



**Fabrication and characterisation of Slippery Icephobic Coatings for application  
to High Voltage Insulators**

**By**

**Samaneh Heydarian Dolatabadi**

**Under supervision of Prof. Gelareh Momen and co-supervision of Prof. Reza Jafari**

**Manuscript-Based Thesis Presented to Université du Québec à Chicoutimi in Partial fulfillment  
of the Requirements for the Degree of Doctor of Philosophy Ph.D.**

**Defended on 12<sup>th</sup> June, 2023**

BOARD OF EXAMINERS:

Professor Issouf Fofana, department of Applied Sciences at UQAC, President of the board of examiners

Professor Ali Nazemi, Department of Chemistry at UQAM, External Member of the Board

Professor Eric Villeneuve, Department of Applied Sciences at UQAC, Internal Member of the Board

Professor Gelareh Momen, Department of Applied Sciences at UQAC, Internal Member of the Board

Professor Reza Jafari, Department of Applied Sciences at UQAC, Internal Member of the Board

Québec, Canada

© Samaneh Heydarian Dolatabadi, Summer 2023

## Résumé

La surface poreuse glissante infusée de liquide (SPGIL), inspiré de la plante sarracénie, suscite un intérêt croissant dans de nombreuses applications, notamment pour les dangers associés à la formation de la glace. Outre la démonstration de leur potentiel hydrophobe, ces surfaces possèdent une faible hystérésis d'angle de contact inférieure à  $2.5^\circ$  et un faible angle d'inclinaison inférieur à  $5^\circ$ . Toutefois, les (SPGIL), sont confrontées à des défis liés au lessivage de l'huile qui réduit leur durée de vie. Ici, deux approches distinctes, notamment la micro-texturation et l'utilisation d'absorbants d'huile, sont présentées dans l'optique de produire efficacement des surfaces glissantes pour améliorer la durabilité de ces matériaux imprégnés de lubrifiant.

Dans la première approche, la méthode de réplique a été employée pour produire des surfaces texturées imprégnées de liquide (STIL) par le biais de la technique de gravure chimique. Des analyses, comme la déplétion/récupération du lubrifiant, ont confirmé que la présence de micro-textures couplée à la viscosité du lubrifiant peuvent jouer un rôle significatif dans la régulation du taux de migration de l'huile. De plus, la combinaison de la micro-texturation et de la glissance dans les STIL peut améliorer de manière considérable les performances glaciophobes. En effet, une telle surface a démontré une contrainte d'adhérence de la glace inférieure à 20 kPa, ce qui représente quatre ordres de grandeur de moins que celle de la surface d'origine non traitée dépourvue de micro-textures. En plus, leur glaciophobicité a été montrée plus stable au fil du temps comparée à la surface d'origine dépourvue de micro-textures.

Pour la deuxième stratégie, des porteurs chargés de lubrifiant ont été utilisés pour empêcher la consommation rapide d'huile, prolongeant ainsi la durée de vie des revêtements préparés. En conséquence, une pression négative a été appliquée pour favoriser l'incorporation du lubrifiant dans les pores des porteurs et augmenter ainsi sa capacité de charge. Afin, d'évaluer quantitativement l'infusion de lubrifiant, une analyse thermogravimétrique (TGA) et la méthode BET (Brunauer, Emmett et Teller) ont été utilisées. Habituellement, un taux élevé de lubrifiant (avoisinant 50 % m/m) est couramment utilisé pour améliorer les performances glaciophobes. Cependant, la présence d'une quantité excessive de lubrifiant dans la matrice peut entraîner une diminution des caractéristiques mécaniques des surfaces préparées.

La combinaison de différents mécanismes anti-givres, comme la localisation de contrainte, la glissance et la formation de molécules non gelées, peut être bénéfique pour l'obtention des propriétés glaciophobes désirables à partir de faibles concentrations de lubrifiant. Ces mécanismes ont été obtenus en utilisant une matrice faite d'un mélange de résines, un lubrifiant infusé et un lubrifiant hydroxyl-terminé.

Le revêtement glissant résultant a été développé en imprégnant des supports chargés de lubrifiant hydroxyle-terminé dans un mélange de résines polydiméthylsiloxane (PDMS) et d'alkoxy-siloxane. Le revêtement préparé a montré des capacités d'anti-givrage et de dégivrage intéressantes, ainsi qu'une bonne résistance à l'exposition aux UVs et à l'humidité. Les caractéristiques glaciophobes du revêtement peuvent être attribuées à sa glissance et à la formation de molécules non gelées. Les propriétés électriques du revêtement ont été évaluées à l'aide d'un ensemble complet de

méthodes, notamment la spectroscopie diélectrique, les tests de contournement, de condensation et de plan incliné. En comparaison avec l'échantillon de référence, le revêtement contenant des porteurs chargés de lubrifiant a montré une permittivité diélectrique et un facteur de perte plus faibles. De plus, une réduction du courant de fuite, dans le cas d'humidité élevée, a été observée avec le revêtement développé. Ce dernier a également montré une augmentation de la tension d'éclatement dans différentes conditions. En somme, les résultats ont confirmé que la solution de revêtement développée contenant des supports chargés de lubrifiant pourrait être considérée comme un candidat potentiel pour une application glaciophobe sur des isolateurs à haute tension.

**Mots-clés:** Surfaces glissantes, Plante carnivore Sarracénie, surfaces biomimétiques, revêtements glaciophobe, Glaciophobicité, surfaces à liquides infusés, surfaces micro/nanostructurées, élastomères de silicone, revêtements infusés de lubrifiant, aérogel de silice, température de nucléation de la glace, temps de congélation, adhérence de la glace, accumulation de glace, absorbant de lubrifiant, absorbants d'huile, isolateur haute tension, fuite.

## Abstract

Slippery liquid-infused porous surface (SLIPS) based on *Nepenthes* pitcher plant has attracted increasing interest in many applications, particularly for mitigating icing hazard. Aside from exhibiting a water repellency, such surfaces have low contact angle hysteresis of  $<2.5^\circ$  and low tilt angle of  $<5^\circ$ . Nonetheless, SLIPS still suffer from challenges related to the oil depletion that reduces their service life. Herein, two different approaches, namely, microtexturing and the use of oil absorbent, are presented to effectively produce the slippery surfaces for the enhanced durability of engineered lubricant-infused materials.

In the first approach, the replication method was employed to produce liquid-infused textured surfaces (LITS) through the chemical etching technique. Analysis such as lubricant depletion/recovery, confirmed that the presence of microtextures and lubricant viscosity can have significant roles in controlling the oil migration rate. Furthermore, merging microtexturing and slipperiness in LITS can enhance the icephobic performance. Such surface demonstrated an ice adhesion strength of less than 20 kPa, which is four orders of magnitude lower than the pristine surface. Furthermore, LITS can offer more long-lasting icephobic properties compared with pristine surface lacking microtextures.

For the second strategy, the lubricant-loaded carriers were used to prohibit the rapid oil consumption, thus prolonging the life service of the prepared coatings. Accordingly, the negative pressure was applied to promote the incorporation of the lubricant within carrier pores and increase the carrier loading capacity. For this purpose, the thermogravimetric analysis (TGA), and the BET (Brunauer, Emmett and Teller) method have been used to evaluate the lubricant infusion quantitatively. High oil content (around 50 wt. %) has been commonly used to enhance icephobic performance, but the presence of excessive amount of lubricant within the matrix can result in decreased mechanical characteristics of the prepared surfaces. The combination of different anti-icing mechanisms, such as stress localization, slipperiness, and the formation of nonfrozen molecules can be helpful to obtain desirable icephobic properties at low oil contents. These mechanisms were achieved using blended matrix, infused lubricant, and hydroxyl-terminated lubricant.

The slippery coating was developed by impregnating hydroxyl-terminated-lubricant-loaded carriers into a blend of polydimethylsiloxane (PDMS) and alkoxy-siloxane resin. The prepared coating showed desirable anti-icing and de-icing properties and long-lasting stability against UV exposure and humidity. The icephobic characteristics of the coating can be attributed from its slipperiness and formation of unfrozen molecules. The electrical properties of the coating were evaluated using a comprehensive set of methods, including dielectric spectroscopy, flashover, condensation, and inclined plane tests. In comparison with the reference sample, the coating containing lubricant-loaded carriers exhibited lower dielectric permittivity and loss factor. Moreover, the coating reduced the leakage current under high humidity. The lubricant-loaded-carrier-containing coating also heightened the flashover voltage in different conditions. The results confirmed that the coating containing lubricant-loaded carriers could be considered as a potential candidate for applying on high-voltage insulators.

**Keywords:** Slippery surfaces, *Nepenthes* pitcher plant, biomimetic surfaces icephobic coatings, icephobicity, liquid-infused surfaces, micro/nanostructured surfaces, silicone elastomers lubricant-infused coatings, silica aerogel, ice nucleation temperature, freezing time, ice adhesion, ice accumulation, lubricant absorbent, oil absorbents, high voltage insulator, leakage current, flashover

## Table of contents

Résumé.....	i
Abstract.....	iii
List of figures.....	ix
List of Tables.....	xiv
List of symbols.....	xvii
Introduction.....	1
Problem definition.....	1
Objectives.....	6
Originality Statement.....	7
Methodology.....	9
Outline.....	11
<b>Chapter 1: Literature review.....</b>	<b>15</b>
1.1 Introduction.....	15
1.2 Icephobicity.....	16
1.3 Coatings for high voltage insulators.....	18
1.4 From superhydrophobicity to slipperiness: theoretical aspect of wetting.....	20
1.5 Fabrication and icephobic properties of SLIPS.....	27
1.5.1 Lubricated micro/nanotextured surfaces.....	27
1.5.2 Oil-infused polymeric systems.....	39
1.5.3 Self-lubricating slippery surfaces.....	41
1.6 Lubricant types and characterization.....	45
1.6.1 Lubricant selection in slippery liquid infused surface.....	45
1.6.2 Effect of lubricant characteristics on the icephobic behavior of SLIPS.....	48
1.7 Durable icephobic slippery surfaces.....	51
1.7.1 Interfacial Slippage.....	55
1.7.2 Slippery omniphobic covalently attached liquid (SOCAL) surfaces.....	56
1.7.3 Oil absorbent materials.....	58
1.8 Characterization of lubricant loaded Carriers.....	59
1.8.1 Thermogravimetric analysis.....	59

1.8.2	B.E.T .....	60
1.9	Conclusion .....	60
<b>Chapter 2: Fabrication of liquid-infused textured surfaces (LITS): the effect of surface textures on anti-icing properties and durability .....</b>		<b>63</b>
2.1	Abstract.....	63
2.2	Introduction.....	64
2.3	Materials and methods .....	67
2.3.1	Fabrication of the oil-infused microtextured silicone material.....	67
2.3.2	Surface characterization.....	69
2.3.3	Mechanical Properties .....	70
2.3.4	Icephobic Properties .....	71
2.3.5	Durability Properties .....	72
2.4	Results and discussion .....	73
2.4.1	Surface characterization.....	73
2.4.2	Surface wettability.....	79
2.4.3	Water-repellency properties .....	81
2.4.4	Depletion/recovery cycle tests.....	83
2.4.5	Anti-icing properties.....	85
2.5	Conclusions.....	95
<b>Chapter 3: Icephobic Behavior of a Slippery Coating Containing Nanoporous Particles as Lubricant-Loaded Carriers.....</b>		<b>98</b>
3.1	Abstract.....	98
3.2	Introduction.....	99
3.3	Experimental section .....	104
3.3.1	Materials.....	104
3.3.2	Preparation of the lubricant-loaded carriers .....	104
3.4	Fabrication of the coatings.....	105
3.5	Material characterization.....	106

3.5.1	Morphology .....	106
3.5.2	Thermogravimetric analysis.....	106
3.5.3	Surface area measurements .....	106
3.5.4	Surface characterization.....	107
3.5.5	Mechanical characterization.....	107
3.5.6	Icephobic Properties .....	107
3.6	Results and discussion .....	109
3.6.1	Characterization of the lubricant-loaded aerogel.....	109
3.6.2	Selection and characterization of the matrix .....	112
3.6.3	Characterization of the coatings containing the lubricant-loaded carriers .....	113
3.6.4	Icephobicity .....	116
3.6.5	Coating durability.....	124
3.7	Conclusions.....	126
<b>Chapter 4: Icephobicity and Electrical Assessment of Slippery Coating Impregnated with a Stabilized Hydroxyl-terminated Lubricant for High Voltage Insulation Application .....</b>		<b>129</b>
4.1	Abstract.....	129
4.2	Introduction.....	130
4.3	Materials and methods .....	134
4.3.1	Fabrication of coatings containing lubricant-loaded carriers .....	134
4.3.2	Surface characterization.....	135
4.3.3	Icephobic Properties .....	136
4.3.4	Durability.....	138
4.3.5	Electrical properties.....	139
4.4	Results and discussion .....	142
4.4.1	Surface characterization.....	142
4.4.2	Icephobicity .....	143



4.4.3	Durability.....	146
4.4.4	Electrical characterization.....	149
4.4.5	Flashover .....	151
4.4.6	Condensation test .....	153
4.4.7	Inclined plane test (IPT) .....	154
4.5	Conclusions.....	156
	<b>Chapter 5: Conclusions .....</b>	<b>158</b>
	<b>Chapter 6: Recommendations.....</b>	<b>165</b>
	APPENDIX I.....	167
	APPENDIX II.....	170
	APPENDIX III.....	172
	References.....	175
	Publications .....	198

## List of figures

<b>Figure 1-1.</b> Schematic showing (a) Young's model, and (b) contact angle hysteresis [117].	21
<b>Figure 1-2.</b> Schematic showing (a) a Cassie state, and (b) a Wenzel.	22
<b>Figure 1-3.</b> The image of a pitcher plant <i>Nepenthes</i> (left), and its scanning electron microscope (SEM) micrographs (right) [123].	23
<b>Figure 1-4.</b> Schematic showing of different wettable configurations for a four-phase system (air, liquid-1, liquid-2, solid) [37].	25
<b>Figure 1-5.</b> Comparison of the ice adhesion strengths of various low-surface-energy [48].	29
<b>Figure 1-6.</b> Sequence of ESEM images of frost formation via droplet condensation and freezing on (a) 10- $\mu\text{m}$ SHS and (b) 10- $\mu\text{m}$ LIS [94].	30
<b>Figure 1-7.</b> (a) Schematic illustrating the fabrication procedure of the oil-infused, microtextured polydimethylsiloxane (PDMS) material [144]. (b) The ice adhesion strengths of oil-infused, microtextured PDMS having different oil viscosities and infusion levels (2–15 wt %) [144].	31
<b>Figure 1-8.</b> Schematic illustration of the fabrication of the SLIP [32].	33
<b>Figure 1-9.</b> Schematic of the electrochemical coating process of a rough polypyrrole [33].	34
<b>Figure 1-10.</b> Schematic model of the icephobic mechanisms of (a) SHS and (b) SLIPS coatings, depicting the decay of the water CA [146].	35
<b>Figure 1-11.</b> (a) Comparison of ice adhesion strengths of lubricant-impregnated surfaces with different amounts of lubricant [48]. (b) Influence of texture density on the ice adhesion strength of different LIS [48].	37
<b>Figure 1-12.</b> Schematic illustrating lubricant depletion after frosting–defrosting cycles [94].	38
<b>Figure 1-13.</b> (a) Schematic showing the migration of infused oil toward the surface. (b) Preparation and surface release of liquid paraffin-organ gel (LP-OG) [157]. (c) Preparation and surface release of liquid paraffin-organ gel (LP-OG) [157].	41
<b>Figure 1-14.</b> (a) The aqueous layer on ice as observed by molecular-dynamic calculations. The gray and black spheres represent oxygen and hydrogen atoms, respectively [165]. (b) Schematic of the formation of a self-lubricating liquid water layer and its de-icing functionality [159]. (c) Schematic showing the polyelectrolyte brushes for inhibiting ice accumulation on a surface. [168].	44

**Figure 1-15.** (a) Schematic illustrating the formation of a liquid–liquid interface on a MAGSS and compared with superhydrophobic and liquid-infused surfaces [193], (b) the fabricating steps of the UV-cured SLIPS [197]., (c) the repeated icing/de-icing tests for oil-only (red), oil+1360 (yellow), and oil+350 (blue) SLIPSs [197]. .....53

**Figure 1-16.** The release of an antifreeze liquid, and the consequent ice melt, in response to icing [198]. .....55

**Figure 1-17.** Formation of the slippery covalently attached liquid coatings through acid-catalyzed polycondensation of dimethyldimethoxysilane on a substrate [207]. .....57

**Figure 2-1.** SEM images of (a) the chemical etched coupons, (b) the pristine PDMS elastomer and (c) the replicated microtextured PDMS without infused oil. ....74

**Figure 2-2.** Micrographs of liquid-infused textured surfaces containing silicone oil with 50 cSt viscosity. (a) 10 wt.%, (b) 30 wt.%, and (c) 50 wt.% of oil at 500x magnification. (d) 10 wt.%, (e) 30 wt.%, and (f) 50 wt.% of oil at 1000x magnification. ....75

**Figure 2-3.** Micrographs of liquid-infused textured surfaces containing silicone oil with 500 cSt viscosity. (a) 10 wt.%, (b) 30 wt.%, and (c) 50 wt.% of oil at 500x magnification. (d) 10 wt.%, (e) 30 wt.%, and (f) 50 wt.% of oil at 1000x magnification. ....75

**Figure 2-4.** Silicon content of the samples in relation to the infusion level of the silicone oil, as obtained by energy-dispersive X-ray spectroscopy. ....76

**Figure 2-5.** AFM images of microtextured elastomer containing (a) no oil, (b) 10 wt.% 50 cSt oil, (c) 50 wt.% 50 cSt oil, and (d) 10 wt.% 500 cSt oil surfaces. ....78

**Figure 2-6.** Water contact angle in relation to oil content (wt.%) for two oil viscosities (50 cSt and 500 cSt). ....80

**Figure 2-7.** Water droplet velocity across the LITS as a function of infusion percentage and lubricant viscosity. ....82

**Figure 2-8.** The rate of weight loss for LIS and LITS samples in relation to the number of test cycles of oil recovery/depletion. ....85

**Figure 2-9.** Ice nucleation temperatures for samples infused with oils having (a) 50 cSt and (b) 500 cSt viscosities, as determined by differential scanning calorimetry. ....87

<b>Figure 2-10.</b> Ice nucleation time on the surface of samples having various levels of oil infusion for the 50 and 500 cSt viscosity oils.....	88
<b>Figure 2-11.</b> Ice adhesion of samples containing various amounts of infused silicone oil over multiple icing/de-icing cycles for oils of (a) 50 cSt and (b) 500 cSt viscosities. ....	89
<b>Figure 2-12.</b> Ice adhesion behavior of LITS and LIS during resting periods for samples (a) 10 wt.% oil infusion and 50 cSt viscosity and (b) 10 wt.% oil infusion and 500 cSt viscosity.....	91
<b>Figure 2-13.</b> Hardness values in relation to oil viscosity and oil infusion level. ....	94
<b>Figure 2-14.</b> Variation of the ice adhesion strength before and after the 300-h-QUV-accelerated-weathering test for samples containing various content of silicone oil with viscosity of (a) 50 cSt, and (b) 500 cSt. ....	95
<b>Figure 3-1.</b> Schematic illustration of the preparation process of the lubricant-loaded carriers.....	105
<b>Figure 3-2.</b> Micrographs of the (a) as-received aerogel, (b) silicone oil-loaded carriers, (c) hydroxyl-terminated silicone oil-loaded carriers. ....	110
<b>Figure 3-3.</b> Thermographic curves for the as-received aerogel and aerogel carriers loaded with silicone oil (SO/A), and hydroxyl-terminated silicone oil (HTSO/A).....	111
<b>Figure 3-4.</b> The contact angle hysteresis of samples containing (SO/A) and (HTSO/A) in relation to concentration of the lubricant-loaded carriers.....	114
<b>Figure 3-5.</b> 3D topographical maps of the (a) reference and samples containing (b) 5%, and (c) 15% silicone oil-infused aerogels and samples containing (d) 5% and (e) 15% hydroxyl-terminated silicone oil-infused aerogels.....	115
<b>Figure 3-6.</b> Evaluation by differential scanning calorimetry (DSC) of ice nucleation temperatures corresponding to samples containing carriers loaded with (a) silicone oil-infused aerogels (SO/A) and (b) hydroxyl-terminated silicone oil-infused aerogels (HTSO/A). ....	117
<b>Figure 3-7.</b> Water droplet freezing time on the surface of the samples containing silicone oil-infused aerogels (SO/A) and hydroxyl-terminated silicone oil-infused aerogels.....	118
<b>Figure 3-8.</b> Ice accumulation on samples containing (a) silicone oil-infused aerogels (SO/A) and (b) hydroxyl-terminated silicone oil-infused aerogels (HTSO/A) on surfaces inclined at 0°, 45°, and 80°, as measured by a static accumulation test. ....	120

<b>Figure 3-9.</b> Infrared thermographs of the samples on surfaces inclined at 80° after 5 min of precipitation. .....	121
<b>Figure 3-10.</b> Ice adhesion strength of samples containing silicone oil–infused aerogels (SO/A) and hydroxyl-terminated silicone oil–infused aerogels (HTSO/A), obtained using (a) push-off and (b) centrifuge tests. ....	123
<b>Figure 3-11.</b> Ice adhesion strength in samples containing (a) silicone oil–infused aerogels (SO/A) and (b) hydroxyl-terminated silicone oil–infused aerogels (HTSO/A) over 20 icing/de-icing cycles, as measured by push-off tests.....	124
<b>Figure 3-12.</b> Root mean square ( $R_q$ ) of surface roughness after 20 icing/deicing cycles. ....	125
<b>Figure 4-1.</b> Schematic of micro-push-off apparatus. ....	137
<b>Figure 4-2.</b> (a) Top view of the flashover and (b) condensation setups. ....	140
<b>Figure 4-3.</b> (a) Schematic illustrating the test setup for inclined plane test (IPT); (b) and (c) parts used for mounting the samples for IPT.....	141
<b>Figure 4-4.</b> Variation of contact angle and contact angle hysteresis as a function of LLC content. ...	143
<b>Figure 4-5.</b> 3D topographical maps of the (a) reference and LLC-5, (b) LLC-10, and (c) LLC-15....	143
<b>Figure 4-6.</b> (a) DSC evaluation of ice nucleation temperatures corresponding to samples with LLC content. (b) Ice accumulation on samples inclined at 0°, 45°, and 80°, as measured by SAT. (c) Ice adhesion strength of samples, as obtained using micro-push-off test. (d) Ice adhesion strength in samples containing LLC over 20 icing/de-icing cycles, as obtained by push-off test.....	146
<b>Figure 4-7.</b> Evaluation of ice adhesion strength corresponding to samples during 45-day accelerated weathering test. ....	148
<b>Figure 4-8.</b> The rate of weight loss the coating containing LLC and the reference (the coating containing the same amount of oil but without aerogel) in relation to the number of test cycles of oil recovery/depletion.....	149
<b>Figure 4-9.</b> Variation of (a) real ( $\epsilon'$ ) and (b) imaginary ( $\epsilon''$ ) parts of permittivity and (c) dissipation factor ( $\tan\delta$ ) in relation to frequency. ....	150

**Figure 4-10.** Evaluation of flashover voltage during 10 subsequent cycles under (a) non-polluted/dry, (b) polluted/dry, and (c) polluted/wetted conditions. (d) Evaluation of first flashover voltage at  $-10\text{ }^{\circ}\text{C}$ ,  $-5\text{ }^{\circ}\text{C}$ , and  $0\text{ }^{\circ}\text{C}$ . ..... 152

**Figure 4-11.** Evaluation of leakage current versus time on samples for a) three repetitive cycles and b) their averages, as obtained by condensation test. .... 154

**Figure 4-12.** (a) Thermal camera images of samples at the final minutes of IPT. (b) and (c) Images of the samples after the test. (d) Evaluation of leakage current over time during IPT. .... 156

## **List of Tables**

<b>Table 3-1.</b> Surface area analysis of the carriers using the BET method. ....	111
<b>Table 3-2.</b> Hardness values of the fabricated samples, as obtained by the Shore A durometer. ....	113
<b>Table 3-3.</b> Surface roughness parameters of the fabricated coatings. ....	115

### List of abbreviations

---

<b>AFM</b>	Atomic Force Microscopy
<b>Al</b>	Aluminum
<b>AMIL</b>	Anti-Icing Materials International Laboratory
<b>B.E.T</b>	Brunauer, Emmett, and Teller
<b>CA</b>	Contact Angle
<b>CAH</b>	Contact Angle Hysteresis
<b>CAT</b>	Centrifuge Adhesion Test
<b>CB</b>	Cassie-Baxter
<b>cSt</b>	Centistokes
<b>DC</b>	Direct Current
<b>DSC</b>	Differential Scanning Calorimetry
<b>EDS</b>	Energy-dispersive X-ray spectroscopy
<b>H<sub>2</sub></b>	Hydrogen
<b>HTSO/A</b>	Aerogel infused with hydroxyl-terminated silicone oil
<b>IPT</b>	Inclined Plane Test
<b>LIS</b>	Liquid-infused surfaces
<b>LIS</b>	Liquid-infused surfaces
<b>LITS</b>	Liquid-infused textured surfaces
<b>LLC</b>	Lubricant-loaded carrier
<b>MAGSS</b>	Magnetic slippery surfaces
<b>N<sub>2</sub></b>	Nitrogen
<b>NH<sub>4</sub>Cl</b>	Ammonium Chloride
<b>NSERC</b>	Natural Science and Engineering Research Council of Canada
<b>OH</b>	Hydroxyl
<b>OTS</b>	Octadecyltrichlorosilane
<b>PDMS</b>	polydimethylsiloxane
<b>PEG</b>	Poly (ethylene glycol)
<b>PEMA</b>	Poly (ethyl methacrylate)
<b>PFD</b>	Perfluorodecalin
<b>PFPE</b>	Perfluoropolyether



<b>POSS</b>	Polyhedral Oligomeric Silsesquioxanes
<b>PPy</b>	Polypyrrole
<b>PTFE</b>	Polytetrafluoroethylene
<b>RTV</b>	Room Temperature Vulcanized
<b>SA</b>	Sliding angle
<b>SAM</b>	Self-assembled monolayer
<b>SAT</b>	Static accumulation test
<b>SEM</b>	Scanning Electron Microscopy
<b>SHP</b>	Superhydrophobic
<b>SiO<sub>2</sub></b>	Silicon Oxide
<b>SLIPS</b>	slippery liquid-infused porous surfaces
<b>SO/A</b>	Aerogel infused with silicone oil
<b>SOCAL</b>	Slippery omniphobic covalently attached liquid
<b>TEOS</b>	Tetraethoxysilane
<b>TGA</b>	Thermogravimetric Analysis
<b>TPFS</b>	Trichloro(1H,1H,2H,2H-perfluorooctyl) silane
<b>UV</b>	Ultra-Violet

## List of symbols

---

$I_C$	Capacitive currents
$I_R$	Resistive current and
$f_{SL}$	fractions of solid–liquid interface
$\gamma_{LG}$	the interfacial surface tensions of solid–gas
$\gamma_{oa}$	Oil–air surface tension
$\epsilon''$	Imaginary part of Dielectric Permittivity
$\epsilon'$	Real part of Dielectric Permittivity
$\epsilon_0$	Permittivity of Free Space
$\emptyset$	Texture density
$\Delta G_f^*$	Gibbs free energy
$\Delta g_{ac}$	Activation energy barriers
$D$	The chain self-diffusion coefficient
$f$	Frequency
$J$	Ice nucleation rate
$K_B$	Boltzmann constant
$R$	Contact radius
$R$	surface roughness
$R_h$	Polymer hydrodynamic radius
$S_{ow}$	oil–water spreading parameter
$S_q$	Root-Mean-Square Height of Area Roughness
$S_{sk}$	Skewness Coefficient of Area Roughness
$T$	Absolute temperature
$\tan \delta$	Dissipation factor
$V$	Droplet velocity
$v$	Water droplet sliding speed
$W$	Droplet weight
$\alpha$	Angle corresponding inclination
$\alpha$	Tilt angle
$\eta$	Viscosity

$\mu$                       Viscosity of the infused liquid  
 $\theta$                       Contact angle

## **Dedication**

To the loving memory of my father,  
to my mother, *Zahra Yadegar*, for her unwavering love, sacrifice, and resilience, who has  
shaped my world and lighten my path with her love,

and

to my loving husband, *Mohammadreza Shamshiri*, my constant source of encouragement  
and inspiration. Without his support and love, this achievement would not have been  
possible.

## Acknowledgements

I would like to express my gratitude to my research supervisor, *Prof. Gelareh Momen*, for her exceptional encouragement, kindness, and mentorship throughout my doctoral journey.

I extend my sincere appreciation to my co-supervisor, *Prof. Reza Jafari* for his support, insightful feedback, and continuous involvement in my project, even during the most challenging times.

I am deeply grateful to the members of my committee, *Prof. Issouf Fofana*, *Prof. Ali Nazemi*, and *Prof. Eric Villeneuve* for their invaluable guidance and insightful comments.

I would like to express my appreciation to *Ms. Helene Gauthier*, Chercheuse Métallurgie et génie des Matériaux, IREQ, Hydro Québec, for her feedbacks and support during this academy-industry collaboration.

I would like to warmly thank *Prof. Stephan Brettschneider*, professor of electrical engineering department at the Université du Québec à Chicoutimi, and *M. Fredric Munger*, graduate student at the Université du Québec à Chicoutimi, for their collaborations, and involvement in performing the electrical analyses.

I would also like to extend my thanks to all the professionals and technicians for their assistance in this project, especially *Ms. Caroline Blackburn*, *Ms. Nathalie Gagné*, and *Ms. Shan Yang* at the Anti-icing Materials International Laboratory (AMIL), UQAC, *Mr. Luc Chatigny*, technician of Laboratoire Revêtements glaciophobes et ingénierie des surfaces (LARGIS), *Ms. Caroline Potvin*, the laboratory assistant of the chemistry department and *Ms. Kouba Marie Lucia Yapi* for the dielectric spectroscopy analyses.

I would like to express my sincere appreciation to *Hydro-Québec*, Québec, Canada, Natural Sciences and Engineering Research Council of Canada (NSERC), and le Pôle Recherche Innovation en Matériaux avancés du Québec (PRIMA Québec), Canada, for providing the financial support that made my research possible.

Last but not least, I would like to sincerely thank my family and friends in LARGIS especially *Anahita Allahdini*, *Saba Goharshenas*, *Elham Vazirinasab*, *Khosrow Maghsoudi*, *Helya Khademsameni* and *Mohammadsadegh Koochaki* that their presence has been a constant source of support making this academic journey all the more meaningful and memorable.

## **Introduction**

### **Problem definition**

Insulators are among the most essential components in the power transition system, which have been used for mechanical support and making the distance between high-voltage line conductors. Ice accretion over the surface of insulators in cold-climate regions can affect their mechanical and electrical performance. As the high-voltage insulators are exposed to ice accumulation in countries such as Canada, severe damages such as deformation, flashovers, and power outage can be expected, resulting in the loss of millions of dollars. The presence of ice and contaminants over the insulator surface creates a highly conductive film that promotes leakage of current and facilitates the short circuit. Such phenomena can lead to arc formation on insulators and cause flashover in some conditions [1,2]. The deformation and collapse of structures are expected caused by increase on weight, resulting from the ice accumulation over the surface of insulators. These problems come with enormous costs and loss of energy. On the December 2013, an extreme winter storm in Canada, left over a million people without power for days and the cost of loses due to ice storm was estimated around 200 million dollars [3]. Thus, many research works have focused on protecting the insulator surface against icing and preventing such damages in transition lines [4,5].

High-voltage outdoor insulators are generally fabricated from glass, porcelain, and composite polymer materials such as silicone rubbers. Since the 1900s, ceramic insulators based on porcelain and glass have shown acceptable performance in the transition line industry. Despite their high mechanical strength and suitable

environmental aging resistance, a conductive water layer over insulators can cause problems such as flashover because of their hydrophilic characteristic [6]. The formation of a conductive layer over the insulator surface can increase the leakage current and thus create dry regions on the surface, leading to dry band arcing and electrical discharge. Therefore, under heavy icing conditions, they cannot be completely effective, and anti-icing strategies such as active and passive methods can be used to improve their efficiency [4,7]. In active de-icing methods, ice can be mechanically and/or thermally removed using an external source of energy, while passive icephobic strategies such as the application of coatings do not need any external source. The latter methods can be intrinsically water repellence and are more economical than active de-icing approaches [8–11].

In recent years, the application of hydrophobic RTV (room temperature vulcanizing) silicon materials on porcelain and glass insulators has been suggested to gain water repellency properties [12,13]. These silicone-based materials are well-known for their unique properties, such as high electrical insulation, thermal stability, and weathering resistance. However, their water contact angle is approximately  $110^\circ$ , and such a low hydrophobicity level can not effectively have water repellency and prevent ice formation over the substrate. Besides, other factors such as high humidity and harsh weather climates can reduce their hydrophobicity [14,15]. Therefore, the use of RTV materials to prevent insulators from icing flashover is not completely efficient. The superhydrophobic surfaces inspired from nature can offer water repellency characteristics and desirable ability for the reduction of severe ice accumulation [10,16]. Therefore, the idea of employing such coatings has been

proposed to decrease ice buildup over insulators and optimize their efficiency [17–19]. Despite the many efforts on the fabrication of superhydrophobic surfaces, some drawbacks are encountered, including mechanical durability and abrasion, which limit their applications for high-voltage insulators [20,21]. Under harsh cold weather conditions, the porous structure of superhydrophobic surfaces can be filled with condensed water. This loss promotes the mechanical interlocking between ice and the surface, thus increasing ice adhesion markedly [22,23]. This challenge can be overcome by developing a strategy that can prohibit the humidity condensation within surface asperities.

This PhD thesis proposes the slippery liquid infused texture surfaces (SLIPS) as a state-of-the-art generation of icephobic coatings that significantly diminish such drawbacks. The most vital difference between superhydrophobic surfaces and SLIPS is the type of substance stuffed in their structures. In slippery surface, liquid substance is trapped in the pores instead of air, and this phenomenon can be used to avoid some limitations of superhydrophobic surfaces. These nature-inspired liquid-infused surfaces (LIS) are characterized by high water repellency, low contact angle hysteresis, and low sliding angle. Therefore, they can show a high potential in application for high-voltage insulators, such as anti-icing coatings. Notably, this research work is defined as an academic-industry collaboration to propose the icephobic coatings for applying on high-voltage porcelain insulators by *Hydro Québec Company*.



## Overview

In the past decades, many studies have introduced different types of anti-wetting surfaces with desirable properties. Superhydrophobic and lubricant infused slippery surfaces are among the well-known non-wettable surfaces that are inspired from the nature [24–28]. Based on the extraordinary properties of superhydrophobic surfaces, they have been used as icephobic surfaces. However, they suffer from some downsides, such as water condensation and high ice adhesion in humid environments. These challenges attached to superhydrophobic surfaces can be addressed by developing icephobic coatings based on the slippery characteristics of pitcher plant [29,30].

The smoothness and homogeneity of SLIPS exhibited low contact angle hysteresis and sliding angle; therefore, they can repel various liquid and solid substances, such as crude oil, blood, and ice [31–34]. Therefore, SLIPS can be used to develop durable icephobic surfaces. Generally, a lubricant and porous structure are essential for slippery surfaces. The presence of lubricant over the surface can diminish the frost condensation in pores and reduce interaction between ice and surface, thus decreasing ice adhesion [35–38].

Although liquid infused slippery surfaces can be used extensively as icephobic coatings, the vital challenge of lubricant depletion through gravity and shear stress restricts their large-scale applications [39,40]. Accordingly, several efforts have been done to enhance the slippery coating durability. Lubricant-infused polymeric systems can maintain the lubricant within their chain networks and replenish the uppermost oil layer when lubricant depletion occurs. In this type of slippery surfaces, the lubricant infused into the polymeric bulk can diffuse into the surface with the help of

concentration gradient and capillary pressure [41–46]. Micro texturing can also trap the lubricant over the surface. Liquid infused textured surfaces exhibit enhanced anti-icing properties, and their texture has a critical role in preserving the lubricant over the surface [47–49].

In the present project, the combination of lubricant infusion in polymeric matrix and creating texture over the surface has been employed to minimize the rate of lubricant depletion and enhance coating durability. Texture was applied over the oil infused polymeric surface by using a replication approach. For this purpose, a metal substrate was chemically etched, and then the texture was transferred from the prepared insert into polymeric surfaces.

Oil-absorbent materials can be used to obtain a coating with optimized stability that can be used for a wide range of applications, particularly high-voltage insulator. Absorbent materials such as zeolite, polymers, and nano-porous materials are widely used in different applications [50]. Therefore, the main concept of this thesis in the second step is the use of porous materials as the lubricant-absorbent and incorporating them in a polymeric matrix. The presence of these absorbents can significantly control the migration rate of lubricant toward the uppermost surface. Finally, the effects of lubricant carriers on the icephobic characteristics of the coatings were comprehensively evaluated. The fabricated coatings should meet the required criteria for application on high-voltage insulators. Hence, the electrical performance of coatings was also investigated precisely.

## Objectives

This project mainly aimed to develop slippery oil-infused polymeric systems by applying different strategies to obtain durable icephobic coatings for high voltage insulators. The subcategorized objectives are as follows:

- Design of a specific methodology for the development of a durable slippery surface based on micro-texturing.
- Selection of the lubricant and polymeric matrix with desirable icephobic characteristics.
- Investigation of the effect of the structural modification on the rate of lubricant depletion and icephobic characteristics of the prepared surfaces.
- Evaluation and optimization of the lubricant parameters, such as viscosity and percentage on the icephobicity and durability of surfaces.
- Development of slippery coating with high lubricant retention ability by using lubricant-loaded carriers.
- Selection of suitable oil absorbent materials compatible with lubricants and polymeric matrix.
- Selection of different types of lubricant with hydrophobic and hydrophilic functionality compatible with polymeric matrix.
- Evaluation of the effect of lubricant-loaded carrier content on the icephobic properties and durability of the fabricated slippery coatings.
- Evaluation of the electrical behaviors of the formulated coatings by carrying out a comprehensive set of electrical analyses.

## **Originality Statement**

This project proposes the fabrication of slippery liquid infused polymeric coatings as a specific type of icephobic coatings that have been inspired from a pitcher plant. For this purpose, coatings with different compositions and properties will be fabricated and applied to solve icing concerns on high-voltage insulators.

Generally, the present study aims to enhance the lubricant retention and durability by either surface micro texturing or using lubricant absorber materials. As the first strategy, it was aimed to combine the textured micromorphology and slipperiness of a lubricant-infused silicone elastomer via replication. Therefore, this study focuses on lubricant infusion in the polymeric matrix. Furthermore, the effect of micro texturing on the lubricant depletion and long-term durability were investigated.

The presence of porosity over SLIPS can play a critical role for lubricant preservation over the surface. Various methods have been used for the production of textured surfaces, such as lithography, laser, spray coating, and plasma [51–54]. However, the method suffers from some drawbacks that are related to the abovementioned fabrication methods, such as high time consumption, complicated procedure, environmental issues, and expensive infrastructures. In present study, textured insert was used for the transformation of microtextures from Al template to polymeric surfaces. For the creation of texture, the chemical etching method via one-step procedure was used. The significance of the strategy is that the use of textured insert is relatively simple and applicable in a wide range of materials, such as rubbers, resins, and thermoplastics polymers with low production time and cost. Unlike other

methods, such textured inserts also benefit from repeatability and reproducibility for the production of micro textures over polymeric surfaces.

The use of texturing along with lubricant infusion into the bulk to enhance the durability of SLIPS is a novel idea. Moreover, only a few research have focused on these fields, particularly in its application on insulators. Furthermore, the available studies are mostly in their initial stages, and they still need to be well developed to apply in real conditions.

In the second phase of the project, lubricant-loaded carrier materials were used to improve the lubricant retention and durability of the surfaces. This strategy involved two separated steps, namely, the preparation of the lubricant-loaded carriers and fabrication of the coatings. A process that involves negative pressure was used to enhance the infusion of the lubricant into the pores of absorbents to lengthen the service life of the coating. To the best of our knowledge, the stabilization of the lubricant in absorbent structure has not been studied.

A slippery coating can be fabricated by changing either the lubricant or matrix. Most studies in both procedures are not well-developed, and they still need further investigation. Both the matrix and the lubricant were modified to obtain more desirable characteristics for this application. Based on the formulation design, the novelties of this research are more related to the combination of three different anti-icing strategies, namely, stress-localization, formation of non-frozen water molecules, and slippage. This set-up can minimize some drawbacks of slippery coatings, such as oil depletion and the influence of excessive oil content on mechanical properties.

The fabrication method of slippery surface is versatile, and balancing the trade-off between low ice adhesion and coating durability has been introduced as their main challenge [55]. The formulation of the coatings was changed in terms of matrix combination and lubricant type to achieve an optimized icephobicity, mechanical properties, and durability.

Finally, a comprehensive set of tests was used to characterize the icephobic and electrical properties of the fabricated coating. In most previous works in the field of slippery coatings, the samples were characterized using only two or rarely three icephobic methods. However, in the present research, the icephobic characteristics of the prepared coatings were evaluated from different aspects. Furthermore, considering the final application of the coatings for high-voltage insulator, the samples were characterized using various methods, such as flash over voltage, leakage current, and erosion resistance via the special-designed equipment in our group. The use of this coating system in the high-voltage insulation industry is a new field of technology.

## **Methodology**

The main objective of this study is to fabricate the slippery oil-infused polymeric coatings having durable icephobic characteristics for use in the high-voltage insulator applications. For this purpose, surfaces and coatings were developed in terms of the main matrix and lubricant characteristics. The overall procedure can be categorized into three phases.

In the first phase, the slippery surfaces were developed by merging surface morphology and slipperiness through infusing silicone oil in a micro-textured silicone

elastomer. To achieve this, the textured templates were first, fabricated using the chemical etching method, followed by applying anti-stiction coating on prepared templates. Then, the microtextures were transferred to the oil-infused silicone elastomer via the replication method. Afterward, the effects of viscosity (50 and 500 cSt) and lubricant contents (10, 20, 30, 40, and 50 wt.% of the silicone oil) on the morphology and icephobic properties of the fabricated surfaces were investigated. Wettability and morphology of the fabricated samples were evaluated using a goniometer, and scanning electron microscopy (SEM), respectively. Moreover, the localized surface elasticity maps of the surfaces were obtained by the atomic force microscopy (AFM). Furthermore, the icephobic performance of the samples was assessed through differential scanning calorimetry (DSC), push-off tests, and freezing delay time measurements.

The second phase of this study involved improving the lubricant retention capability by incorporating oil-absorbent materials within the polymeric blend. Therefore, two different lubricants namely silicone oil and hydroxyl-terminated silicone oil were separately loaded within hydrophobic silica aerogel as a lubricant carrier by applying negative pressure via a three-step procedure. The lubricant-carrier powders were then added into a PDMS- alkoxy siloxane blend at various percentages. It is noteworthy that the blend ratio was studied to obtain the optimized mechanical properties. The loading capacity of the lubricant-loaded carriers was evaluated by scanning electron microscopy (SEM), thermogravimetric analysis (TGA), and BET (Brunauer, Emmett and Teller) method. Furthermore, a comprehensive series of methods was conducted to assess both anti-icing and de-icing properties of the

fabricated coatings. The amount of ice accumulated on the surfaces was measured by the static accumulation test (SAT), and the effect of their ice adhesion strengths on ice accumulated ice was studied using two different methods, namely the push-off and centrifuge adhesion tests. The durability of the coatings over repeated icing/de-icing event was assessed via the push-off adhesion test.

Based on the previous phase, the coatings containing hydroxyl-terminated-silicone-oil carriers were identified as potential candidates to evaluate their electrical properties. In the last phase, a comprehensive set of electrical tests was carried out to find the optimal candidate among them for application on high voltage insulators. The permittivity and loss factor of the fabricated samples were measured via the dielectric spectral analysis. Moreover, the maximum tolerance of the coatings under applying high-voltage stress was assessed using the flashover test in different conditions, including clean/dry, polluted/dry, and polluted/wet states. The flashover voltage of the samples was also investigated at  $-10\text{ }^{\circ}\text{C}$ ,  $-5\text{ }^{\circ}\text{C}$ , and  $0\text{ }^{\circ}\text{C}$ . Additionally, the electrical performance of the coatings was studied under controlled humidity conditions via the condensation test. Finally, the inclined plane test (IPT) was conducted to determine the resistance of fabricated coatings against tracking and erosion under electrical voltage. It is worth mentioning that the behavior of the coatings was also assessed under weathering conditions, including harsh condensation cycles and UV exposure using QUV, which simulated exposing to outdoor circumstances.

## **Outline**

The outline section provides a brief overview of the six chapters composing this thesis. First, a literature review is presented for the readers to provide some general



ideas about the slippery LIS. The fundamental wettability processes of the LIS are thus provided. Furthermore, the different fabrication methods of such surfaces are presented, and the icephobic characteristics of the prepared surfaces are listed. The durability of the slippery LIS, as one of the main challenges, is widely addressed, and various strategies to tackle this issue are provided. Notably, a major part of this chapter is related to our review article entitled “Recent progress in the anti-icing performance of slippery liquid-infused surfaces” published in the journal of *Progress In Organic Coatings* [35]. The three following chapters correspond to each written article of this Ph.D. research work.

In chapter 2, the fabrication of the liquid-infused textured surfaces (LITS) by using a replication method is presented. By merging microtexturing and slipperiness, the development of an icephobic surface with enhanced durability was aimed. The wettability, morphology, and localized surface elasticity maps of the prepared surface were studied in terms of lubricant viscosity and content via goniometry, scanning electron microscopy (SEM), and atomic force microscopy (AFM), respectively. Furthermore, various icephobic characteristics of the surfaces, including the ice nucleation temperature, complete freezing time, and ice adhesion were evaluated. The obtained results are presented in the journal article of “Fabrication of Liquid-Infused Textured Surfaces (LITS): The Effect of Surface Textures on Anti-Icing Properties and Durability” published in *Journal of Materials Today Communications* [56].

In chapter 3, the fabrication of a durable icephobic coating was obtained by incorporating lubricant-loaded carriers within a polymeric blend. The use of aerogel as an oil absorbent material can be considered as an effective strategy to control the rate of the lubricant consumption in the fabricated slippery coatings. The loading capacity

of the carriers was studied using thermogravimetric analysis (TGA) and Brunauer, Emmett, and Teller (BET) test. Furthermore, the anti-icing properties of the prepared coatings were evaluated by differential scanning calorimetry (DSC) and using the Peltier cooling machine. The de-icing characteristics of the coatings were investigated using various methods, such as push-off test, centrifuge test, and static accumulation test (SAT). The long-term durability of the fabricated coatings was assessed by combining 20 subsequent icing/de-icing events and push-off test. The obtained results are presented as the journal article entitled “Icephobic Behavior of a Slippery Coating Containing Nanoporous Particles as Lubricant-Loaded Carriers” published in *Surfaces and Interfaces journal* [57].

In chapter 4, the slippery coating was obtained by embedding the hydroxy-terminated-silicone-oil-loaded carriers into a polymeric matrix. The icephobicity and weathering resistance of the fabricated coating were thoroughly surveyed in this chapter. For the evaluation of the icephobic performance of the coatings, various methods such as DSC, micro-push-off adhesion test, and SAT were employed. A comprehensive set of tests was performed to evaluate the electrical characteristics of the coating that included the dielectric, flashover, condensation, and inclined plane tests. The obtained results are presented as the journal article entitled “Icephobicity and Electrical Assessment of Slippery Coating Impregnated with a Stabilized Hydroxyl-Terminated Lubricant for High Voltage Insulation Application” published in *journal of Material Science* [58].

In chapter 5, the important results of this PhD project were provided in the conclusion chapter. The main results corresponding to each article were first listed as partial conclusions. The general conclusions are presented afterwards.

In chapter 6, particular measures or directions that can be helpful for the future research work are presented as recommendations based on the findings and literature review.

## Chapter 1: Literature review

### 1.1 Introduction

Ice formation on solid surfaces raises both safety and cost concerns for many outdoor infrastructures, including transportation networks, power plants, wind turbines, railways, and telecommunication systems [59–62]. Particularly ice accumulation on insulators restricts their performance and leads to many technical problems and costs [63–65]. To develop means of reducing the ice build-up on solid surfaces, the academic and industrial sectors have investigated the properties, energy, and topography of surfaces for a range of materials [66–68].

Generally, there are two approaches to remove ice from the exposed surfaces including active and passive methods. In comparison with active de-icing methods, which need an external source of energy to ice removal mechanically and thermally, using the passive icephobic strategies can be along with many advantages. Indeed, such methods not only have intrinsic water repellency ability, but also are more economical than other icephobic approaches [8–11]. Moreover, active methods cannot be completely effective under heavy icing conditions, and therefore, utilizing passive anti-icing methods such as applying coatings has got more attention [7].

Recently, slippery liquid-infused porous surfaces (SLIPS) have been introduced; these surfaces are inspired by those of the *Nepenthes* pitcher plant [69–71]. By replacing the liquid–liquid contact with an air–liquid contact, SLIPS eliminate water condensation in pores and significantly reduce ice adhesion, even under conditions of high humidity. SLIPS technology has enhanced the performance of

surfaces in various fields and has shown a high potential for new applications [72–74], including anticorrosion, biomedical, antifouling, and anti-icing needs [37,49,83,75–82]

In this chapter, we review the icephobic characteristics of these slippery surfaces and their anti-icing mechanisms. We first investigate the fundamental wettability processes of liquid-infused surfaces. We then summarize the various fabrication methods of slippery surfaces regarding surface properties (ordered, disordered, polymeric), and detail the anti-icing behavior of the developed surfaces. The characteristics of lubricants as one of the most vital factors for fabrication procedures are discussed completely. We also survey the effects of surface morphology and lubricant properties on icephobicity. Moreover, since durability is one of the main challenges of SLIPS, this issue is widely addressed, and different strategies are presented to tackle this problem. This chapter proceeds with characterization methods for lubricant-loaded carriers, and finally some fabrication methods are summarized.

## **1.2 Icephobicity**

The strategies used to combat icing can be divided into anti-icing and de-icing approaches, which may be either active or passive. Removing ice that has accumulated on a surface is referred to as de-icing; an example is removing ice from a car windshield using a defroster. These methods are active de-icing approaches because an external energy input is required. Many active de-icing approaches have been developed, including mechanical breakage, cutting, thermal, or electro-impulse methods [8,84]. These methods are often expensive and also involve more energy use than passive methods. Melted ice can refreeze at a different location on the surface, thus only transferring the problem to another part of the surface. Anti-icing approaches aim to

prevent ice growth on a surface, such as applying a defroster to the substrate for an extended period and preventing water on the surface from freezing. Such strategies are active anti-icing methods [9,85,86]. Active methods cannot, however, solve all icing problems. Many techniques are inefficient over the long term and can be quite harmful to the environment. Passive methods involve fewer of these types of problems and do not require an external energy input during their service life. In passive anti-icing, the surface should be able to repel water before any freezing occurs to keep the surface free of ice. With de-icing strategies, the ice adhesion may be very low, and wind or weak external forces can easily eliminate the ice [87–89]. A lot of research works have aimed at fabricating icephobic surfaces such as superhydrophobic and lubricant infused coatings[90,91]. Although there is a lack of a standard definition for an icephobicity in the literature.

Definitions of icephobicity can be defined as having a low ice formation temperature and low ice adhesion strength between ice and a surface, or identified as a surface possessing a low ice accretion rate [90–92] . Ice adhesion strength can be measured by calculating the critical shear stress, defined as the magnitude of shear stress required to remove an amount of ice on a surface [93,94]. These definitions are, however, not comprehensive and are sometimes not applicable, such as for superhydrophobic surfaces. For these latter surfaces, icephobic characteristics that delay ice formation do not necessarily reduce ice adhesion [22,95,96]. In fact, the ice adhesion on superhydrophobic surfaces can be affected by critical parameters such as dimension of voids at the interface. Therefore, icephobicity may also be defined as the capacity of a surface to prevent ice formation by delaying heterogeneous ice nucleation within a supercooled water droplet at the interface [97].

From the aforementioned definitions, a coating should fulfill some or all of the following requirements to be considered as an icephobic coating. First, an icephobic coating reduces interactions between the surface and the water droplet, leading to a decreased accumulation of water on the surface. This condition is, to some extent, similar to the capability of a superhydrophobic surface in repelling incoming water droplets. An icephobic surface should also inhibit heterogeneous nucleation. Such a coating should be able to minimize adhesion strength at the ice–coating interface [98–101].

### **1.3 Coatings for high voltage insulators**

Various types of icephobic strategies have been proposed to prevent ice formation and ice accumulation on the insulators [102]. For instance, porcelain and glass insulators were coated with hydrophobic RTV silicone rubber materials to prevent outages of the power network, resulting from ice accretion [13]. The main component of RTV silicon rubber coatings is poly (dimethylsiloxane) (PDMS), and because of the presence of CH<sub>3</sub>– groups on the molecular chains, it provides a certain degree of hydrophobicity. However, at very cold weather conditions and low temperatures, the performance of these coatings decrease drastically and there is no guarantee to prevent insulators from icing flashover for a long time [12,103]. Semi-conductive silicone coatings were also fabricated in which thermal energy was used to remove ice from insulators [104]. In such coatings, conducting particles like ZnO and carbon fibers were responsible for heating the surface using the leakage current heat. Despite their fascinating anti-icing performance, the high-power consuming and low degradation durability of such coatings have limited their applications [104,105]. By

the advent of superhydrophobic surfaces, the idea of employing such coatings to decrease ice buildup over insulators has been developed [18]. These surfaces possess water contact angles higher than  $150^\circ$  and contact angle hysteresis (CAH) lower than  $10^\circ$ . Surfaces with low CAH and low wettability show lower ice adhesion and longer delays in freezing times [106–109]. Superhydrophobic (SHP) coatings could also be utilized as icephobic surfaces for insulators [110–114]. Lie et al. developed a SHP coating using a sol-gel method, and investigated its anti-icing properties on glass and porcelain insulators. Since the contact time between a cold SHP surface and water droplet was considerably low, such surface showed the potential for applying as an icephobic coating on insulators [16]. In another work, a hybrid coating was developed via self-assembly of a super-hydrophobic layer on a semi-conducting layer. In fact, the coating consisted of a PDMS-modified nano-silica/ Carbon hybrid and its anti-icing properties were compared with RTV coatings. The results showed that the minimum flashover voltage of ice-covered insulators for the proposed coating was greater than that of RTV silicone rubber coatings [115]. It is worth mentioning that under harsh environmental conditions such as high humidity, the superhydrophobic surfaces lose their icephobic characteristics owing to water condensation in the structure porosity and lack of air voids in the texture [71]. By providing the condition that prevents the water condensation in a porous structure, this obstacle can be removed. The idea of slippery liquid-infused surfaces has been providing an insight to develop a new generation of the icephobic surfaces applicable on insulators.



#### 1.4 From superhydrophobicity to slipperiness: theoretical aspect of wetting

The wettability of solid surfaces has attracted increasing interest from both a fundamental and practical perspective through the tailoring of specific surface topographies and surface chemical compositions. Wettability is usually determined by measuring the contact angle (CA) of a liquid droplet on the solid surface. The fabrication of superhydrophobic surfaces requires combining hierarchical surface roughness with a low surface free-energy material. Aside from an apparent water CA  $>150^\circ$ , the superhydrophobic surface also must show a low sliding angle (SA) of  $<10^\circ$  [116].

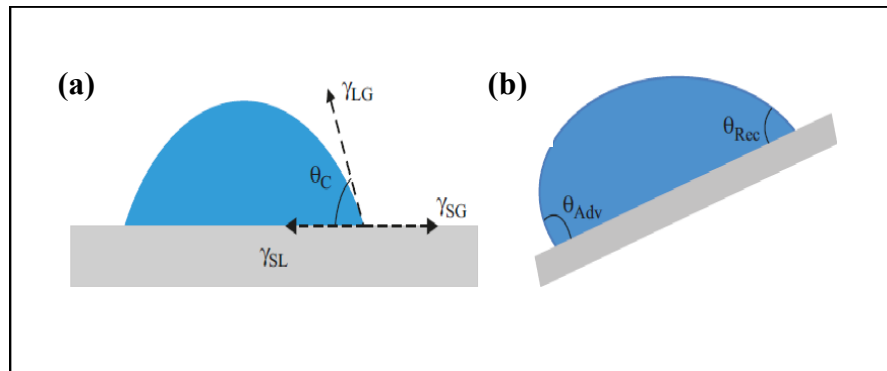
Both the interfacial wettability and interfacial force play essential roles in the development of superhydrophobic surfaces [117,118]. In surface sciences, interfacial wettability phenomena are critical factors. Several models exist to interpret these phenomena and describe the wetting process. In 1805, Thomas Young proposed an initial model that has been very useful for investigating the state of a liquid on an ideal flat surface. It is described by the Young equation (Eq. 1-1):

$$\gamma_{SG} = \gamma_{SL} + \gamma_{LG} \cdot \cos\theta \quad (\text{Eq. 1-1})$$

where, as depicted in Figure 1-1a,  $\theta$  is the contact angle, and  $\gamma_{SG}$ ,  $\gamma_{SL}$ , and  $\gamma_{LG}$  are the interfacial surface tensions of solid–gas, solid–liquid, and liquid–gas, respectively.

The structure and chemical heterogeneity of a surface under actual conditions can affect the contact angle [119]. Contact angle hysteresis can be defined as the difference between the advancing contact angle ( $\theta_a$ ) and the receding contact angle ( $\theta_r$ ) (Figure 1-1b) and represents the ability of a droplet to move or roll on a surface.

It is worth mentioning that this concept is only applied to surfaces that are chemically homogeneous and atomically smooth.

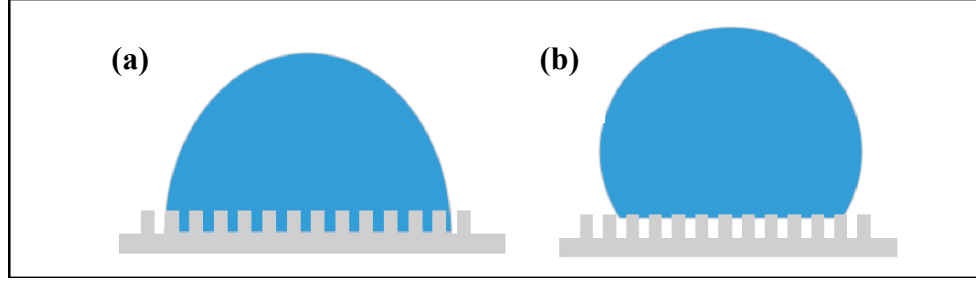


**Figure 1-1.** Schematic showing (a) Young's model, and (b) contact angle hysteresis [118].

In reality, most surfaces are not perfectly smooth; therefore, to include this roughness, the simple model requires modification [120]. In 1936, Wenzel proposed a model in which the contact angle on a rough surface was presented by modifying Young's equation, as Eq. 1-2:

$$\cos\theta_W = r \cdot \cos\theta_Y (r \geq 1) \quad (\text{Eq. 1-2})$$

where  $\theta_W$  and  $\theta_Y$  are respectively the apparent contact angle and Young's contact angle for ideal flat surface, and  $r$  is the surface roughness factor, defined as the ratio of the true area of the solid surface to the apparent area. From Figure 1-2a, the true area is clearly larger than the apparent surface area; therefore, the value of  $r$  is  $>1$ . Thus, if  $\theta_Y < 90^\circ$ , a larger value of  $r$  would produce a more hydrophilic surface; when  $\theta_Y > 90^\circ$ , a larger value of  $r$  would lead to a more hydrophobic surface. Note, however, that the Wenzel model applies only to a thermodynamically stable state and a single chemical component surface; these issues limit its application [121].



**Figure 1-2.** Schematic showing (a) a Cassie state, and (b) a Wenzel.

Cassie and Baxter introduced Eq. 1-3, which was appropriate for heterogeneous interfacial areas:

$$\cos \theta = f_1 \cos \theta_1 + f_2 \cos \theta_2 \quad (f_1 + f_2 = 1) \quad (\text{Eq. 1-3})$$

where  $\theta$  is the apparent contact angle,  $\theta_1$  and  $\theta_2$  are the intrinsic contact angles of component 1 and component 2, respectively, and  $f_1$  and  $f_2$  are the apparent area fractions of the mentioned components. If the equilibrium state consists of the liquid sitting on top of asperities and air pockets (Figure 1-2b), the Cassie-Baxter model for this composite interface is described by Eq. 1-4:

$$\cos \theta_{CB} = f_{SL} \cos \theta_c - f_{LV} \quad (\text{Eq. 1-4})$$

In Equation 1-4,  $\theta_{CB}$  is the Cassie-Baxter CA, and  $f_{SL}$  and  $f_{LV}$  are fractions of solid–liquid and liquid–air interfaces, respectively. Eq. 1-4 is, however, only valid for specific geometries, and the surface roughness has not been considered. Using the Wenzel equation, Eq. 1-4 can be modified to include microstructures or hierarchically rough surfaces as Eq. 1-5:

$$\cos \theta_{CB}^W = r f_{SL} \cos \theta_c - f_{LV} \quad (\text{Eq. 1-5})$$

Again, this model assumes that air is trapped between the liquid and solid phases and that the liquid is in contact with the solid only at the top of the surface structure; the full solid surface is therefore not wetted by the liquid [122].

Superhydrophobic surfaces have some drawbacks that can affect their icephobic properties and reduce their efficiency. These drawbacks relate to the loss of the air voids in the porous structure of the surface between the ice and the substrate. This scenario is caused by the condensation of water within the porous structure of the superhydrophobic surface. This condensed water anchors the ice to the surface after freezing, thereby increasing the ice adhesion strength. Besides this failure in reducing ice adhesion, the design of superhydrophobic surfaces is not readily scalable, and these surfaces have issues with high-pressure impingement and high-temperature applications [109,123]. The peristome of the *Nepenthes* pitcher plant is composed of crescent-shaped microstructures in which a thin layer of water becomes trapped (Figure 1-3).



**Figure 1-3.** The image of a pitcher plant *Nepenthes* (left), and its scanning electron microscope (SEM) micrographs (right) [124].

This trapped water produces a slippery interface. It is this interface that contacts the legs of insects that venture into the plant and causes the insects to slide on the slippery peristome and fall into the plant's digestive organ [125]. Liquid-infused surfaces (LIS) have been developed that imitate the morphology of the *Nepenthes* peristome [124,126]. These LIS was discussed in the following sections.

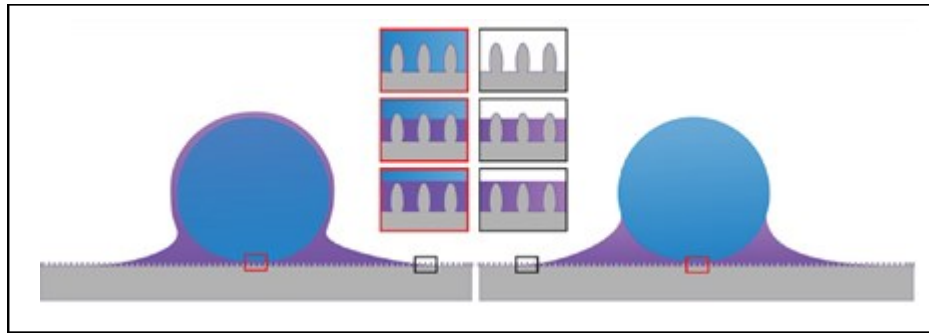
LIS surfaces exhibit extreme liquid repellency, characterized by a low contact angle hysteresis of  $<2.5^\circ$  and a low sliding angle of  $<5^\circ$ . They are also incredibly slippery and pressure stable. Air-trapped structures, such as those on superhydrophobic surfaces, the manner of surface wetting, and the transition from a Cassie to a Wenzel state are all influenced by the Laplace pressure, which depends on surface geometry. In the case of oil-infused surfaces, the design of the substrate texture is vital for holding lubricant as Laplace pressure increases and, therefore, boosting the pressure resistance of the surface. SLIPS can retain their water repellency properties at a pressure of 676 atm, and they demonstrate significant pressure stability [127,128].

Such properties, therefore, make these surfaces able to handle liquids having a low surface tension. Three main design criteria must be considered to properly create a liquid-infused surface: (i) the lubricant and the repellent liquid must be immiscible; (ii) the lubricating fluid must have more affinity for solids rather than for the test liquid and be spread out completely over the solid substrate; and (iii) the solid surface preferably has a surface roughness and a higher affinity for the lubricating liquid over the probing liquid to increase the surface area for the adhesion and the retention of the lubricating fluid [128,129].

As four different phases that must be considered—solid, repellent liquid, lubricating liquid, and air phases—the analysis of the wetting process of these systems

is very complicated. Accordingly, Smith et al. introduced the fundamental wetting configuration principles for the above criteria and determined 12 thermodynamic conditions that describe these four-phase systems [130].

For instance, if the four-phase system, presented in Figure 1-4, includes water, lubricant, air, and solid substrate, the behavior of water could vary on the lubricated surface [131].



**Figure 1-4.** Schematic showing of different wettable configurations for a four-phase system (air, liquid-1, liquid-2, solid) [37].

The spreading factor ( $S_{ow}(a)$ ) can be defined to interpret the situation of the water droplet and the oil in relation to each other. Here, “o,” “w,” and “a” represent oil, water, and air, respectively. If  $S_{ow}(a) > 0$ , the water droplet will be completely encapsulated by the oil (Figure 1-4, left); if  $S_{ow}(a) < 0$ , the droplet will lie on top (Figure 1-4, right). This issue is key because once water droplets are shed from the surface, cloaking results in the progressive loss of impregnated oil through entrainment in the water droplets. The oil–water spreading parameter ( $S_{ow}$ ) is defined as Eq. 1-6 [131]:

$$S_{OW}(a) = \gamma_{wa} - \gamma_{ow} - \gamma_{oa} \quad (\text{Eq. 1-6})$$

In this equation,  $\gamma_{aw}$ ,  $\gamma_{ow}$ , and  $\gamma_{oa}$  are the water–air surface tension, the oil–water surface tension, and the oil–air surface tension, respectively.

Eq. 1-7 and Eq. 1-8 can also determine the spreading factor of oil on a solid substrate when they are in contact with air or water, respectively:

$$S_{os}(a) = \gamma_{sa} - \gamma_{os} - \gamma_{oa} \quad (\text{Eq. 1-7})$$

$$S_{os}(w) = \gamma_{sw} - \gamma_{os} - \gamma_{ow} \quad (\text{Eq. 1-8})$$

Therefore, depending on the type of four-phase system, the oil could undergo different phenomena; the surface might be either completely or slightly wetted by the oil. The substrate roughness is another effective factor in oil penetration that can affect the contact line (the line at which different phases face each other), following Eq. 1-9 [130]:

$$\cos\theta = \frac{\phi-r}{r-1} \quad (\text{Eq. 1-9})$$

In this equation,  $r$  is the surface factor, and  $\phi$  is the fraction of the projected area occupied by the liquid, which is comparable with the fraction factor in Cassie's equation. According to the conditions that must be fulfilled to have a liquid-infused surface, a solid can obtain a higher affinity for oil than water if  $\frac{-\gamma_{ow}(r-1)}{r-\phi} < S_{os} < 0$ . Furthermore, to encapsulate the surface by the lubricant, the condition of  $S_{os}(a) \geq 0$  should be established [130,131]. The other conditions are presented in APPENDIX I (Table A.I.1), and three possible configurations can be assumed for the oil–solid–air interface outside of the droplet. According to APPENDIX I (see Table A.I.1), however, this interface underneath the droplet in the same environment has three other possible configurations. The stable configuration should clearly possess the lowest total interface energy. The following possibilities are expected: (a) the lack of the lubricant between the substrate and the droplet causes the droplet to be pinned on the substrate,

resulting in a Wenzel state; (b) the partial presence of the oil leads to droplet slides; however, it will be influenced by frictional forces [132].

Schellenberger et al. demonstrated that each type of lubricant generates a special wetting ridge against the probing water [131]. These combinations were tested under dynamic conditions, including advancing and receding contact angles on a liquid-infused surface. The contact between the droplet and solid affected this contact angle; the multiple possible liquid–liquid surface tension interactions therefore heighten the importance of selecting the appropriate roughness and liquids. The next section focuses on the fabrication of SLIPS, and various approaches and strategies to investigate their anti-icing behavior are presented.

## **1.5 Fabrication and icephobic properties of SLIPS**

### **1.5.1 Lubricated micro/nanotextured surfaces**

The first group of SLIPS is a micro/nanotextured surface structure that holds large spaces for absorbing and storing a lubricant. Aizenberg et al. were among the first to report micro/nanostructured epoxy resin–based surfaces with a perfluorinated lubricant infused into a textured surface [128]. Their produced surface showed extraordinary ice-repellency and pressure stability. These coatings also possessed a low contact angle hysteresis, low sliding angles, and self-healing properties. Since this early work, other SLIPS comprising different liquids and substrates have received much attention and study [33,133,134].

Using a superhydrophobic surface is the most common method for fabricating slippery coatings in which a textured structure holds an infusing oil. Two types of

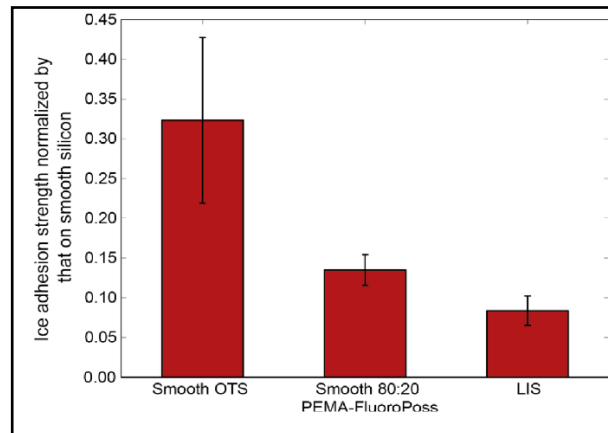


structures can favor superhydrophobicity: ordered and disordered structures [135,136]. In ordered structures, the surfaces are designed entirely prior to their fabrication and have various textures such as micro-posts. Ordered surfaces are then fabricated using lithography, laser, CNC, etc. [137–139]. For disordered structures, the surface has a random porous pattern. These surfaces are obtained through methods such as etching, plasma, and spin coating [52,140–142]. Relying on this classification, the typical means of preparing textured surfaces for generating anti-icing properties were summarized here.

#### *1.5.1.1 Ordered textured surfaces*

Lithography techniques are top-down methods that are used extensively for producing patterned and ordered structure surfaces having a specific shape and structure [143]. To generate a porous slippery layer, Varanasi et al. used standard photolithography to fabricate silicon micro-posts. The authors then coated the samples with OTS (octadecyltrichlorosilane) to improve surface hydrophobicity. The silane-coated samples were lubricated using a dip coater to ensure an effective impregnation of the OTS. The dip coater was then withdrawn at a controlled velocity from the bath of lubricant to prevent an excess oil film. Varanasi et al. compared the ice adhesion strength of high-texture-density LIS with other low-surface-energy coatings. The slippery surface with the highest texture density had a considerably lower ice adhesion strength than a PEMA-Fluoro POSS-coated smooth surface, a material having one of the lowest known surface energy values, and a smooth surface coated with OTS (Figure 1-5). The ice adhesion strength of LIS in a thermodynamically stable state was also greater than that for the excess lubricant layer. Ice adhesion strength on a slippery

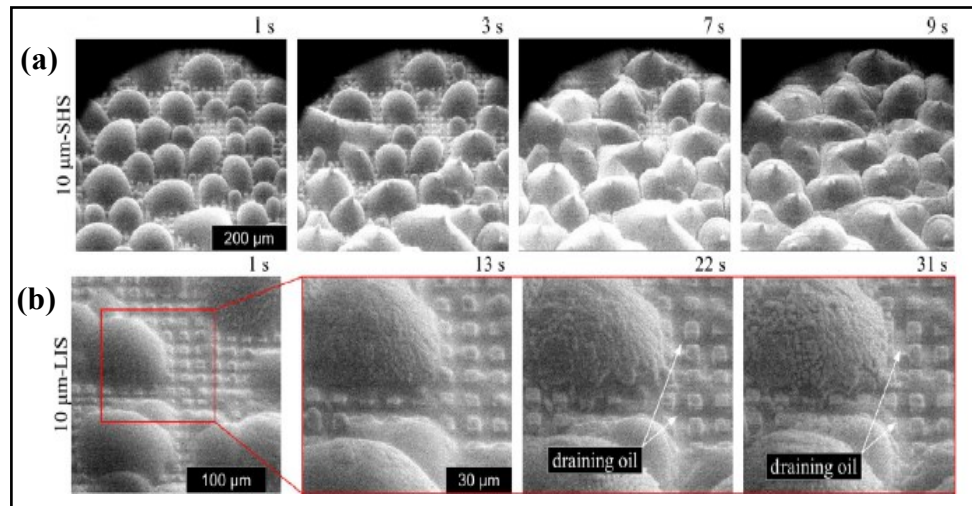
surface with a stable lubricant layer thus depends on texture, and this ice adhesion decreases with increased texture density [48].



**Figure 1-5.** Comparison of the ice adhesion strengths of various low-surface-energy [48].

Varanasi et al. also investigated condensation frosting on superhydrophobic surfaces (SHS) and liquid-infused surfaces [95]. They fabricated a nanostructured superhydrophobic surface by vapor-phase-deposited alumina nanoparticles and silicon nanowires. Silicon micro-posts were also used to produce the microstructured SHS. Perfluorinated oil lubricated the surface, and the authors used a dip-coating procedure to avoid excess oil on the surface. Frost forms on a surface through two means. One is through the freezing of a subcooled liquid; the other is via desublimation. Varanasi et al. focused on condensation frosting. As illustrated in Figure 1-6a and Figure 1-6b, a 10- $\mu\text{m}$  SHS (where 10  $\mu\text{m}$  corresponds to the interpost spacing) did not maintain surface superhydrophobicity during condensation. As a result, droplets froze within 1–2 s because of the large solid–liquid contact area of the surface. However, the effective thermal resistance of the interface increased with the volume fraction of oil, which

explained the slightly increased time for the complete frosting of the microstructured LIS because of a decreased micropost density [95].



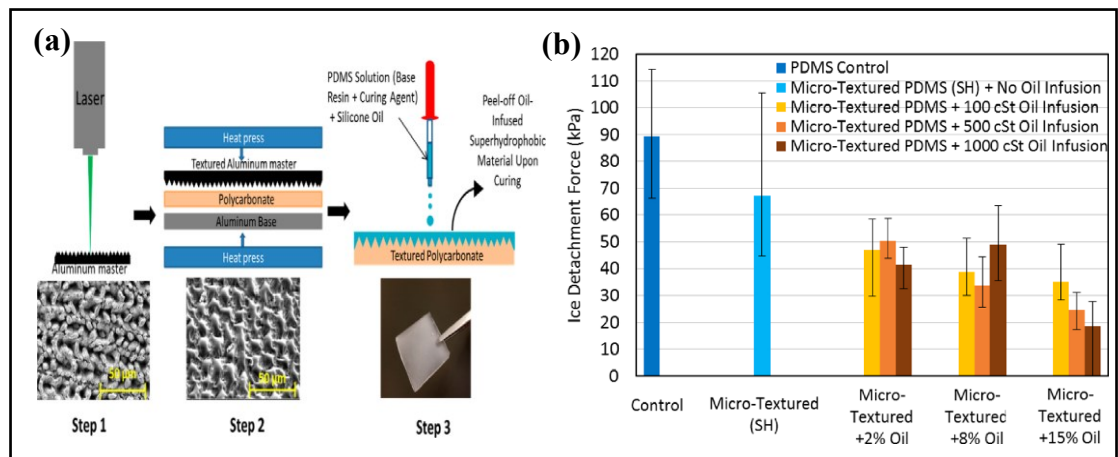
**Figure 1-6.** Sequence of ESEM images of frost formation via droplet condensation and freezing on (a) 10- $\mu\text{m}$  SHS and (b) 10- $\mu\text{m}$  LIS [95].

Replication methods are a commonly used technique for obtaining nano-microstructures on polymeric surfaces [144]. Gupta et al. used a replication method for fabricating slippery oil-infused elastomeric surfaces and maintaining the superhydrophobicity of the surface. Laser irradiation created macro textures on an Al surface. Polycarbonate was used as an intermediate, and the texture was then transferred to the silicon material (Figure 1-7a). The study obtained a surface having a combination of superhydrophobicity, elasticity, and slippage by oil infusion [145].

Studies have also evaluated the effect of oil infusion on surface morphology and ice adhesion [145]. Microtextured polydimethylsiloxane (PDMS) materials exhibited a significant reduction in ice adhesion strength compared to the smooth and

microtextured material without oil infusion, regardless of oil viscosity and percentage. Infusing only 2% of silicon oil (100 cSt) reduced ice adhesion by almost 50% (89 kPa to 46 kPa) relative to no-oil samples (Figure 1-7b).

It is therefore possible to reduce ice adhesion markedly by combining superhydrophobicity—to maximize the water repellency of the surface—and silicon oil to improve slippage on the surface. Increasing the flexibility of elastomeric materials with the presence of oil can also accelerate ice release and the icephobic capability of the surface [145].



**Figure 1-7.** (a) Schematic illustrating the fabrication procedure of the oil-infused, microtextured polydimethylsiloxane (PDMS) material [145]. (b) The ice adhesion strengths of oil-infused, microtextured PDMS having different oil viscosities and infusion levels (2–15 wt %) [145].

### 1.5.1.2 Disordered textured surfaces

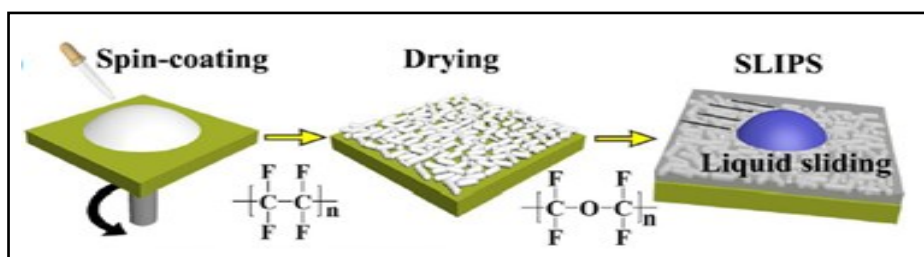
Wang et al. designed SLIPS coatings by spraying a modified SiO<sub>2</sub> suspension onto substrates to form superhydrophobic/oleophilic surfaces [134]. The infusing lubricant was perfluorinated, and it was completely infused within the rough surface.

This surface repelled hexane, kerosene, diesel oil, water, and milk, thereby exhibiting an exceptional oleophobicity compared with superhydrophobic surfaces.

The evaluation of anti-icing performance on surfaces confirmed that the formation of a meniscus force between a water droplet and a cold superhydrophobic surface causes the adhesion strength to increase greatly and deactivates the anti-icing capacity of the surface. However, by replacing the air pockets under a water droplet with oil, in  $-20\text{ }^{\circ}\text{C}$  conditions, a capillary bridge cannot form on the slippery surface. Thus, the slippery surface produced anti-icing properties that were superior to those of a superhydrophobic surface [134]. Under cold conditions having a high condensation rate, the formation of a water-capillary force increases ice adhesion and the loss of water repellency for superhydrophobic surfaces.

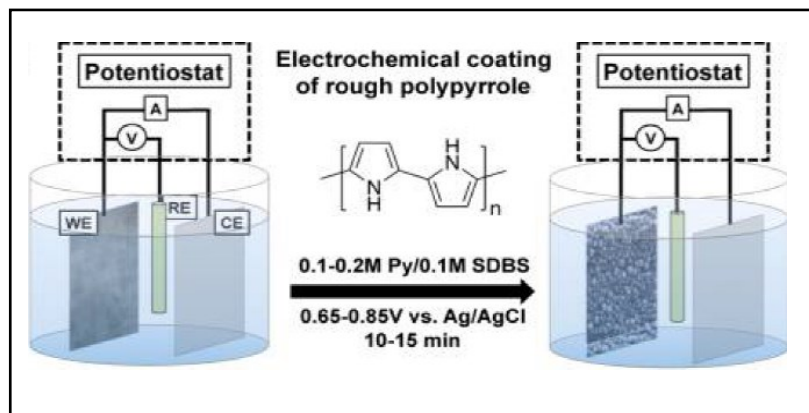
Another study [32] used a spin-casting method to fabricate slippery surfaces on various substrates, including a Si-wafer, glass, and a Cu plate (Figure 1-8). The authors packed an aqueous suspension of polytetrafluoroethylene (PTFE) with nanoparticles of an appropriate size and shape to form a transparent nano-porous monolayer and lock in the perfluoropolyether (PFPE) lubricants. After adding the lubricant, the lubricant quickly infused into the nanolayer via the capillary effect. Evaluation of anti-icing behavior of slippery surfaces confirmed that ice crystals appeared on the oil-infused coating (glass@PTFE@PFPE) with a longer ice formation time (13 min) compared with the original glass (5 min) and the glass@PTFE (7 min). The presence of the nanoparticle layer created a heat-transfer barrier, which delayed ice formation. However, the lubricated surface also facilitated the mobility of water droplets and therefore minimized the number of ice nucleation sites [32]. During the deicing process, the ice quickly slid off the surface (within 20 s), whereas the ice stuck firmly

to the surfaces of glass and glass@PTFE. Thus, these SLIPSs showed obvious anti-freezing properties and reduced ice adhesion.



**Figure 1-8.** Schematic illustration of the fabrication of the SLIP [32].

Kim et al. [33] used the electrodeposition of textured polypyrrole (PPy) to create porous superhydrophobic surfaces (Figure 1-9). To build SLIPS, the authors fluorinated and infiltrated the PPy-coated aluminum samples with a low-viscosity perfluorinated lubricating liquid [33]. An advantage of electrodeposition is that by changing the parameters, such as deposition time, the applied potential, and the concentration of monomers, the nanometric morphology of the surface can be controlled. An evaluation of SLIPS-Al as an icephobic surface revealed an ice adhesion of 15.6 kPa, illustrating a considerable reduction in ice adhesion compared with bare Al (1359 kPa) and other types of icephobic materials [146]. On a slippery surface, solid–liquid interfaces provide the smooth surface with minimum heterogeneity and few pinning points, whereas a superhydrophobic surface having a solid–solid interface has issues with pinning and high ice adhesion. Thus, SLIPS strongly limit ice nucleation and also reduce sliding droplet size and ice adhesion to provide an effective icephobic surface [33].

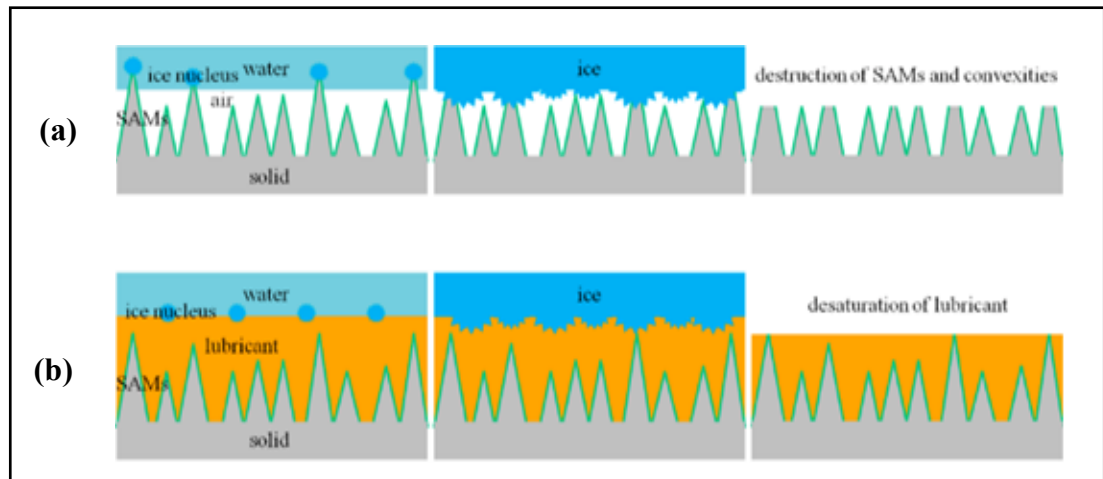


**Figure 1-9.** Schematic of the electrochemical coating process of a rough polypyrrole [33].

Zhang et al. fabricated a double-layered structure on an AZ31 Mg alloy with anti-icing and anticorrosion properties [147]. On such a surface, the top layer was a porous slippery surface for anti-icing purposes, and the underlying layer was a compact surface, created via a hydrothermal procedure, to provide anti corrosion protection. The hierarchical porous structures lock in perfluoropolyether, used as an infusing lubricant, through capillary action. With this method, Zhang et al. obtained SHS and SLIPS hydrothermally, and they created surface textures through the conventional surface modification method. A comparison of the anti-icing performances of the SHS and SLIPS coatings highlighted that the roles of the hierarchical micro-nanostructures in relation to ice formation differed between the surfaces. This difference occurred because of the smaller size of the condensed droplets than the micro-nanostructure pores; thus, the mechanism of the Cassie-Baxter wetting mode no longer held in this case.

The SHS delayed the process of ice nucleation, although after sufficient time, the SHS lost its anti-icing capacity, and a frost layer formed. The lubricant-infused

surface, on the other hand, resisted the onset of ice nucleation for a longer time. The lubricated surface allows fewer ice nucleation sites and prevents moisture condensation (Figure 1-10a and Figure 1-10b). As well, the partly formed ice can be removed easily by a simple tilting of the sample. Therefore, the slippery surface can reduce heterogeneous ice nucleation and delay ice formation [147].



**Figure 1-10.** Schematic model of the icephobic mechanisms of (a) SHS and (b) SLIPS coatings, depicting the decay of the water CA [147].

### 1.5.1.3 Effect of surface morphology on the icephobic behavior of SLIPS

Slippery liquid-infused porous surfaces show much potential for use as an icephobic coating. However, losing lubricant over time could be a problematic issue that limits their application. In particular, the lubricant within textured porous substrates could be affected by external environmental conditions, such as repeated icing/de-icing cycles, high-shear water flow, and evaporation. Therefore, the relationship between the morphology of the surface and ice adhesion must be determined to enhance the durability of these coatings and study their anti-icing

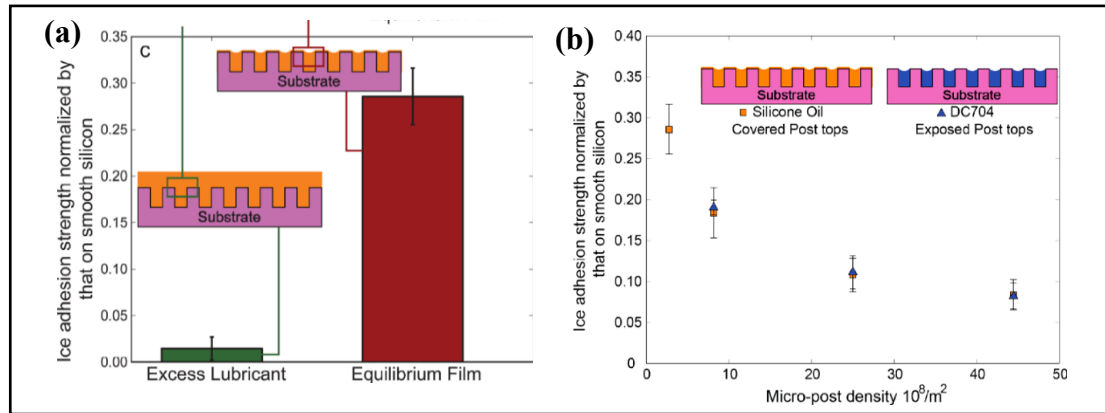


behavior. Varanasi et al. have investigated this relationship using lithography methods to create structured textures with different lubricants [48,95,130,148]. They have investigated various parameters, including the topography of the surface texture, the surface tension of the solid–liquid interface, and the effect of liquid infusion levels, and we will detail these studies in the following paragraphs.

The draining of excess lubricant by external forces such as gravity relates to the tendency of the system to be in a thermodynamically stable state [48]. Although surfaces with excess lubricant film show a considerably lower ice adhesion, the complete covering of the textures causes the surface to lose its anti-icing capacity over time as the lubricant is depleted (Figure 1-11a).

The ice adhesion strength of SLIPS in a thermodynamically stable state is affected by texture, and increased texture density reduces ice adhesion strength. Infusing a small amount of ice between the surface posts initiates cracks, which occur because of the stress produced from the corner of posts on providing points. As seen in Figure 1-11b, increasing the texture density therefore reduces the possibility of diffusing ice within textures.

After a few defrosting cycles, the slippery surfaces lost their anti-icing characteristics. The capillary force generated from the nucleation of nano-icicles caused the lubricating liquid to migrate from the ridge and porous substrate into the frozen droplet (Figure 1-12). The nucleation of nano-icicles in textured surfaces also caused the simultaneous competition between infusion of oil and frost within the substrate topography via capillary attraction [95,148].

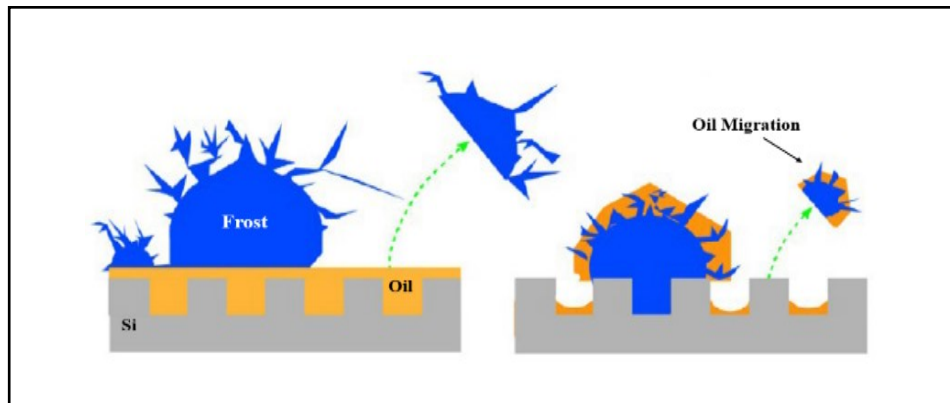


**Figure 1-11.** (a) Comparison of ice adhesion strengths of lubricant-impregnated surfaces with different amounts of lubricant [48]. (b) Influence of texture density on the ice adhesion strength of different LIS [48].

Therefore, this explanation requires the scale (micro vs. nano) of the substrate texture during frost growth to play an important role in holding on to the lubricant. Examination of the surface morphology confirmed that oil draining from a microtextured slippery surface was more likely with a single defrosting step than from a nanostructure liquid-infused system subjected to a greater number of frosting–defrosting cycles.

Aizenberg et al. proposed a closed-cell system to improve the properties of substrate morphology for generating a durable slippery surface. Their proposed surface was a transparent and nanostructured slippery composite having an inverse colloidal monolayer. The lubricant was trapped within the textures and could remain trapped for more than nine months. The ice adhesion strength of the surface was around 10 kPa. Such a structure can also provide suitable mechanical properties because of the presence of a firm layer. Closed-cell SLIPS can tolerate a range of mechanical tests,

including wiping, touching, and tape peeling. Open-cell types are damaged under these tests [73,149].



**Figure 1-12.** Schematic illustrating lubricant depletion after frosting–defrosting cycles [95].

Besides the methods detailed above, other approaches exist for creating the rough textures required for fabricating slippery surfaces. Regardless of the approach, the desired icephobic characteristics for slippery coatings with textured surfaces are strongly affected by the properties of the rough substrate. The design of ordered structures on surfaces can be adjusted to obtain the optimal surface characteristics. Although this facilitates achieving the desired anti-icing properties compared with using non-ordered methods, the latter approach of creating non-ordered surfaces is easier and more practical. Scalability is also an essential aspect when fabricating porous substrates. Many porous coatings cannot be used at a large scale because of the procedures used to create their small-scale surface architecture. Therefore, other types of easily fabricated and easily applied SLIPS are needed, such as oil-infused polymeric surfaces. In such methods, lubricants and plasticizers are incorporated into crosslinked polymers to produce slippery surfaces.

### 1.5.2 Oil-infused polymeric systems

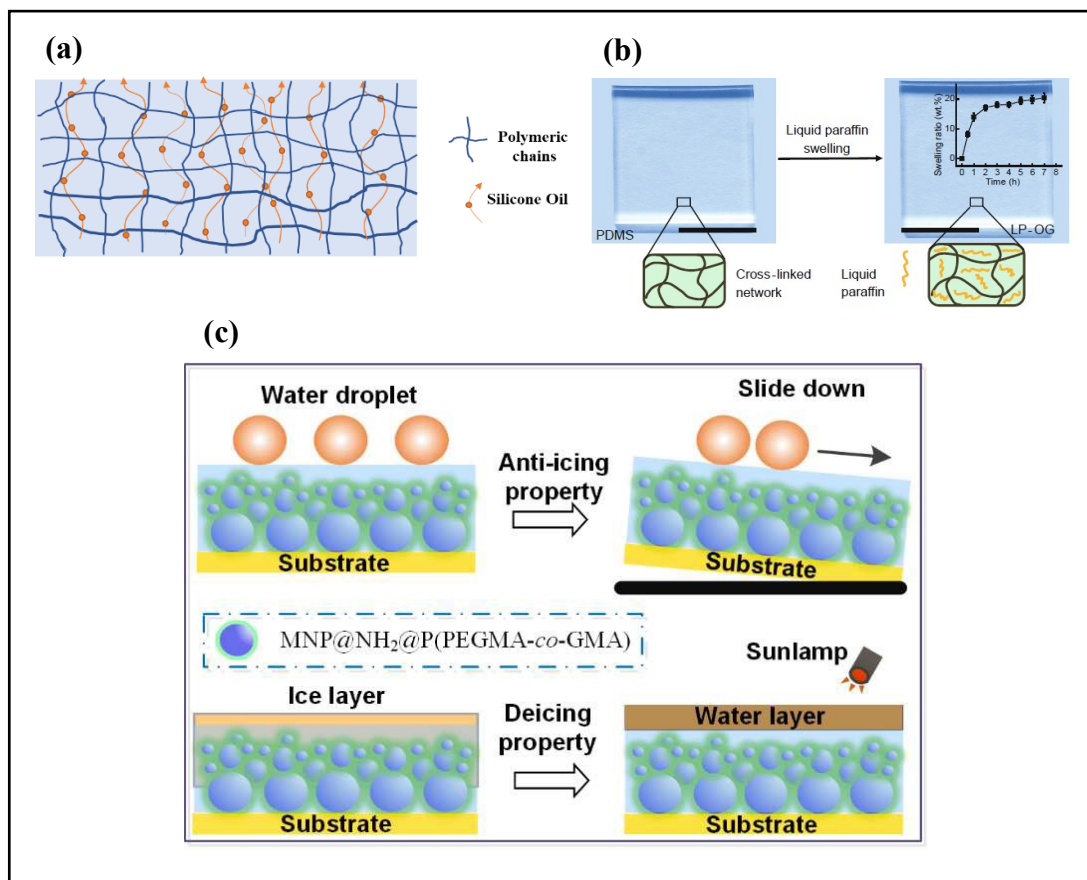
Lubricant-infused polymeric systems rely on crosslinked polymers having a very low ice adhesion strength. Infusing oil into polymers decreases ice adhesion considerably and provides an appropriate matrix for blocking and encapsulating the lubricant over an extended period. This polymer can also maintain low ice adhesion after lubricant loss owing to its low surface energy and smooth surface [43,150–153].

Although most slippery-coating lubricants infuse into preformed structures, as with porous material or sponges [74,154–156], the lubricant can also be infused into a polymer matrix as a precursor solution of the final surface. Wang et al. applied this method to fabricate silicon oil-reinfused PDMS coatings. Using PDMS with a low glass transition temperature provided a large free volume in which the infused lubricant could be retained. In fact, the presence of 20–40 wt% silicone oil significantly reduced ice adhesion compared with pure PDMS coated on aluminum surface [157]. This coating also maintained its performance after multiple icing/de-icing tests, highlighting its durability. This high durability occurs because of the large free volume of the polymer, which provides a medium for mobile infusing oil to migrate over the surface when de-icing causes a loss of lubricant (Figure 1-13a).

Similar effects occur through infusing liquid paraffin within a polydimethylsiloxane polymeric matrix [158]. The infusion causes the swelling of the cured polymer network with compatible oils (Figure 1-13b). This approach produced exceptional results for ice adhesion strength (only 1.7 kPa at  $-30\text{ }^{\circ}\text{C}$ ), and ice adhesion strength remained  $<10\text{ kPa}$  down to a temperature of  $-70\text{ }^{\circ}\text{C}$ . In this type of anti-icing coating, the crosslinked network of polymers is critical, as its capacity to hold a liquid

inside the structure prevented the loss of this fluid during the ice shedding. The coating showed, therefore, marked durability, as ice adhesion remained at approximately 10 kPa over 100 days and over 35 icing/de-icing cycles [158].

Chen et al. synthesized highly hydrophilic acrylic-based copolymers as a compatible backbone for a polyol lubricant, such as ethylene glycol, by relying on their shared polarity [159]. To improve the capillary action and storage ability of lubricating liquids, they fabricated a micro-nanostructure with amino-functionalized magnetic nano  $\text{Fe}_3\text{O}_4$  in the coating. The slippery coating containing the copolymer and modified nanoparticles was sprayed and then lubricated by immersion in various polyols, including ethylene glycol and triethylene glycol. In this study, the properties of both the crosslinked polymeric media and the porous surface prevented the leakage and evaporation of infused liquid over an extended period. Observations of the anti-icing properties also confirmed that such coatings could delay frost formation for about 45 min. This long duration likely resulted from the ultralow crystallization point of  $-36.8$  °C that could retard the water droplet nucleation process for a longer period. Ice adhesion also had an extremely low value of 0.1 kPa. As depicted in Figure 1-13c, the magnetic  $\text{Fe}_3\text{O}_4$  nanoparticles could be thermally stimulated by exposing them to light energy; this property contributed to an active de-icing of the surface. Indeed, these polyol-infused slippery surfaces exhibited outstanding characteristics that might serve as anti-icing and de-icing coatings [159].



**Figure 1-13.** (a) Schematic showing the migration of infused oil toward the surface. (b) Preparation and surface release of liquid paraffin-organ gel (LP-OG) [158]. (c) Preparation and surface release of liquid paraffin-organ gel (LP-OG) [158].

### 1.5.3 Self-lubricating slippery surfaces

Another form of slippery surfaces involves self-lubricating material relying on aqueous lubrication rather than the use of an oily fluid [160–165]. The intrinsic slippery properties of the pitcher plant relate to the condensed water on the rim surface or rainwater on the hygroscopic nectar at the peristome surface [124]. Therefore, water can be an alternative to oily lubricants. In ice skating, the ice itself contributes to the required slippage for facile skating on the ice. After breaking the hexagonal structure

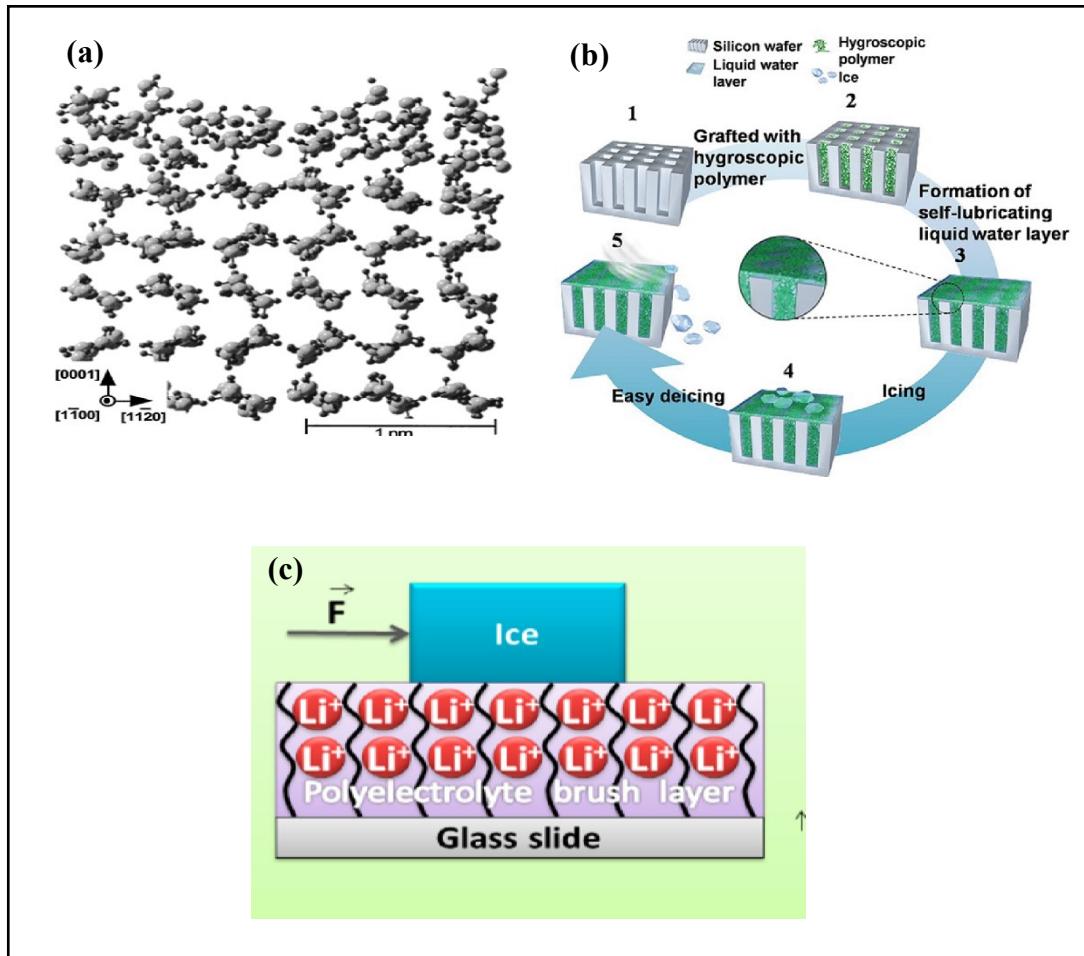
of ice on the surface, a quasi liquid-like layer is created even at sub-zero temperatures, as illustrated in Figure 1-14a [166–168]. The transformation of ice into liquid water occurs through the combined effects of frictional heating and pressure melting. These processes contribute to the creation of a thin layer of aqueous solution, which acts as a lubricant between the blade and the ice surface. Owing to the lubricating water layer over the ice surface, ice adhesion between the skate blades and the surface significantly decreases, thereby making skating possible. Inspired by ice skating, researchers have developed the concept of covering a surface with hygroscopic polymers as a self-lubricating liquid water layer. By grafting hygroscopic materials onto a surface, it is possible to generate a non-frozen, liquid-like layer of water. This process results in the production of surfaces that exhibit hydrophilic characteristics. Hydrophilic polymer layers—cationic, anionic, and nonionic—absorb water, swell, and create a liquid water layer on a surface [149]. So, the interfacial layer of hydrophilic polymers exhibited a significantly higher viscosity compared to hydrophobic polymers.

Jiang et al., inspired by this phenomenon, fabricated a self-lubricating surface by grafting crosslinked hygroscopic polymers inside the micropores of a porous silicon wafer [160]. The ice adhesion strength was about one order of magnitude less than that of superhydrophilic or superhydrophobic surfaces. In this method, a hygroscopic polymer is ionized in water and, as ions exist within the solution, the activity of the water is reduced, lowering the melting and freezing points. Therefore, the hydrophilic side groups can melt ice and snow when they are in contact with snow and ice. Then, the aqueous lubricating layer is created on the surface because the absorption of water by the hygroscopic polymers causes the swelling of the microstructures (Figure 1-14b) [160].

This type of aqueous lubricant is highly durable as long as there is ice on top of the surface. Using this type of surface could also be challenging because below the phase transition temperature, ice adhesion values increase considerably because of the freezing of the aqueous layer. The elimination of such a problem requires the careful consideration of, for example, the type of polymer and the concentration of the polymer network [163].

Hygroscopic surfaces prepared by polymeric structures, and ionic species can also show anti-icing characteristics. As shown in Figure 1-14c, this type of self-lubricating surface contains polyelectrolyte brushes that inhibit ice attachment on the surface through an ion-exchange mechanism with the first layers of the brush, which prevents ice formation. Chernyy et al. investigated the ice adhesion of three polyelectrolyte brushes, including poly [2-(methacryloyloxy) ethyl]-trimethylammonium chloride], poly (3-sulfopropyl methacrylate), and poly (sodium methacrylate). They evaluated the exchange of the counter ions of the polyelectrolytes with 13 different ions ( $H^+$ ,  $Li^+$ ,  $Na^+$ ,  $K^+$ ,  $Ag^+$ ,  $Ca^{2+}$ ,  $La^{3+}$ ,  $C_{16}N^+$ ,  $F^-$ ,  $Cl^-$ ,  $BF_4^-$ ,  $SO_4^{2-}$ , and  $C_{12}SO_3$ ) [169]. The ice adhesion for brushes incorporating  $Li^+$  ions on the glass surface decreased by 40%–70% at  $-18\text{ }^\circ\text{C}$ . All polyelectrolyte brushes showed a 20%–80% reduction in ice adhesion at  $-10\text{ }^\circ\text{C}$ , depending on their ion type. The anti-icing characteristics of the hydrophobic brushes and surfactant, with the exchanged polyelectrolytes, also produced better results than the superhydrophilic brushes. The chemical properties of the polymer brushes may change the capacity of water to crystallize at the water brush interface by influencing the interfacial water layer structure [169].





**Figure 1-14.** (a) The aqueous layer on ice as observed by molecular-dynamic calculations. The gray and black spheres represent oxygen and hydrogen atoms, respectively [166]. (b) Schematic of the formation of a self-lubricating liquid water layer and its de-icing functionality [160]. (c) Schematic showing the polyelectrolyte brushes for inhibiting ice accumulation on a surface. [169].

Chen et al. incorporated a polydimethylsiloxane (PDMS)-poly (ethylene glycol) (PEG) copolymer within a PDMS polymeric matrix to fabricate self-lubricating icephobic coatings. The resulting ice adhesion value of 50 kPa is lower than other hydrophobic solid surfaces used for comparison. Their proposed mechanism for the self-lubricating process of this coating relates to hydrogen bonds between the copolymer and water molecules. These hydrogen-bonded water molecules cannot

transform into a solid state. They formed an aqueous-like layer that acted as a lubricant and decreased ice accumulation on the surface [168].

## **1.6 Lubricant types and characterization**

### **1.6.1 Lubricant selection in slippery liquid infused surface**

The characteristics of both the substrate and lubricant are key factors to consider in the fabrication of slippery surfaces with anti-icing property. Generally, the desired characteristics for slippery surfaces can be achieved by meeting some requirements. Initially, the lubricant should be entirely absorbed in the matrix, and the surface needs to be completely wetted. Moreover, the lubricant must have more affinity to the substrate rather than the repellent liquid. Finally, the immiscibility of the lubricant and test liquid is essential. In addition, for the lubricants used in SLIPS, parameters such as viscosity and the type of organic liquid affect the anti-icing properties [36,170]. The lubricants used in liquid-infused systems are mostly organic fluids, such as fluorinated components or silicon oils, as well as some other lubricants that are briefly discussed in this study.

#### *1.6.1.1 Silicone Oils*

Linear polysiloxane materials known as silicon oil contain repeating units of silicone and oxygen atoms with two functional groups attached to each silicon atom. Polydimethylsiloxane (PDMS), as an important member of this category, is colorless, non-toxic, non-corrosive, and chemically stable [40,171]. Considering the significant properties of silicon lubricants, they are widely used for different applications. The surface tension of such lubricant ( $\sim 210 \text{ J/cm}^2$ ) is lower than that of water. Silicone oil has low solubility in water or oil, and low volatility. Moreover, it is not chemically

active; therefore, it cannot react with other materials in the composition. Notably, silicon lubricants should meet some important requirements for surface and coating application, including desirable electrical insulation, fire-retardancy, and easy release from the mold. Considering the numerous advantages, the use of silicon oil in lubricant infused surfaces can result in some problems for their real-life service. The high thermal expansion coefficient can lead to the production of an overpressure situation, thus decreasing the mechanical characteristics of the developed surfaces. However, the low surface tension of silicon oil facilitates its movement within the matrix, but it can promote oil consumption during its service life [40,171].

#### *1.6.1.2 Fluorocarbon*

Fluorocarbon-based materials that have many desirable characteristics comprise another lubricant category used for oil-infused surfaces. Most of their properties such as hydrophobicity, oleophobicity, low surface tension, and chemical resistance arise from the presence of fluorine atoms in their chemical structures [170,172–174]. The C-F in fluorocarbon is a high-energy bond, allowing them to tighten strongly and resulting in the above-mentioned properties and high transparency. Furthermore, considering that fluorine atoms have a low polarization rate, these materials show hydrophobic characteristics. The two groups of fluorocarbons, including perfluorodecalin and perfluoropolyether, are widely used for lubricant infused surfaces. Such materials have low vapor pressure, heat resistance, good flow, and significant dielectric properties [175]. Considering these distinctive characteristics, fluorocarbon-based lubricants can be commonly used in different applications, but they are extremely harmful for nature and human life [176,177]. This negative point

significantly restricts their usage in practical applications, such as LIS. They have a complex degradation process, and even after degradation, the obtained products are very toxic and remain stable for a long time. Considering the lack of an appropriate biodegradation process, their by-products cannot be easily recycled, thus damaging the ecosystem and biological activity. Consequently, environmental issues limit the use of such lubricants despite their desirable properties.

#### *1.6.1.3 Other lubricants:*

Other types of lubricants are also incorporated into lubricant-infused-surfaces, including vegetable oils, ionic liquids and polyols [46,178–181]. Generally, vegetable oils are extracted from different types of plants, such as peanuts, corn, soybean, coconut, and olive. Vegetable oils have been conventionally used as a lubricant. Considering the advent of mineral oils, vegetable oil usage decreased in the industry, but still have some advantages over mineral oils. Such substances have low flash point, high lubricant ability, low volatility, and solvent miscibility. However, one of their most vital downsides of these lubricants is their undesirable characteristics in low temperatures. This issue can affect their appearance such as haziness, solidification, and low fallowness at room temperature.

Ionic liquids are also another group of materials that are used as lubricants [182–184]. These materials consist of anions and cations, and they can be generally considered as molten salts at a temperature lower than 100 °C. Moreover, hydrophobic characteristics can be produced by modifying the chemical composition of ionic liquid. These materials have a very low vapor pressure, thermal resistance, electrical conductivity, and chemical stability. Based on their properties, these lubricants are

recyclable and environment friendly. Although ionic liquid can be considered as an excellent candidate for liquid infused surfaces application, their high cost restricts their large-scale application.

### **1.6.2 Effect of lubricant characteristics on the icephobic behavior of SLIPS**

Some characteristics, including low surface energy and fluidity apply to all mentioned lubricants. Low-surface-energy liquids reduce intermolecular interactions, such as hydrogen-bonding, between ice and solid surfaces and thereby affect ice adhesion. Lubricants can also cover a surface completely and, therefore, decrease the possibility of anchoring between ice and the textured substrate, which can commonly occur for superhydrophobic surfaces [181,185,186].

Villegas et al. compared heat transformation of an oil-infused surface with another surface having superhydrophobic structures [187]. The anti-icing mechanism of SHS is affected by air trapped within the rough surface; however, the existence of vapor in high-humidity conditions interferes with heat transfer. Therefore, as ice nucleation occurs under low temperatures, the chance of a Cassie–Wenzel (CW) transition and, therefore, high ice adhesion increases significantly [188]. Oil content also affects the anti-icing performance of a slippery surface. Although slippery surfaces having thick lubricant layers over solid surfaces show very low ice adhesion values, they are thermodynamically unstable and can be eventually removed from the system by external forces, such as gravity and drag forces. Therefore, a durable oil-infused surface must produce low ice adhesion but also show durability [189].

Gupta et al. showed that oil at various percentages (2%, 8%, 15%) and viscosities (100–1000 cSt) markedly alters the anti-icing properties of SLIPS. They

designed oil-infused slippery elastomers that could also maintain their superhydrophobic characteristics. Gupta et al. compared the anti-icing behavior of their obtained surfaces with other surfaces, including microtextured SHSs without oil infusion and smooth surfaces coated with PDMS, and observed an approximate 95% reduction in ice adhesion strength for the oil-infused elastomer surface relative to the other surfaces. Increasing viscosity from 100 to 1000 cSt with the highest percentage (15%) of oil resulted in a considerable decrease in the ice detachment force. As mentioned above, the lowest ice adhesion cannot produce a promising slippery surface. The high migration and accumulation of an oil layer on the surface when the viscosity and oil percentage are maximized, reduce the water repellency and stability of the fabricated surface. Gupta et al. determined an optimal state for superhydrophobicity and low ice adhesion strength at 100 cSt viscosity and <8% oil content infused within the microtextured surface [145,190].

The viscosity of the lubricant also affects other slippery-surface properties, including droplet mobility. Tsuchiya et al. investigated the relationship between the viscosity of the infused oil and water droplet velocity [187] using Eq. 1-10:

$$v = V \cdot (1 - T) / \mu \quad (\text{Eq. 1-10})$$

where  $v$  is the water droplet sliding speed on a liquid-infused surface,  $V$  is the volume of the water droplet,  $T$  is the area fraction of the base layer, and  $\mu$  is the viscosity of the infused liquid. They demonstrated that once the solid substrate is fully covered with an adequate oil viscosity, the mobility of water droplets can increase. Therefore, an appropriate combination of three parameters, namely  $V$ ,  $T$ , and  $\mu$ , produces a lubricated surface having a high droplet sliding speed [191–193].

Smith et al. also studied the effect of lubricant viscosity on the repellent liquid droplet velocity and droplet behavior over the lubricant layer. Predicting water droplet behavior on a surface is more complicated when a lubricant is present on the slippery surfaces. When the gravity force on liquid droplets overcomes the pinning force, the velocity of the droplet can determine the wetting performance of the surface. This parameter should be affected by the lubricant viscosity and contact line pinning. Smith et al. demonstrated theoretically that using lubricants having a high viscosity in LIS causes a water droplet to roll rather than slide over the oil. This approach is modeled as Eq. 1-11:

$$\frac{V_i}{V} \sim \left(1 + \frac{\eta_o R}{\eta_w h}\right)^{-1} \quad (\text{Eq. 1-11})$$

In this relation,  $V$ ,  $V_i$ ,  $h$ , and  $R$  are the velocity of the water droplet, the velocity of water at the water-oil interface, the lubricant thickness, and droplet radius, respectively. As well,  $\eta_o$  and  $\eta_w$  are, respectively, the dynamic viscosities of oil and water. It was thus concluded that although most LIS systems involve sliding of a droplet over the surface, the viscosity of the two liquids greatly affects this property [130].

Another group worked with various lubricants of both higher and lower viscosities than water. When the viscosity of the water droplet is much higher than that of the lubricant ( $\eta_w \gg \eta_o$ ), the droplet velocity is related to sliding angle ( $\alpha$ ), according to Eq. 1-12 [132]:

$$V \sim \frac{\rho g R^2}{\eta_w} \cdot \sin \alpha \quad (\text{Eq. 1-12})$$

The friction force therefore appears linear for the droplet. Furthermore, if  $\eta_w \ll \eta_o$ , the droplet experiences nonlinear frictional forces. Here, the fraction of a material in contact with the water droplet is defined by Eq. 1-13:

$$V \sim \frac{(\rho g)^{3/2} R^3}{\gamma_{oa} \phi^{3/2} \beta \eta_w} \cdot \sin^{3/2} \alpha \quad (\text{Eq. 1-13})$$

where  $\phi$ ,  $\gamma_{oa}$  and  $\beta$  represent the texture density, the oil–air surface tension, and the numerical factor that reflects the dissipation at the tip of the wedge. When  $\eta_w \gg \eta_o$ , the velocity of the droplet over a surface is independent of surface microstructure; however, if the viscosity of water is less than that of the lubricant, the velocity is scaled as  $1/\phi^{3/2}$ .

Thus, in four-phase surfaces with lubricants, the properties of both the repelling liquid and the infusing liquid can considerably affect the functionality of the surface. The presence of two active mobility regimes influences the anti-icing characteristics of the coating.

### 1.7 Durable icephobic slippery surfaces

New paths have emerged for producing slippery icephobic materials having a high durability. Irajizad et al. developed new anti-icing surfaces using ferrofluids as slippery lubricant layers with an exceptionally low ice adhesion strength [194]. These magnetic slippery surfaces (MAGSS) benefitted from the concept of stress localization to create low-energy liquid–liquid interfaces and reduce ice adhesion strength between the surface and the ice. Exposing the surface to a magnetic field blocked the thin liquid film in the structure without a need for micro-nano textures. This locking action increased the durability of the surface, which maintained its reduced ice adhesion strength even under high shear stress and frictional forces. The ice adhesion values for



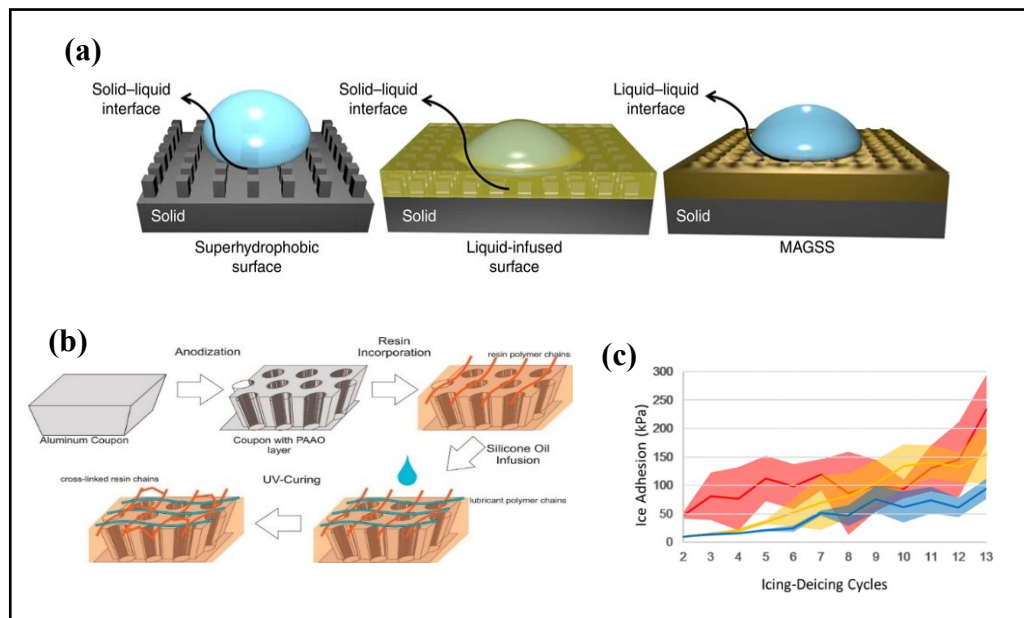
such a surface were about 1–10 kPa, and the surface also showed self-healing characteristics and a mechanical durability. MAGSS, compared with other icephobic systems such as superhydrophobic surfaces, produce more extensive liquid–liquid interfaces that provide low-energy sites and high free-energy barriers to heterogeneous ice nucleation (Figure 1-15a) and, as a consequence, a colder ice nucleation temperature [195].

The heterogeneous ice nucleation temperature of the MAGSS was  $-34 \pm 1$  °C, much colder than that of superhydrophobic and liquid-infused surfaces at  $-23$  °C and  $-26$  °C, respectively. The ice nucleation delay observed in this study was three orders of magnitude longer than for other icephobic surfaces. Increasing the intensity of the imposed magnetic field improved this initial result even further. Thus, MAGSS exhibited much lower ice adhesion values than other icephobic surfaces. These surfaces with very low ice adhesion have an extraordinary potential for inhibiting heterogeneous ice nucleation [196]. Difficulties remain when applying this surface to outdoor applications, related to the problem of maintaining magnetic fields for an extended period. Thus, there remains a need to develop more practical surfaces [194,197].

Coady et al. developed UV-cured polymer networks incorporated into slippery lubricant-infused porous surfaces to improve the operational durability and icephobicity of SLIPS [198]. Their surface preparation involved submerging the coupons in two different UV-cured resins and then infusing them with the silicon oil (Figure 1-15b). In this UV-curable SLIPS surface, the authors combined hexacrylated resin (Ebecryl 1360) and diacrylated silicone resin (Ebecryl 350) with silicon oil.

Coady et al. tested how acrylate functionality and the crosslinking density of the polymeric network affected ice adhesion. UV-cured slippery surfaces (Figure

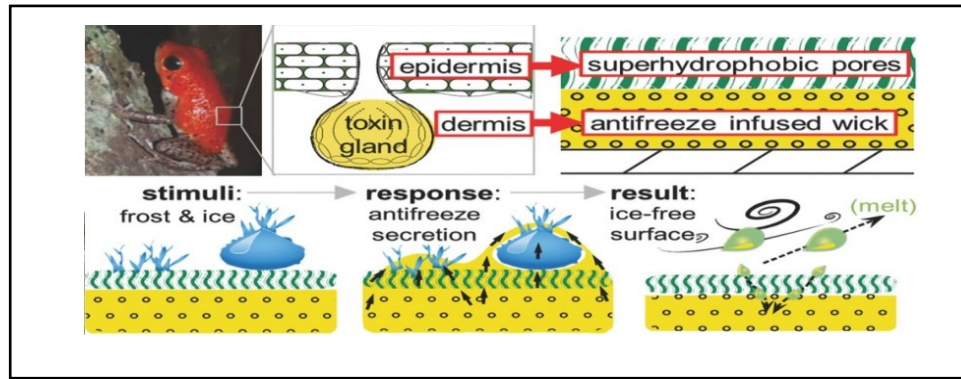
1-15c) showed a high durability after 14 icing/de-icing cycles, whereas other surfaces used for comparative purposes markedly increased their ice adhesion after only four de-icing tests [198]. The reported anti-icing characteristics illustrated that the silicone resin Ebecryl 350 exhibited an improved ice adhesion value below 10 kPa. Such a low value relates to the low crosslink density of this resin, which makes this surface more flexible than the highly crosslinked and brittle hexa-acrylate resin (Ebecryl 1360). This result was confirmed by work that found polymers having a lower crosslink density exhibited lower ice adhesion and were practical as icephobic materials [94].



**Figure 1-15.** (a) Schematic illustrating the formation of a liquid-liquid interface on a MAGSS and compared with superhydrophobic and liquid-infused surfaces [194], (b) the fabricating steps of the UV-cured SLIPS [198], (c) the repeated icing/de-icing tests for oil-only (red), oil+1360 (yellow), and oil+350 (blue) SLIPs [198].

After repeated icing/de-icing tests, the adhesive force increased to 50 kPa; however, this increase was not related to oil depletion [198]. The authors argued that the penetration of silicon oil into a crosslinked network of UV-cured polymers prevented oil depletion. SEM/EDX analyses suggested that the resin-oil layer may have been lost after the initial icing/de-icing cycles and was not simply the loss of the lubricant. Modifications, such as using resins having more abrasion resistance, would also favor these surfaces for use as durable icephobic surfaces [198].

Sun et al. introduced an anti-icing coating inspired by tropical frogs that release functional liquids in response to external stimuli. For this purpose, as shown in Figure 1-16, the developed icephobic surface released an antifreeze liquid when the surface was stimulated by icing. Such a surface comprises a bilayer structure, which includes a porous superhydrophobic epidermis on top and a reservoir for antifreeze in the bottom. To obtain this coating, they sprayed polymeric superhydrophobic shells (Hydrobead) onto a nylon membrane, and the dermis layer was infused with propylene glycol. Once ice or frost formed on the surface, the antifreeze liquid was gradually released through the bottom layer. This layer acted as a melting layer between the ice and the surface and melted the ice and frost. The analysis of the ice formation time showed that the surface could delay ice formation for approximately half an hour; in contrast, other types of icephobic samples experienced ice formation in under five minutes. As well, the antifreeze liquid had an optimal value ( $0.01\text{-}0.03 \text{ mL} \cdot \text{cm}^{-2} \cdot \text{h}^{-1}$ ), and once it was removed from the surface, it could be restored [199].



**Figure 1-16.** The release of an antifreeze liquid, and the consequent ice melt, in response to icing [199].

### 1.7.1 Interfacial Slippage

Golovin et al. recently proposed the concept of interfacial slippage. The ice adhesion measurement on polymers confirmed that, compared with thermoplastic polymers, elastomers showed lower ice adhesion [94,200–202]. The viscoelastic nature of elastomers fulfilled the required conditions for interfacial slippage and the initiation of cracks in the ice [203–206]. Regardless of the polymers' respective chemistries, changing the crosslink density of elastomers—lubricated with synthetic and natural oils to obtain the interfacial slippage—affected ice adhesion. The ice adhesion of elastomers having a low crosslink density was less than that for highly crosslinked elastomers. By adding lubricant and having interfacial slippage, a  $\tau_{ice}$  of  $<0.2$  kPa could be achieved. The lubricant, as an uncross-linked polymer chain, was mobile at the surface and increased the interfacial slippage along the solid–solid interface. This behavior promoted slippage between the ice, as a hard surface, and the soft oil-infused elastomer, thereby producing ultra-low ice adhesion [94].

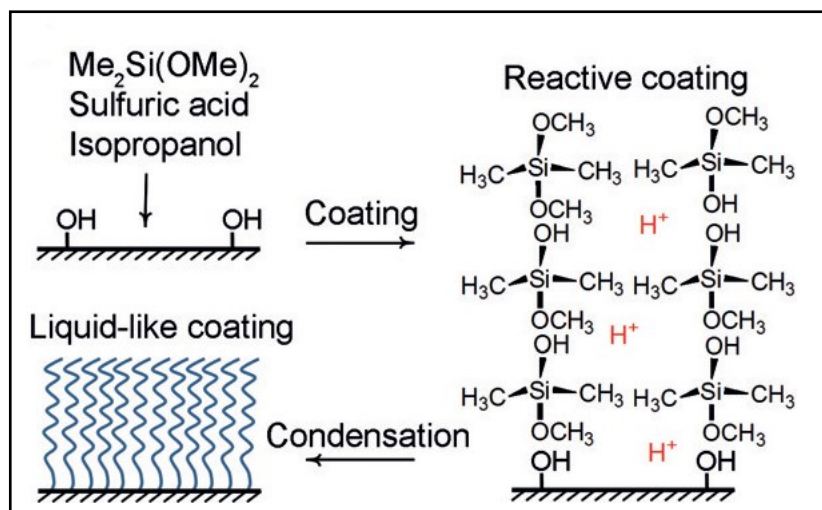
These surfaces showed good abrasion resistance, maintained their ultra-low ice adhesion, and had exceptional durability over several abrasion cycles. These elastomers, therefore, have an inherent icephobicity and produce durable anti-icing surfaces [200].

### **1.7.2 Slippery omniphobic covalently attached liquid (SOCAL) surfaces**

Covalent immobilization has been suggested for preventing lubricant depletion and obtaining more durable slippery surfaces. This process can be performed by covalently attaching either flexible functional groups or a lubricant to smooth surfaces [185,207]. In the former method, the grafted groups provide the solid surface liquid-like properties that cannot be dissolved or displaced by external liquids. Wang et al. fabricated the slippery covalently attached liquid surfaces using acid-catalyzed hydrolysis and the graft polycondensation of dimethyldimethoxysilane (Figure 1-17) [208]. The smooth surfaces demonstrated incredibly low contact angle hysteresis ( $\leq 1^\circ$ ) and low sliding angles for liquids such as water and hexane across a range of surface tensions (78.2–18.4 mNm<sup>-1</sup>).

Zhao et al. fabricated an anti-scaling coating by combining a slippery covalently attached liquid coating with a SiO<sub>2</sub> coating. The low surface energy and high homogeneity of such surfaces have been used to easily remove salt after scaling [209]. Given that the lubricant can be covalently attached to the substrate, Krumpfer et al. fabricated such a surface using the reaction of silicone oil with the surfaces of inorganic oxidized silicon, titanium, aluminum, and nickel [210]. The immobilized lubricant gel surfaces produced through this approach presented a low contact angle

hysteresis. The high affinity between the lubricant and surfaces allowed the grafted silicones to withstand a one-week exposure to toluene.



**Figure 1-17.** Formation of the slippery covalently attached liquid coatings through acid-catalyzed polycondensation of dimethyldimethoxysilane on a substrate [208].

Slippery liquid-immobilized surfaces have also been obtained by reacting a silicone lubricant and a polyelectrolyte layer containing  $\text{Ag}^+$  ions [211]. Because of gelation and immobilization of the lubricant, these slippery surfaces were highly durable both chemically and physically. The fabricated liquid-immobilized films also provided a high level of slipperiness compared with other liquids, such as water, ethanol, hexadecane, and oleic acid. Both the slippery covalently attached liquid-like surfaces and covalently attached-lubricant surfaces show great potential for anti-icing applications because of their low contact angle hysteresis (CAH) and high homogeneity, which improve water repellency and reduce ice nucleation sites, respectively.

### 1.7.3 Oil absorbent materials

Adsorbents are another group of materials that can be used in LIS to improve their lubricant stability and long-lasting durability. Such substances are usually in micro- and nanometer size and can attract oil and hydro-carbonic impurities from polluted sites, such as marine ecosystems [212–214]. In this regard, various types of materials, such as polymers, zeolite, nanocomposites, and aerogels, have been used as adsorbents. The most distinctive characteristic of these non-porous materials is their pore size distribution, including the macro, micro and mesopore size. Generally, such adsorbent with desirable porosity and surface area can be applied in different fields and applications [215–217].

Aerogel is a non-porous substance with different applications. The fabrication of aerogels via the sol-gel process has been widely studied, and some of these materials are commercially available in large scale. Nanostructured silica aerogels have extremely unique properties, such as high porosity, desirable carrier capacity, high surface area, and ultralow density. The high porosity and surface area of aerogel provide appropriate conditions for absorbing and carrying materials, such as catalysts, corrosion inhibitors, and lubricants [218–220]. Moreover, these materials are non-toxic and eco-friendly materials with widespread applications, especially as lubricant-absorbent material. Considering the hydrophobic nature of most oils, the hydrophilic structure of aerogels should be chemically modified as hydrophobic materials. For this purpose, the surfaces of aerogels can be treated with hydro carbonic silica groups[221–223].

Kim et al. used silica aerogels to absorb silicone oil, and then mixed them with PDMS polymeric matrix [224]. The presence of these carriers can slow down the migration rate of lubricants through the matrix. The developed coatings had an ice adhesion lower than 20 kPa, which was maintained over 20 icing/deicing cycles.

APPENDIX I (see Table A.I.2) presents a general overview of the fabrication methods of the slippery surfaces, their material composition, type of the infusing lubricant, and their characteristics.

## **1.8 Characterization of lubricant loaded Carriers**

There are some techniques that have a potential to be used for determining the amount of the lubricant infused in the pores. In fact, these measurements can be helpful to ensure the lubricant would be available during the subsequent de-icing events. The methods such as fluorescence microscopy was utilized to evaluate the presence of lubricant in the surface qualitatively [130,131]. Here, two test methods namely thermogravimetric analysis and B.E.T have been used to quantify the lubricant infused in the pores.

### **1.8.1 Thermogravimetric analysis**

TGA is an analytical technique, in which the variation of sample mass is monitored against time or temperature. This analysis performed on the thermogravimetric analyzer instrument. The analyzer measures the change in sample mass when temperature increases over time. Mass, temperature, and time are basic data that can be derived from this technique, from which additional analyses can be carried out [225,226]. This technique is usually used for investigating material degradation temperatures, residual solvent levels, adsorption, and the amount of inorganic fillers in



composite materials [227,228]. In the PhD research work, TGA was used to evaluate the loading capacity of the lubricant carriers.

### **1.8.2 B.E.T**

BET theory was used to explain the process of gas molecule adsorption over solid surfaces. This method is commonly used for the evaluation of the specific surface area of solid materials. Generally, this theory is based on the gas-sorption process. It usually requires that the probing gas adsorbate should not chemically react with adsorptive materials. Nitrogen gas is commonly used for probing material surfaces. Initially, the samples are vacuumed for some time at a certain temperature (e.g., 18.5 h at 140 °C). N<sub>2</sub> gas is also used for vacuuming. Then, the adsorption of gas molecules is done under vacuum, and a thin layer of gas is formed on the surface [229,230]. Based on the B.E.T theory, the gas molecule number over the surface can be estimated. This process is repeated for several times until the full coverage of the surface with the N<sub>2</sub> gas. In fact, when a multilayer of gas molecules is formed over the surface, and all the pores are filled with nitrogen gas, the saturation occurs. Therefore, this method can be used to determine the pore volume of particles [231–233].

### **1.9 Conclusion**

The presence of ice can reduce the effectiveness and functionality of equipment and infrastructure. To reduce ice accretion, research has focused on developing icephobic surfaces. This section reviewed the general idea about SLIPS, a new generation of icephobic coatings inspired by pitcher plants. To begin with, a theoretical background of superhydrophobic and slippery liquid-infused surfaces were extensively

addressed to get a better understanding about their differences and fundamental characteristics.

The assessment of fabrication methods and anti-icing characteristics of SLIPS confirmed that substrate morphology, including created textures, and the use of crosslinked polymers affect anti-icing performance. The characteristics of the infused lubricant, such as viscosity and its content percentage, affect the mobility of the repellent liquid over a surface as well as ice nucleation and ice adhesion.

The development of slippery surfaces faces challenges, including issues of durability and long-life applicability, especially in their first-generation fabrication methods. Textured surfaces covered with lubricant can reduce the loss of infused oil, normally lost through evaporation, gravity, or icing/de-icing. Employing novel fabrication methods, including microtexturing techniques and incorporating porous substances like aerogels can be considered as promising strategies to reduce oil depilation and enhance the durability of slippery coatings. By introducing microscale textures on the surface, consumption of oil can be minimized, leading to improved longevity and performance of the coating. Additionally, porous substances like aerogels can act as lubricant-absorbent materials that prevents oil from depleting and adjusts its migrating from the coating, thereby maintaining its lubricating properties for an extended period. These strategies offer several advantages, including ease of handling, cost-effectiveness, and favorable processability, making them attractive alternatives to other methods.

The use of silicone-based materials either as the matrix or lubricant, offers numerous desirable characteristics, including chemical stability, compatibility, low surface tension, and electrical insulation. Silicone-based materials provide durability,

resistance to degradation, and low ice adhesion. Additionally, their electrical insulation capabilities ensure the safe operation of electrical systems. Overall, silicone-based materials contribute significantly to the performance and reliability of coatings.

Finally, evaluating the long-term durability of these developed surfaces under harsh environmental conditions is essential to ensure their effectiveness over extended periods.

## **Chapter 2: Fabrication of liquid-infused textured surfaces (LITS): the effect of surface textures on anti-icing properties and durability**

Samaneh Heydarian<sup>1\*</sup>, Khosrow Maghsoudi<sup>1</sup>, Reza Jafari<sup>1</sup>, Hellene Gauthier<sup>2</sup>,  
Gelareh Momen<sup>1</sup>

<sup>1</sup>Department of Applied Sciences, University of Quebec at Chicoutimi (UQAC), 555, boul. de  
l'Université, Chicoutimi, Quebec, G7H 2B1, Canada.

<sup>2</sup>Institut de recherche d'Hydro-Québec (IREQ) 1800 boul. Lionel-Boulet, Varennes (Québec), J3X  
1S1, Canada

\*Corresponding author: E-mail address: samaneh.heydarian-dolatabadi1@uqac.ca. Tel:001(418)  
545-5011

### **2.1 Abstract**

Icephobic surfaces offer an effective solution to protect the infrastructures subjected to harsh cold-weather environment and increase their efficiency. Inspired by the *Nepenthes* pitcher plant, liquid-infused coatings have received much interest as a potential cost-effective anti-icing solution. In this paper, we developed liquid-infused textured surfaces (LITS) through chemical etching followed by a replication method. We assessed the effect of viscosity (50 and 500 cSt) and the infusion percentages of lubricant on the morphology and icephobicity of the produced surfaces. Lubricant-infused silicone surfaces are normally obtained by combining a textured surface morphology and slipperiness. We therefore evaluated the wettability, morphology, and

the localized surface elasticity maps of the fabricated surfaces using a goniometer, scanning electron microscopy (SEM), and atomic force microscopy (AFM), respectively. The icephobic performance of the samples was studied by differential scanning calorimetry (DSC), push-off tests, and freezing delay time measurements. Our observations of the anti-icing nature of the produced LITS confirmed that the heat insulation effect of the lubricant lowered the ice nucleation temperature considerably compared with non-oil surfaces. The prepared LITS presented an ice adhesion strength of less than 20 kPa, four orders of magnitude lower than that of a pristine surface. Surficial microtextures are critical for reducing the rate of oil depletion through the trapping of oil within the surface microstructures. Our designed lubricant-infused surfaces present more durable and stable anti-icing characteristics over the long term than smooth lubricant-infused surfaces.

**Keywords:** icephobic surfaces and coatings, slippery coatings, liquid-infused surfaces, micro/nanostructured surfaces, superhydrophobic surfaces, silicone elastomers

## 2.2 Introduction

Ice accumulation and ice formation on the exposed surfaces can cause both operational problems and economic losses [63–65]. There is much effort, devoted to developing strategies to prevent ice accretion on surfaces and prevent related damage [10,38,66–68,234,235]. A large number of studies have focused on the use of superhydrophobic surfaces as water-repellent surfaces to use for anti-icing purposes [236–238]. High humidity conditions can damage anti-icing properties of these

surfaces due to water condensation within their surface textures, resulting in mechanical interlocking between the ice and the surface [22,23]. Inspired by *Nepenthes* pitcher plants, slippery liquid-infused porous surfaces (SLIPS) have been developed in which an air-liquid interface is replaced by liquid-liquid contact. Reducing ice adhesion by 10 kPa (usually measured by non-impact bulk ice) makes SLIPS a potential candidate for passive icephobic materials [35,74,80].

SLIPS benefit from their porosity to preserve an amount of lubricant on the surface and generate a liquid layer. This layer can remove; thus, a water drop can easily slide over the surface at very low roll-off angles [72]. One of the key design factors in the fabrication of a liquid-infused surface is its porosity. Indeed, by preserving the lubricant, a liquid layer can be formed on the surface that prevents producing pinning spots on the surface.

Both ordered and disordered textures can serve to produce the porous structure of SLIPS. Ordered surfaces can be fabricated using lithography, lasers, and computer numerical control (CNC) methods [137–139]; while, the disordered textures are usually produced by dip coating, spray coating and plasma , resulting in a random porous pattern [52,140,141]. The mentioned methods have many drawbacks, including complexity, long procedure times, expensive facilities, and environmental concerns. In contrast, using textured templates (also known as insert or coupon) to obtain replicates having micro-nanotextures on the surface, as a relatively simple method, may be desirable for reducing the processing time and costs, for applying to a wide range of materials like thermoplastic polymers, rubber and resins and for simplifying the use

and reproducibility of micro-nanotextures. The textured template can be fabricated using various methods such as chemical etching procedure [144,145].

Infusing oil into the polymeric matrix is one of the effective approaches for decreasing ice adhesion on the surface. In this method, a suitable matrix is used to incorporate the lubricant for a longer period. Due to low surface energy and surface smoothness, polymers can keep their low ice adhesion strength, even after oil depletion [32,33,48,150]. Thus, by combining elasticity and the presence of a lubricating layer, a considerable reduction in ice adhesion strength is possible. It has been shown that elastomers can offer a lower ice adhesion strength than thermoplastic polymers owing to their viscoelastic characteristic. This property promotes interfacial slippage which results in ice detachment [43,94,200,203,204,239]. Furthermore, the polymer stiffness is the mechanical property that can be affected by lubricant infusion, resulting in ice adhesion strength lower than 20 kPa [94]. For instance, liquid paraffin was infused in polydimethylsiloxane (PDMS) that oil infusion led to swelling the elastomeric matrix. An ice adhesion strength of 1.7 kPa was obtained at  $-30\text{ }^{\circ}\text{C}$ , which remained below 10 kPa until  $-70\text{ }^{\circ}\text{C}$ . The increase of ice adhesion can be resulted from rise of oil viscosity when temperature decreased [158].

Losing lubricant over time can cause problems in SLIPS, and influence their efficiency. The uppermost lubricant layer can be removed due to conditions such as icing/de-icing cycles, and evaporation [48,95,130]. So, much effort has been focused on finding relationship between surface morphology and ice adhesion to promote the durability of SLIPS [48,73,148]

Here, we successfully fabricated liquid-infused surfaces (LIS) and liquid-infused textured surfaces (LITS) through a replication method. We then, studied the effect of viscosity and lubricant contents on the morphology and icephobicity of the produced surfaces. It is worth mentioning that LITS can be considered as a developed subcategory of conventional slippery liquid-infused porous surfaces (SLIPS); while LIS presents liquid infused surface without texture. Therefore, using these surfaces allows us to study the effect of textures on surface characteristics. The focus of this study is on the lubricant infusion in the bulk and investigation of the effect of surface textures on the long-time durability. While the conventional SLIPS benefit from lubricant impregnated only on the surface, here, the lubricant is embedded in the elastomeric matrix which endows enhanced properties.

We embedded a lubricant of two different viscosities (50 and 500 cSt) into the elastomeric matrix at various lubricant contents (10, 20, 30, 40, and 50 wt.% of the silicone) and transferred the microtextured templates from a textured aluminum template. We then performed cyclic icing/de-icing tests on the LITS samples and examined the relationships between lubricant contents, oil viscosity, and LITS durability.

## **2.3 Materials and methods**

### **2.3.1 Fabrication of the oil-infused microtextured silicone material**

To obtain microtextures on the silicone surfaces, we cut an A5052 aluminum sheet into 2.5 cm × 3 cm coupons. They were ultrasonically cleaned in acetone and deionized water for 0.5 h, followed by drying in an oven at 70 °C for 1 h. The coupons



were then chemically etched by being placed in 15 wt.% hydrochloric acid for 2h. This etching process has been successfully used in our group's previous research work [144]. The above cleaning and drying procedures were repeated to remove any residual particles from the Al coupons.

Throughout the replication process, the elastomer material can stick to the template surface and heighten the difficulties of replication. Although various strategies have been proposed to solve this issue, we applied anti-stiction coatings on the textured surface to improve the quality of the insert surface and the uniformity of the textures. Applying an anti-stiction coating allows the templates to be used in the replication process. The most commonly used anti-stiction coatings are low-surface-energy coatings applied via the self-assembled monolayer (SAM) method. To facilitate releasing surfaces from the templates, we prepared a 6 mM solution of diluted Trichloro (1H,1H,2H,2H-perfluorooctyl) silane in methanol (TPFS= $\text{CF}_3(\text{CF}_2)_5\text{CH}_2\text{CH}_2\text{SiCl}_3$ ) as the anti-stiction coating, and samples were immersed in the solution for 2 h at a temperature of 70 °C. The dip-coated aluminum templates were then dried at 70 °C for 1 h.

Sylgard 184 PDMS was received from Dow Corning, and the base resin was mixed with a curing agent in a standard weight ratio of 10:1. Then, we mixed various percentages (10, 20, 30, 40, and 50 wt.%) of each silicone oils (two viscosities of 50 and 500 cSt from Dow Corning, Xiamater PMX-series) into the PDMS mixtures. We therefore created ten combinations of viscosity and infusion levels for the prepared samples.

The microtextures were then replicated to the oil-infused silicone elastomer. The surface of the textured templates was covered with the oil-infused elastomer mixtures, and the template–mixture preparations were placed in a vacuum chamber to degas and increase the penetration of the mixtures into the polymeric materials within the microtextures. They were then cured at 90 °C for 30 min. The cured elastomers were removed from the template surface to obtain the replicated silicone elastomer having microtextured surfaces.

In addition to the oil-infused microtextured materials, we also fabricated microtextured and smooth PDMS materials without oil infusion and smooth PDMS materials with oil infusion (resembling SLIPS surfaces) to serve as control substrates for the ice adhesion tests.

### **2.3.2 Surface characterization**

The wettability of oil-infused microtextured surfaces was examined using a contact angle goniometer (Kruss<sup>TM</sup> DSA100). A 4- $\mu$ L water droplet was used for the static contact angle measurement (CA). The droplet was deposited onto the surface, and the CA was calculated using the Young-Laplace approximation. Contact angle measurements were repeated at five different points on the substrate to consider any variation in wettability performance, and we calculated the average CA. We also obtained water and diiodomethane contact angles to calculate surface energy of our fabricated samples using Fowkes model [240].

To measure the water droplet velocity, a 5- $\mu$ L water droplet was placed onto the surfaces sloped at an angle of  $\sim 30^\circ$ , and we recorded the time for a water droplet to travel along a given distance.

The characterization of the microtexture morphology of the replicated silicone elastomer surfaces was performed using a scanning electron microscope (JSM-6480 JEOL SEM manufactured by JEOL Japan). Prior to the analysis, the samples were coated with a thin layer of gold alloy to enhance imaging. We also used an attached energy-dispersive X-ray spectroscopy (EDS) to study the elemental composition of the surface.

To improve our understanding of the produced surfaces, we obtained localized surface elasticity (stiffness) maps through atomic force microscopy (AFM), using a Dimension ICON microscope (Bruker, USA) in tapping mode, to qualitatively assess changes in the surface composition of samples. The qualitative maps were generated on the basis of the contrasting viscoelastic properties of various components across the surface.

### **2.3.3 Mechanical Properties**

To examine the mechanical properties of the prepared samples, we measured the hardness values using a 2000 max-hand Shore A durometer (Rex Gauge, USA). Samples having a minimum thickness of  $4.0 \pm 0.1$  mm were used for these measurements. To guarantee the accuracy of our measurements, we performed five separate measurements with a constant load for each sample at room temperature ( $\sim 23^\circ\text{C}$ ).

### 2.3.4 Icephobic Properties

To investigate the effect of surface properties on the ice nucleation, we ran differential scanning calorimetry (DSC). For this purpose, a 5-mg deionized water droplet was poured into T-zero aluminum pans, each pan coated with a very thin layer of a coating and sealed with lids. The measuring process included the cooling down of a prepared sample (from 30 to  $-40$  °C at a 3 K/min ramp) and an empty sealed pan as a reference.

The freezing delay times were measured using a Kruss machine equipped with a cold chamber and a Peltier stage that can cool down to  $-30$  °C. To minimize the effect of condensation on the measurements, we used anhydrous calcium sulphate desiccants. The freezing delay time was described as the time at which a water droplet, placed on the surface, began to freeze.

Ice adhesion on the sample was measured via a homemade push-off apparatus [67,195]. In this test, a cylindrical plastic mold, having a diameter of 1 cm, was placed on the prepared surface and filled with deionized water. Samples with their respective filled plastic molds were then placed into a cold chamber at  $-10$  °C for 24 h to obtain an ice cylinder on the sample surface. The samples were then placed into the holder of the apparatus and fixed using a vacuum. The test began as the probe of the force meter approached the cylinder at a rate of  $0.1 \text{ mm}\cdot\text{s}^{-1}$  and pushed on the cylinder. The force shear was measured by the force meter and recorded the breaking point when the ice detached from the surface. We obtained ice adhesion shear stress by dividing the maximum force by the icing area.

### 2.3.5 Durability Properties

#### 2.3.5.1 Lubricant depletion/recovery

The oil replenishment capability of the fabricated samples was evaluated by depletion/recovery repeating tests [241]. We assessed the recovery capability of the fabricated samples via the procedure, described in the reference [241]. First, the sample was weighed using a balance (Sartorius Co., precision 0.1 mg), and the measured value was recorded as  $m_0$ . In a second step, an oil-absorbing paper was applied to remove oil film off the sample's surface, and the sample was then reweighed. This step was repeated for  $n$  cycles, and the corresponding weight was recorded as  $m_n$ . We used Eq. 2-1 to calculate the rate of weight loss.

$$\text{Rate of weight loss} = \frac{m_0 - m_n}{m_0} \times 100 \quad (\text{Eq. 2-1})$$

#### 2.3.5.2 Icing/de-icing cycles

We combined the push-off adhesion test and icing/de-icing cycle to assess the durability of the samples. For this purpose, we subjected samples to multiple icing/de-icing cycles, and repeated push-off test seven times with the same method.

#### 2.3.5.3 Weathering test

We utilized a QUV accelerated weathering tester to analyze the effect of ultraviolet radiation followed by moisture condensation on the destruction of the sample. This test method allowed us to assess the durability property of the fabricated samples when exposed to simulated outdoor conditions. The test method was carried

out based on ASTM G154 using UVA-340 fluorescent lamps. The test consisted of 300 h UV light exposure as a test cycle of 8 h, a temperature of 60 °C, and an irradiance of 0.89 W.m<sup>-2</sup>, followed by 4 h of condensation at 50 °C.

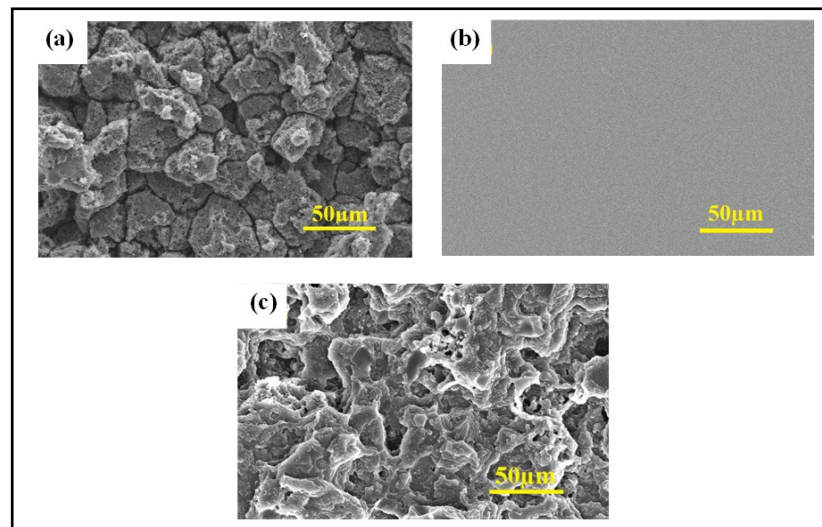
## **2.4 Results and discussion**

### **2.4.1 Surface characterization**

Figure 2-1 illustrates the surface morphology of smooth PDMS, the etched Al coupon and micro-textured PDMS materials. We tried to optimize the effect of etching conditions on replicated surfaces in terms of acid concentration and etching time. However, it was verified that using the etching conditions of 15 wt.% hydrochloric acid for 2 h was successfully created microtextures, as the same as previous work in our group [144]. It can be confirmed that the replication was clearly done on the elastomeric matrices.

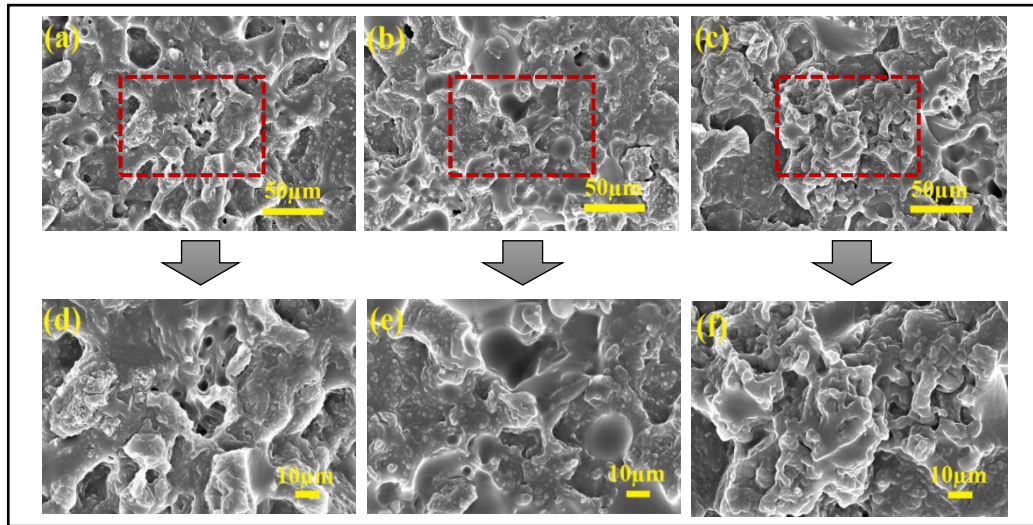
The evaluation of the SEM images (Figure 2-2 and Figure 2-3) revealed differences in the surface morphologies caused by oil viscosity and the percentage of oil infusion. For the 50 cSt oil-infused surfaces, regardless of oil infusion percentages, the microtextures were clearly visible. To get better understanding, we marked the specific location in lower magnifications where the higher magnification has been taken to make the identification clearer. As the oil content increased from 10 to 50 wt.%, the sharpness of the microtextured edges gradually decreased, which confirmed the slight presence of oil on the surface (Figure 2-2). On the other hand, the surface textures were considerably changed in the samples containing oil with 500 cSt viscosity. Increasing the oil percentage of this 500 cSt oil caused the microtextures to

gradually vanish. Although the sample containing 10 wt.% infused oil presented surface microtextures, few microtextures were observed on the 50 wt.% oil-infused surface (Figure 2-3). Therefore, for surface containing oil with 50 cSt viscosity, the microstructures produced by the replication were more obvious in comparison with those containing lubricant with 500 cSt viscosity.

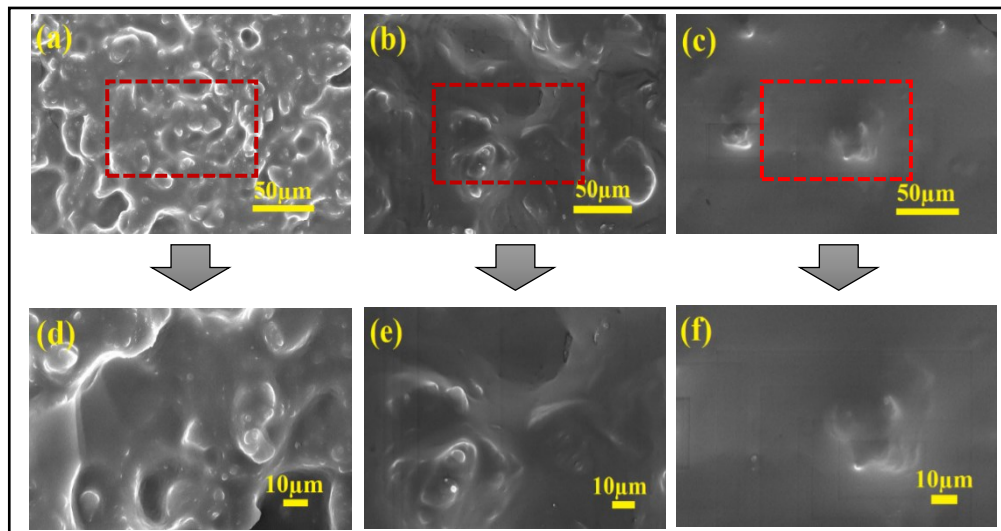


**Figure 2-1.** SEM images of (a) the chemical etched coupons, (b) the pristine PDMS elastomer and (c) the replicated microtextured PDMS without infused oil.

In the sample without microstructures, the oil migration can result in excessive availability of oil on the surface and therefore, covering the asperities. The surface morphologies of these oil-infused microtextured materials affect the wetting characteristics of the coatings (discussed in the following section). This wide range of oil–texture combinations provided us the opportunity to scrutinize the contribution of each variable (oil and surface microtextures) on the icephobic properties of the produced surfaces.



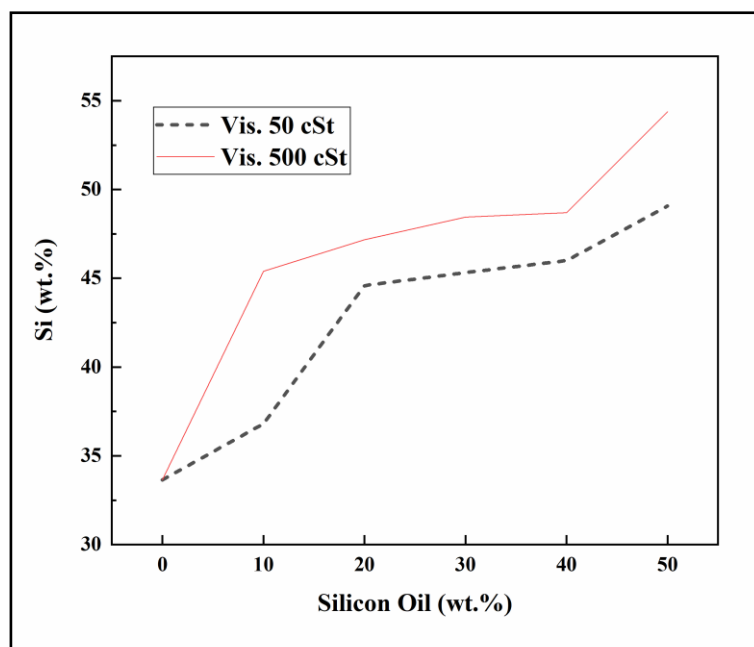
**Figure 2-2.** Micrographs of liquid-infused textured surfaces containing silicone oil with 50 cSt viscosity. (a) 10 wt.%, (b) 30 wt.%, and (c) 50 wt.% of oil at 500x magnification. (d) 10 wt.%, (e) 30 wt.%, and (f) 50 wt.% of oil at 1000x magnification.



**Figure 2-3.** Micrographs of liquid-infused textured surfaces containing silicone oil with 500 cSt viscosity. (a) 10 wt.%, (b) 30 wt.%, and (c) 50 wt.% of oil at 500x magnification. (d) 10 wt.%, (e) 30 wt.%, and (f) 50 wt.% of oil at 1000x magnification.



The Si content on the developed surfaces were measured by the energy-dispersive X-ray spectroscopy. As can be seen, regardless of the oil viscosity, the presence of oil increases the Si content on the surface. Although the Si content of samples having no oil infusion was identical for both viscosities (50 and 500 cSt), as the weight percentage of silicone oil increased, the weight percentage of Si on the surface increased more for samples with the infused 500 cSt silicone oil than those having the 50 cSt oil. These measurements agreed well with the SEM images were more oil contents resulted in more microstructures covered by oil. As silicone oils contain Si content, it would enhance the overall silicone content on the surface. So, it confirmed the presence of lubricant over the surface compared to no oil samples.



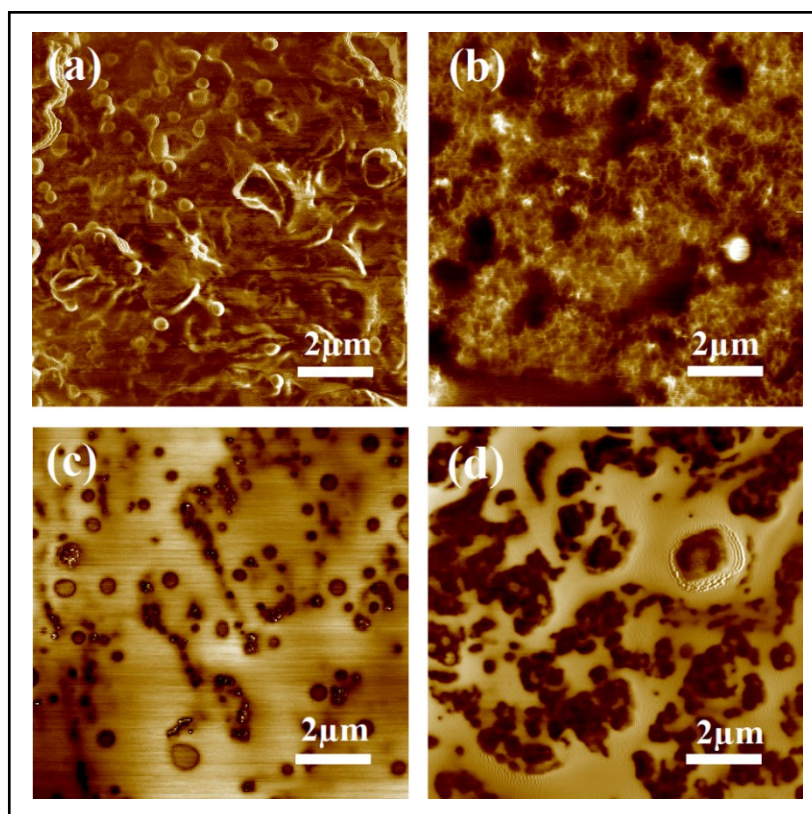
**Figure 2-4.** Silicon content of the samples in relation to the infusion level of the silicone oil, as obtained by energy-dispersive X-ray spectroscopy.

Atomic force microscopy (AFM) produced the localized surface elasticity (stiffness) maps to provide information about the composition of materials on the surface in terms of their viscoelastic properties (Figure 2-5). Phase contrast microscopy detected compositional changes across the polymeric surface and lubricated surfaces. Phase change usually occurred owing to the interaction between the surface and the AFM stylus tip. The mechanical characteristics of the surface, such as stiffness and frictional properties, also affect the observed phase [242].

A parameter used in this technique is the contrast of viscoelastic properties acquired from the various viscous energy dissipations of the materials across the surface [243]. Materials having limited viscoelastic properties showed lower phase angles. Domains with different mechanical properties could be determined using the contrast of the phase images with a high lateral resolution. Generally, the lighter regions illustrate areas having a low phase shift, and the darker areas represent regions having a higher phase shift [243].

The no-oil sample showed no real phase contrast (Figure 2-5a). We observed only cross-talk, which is the inherent error in the AFM method arising from lateral and normal signals [244]. The sample surface was homogeneous in terms of phase contrast; thus, no viscoelastic contrast was observed. In the oil-containing samples, however, the lighter brown and darker brown areas illustrated a real phase contrast, suggesting some heterogeneity in the distribution of the oil. For samples containing 10 wt.% lubricant with 50 cSt viscosity (Figure 2-5b), the phase contrast was considerably stronger than for the no-oil sample. In the lighter brown domains, the surface was covered with oil, and the darker brown phase area was oil-free, which stemmed from the difference in

modulus and viscoelastic properties of the lubricant and cured polymeric matrix. Accordingly, the phase contrast clearly showed the oil distribution and heterogeneity across the surface. As expected, the proportion of lighter brown areas increased in the oil-infused sample (50 wt.%, 50 cSt), which confirmed the higher coverage of the surface by the lubricant (Figure 2-5c). In addition, the AFM imagery of oil-infused elastomer (10 wt.%, 500 cSt) showed considerably more lubricant on the surface compared with samples containing 50 cSt oil viscosity at the same infusion level (Figure 2-5d).

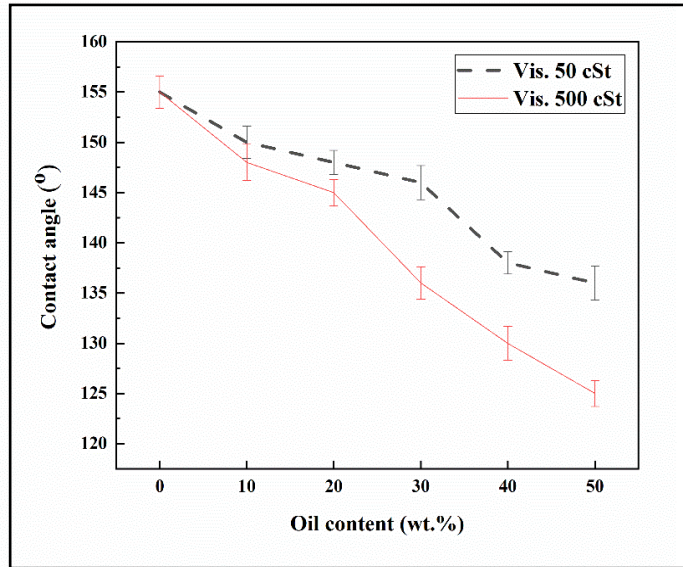


**Figure 2-5.** AFM images of microtextured elastomer containing (a) no oil, (b) 10 wt.% 50 cSt oil, (c) 50 wt.% 50 cSt oil, and (d) 10 wt.% 500 cSt oil surfaces.

A comparison between the lighter brown areas of the 10 wt.% 50 cSt and 10 wt.% 500 cSt samples revealed that 50 cSt oil was less present between the surficial microtextures than the 500 cSt oil. The 10 wt.% 50 cSt sample showed a heterogeneous surface as indicated by the darker brown areas. These relatively darker areas represent the effect of the underlying microtextures. The strong homogeneity of the lighter brown areas of the 10 wt.% 500 cSt sample indicated a thicker layer of lubricant, which did not allow the underlying microtextures to be exposed. The thick layer of lubricant covering the 50 wt.% 500 cSt samples prevented the evaluation of its surface using the AFM technique.

#### **2.4.2 Surface wettability**

After evaluating the distribution of the lubricant material on the microtextured surfaces and its effect on the microtopography, we assessed the surface wettability and surface energy of the oil-infused silicone elastomers. Increased oil content decreased the water CA (Figure 2-6). Also, samples containing oil with viscosities of 50 and 500 cSt showed an increase in surface energy from 20.64 and 21.48 mN/m to 24.57 and 25.35mN/m, respectively, when oil content increased (based on Fowkes model calculations). This overall trend is resulted from the filling of the microtextures with oil.



**Figure 2-6.** Water contact angle in relation to oil content (wt.%) for two oil viscosities (50 cSt and 500 cSt).

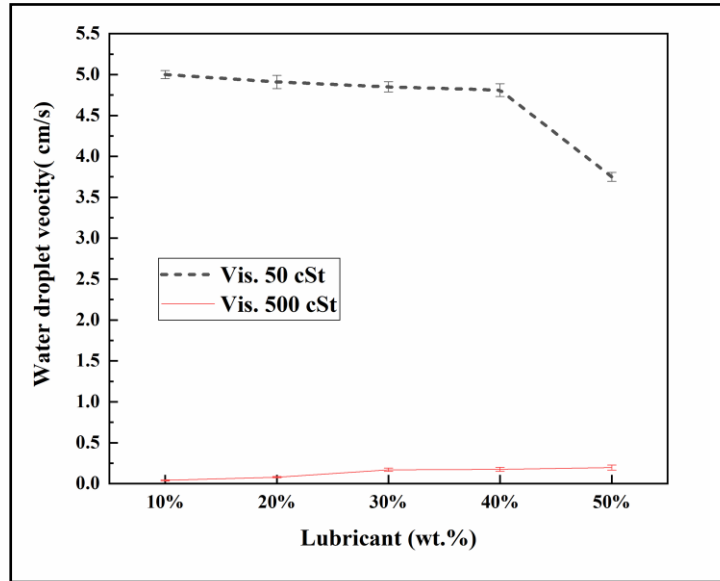
The higher surface energy of the silicone oil than that of the trapped air between the microtextures led the water droplet to spread out more on the surface and consequently wet the surfaces of the samples containing the lubricant. Moreover, the samples containing oil with 50 cSt viscosity produced a higher CA than the 500 cSt samples, regardless of the percentage of oil infusion. This observation agreed with the SEM imagery and demonstrated that samples containing 50 cSt silicone oil still benefited from a microtextural contribution to the anti-wetting properties, whereas for samples having 500 cSt silicone oil, a layer of oil covered the surface microtextures of the samples.

### 2.4.3 Water-repellency properties

To better evaluate the contribution of surface microtextures to the dynamic behavior of water droplets on the LITS, we measured water droplet velocity to predict the mobility behavior of a water droplet on the lubricated surfaces [130][245]. We also analyzed the role of lubricant viscosity and oil infusion level on water droplet velocity. We observed a marked difference between water droplet velocities for the surfaces containing low-viscosity (50 cSt) and high-viscosity (500 cSt) lubricants (Figure 2-7). Water droplet velocity was much higher on the slippery surfaces containing 50 cSt lubricant than those containing the 500 cSt lubricant. The relationship between droplet velocity ( $V$ ) and oil viscosity is presented in Eq. 2-2 [132], in which the effect of lubricant viscosity on the repellent liquid droplet velocity and droplet behavior over the lubricant layer are considered. The droplet velocity is inversely proportional to oil viscosity.

$$V \sim \frac{(\rho g)^{3/2} R^3}{\gamma_{oa} \phi^{3/2} \beta \eta_0} \cdot \sin^{3/2} \alpha \quad (\text{Eq. 2-2})$$

where  $R$ ,  $\gamma_{oa}$ ,  $\phi$ ,  $\eta_0$ ,  $\alpha$ , and  $\beta$  represent the contact radius, oil–air surface tension, texture density, oil viscosity, tilt angle, and the factor that present the dissipation at the tip of the wedge, respectively.  $(\rho g)^{3/2} R^3$  is related to the droplet weight.



*Figure 2-7. Water droplet velocity across the LITS as a function of infusion percentage and lubricant viscosity.*

The lubricant infusion percentage also affected the behavior of water droplets on the surfaces. Given that the thickness of the lubricant layer over LITS for the 500 cSt oil was obviously higher than that of the lower viscosity 50 cSt oil, we observed that by increasing infusion percentages, the speed of the droplets increased. According to Eq. 2-1,  $V$  is inversely proportional to  $\beta$  (the factor that corresponds to the dissipation at the tip of the wedge).  $\beta$  is related to the thickness of the lubricant by  $\beta \approx \ln(L/h)$ , where  $L$  and  $h$  are the typical size of the surrounded liquid by the lubricant materials and lubricant thickness, respectively [132]. Accordingly, by increasing thickness,  $\beta$  decreases, thereby producing a greater water droplet velocity (Eq. 2-1). Consequently, for a given lubricant viscosity, a greater lubricant infusion followed by an increased thickness results in the increased water droplet velocity across the lubricated surface.

For the surfaces infused with the low-viscosity lubricant (50 cSt), however, the relationship between the oil infusion level and water droplet velocity was very different. Greater infusion levels of lubricant reduced the water droplet velocity over the surfaces. Unlike the fully lubricated surfaces of the high-viscosity lubricant (500 cSt) samples, the microtextures, as seen in SEM images, were more exposed on the samples infused with a low-viscosity lubricant (50 cSt). Therefore, on such surfaces, the water droplet velocity depended on microtextures to a much greater extent than on lubricant thickness. At low levels of oil infusion (10 wt.%), the oil-infused surface showed a CA  $>150^\circ$ , which acted as a key factor affecting water droplet roll-off and the increased velocity (Figure 2-7). By heightening the lubricant content, the surface microtextures became increasingly covered by the lubricant, and, consequently, the CA decreased. As such, the surface lost its roll-off properties, resulting in a reduced water droplet velocity.

#### **2.4.4 Depletion/recovery cycle tests**

The replenishment of lubricant is a distinguishable characteristic of oil-infused slippery surfaces by which the long-term durability of such surfaces is possible [246,247]. We compared the lubricant weight loss of liquid-infused surfaces (LIS) and liquid-infused textured surfaces (LITS) per number of cycles of testing (Figure 2-8). Regardless of lubricant viscosity, the oil loss gradually increased, and this oil loss for LIS samples was significantly higher than that observed for the LITS samples. This trend confirmed that untextured surfaces (LIS) provide more available lubricant on the surface for each cycle and highlighted the importance of microtextures in the oil-infused samples; microtextures are very important for reducing the rate of lubricant



depletion considerably, thereby optimizing the recovery of surface lubrication. A textured surface increases the available volume to trap more oil; therefore, once the silicone oil is diffused into the surface, it becomes trapped within the microtextures. Wiping the surface with oil-absorbent paper did not easily remove the trapped lubricant, allowing the LITS surfaces to display enhanced durability. For LIS, the lubricant was more available on the surface and permitted a greater oil depletion by external forces.

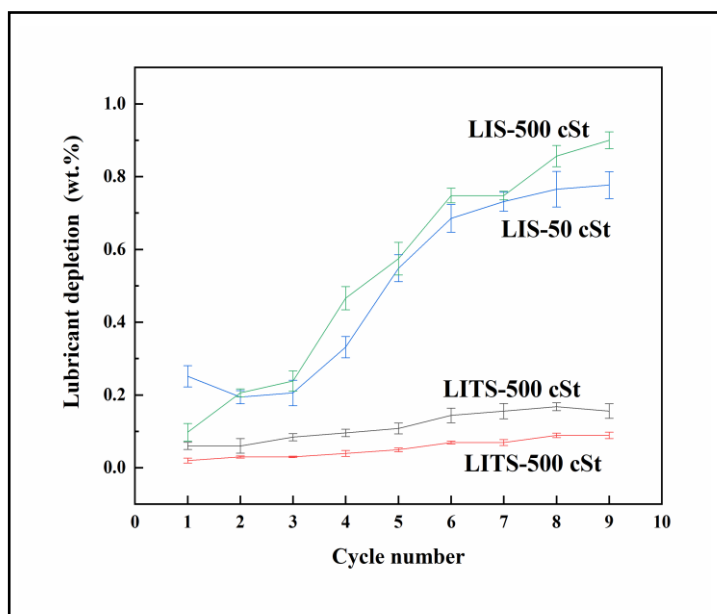
The oils in the oil-infused samples for all oil combinations of infusion levels and viscosities can migrate to the surface; however, the migration rate differed between the low- and high-viscosity oils. The migration rate for samples of 500 cSt oil was greater than that for samples containing 50 cSt oil (Figure 2-8). This behavior can be attributed to the different diffusion rates of oil molecules through the free volumes of the cross-linked polymeric network. From the Stokes–Einstein relationship [248] , Eq. 2-3, the chain self-diffusion coefficient  $D$  can be related to viscosity ( $\eta$ ) as:

$$D \propto \frac{1}{\eta \cdot R_h} \quad (\text{Eq. 2-3})$$

where  $R_h$  is the polymer hydrodynamic radius. This equation is usually used to interpret the behavior of a polymer in a dilute solution. In this study, silicone oil is considered to be the solvent owing to its lower molecular weight than the main matrix. As such, according to this equation, at a high viscosity (500 cSt), a lower diffusion of the oil within the polymeric network is expected. Furthermore, at 500 cSt viscosity, the silicone oil molecules have a greater tendency to migrate from the bulk material toward the surface than the 50 cSt oils because they are not trapped within the cross-linked

network. In other words, the low-viscosity silicone oil molecules diffuse in greater amounts into the free volumes, thereby becoming trapped in the cross-linked network. Consequently, these molecules are gradually released to migrate toward the surface.

The observed differences in behaviours are of great importance for the anti-icing properties, in particular for the durability of anti-icing properties of the produced oil-infused surfaces. This will be discussed in the following sections.



**Figure 2-8.** The rate of weight loss for LIS and LITS samples in relation to the number of test cycles of oil recovery/depletion.

### 2.4.5 Anti-icing properties

We evaluated the anti-icing properties of LITS in regard to its resistance against icing and the material's icephobic properties. The resistance against icing involves reducing the ice crystallization point to delay heterogeneous ice nucleation and, consequently,

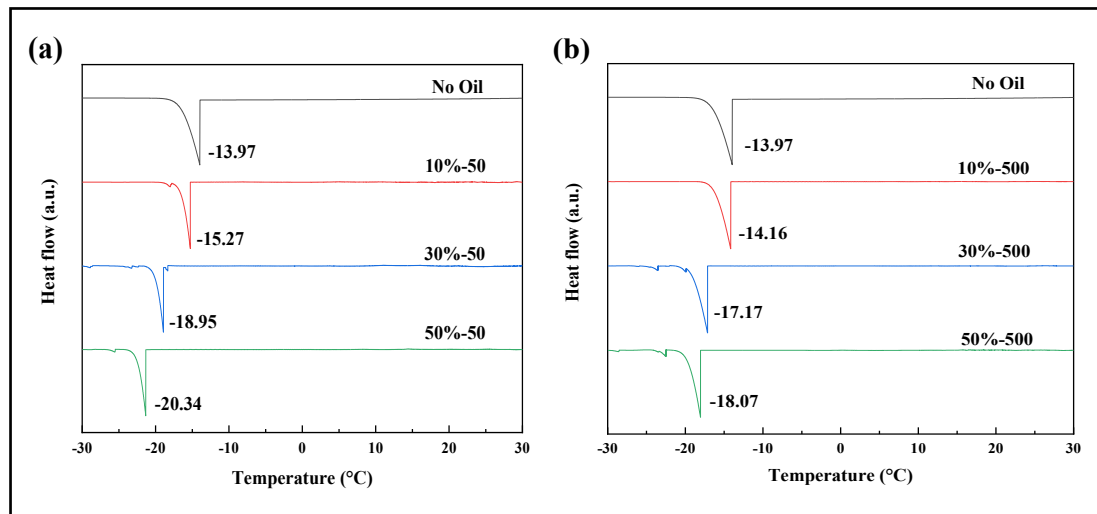
ice formation on the surface. Icephobic properties relate to a decreased ice adhesion strength on a surface that is already covered by ice. Therefore, we evaluated the delay in ice nucleation temperature, the delay in freezing time, and the ice adhesion strength of the textured slippery surfaces in relation to viscosity and silicone oil content.

#### *2.4.5.1 Ice nucleation*

Ice nucleation was determined by DSC analysis of all samples and the contact with droplets of deionized water (Figure 2-9). Compared with the ice nucleation temperature of the PDMS sample without oil (about  $-14\text{ }^{\circ}\text{C}$ ), increasing the oil percentage to 50 wt.% for both oil viscosities (50 and 500 cSt) resulted in a lower ice nucleation temperature to near  $-20\text{ }^{\circ}\text{C}$  and  $-18\text{ }^{\circ}\text{C}$ , respectively. This can be attributed to the heat insulation effect of the lubricating layer that extended the freezing time of water in contact with the surface. The used silicone fluids have a lower thermal conductivity ( $0.00037\text{ cal/s}\cdot\text{cm}\cdot^{\circ}\text{C}$ ) compared with that of the silicone elastomeric matrices ( $0.00062\text{ cal/s}\cdot\text{cm}\cdot^{\circ}\text{C}$ ). It is worth mentioning that thermal conductivity can be described as the capability of a material to transfer heat. Indeed, the heat conducting capability of the material is affected by its thermal characteristics [249]. By increasing the lubricant content, the overall thermal conductivity of oil-infused surfaces decreased. According to the mechanism of ice nucleation, heat transfer through the water droplet–substrate interface plays a vital role in ice nucleation phenomena, and lowering the thermal conductivity can delay ice nucleation [195].

The results showed that the viscosity of the silicone lubricant had no considerable effect on ice nucleation temperature. However, the samples containing a

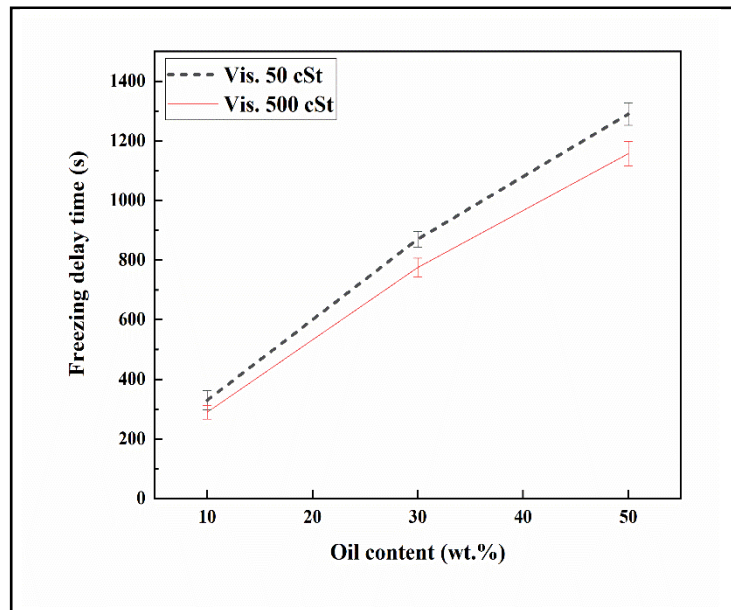
silicone lubricant with 500 cSt viscosity showed a slightly higher ice nucleation temperature than those with a 50 cSt viscosity. The thermal conductivity of polymers depends on physicochemical properties such as viscosity and the molecular weight of polymers. Furthermore, it has been found that thermal conductivity increases as molecular weight and consequently the viscosity of the polymer increases [250]. Therefore, our results confirm that lower viscosity (50 cSt) LITS have a lower thermal conductivity, which leads to slightly lower ice nucleation temperatures relative to those of the 500 cSt LITS.



**Figure 2-9.** Ice nucleation temperatures for samples infused with oils having (a) 50 cSt and (b) 500 cSt viscosities, as determined by differential scanning calorimetry.

We then measured the icing delay time of water on different surfaces. The measurements confirmed the previous results obtained from DSC that the presence of the oil affected the freezing delay time. The freezing delay time for samples containing 50 wt.% silicone oil with viscosities of 50 and 500 cSt increased to about 1300 and

1160 s, respectively (Figure 2-10). The freezing delay time for the sample containing no oil was about 200 s. APPENDIX II (see Figure A.II.1) shows more detailed information about unset ice nucleation and complete freezing time corresponding to each sample.

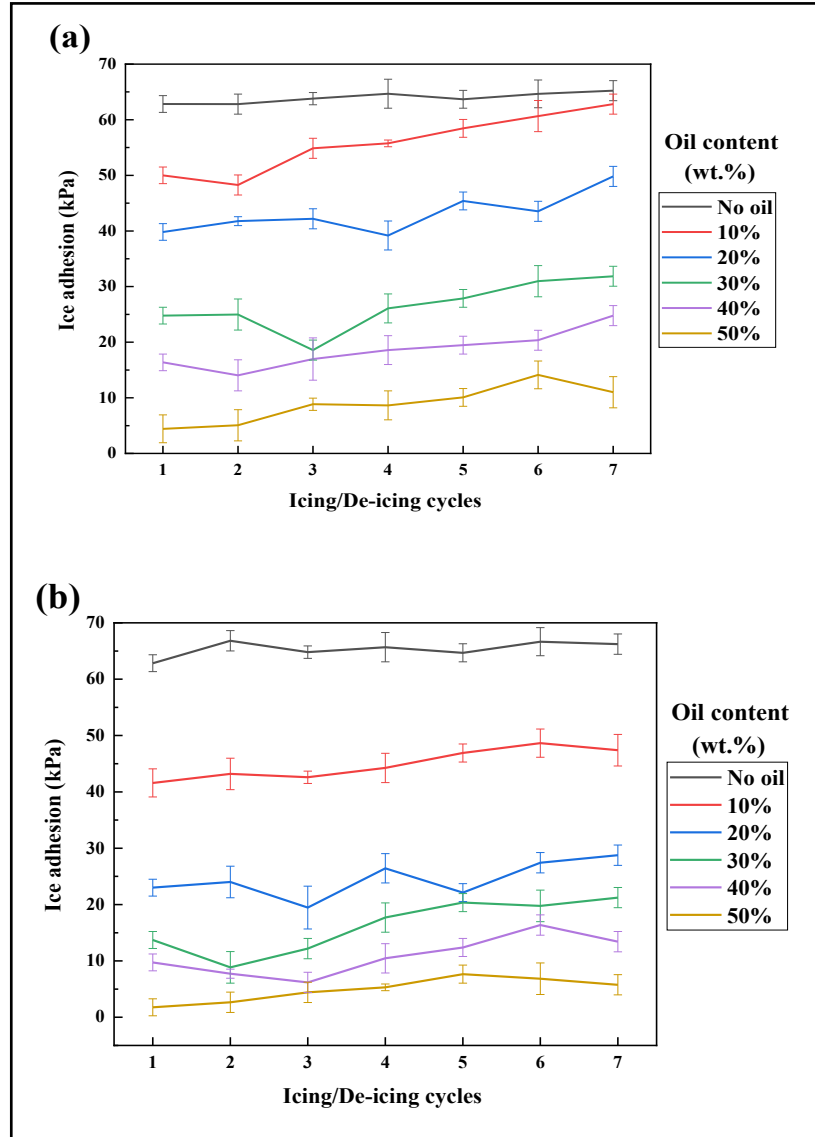


**Figure 2-10.** Ice nucleation time on the surface of samples having various levels of oil infusion for the 50 and 500 cSt viscosity oils.

#### 2.4.5.2 Ice adhesion

The ice adhesion force plays an important role in the icephobic performance of the surfaces covered by ice. We evaluated the change in the ice adhesion strength of the oil-infused textured PDMS surfaces—surfaces differing in oil content and viscosity and a no-oil surface—over seven icing/de-icing cycles (Figure 2-11). A greater oil content for both viscosities markedly decreased ice adhesion strength. This loss of ice

adhesion strength resulted from a higher amount of oil in the ice/surface interface and an increased slipperiness on the surfaces.



**Figure 2-11.** Ice adhesion of samples containing various amounts of infused silicone oil over multiple icing/de-icing cycles for oils of (a) 50 cSt and (b) 500 cSt viscosities.

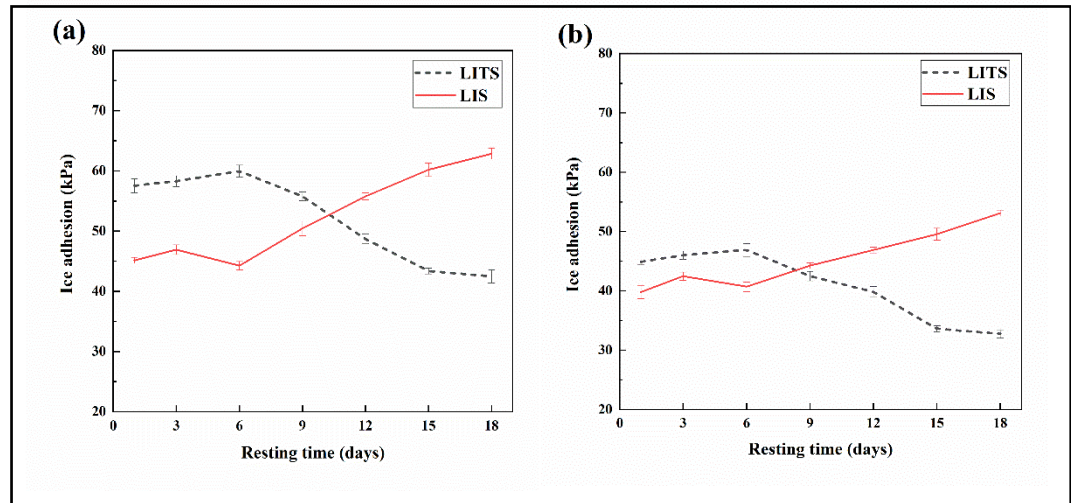
We also observed the general increasing trend in ice adhesion strength over multiple icing/de-icing cycles owing to the depletion of surficial oil after each cycle and resulting in a gradually reduced icephobic performance. Samples containing more than 30 wt.% lubricant (at 50 cSt viscosity) had ice adhesion strengths almost always below 20 kPa (Figure 2-11a), and surfaces infused with the 500 cSt oil required only more than 20 wt.% lubricant to attain similar results (Figure 2-11b). The ice adhesion strength highly depends on the extent of the lubricant presence on the surface.

The lowest ice adhesion strength (<10 kPa) was achieved at the highest level of oil infusion for both oil viscosities (Figure 2-11); because oil migrated more from the bulk material to the surface [251]. Consequently, this led to more lubricant available at the surface to facilitate a greater slippage between ice and surface. It is noteworthy that the high oil content can increase the risk of contaminations in long-term [252].

Moreover, our results showed that the presence of silicone oil on the surface was not considerable at infusion percentages of 10 and 20 wt.% in both viscosities. This low amount of oil on the surface nonetheless increased the slipperiness between ice and the surface. Hence, we concluded that both the low slipperiness and the microtextures were responsible for the observed reduction in the ice adhesion strength compared with the no-oil surfaces.

Given the importance of the rate at which the infused silicone oil migrates from the bulk material to the surface, we conducted an additional investigation to study the impact of resting time, following the preparation of the polymers, on the migration of the silicone oil and, consequently, the ice adhesion strength. We evaluated the ice

adhesion strength of non-textured (LIS) and microtextured (LITS) silicone surfaces at low infusion levels (10 wt.%) for the two oil viscosities of 50 cSt and 500 cSt. (Figure 2-12) to clarify the contribution of both microtextures and the infused oil to ice adhesion strength over time.



**Figure 2-12.** Ice adhesion behavior of LITS and LIS during resting periods for samples (a) 10 wt.% oil infusion and 50 cSt viscosity and (b) 10 wt.% oil infusion and 500 cSt viscosity.

Unlike the LIS samples, immediately after the fabrication of the LITS there was insufficient lubricant on the surface to reduce ice adhesion strength. Because of the mechanical interlocking between the microtextures and the ice, the ice adhesion strength was greater than that of the LIS. The smooth surface of the LIS provided a pinning-point-free surface. As observed in the oil replenishment test (Figure 2-8), the migration rate of lubricant through the LIS samples is greater than that through the LITS. This results in the more visible presence of oil on the LIS even shortly after the



fabrication. Thus, for the LIS, following a resting time and multiple icing/de-icing cycles (3 days), the ice detachment from these slippery smooth surfaces removed oil from the surface and, therefore, increased the ice adhesion strength. In the case of LITS, which have a slower rate of silicone oil migration to the surface than the LIS, the amount of oil on the surface increased markedly after about three rest cycles, leading to a greater slippage between the LITS and the ice. We conclude that, over the long term, the stability of oil on microtextured surfaces is greater than that for untextured surfaces. The microtextures on the LITS samples act as reservoirs for the infused oil and maintain a low ice adhesion strength for a longer duration.

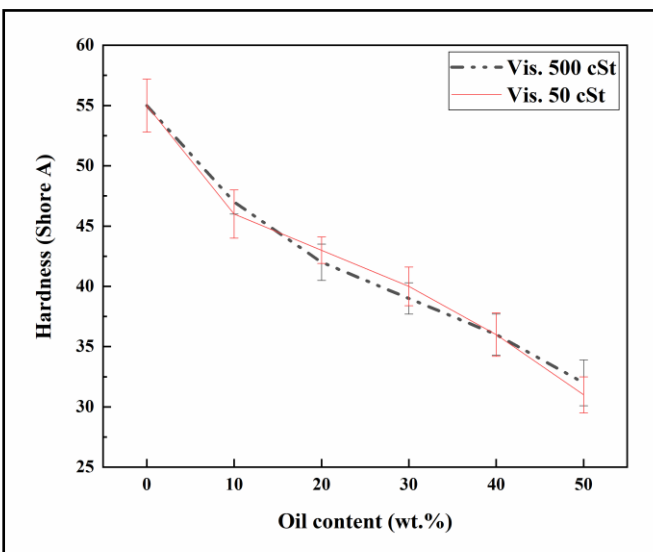
In terms of the role of lubricant viscosity, we observed very similar trends for both low (50 cSt) and high (500 cSt) viscosities for reducing ice adhesion after resting periods (see Figure 2-12). LITS having an oil viscosity of 500 cSt, owing to its relatively higher rate of oil migration toward the surface, retained a sufficient amount of oil on the surface, even at the beginning of the resting test (Figure 2-12b). Hence, it showed relatively stable ice adhesion strengths. As well, the reduction rate of its ice adhesion was lower than samples containing 50 cSt oil. Such surfaces (50 cSt), although showing an increased ice adhesion strength at the beginning of the resting periods, had considerable amounts of oil reaching the surface after three rest cycles; this resulted in a marked reduction in ice adhesion strength. These observations confirmed the important synergetic effect of microtextures and infused oil on the icephobic properties of the LITS samples.

In fact, the presence of microtextures can play a complementary role in icephobic characteristics of the samples beside the oil infusion. Because the

microtextures act as oil reservoirs, ice adhesion strength remains low due to the controlled and prolonged presence of oil on the surface. So, the produced LITS samples can, therefore, be used in practical applications for long periods.

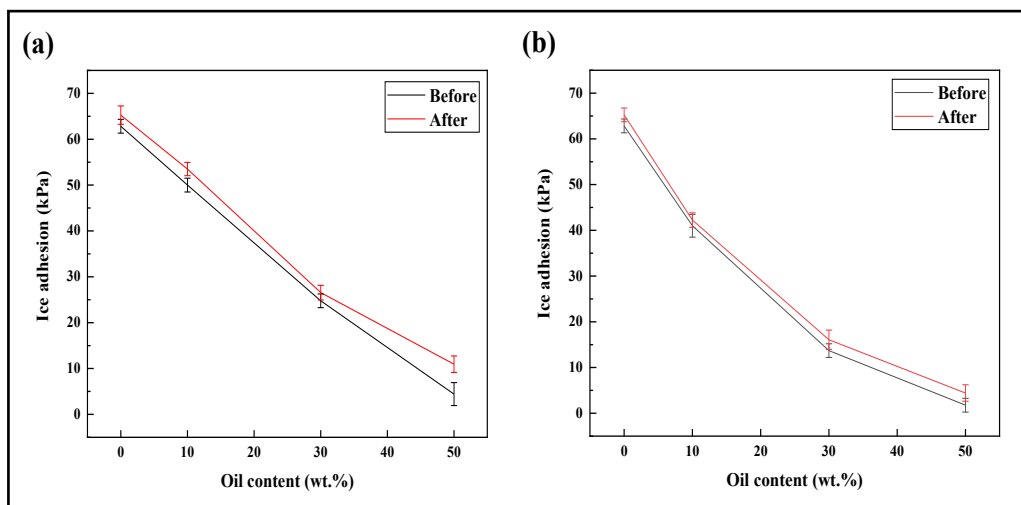
To evaluate the effect of infused oil on the mechanical properties of the produced samples, we conducted hardness tests (Figure 2-13). An increase in the hardness of materials increases modulus elasticity [253]. The surface hardness decreased markedly by as the oil content increased, and this was followed by the reduction of the modulus (Figure 2-13).

Based on the literature, the Young's modulus of ice is between 0.3 and 3.6 GPa; while silicone based coatings usually showed a Young's modulus less than 10 MPa [254,255]. As such, the difference between the modulus of the ice and the surface was heightened. These different mechanical characteristics, which create different strain values under the given applied stress, facilitated the ice detachment from the surface. It is noteworthy that for a rubbery material, the stress distribution is not uniform and is more concentrated at the interface. This phenomenon can help facilitate ice release from the surface [256].



*Figure 2-13. Hardness values in relation to oil viscosity and oil infusion level.*

The ultraviolet radiation and humidity as the weathering conditions can also have a destructive impact on elastomeric surfaces, resulting in their degradation. Here, the effect of such conditions on icephobic properties of fabricated surfaces has been evaluated. The ice adhesion strength did not change significantly after being exposed to 300 h UV light along with humidity condensation, representing about one year and half under real outdoor conditions [5] (Figure 2-14). Thus, it can be claimed that the fabricated surfaces offered an acceptable resistance capability against accelerated UV-light and high humidity.



**Figure 2-14.** Variation of the ice adhesion strength before and after the 300-h-QUV-accelerated-weathering test for samples containing various content of silicone oil with viscosity of (a) 50 cSt, and (b) 500 cSt.

## 2.5 Conclusions

Liquid-infused surfaces (LIS) and liquid-infused textured surfaces (LITS) were successfully fabricated to study the effect of microtextures and lubricant infusion on ice adhesion, ice nucleation, and the long-term durability of such surfaces. We aimed to combine the textured micromorphology and slipperiness of a lubricant-infused silicone elastomer via a replication method. To fabricate microtextured templates, we used a chemical etching method and then applied an anti-stiction coating on microtextured aluminum via SAM. The replication process was completed by transferring the microtextures to a lubricant-infused polymeric surface. Silicone oil of different viscosities (50cSt, 500cSt) were infused at various levels (10, 20, 30, 40, and 50 wt.%) into the silicone elastomeric matrix. A lower oil viscosity produced a higher droplet velocity of the surfaces, although the droplet velocity also depended on the

presence of microtextures and lubricant thickness for the oil viscosities of 50 cSt and 500 cSt, respectively. The heat insulation effect of the lubricant also influenced the ice nucleation temperature; increasing the lubricant percentage for both 50 and 500 cSt viscosity oils reduced the ice nucleation temperature to approximately  $-22\text{ }^{\circ}\text{C}$  and  $-18\text{ }^{\circ}\text{C}$ , respectively, compared with microtextured samples without lubricant (near  $-14\text{ }^{\circ}\text{C}$ ).

The ice adhesion results showed that the designed slippery surfaces can decrease the ice adhesion strength (less than 20 kPa) by four orders of magnitude compared with a reference surface. Oil infusion levels above 30 wt.% for 50 cSt lubricants produced ice adhesion strengths below 20 kPa, and such results were also obtained at infusion levels greater than 20 wt.% for 500 cSt oils. The surficial microtextures also controlled the amount of oil present on the surface and enhanced the durability of the material's anti-icing properties. The microtextures also reduced the rate of oil loss by holding oils at/near the surface. Therefore, relative to the smooth lubricant-infused surfaces, the designed lubricant-infused surfaces produced more durable and stable anti-icing properties for long-term applications.

### **Acknowledgments**

The authors acknowledge all support from the Natural Sciences and Engineering Research Council of Canada (NSERC), Hydro-Québec, and PRIMA Quebec. The authors would like to thank UQAC and CENGIVRE for providing the icing infrastructure. The authors would also like to thank Caroline Potvin at the

Département des Sciences fondamentales, UQAC, for her help in conducting the DSC test.

## **Chapter 3: Icephobic Behavior of a Slippery Coating Containing Nanoporous Particles as Lubricant-Loaded Carriers**

Samaneh Heydarian<sup>1\*</sup>, Reza Jafari<sup>1</sup>, and Gelareh Momen<sup>1</sup>

<sup>1</sup>Department of Applied Sciences, University of Québec at Chicoutimi (UQAC), 555, boul. de

l'Université, Chicoutimi, Québec, G7H 2B1, Canada

\*Corresponding author: samaneh.heydarian-dolatabadi1@uqac.ca

### **3.1 Abstract**

Lubricant-infused surfaces have received increased attention because of their icephobic characteristics. However, the rapid consumption of the lubricant negatively affects the life service of these surfaces. Here we introduced a novel icephobic strategy using the synergistic effect of combining three different anti-icing mechanisms, namely stress localization (matrix), slippery and the formation of unfrozen molecules. Therefore, we fabricated two lubricant-loaded carriers by incorporating silicone oil or hydroxyl-terminated silicone oil within a hydrophobic nanoporous particles. Different quantities of lubricant-loaded carriers were then embedded into an alkoxy silane resin-dimethylpolysiloxane (PDMS) blend having optimized mechanical properties. Using scanning electron microscopy (SEM), thermogravimetric analysis (TGA), and the Brunauer, Emmett, and Teller (BET) method, we confirmed that both types of silicone oils were successfully loaded within the porous aerogels. Even though, the silicone oil-loaded carrier accommodated more lubricant within its structure than the hydroxyl-terminated silicone oil, the coatings with hydroxyl-terminated silicone oil exhibited a

better anti-icing performance. This enhanced anti-icing property can be attributed to the formation of hydrogen bonds between the water molecules and the hydrophilic functional groups of the oil. These coatings also reduced ice accumulation on their surfaces. The coatings containing hydroxyl-terminated silicone oil-loaded carriers (HTSO/A), had a lower ice adhesion strength regardless of their concentration in the filler relative to those containing the silicone oil-loaded carriers. An ice adhesion strength of 15.9 kPa was achieved using 15% hydroxyl-terminated silicone oil-loaded carriers. Reduced ice adhesion in samples containing HTSO/A stems from producing localized stress (matrix), the slippery behavior of the surface and the formation of unfrozen molecules that are hydrogen-bonded with water molecules on their surfaces. The latter mechanism helps these coatings retain stable icephobic characteristics even after 20 icing/deicing cycles.

**Keywords:** Slippery coatings, lubricant-infused coatings, icephobic surface, synergic effect, silicone matrix, lubricant absorbent, hydrogen bonding

### **3.2 Introduction**

Ice accretion can have serious economic, operational, and safety consequences for exposed infrastructure. Ice accumulation events and the associated damage have led to greater interest in reducing the icing of surfaces in harsh cold-weather regions [62,65,257]. Much work has focused on preventing icing on the surfaces by delaying ice formation, limiting ice accretion, and reducing ice adhesion. The innovative use of icephobic coatings is an increasingly sought-after approach for anti-icing applications



because of reduced operational costs for these surfaces and the lack of a need for an external energy input [98,99,258]. Superhydrophobic coatings and slippery liquid-infused porous surfaces (SLIPS) are among those icephobic coatings that have received much recent attention [33,35,84,259,260]. The fabrication of superhydrophobic surfaces usually involves concerns about durability, high costs, and the use of harmful materials, e.g., fluorine-containing substances [68,71,188,197]. On the other hand, SLIPS offer the potential to fabricate durable icephobic surfaces at a reasonable cost. Inspired by *Nepenthes* pitcher plants, SLIPS generally consist of two different parts: a lubricant and a micro-nanostructure infused with the lubricant [78,261]. Unlike superhydrophobic coatings, SLIPS replace a liquid–liquid contact with an air–liquid contact to eliminate water condensation in pores. This scenario reduces ice adhesion considerably, particularly under high-humidity conditions. Moreover, the lubricant can reduce interactions between water droplets and the surface to allow the droplet to slip readily along the surface [37,38,72–74,77,79,80,262].

Crosslinked polymeric systems offer an effective matrix for maintaining the lubricant for an extended duration. In these systems, the lubricant is infused into either a preformed structure, such as a porous material or a polymeric matrix, as a precursor solution for the final coating [23–28]. In the first method, the oil is infused in an already-prepared matrix, resulting in a swelling deformation of the matrix. The second approach can produce more desirable outcomes because there is greater control of the composition of the oil and the matrix to prevent deformation [43,158,246,263,264]. Furthermore, the surfaces can maintain, to some extent, their anti-icing characteristics even after lubricant loss when the matrix is produced from materials having low surface energy or low modulus [200,265].

Wang et al. fabricated silicone-oil-infused dimethylpolysiloxane (PDMS) coatings, in which the low surface energy of both the silicon oil and PDMS and the high mobility of the oil combined to reduce ice adhesion [247]. The very low glass-transition temperature of PDMS also favors the retention of a large free volume at low temperatures in which greater amounts of lubricant can be reserved.

Thus, an effective SLIPS requires a lubricant to meet several criteria. First, the lubricant should be compatible with the matrix. Second, the affinity of the matrix for the lubricant must be much greater than that for the water droplet to be repelled from the surface. Finally, the lubricant should be immiscible with water [128].

Despite having desirable icephobic characteristics, SLIPS have shown limited service time because of lubricant loss, thereby restricting their application. Lubricant can be lost through the capillarity effect, external shear stress, drainage by gravity force, and evaporation [40]. This limited durability remains the key challenge for a wider application of these surfaces.

Several methods have been proposed to enhance SLIPS durability. Aghdam et al. [266] benefited from a layer-by-layer self-assembly technique to fabricate a coating by depositing silica nanoparticles onto a substrate. They then infused a lubricant into the produced porous structure to obtain a slippery surface. The lubricant was trapped in the holes and cracks of the structure to improve the coating's durability, and this thin film preserved 80% of its icephobicity after 50 icing/deicing cycles. Wang et al. [267] fabricated an icephobic coating by infusing the lubricant into a tubular silica composite structure. This coating exhibited a low ice adhesion strength of 17 kPa and reduced the loss of lubricating liquid during the icing/deicing cycles, as the lubricant was locked within the stack-hole structure. Microtexturing can also be used to enhance lubricant

retention. Liquid-infused textured surfaces fabricated with microtextures have a lower ice adhesion and an improved long-term durability. Such surfaces play a critical role in reducing the oil depletion rate because of the oil trapped within the microtextures [47–49].

Using oil-absorbent materials can be considered as another strategy to improve the lubricant retention ability of slippery coatings. The use of oil-absorbent materials (e.g., zeolite, polymers, nanoparticles, and aerogels) has increased in a range of applications [50]. Zhou et al. fabricated the anti-icing surfaces by infusing silicone oil and fumed silica—as an oil reservoir—into the epoxy resin matrix. The prepared surface had an ice adhesion strength of about 10 kPa and maintained a value lower than 20 kPa after multiple icing/deicing cycles [268]. Moreover, aerogels, as 3D nanostructures, are characterized by a high carrier capacity, ultra-low density, a high specific surface area, high porosity, and large interfacial area [269,270]. Their more ecologically benign and nontoxic nature makes these materials preferred over nanoparticles. The particular characteristics of aerogels have made them potential candidates for many applications, in particular as oil-absorbing materials. Kim et al. [224] used a SiO<sub>2</sub> aerogel to hold silicone oil, and this aerogel was dispersed within a PDMS matrix. Using this strategy, the authors tried to decrease the release rate of the oil into the matrix. The fabricate samples showed an ice adhesion strength of <20 kPa at high concentrations of 50-70 wt% (silicone oil-Aerogel/ PDMS), over 20 icing/deicing cycles.

Although in most previous research on SLIPS, the desired icephobic characteristics have been usually obtained through a high oil content, which can cause problems such as mechanical failure during the service life of the surfaces .

Particularly, those studies on oil reservoir have placed less emphasis on the stability of the lubricant in absorbent materials.

The synergistic effect of combining two or more anti-icing strategies can create a more effective coating by avoiding the drawbacks of either strategy [271,272]. It is also noteworthy that in a hybrid anti-icing approach that consists of various strategies, the performance of each strategy should not have any negative effect on the performance of the other. Here, we aim to merge three different anti-icing strategies including stress-localization, slipperiness and producing non-frozen molecules, and fabricate an icephobic coating by incorporating lubricant-loaded aerogels as a carrier within a polymeric matrix. To increase the loading capacity of the carriers and stabilize the lubricant within pores, we use a specific three-step method to incorporate lubricants into the aerogel pores by applying negative pressure. We evaluate the effect of lubricant type on the anti-icing mechanism of the coatings by using two different oils: silicone oil (SO/A) and hydroxyl-terminated silicone oil (HTSO/A). These lubricants are then loaded into hydrophobic silica aerogels that serve as a lubricant carrier. Scanning electron microscopy (SEM), thermogravimetric analyses (TGA), and Brunauer, Emmett, and Teller (BET) tests confirm that the lubricants are successfully loaded into the carrier pores. Furthermore, we add alkoxysiloxane, as a co-binder, into PDMS matrix to compensate for the negative effect of the lubricant on the mechanical properties of the coating. We then design the final coating formula by impregnating various amounts of lubricant-loaded carrier into the prepared matrix. We conducted a comprehensive set of tests and analysis to evaluate the icephobic characteristics of the fabricated coating under various conditions. We determine ice adhesion strength for different ice types using push-off test and centrifuge tests and run differential scanning

calorimetry (DSC) and the Peltier cooling machine to evaluate ice nucleation temperature and freezing time, respectively. We then measure ice accumulation on the samples using a static accumulation test (SAT) and IR camera. Finally, the durability of the samples is assessed by combining the push-off adhesion test with multiple icing/deicing cycles.

### **3.3 Experimental section**

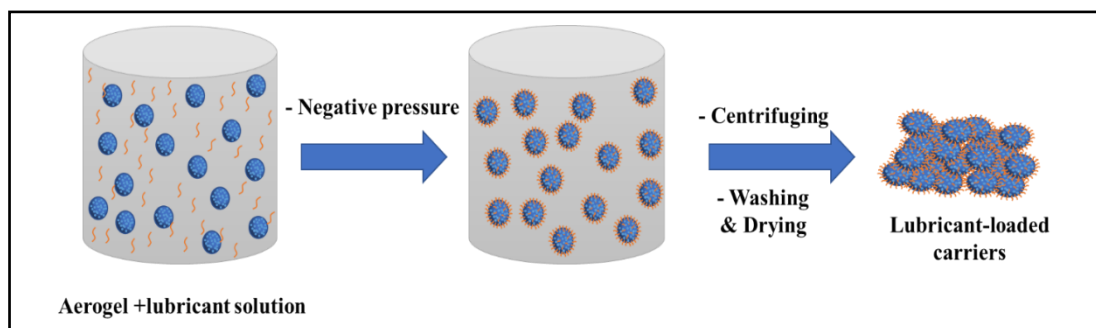
#### **3.3.1 Materials**

Hydrophobic silica aerogel (Enova® Aerogel IC3100), having a 2–40  $\mu\text{m}$  particle size, was purchased from Cabot Aerogel. Sylgard 184 silicone elastomer (polydimethylsiloxane (PDMS)), silicone oil (XIAMETER™ PMX-200 silicone fluid 50 cSt), tetraethoxysilane (TEOS), and reactive alkoxy siloxane resin (DOWSIL™ 2405) were received from Dow Corning. The hydroxyl-terminated silicone oil was obtained from Genesee Polymers.

#### **3.3.2 Preparation of the lubricant-loaded carriers**

The procedure of loading the lubricant inside the carrier comprised three steps (Figure 3-1). First, 10 g of a 60 wt.% solution of lubricant in hexane, as a solvent, was added to 0.1 g of silica aerogel. Second, the prepared mixture was sonicated for 10 min to obtain a uniform dispersion and then vacuumed at 60 kPa at 40 °C for an hour. This step was repeated three times to de-aerate the internal pores of the aerogel. In the final step, a washing procedure with hexane and centrifugation were followed by drying overnight at 60 °C to obtain the lubricant-loaded powders.

We labeled the powders based on the type of lubricant. The lubricant-loaded carriers HTSO/A and SO/A represented silica aerogel infused with hydroxyl-terminated silicone oil and silicone oil, respectively.



*Figure 3-1. Schematic illustration of the preparation process of the lubricant-loaded carriers.*

### 3.4 Fabrication of the coatings

PDMS was blended with alkoxy-siloxane resin at a ratio of 70:30. The alkoxy-siloxane resin acts as a co-binder to enhance the physical performance of coatings. The lubricant-loaded powders were mixed in xylene (as a solvent), and the dispersion was added into the precursor at various percentages on the basis of the weight ratio of lubricant-loaded powders to the precursor (5 wt.%, 10 wt.%, and 15 wt.%). The curing agent was then added to the mixture at a standard ratio of 1: 10 (PDMS: curing agent). TEOS was added to the mixture as a coupling agent. The crosslinking and polymerization reactions between TEOS and alkoxy-siloxane resin create a three-dimensional network structure. The mixture was stirred for 10 min and then applied onto polished aluminum substrates using a Zehntner film applicator. The samples were kept at 80 °C for 24 h to obtain fully cured coatings. The average thickness of cured coatings was about  $100 \pm 5 \mu\text{m}$ , as measured by a micrometer.

### **3.5 Material characterization**

#### **3.5.1 Morphology**

Particle morphology was investigated using a scanning electron microscope (JSM-6480 LV SEM, JEOL Japan).

#### **3.5.2 Thermogravimetric analysis**

Thermogravimetric analysis (TGA) was conducted using a Netzsch STA 449C thermal analyzer under a nitrogen atmosphere to measure the loading capacity of the lubricant carriers. Ten milligrams of each powder was placed into the pan and heated at  $5\text{ }^{\circ}\text{C min}^{-1}$  from an ambient temperature to  $1000\text{ }^{\circ}\text{C}$ .

#### **3.5.3 Surface area measurements**

The specific surface area of the powder sample was obtained by the BET method using a Quadrasorb SI analyzer. Before the analysis, the sample was kept under vacuum for 18.5 h at  $140\text{ }^{\circ}\text{C}$ . Then, the adsorbate, namely  $\text{N}_2$ , was entered into the evacuated chamber. This method is based on the gas-sorption process, in which gas molecules—the adsorbate—form a thin layer on the entire particle surface under vacuum conditions. The amount of gas molecules covering the particle surface is estimated using BET theory. The continued process forms multiple layers of gas molecules that lie parallel to capillarity condensation. Saturation occurs when the pores are filled completely by the  $\text{N}_2$  molecules. Therefore, the total pore volume of the particle can be obtained.

### **3.5.4 Surface characterization**

The static contact angles of deionized water on the fabricated surfaces were measured using a Kruss™ DSA100 goniometer. A 4- $\mu$ L water droplet was deposited onto a surface, and the contact angle was calculated via the Young–Laplace approximation. To account for variability, we repeated our measurements at various places along the surfaces and calculated the average contact angle. The samples' surface profile and roughness were obtained using a confocal laser scanning microscope (Profil3D Filmetrics).

### **3.5.5 Mechanical characterization**

The mechanical properties of the samples were assessed in terms of hardness. We measured the hardness of samples, each having a minimum thickness of  $4.0 \pm 0.1$  mm, using a 2000 max-hand Shore A durometer (Rex Gauge, USA). The accuracy of measurements was ensured by performing five separate tests with a constant load. The measurements were carried out at the ambient temperature of approximately 23 °C.

### **3.5.6 Icephobic Properties**

The ice nucleation temperature of the fabricated samples was evaluated by differential scanning calorimetry (DSC). The inner surface of a DSC lid was coated with a thin layer of each coating, and after the curing process, 5 mg of deionized water was placed onto the coating surface, subsequently sealed by the lid. An empty sealed pan served as a reference. The samples were cooled from 30 to  $-40$  °C. The cooling rate was selected as a 5 K/min ramp.



The freezing time of the water droplets on the samples was obtained using a Kruss contact angle meter. The machine was equipped with a Peltier cooling plate adjusted to  $-20\text{ }^{\circ}\text{C}$ . The effect of humidity on our measurements was minimized by placing anhydrous calcium sulfate desiccants within the cold chamber.

The ice adhesion strength of each sample was evaluated using push-off and centrifugal tests. Different methods were required to determine ice adhesion under variable icing conditions. In the push-off test, nonimpact ice was used; thus, a 1-cm-diameter cylindrical mold placed onto the sample was filled by deionized water and kept in a cold chamber at  $-10.0 \pm 0.2\text{ }^{\circ}\text{C}$  overnight to obtain a cylinder of completely frozen water. The probe of the force meter approached the ice at  $0.05\text{ mm}\cdot\text{s}^{-1}$  into the side of the cylindrical column. We recorded the maximum force required to detach the ice column from the sample surface and then divided this value by the cross-sectional area of the cylindrical column to obtain the ice adhesion strength. The same process was repeated to evaluate the durability of the coatings over multiple icing/deicing cycles.

In the centrifuge test, supercooled water microdroplets were sprayed onto the samples, glued to aluminum beams, at  $-10\text{ }^{\circ}\text{C}$  to produce glaze ice with an average thickness of  $7 \pm 1\text{ mm}$ . The beams were placed onto the centrifuge apparatus to obtain the maximum centrifugal force required to detach the deposited glaze ice.

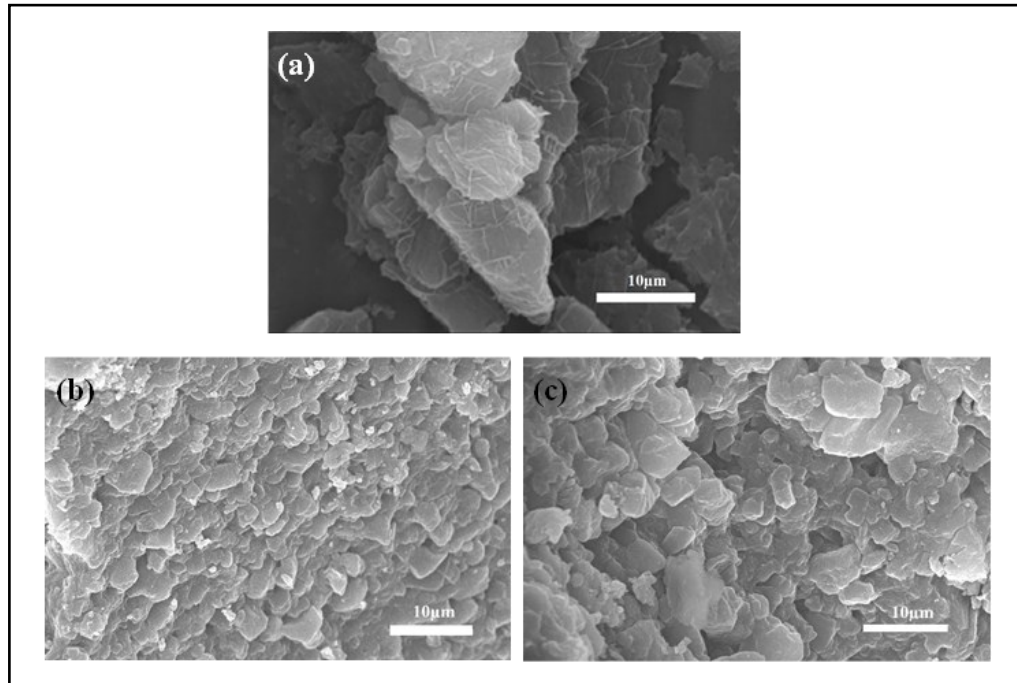
Ice accumulation on the surfaces was evaluated by the static accumulation test (SAT) at various inclinations, including  $0^{\circ}$ ,  $45^{\circ}$ , and  $80^{\circ}$ . The coatings were applied to  $3\text{ cm} \times 15\text{ cm}$  aluminum substrates for this test. The samples were placed onto holders, fixed at the aforementioned angles, and kept at  $-5.0\text{ }^{\circ}\text{C}$ . The samples were then exposed to 15 min of precipitation of microdroplets, having an average diameter of  $327\text{ }\mu\text{m}$ , at

4°C. The samples were then kept at  $-5.0$  °C for 45 min. The amount of ice accumulated on the samples was obtained through the difference between the sample mass before (without deposited ice) and after (with deposited ice) precipitation. Furthermore, an Optris PIX infrared camera was utilized to monitor the surface temperature of sample during SAT.

### **3.6 Results and discussion**

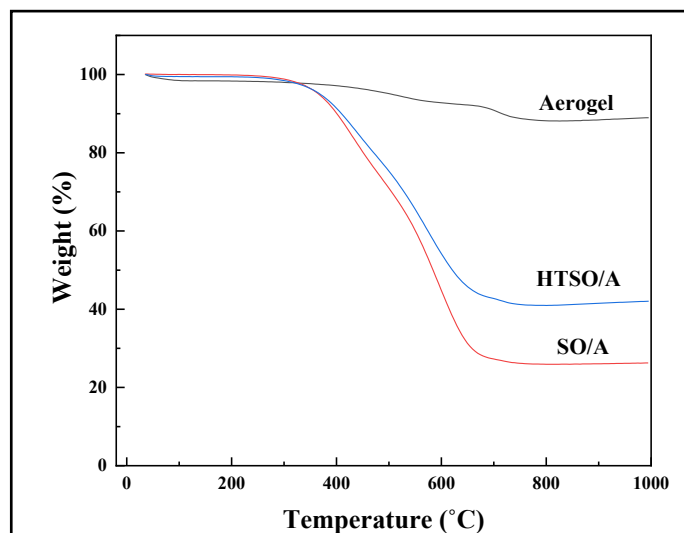
#### **3.6.1 Characterization of the lubricant-loaded aerogel**

The SEM images of the as-received aerogel, silicone oil-loaded aerogel, and hydroxyl-terminated silicone oil-loaded aerogel demonstrate that the sharp edges of aerogel, to some extent, disappeared when it was loaded with lubricant and the oils accommodated within the micropores (Figure 3-2). It was expected that the loaded oils would migrate toward the surface to maintain a slippery surface. The silicone oil can infuse into the pores of the silica aerogel because of the capillarity pressure effect and weak Van der Waals interactions [270]. The silicone oil molecules are adsorbed into pore walls until the inner surface of the pores is covered by the oil. Then, the other molecules of silicone oil are joined onto the adsorbent oil molecules via weak forces, such as Van der Waals; consequently, the pores are filled by the lubricant [270]. This infused lubricant can migrate into the matrix by a concentration gradient pressure and then be delivered into the surface because of the high mobility of the silicone oil within the large free volume of the matrix [157].



**Figure 3-2.** Micrographs of the (a) as-received aerogel, (b) silicone oil-loaded carriers, (c) hydroxyl-terminated silicone oil-loaded carriers.

Thermogravimetric analyses evaluated the loading capacity of the lubricant carrier in terms of the oil type. As the samples were heated to 1000 °C, the residual masses of the as-received aerogel, HTSO/A, and SO/A were approximately 89%, 42%, and 26%, respectively (Figure 3-3). Compared with the mass loss of the silica aerogel (around 11%), the loaded-lubricant mass values for the HTSO/A and SO/A powders were greater at about 47% and 63%, respectively. Thus, the silicone oil had more tendency to be absorbed by the hydrophobic-modified aerogel than the hydroxyl-terminated silicone oil, likely because of the hydrophobic nature of silicone oil.



**Figure 3-3.** Thermogravimetric curves for the as-received aerogel and aerogel carriers loaded with silicone oil (SO/A), and hydroxyl-terminated silicone oil (HTSO/A).

We also used the BET method in which N<sub>2</sub> sorption informs on the loading efficiency of the particles, i.e., the change in particles' porosity and reduction in pore volume can be estimated. Pore volume decreased from 2.173 cc/g for the aerogel to 0.108 cc/g for silicone oil-loaded particles and 0.270 cc/g for hydroxyl-terminated silicone oil-loaded particles; thus, the oils had penetrated the aerogel's pores (see Table 3-1).

**Table 3-1.** Surface area analysis of the carriers using the BET method.

	<i>As-received aerogel</i>	<i>SO/A</i>	<i>HTSO/A</i>
<b>Pore volume (cc/g)</b>	2.173	0.108	0.207
<b>Surface area (m<sup>2</sup>·g<sup>-1</sup>)</b>	536.64	35.022	57.7

Moreover, in agreement with TGA, the loading capacity for the silicone oil was greater than for the hydroxyl-terminated silicone oil. The surface area of the particles also decreased after infusing the lubricant. This decrease reflects the filling of the micropores. This penetration of the lubricant firmly traps the oil and is critical for creating long-lasting slippery behavior.

### **3.6.2 Selection and characterization of the matrix**

Impregnating the lubricant into the matrix can result in low ice adhesion; however, this infusion also alters the mechanical properties of the coating [255]. Thus, given that an excessive amount of silicone oil can affect the mechanical properties of a PDMS coating, we used an alkoxy siloxane-PDMS blend as the main matrix to enhance the mechanical properties of the prepared coating. By blending these polymers, we aimed to obtain a matrix with some properties of each component. In the other word, the prepared blend will have some desired characteristics of both polymers in the right combination [273].

Table 3-2 illustrates the hardness values corresponding to different combinations of PDMS and alkoxy siloxane. Matrix hardness values increase as alkoxy siloxane is added until peaking at a 70:30 ratio (PDMS: alkoxy siloxane) due to the presence of alkoxy siloxane that acts as hard segments like a filler [274]. At the reduced hardness at a 60:40 ratio, we observed a miscibility of the two components, likely because of a saturation of the alkoxy siloxane in PDMS. We therefore used alkoxy siloxane as a co-binder at a ratio of 70:30 to compensate for the negative effect of lubricant on the coating's mechanical properties and enhancing coating durability. So, the matrix would have both icephobic and mechanical characteristics of PDMS and

alkoxysiloxane, respectively. Besides, mixing polymers can promote the free volume in the structure of the prepared blend [273], facilitating the migration of oil from the bulk into the surface.

*Table 3-2. Hardness values of the fabricated samples, as obtained by the Shore A durometer.*

<b>Mixture (PDMS: alkoxy siloxane)</b>	<b>100:0</b>	<b>90:10</b>	<b>80:20</b>	<b>70:30</b>	<b>60:40</b>	<b>0:100</b>
<b>Hardness (Shore A)</b>	55 ± 2	64 ± 1	66 ± 2	68 ± 1	58 ± 1	80 ± 2

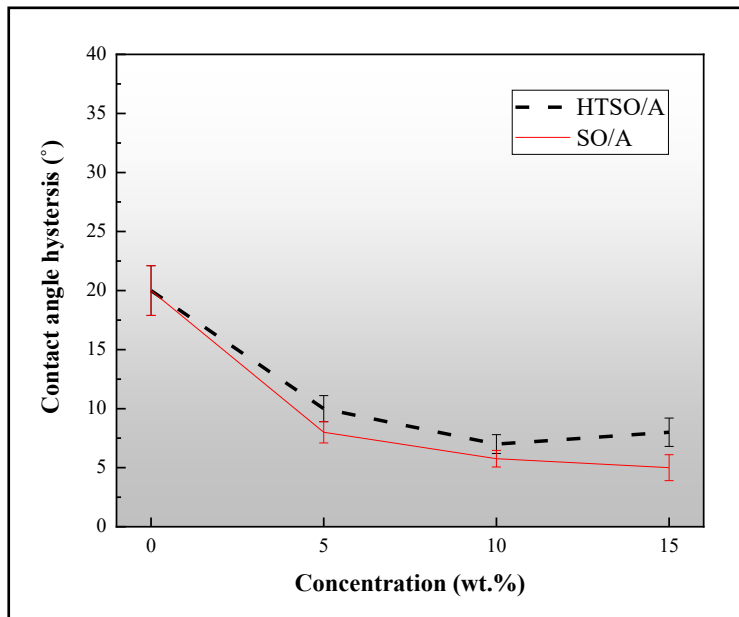
### **3.6.3 Characterization of the coatings containing the lubricant-loaded carriers**

#### *3.6.3.1 Surface characterization*

##### *3.6.3.1.1 Wettability*

Generally, impregnating of lubricant-loaded carrier will affect surface wettability. Using the water contact angle as a measure of wettability, we observed that the contact angle did not change markedly for either oil type in terms of lubricant-carrier content. However, we did note that the water contact angle decreased from about 105° for the reference to approximately 94° and 88° for samples containing SO/A and HTSO/A, respectively.

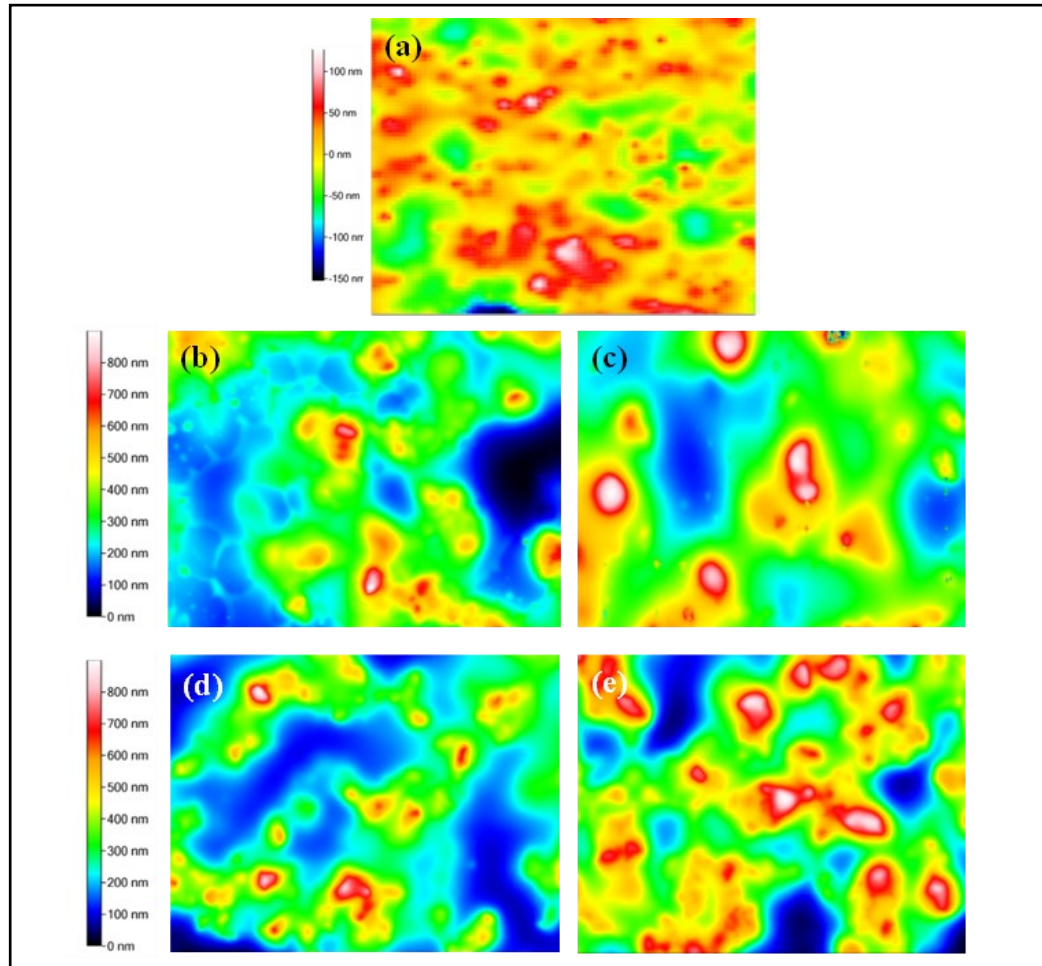
Moreover, increased concentrations of both SO/A and HTSO/A produced a lower water contact angle hysteresis (CAH) (Figure 3-4). A low CAH prevents the pinning of the water droplet and, consequently, eases the removal of the droplet from the surface. Finally, we noted that the CAH values for the HTSO/A samples were slightly higher than those for the SO/A samples.



**Figure 3-4.** *The contact angle hysteresis of samples containing (SO/A) and (HTSO/A) in relation to concentration of the lubricant-loaded carriers.*

### 3.6.3.1.2 Topography

The profilometry technique was used to evaluate topography of samples (see Figure 3-4) as well as their surface roughness (Table 3-3). Surface roughness increased with a greater amount of lubricant-loaded carriers in the coatings. Samples containing HTSO/A had a higher surface roughness than the SO/A samples for a similar carrier concentration (Figure 3-5). TGA demonstrated that the HTSO/A powders consisted of a higher percentage of aerogel than for the SO/A powders; thus, for the same lubricant-loaded carrier content, a higher amount of aerogel was present within the HTSO/A coatings than the SO/A coatings, resulting in the higher surface roughness for the HTSO/A samples.



**Figure 3-5.** 3D topographical maps of the (a) reference and samples containing (b) 5%, and (c) 15% silicone oil–infused aerogels and samples containing (d) 5% and (e) 15% hydroxyl-terminated silicone oil–infused aerogels.

**Table 3-3.** Surface roughness parameters of the fabricated coatings.

Roughness parameters	Reference	SO/A-5	SOA-15	HTSO/A-5	HTSO/A-15
RMS roughness ( $S_q$ -nm)	33.19	121.2	266.8	126	319.5
Skew ( $S_{sk}$ )	-0.149	0.946	0.190	0.5355	0.912

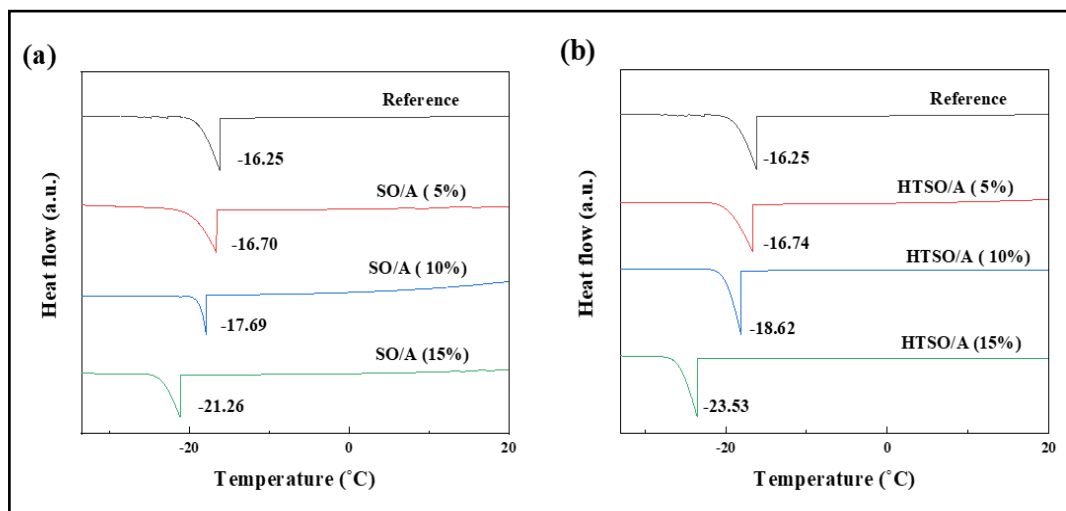


### 3.6.4 Icephobicity

The coating's performance against icing is usually assessed using various measurements, including ice nucleation temperature, average freezing time, ice adhesion strength, and the quantity of ice accumulation. Indeed, these methods can be categorized into two general groups. Some of the mentioned tests, such as measuring ice nucleation time measures delays in icing and the temperature of supercooled water droplets to enable water droplets to slip off a surface *before* freezing. Some other test methods, like ice adhesion measurements evaluate the icephobic performance of the coating in removing ice *after* freezing.

#### 3.6.4.1 Ice nucleation time and temperature

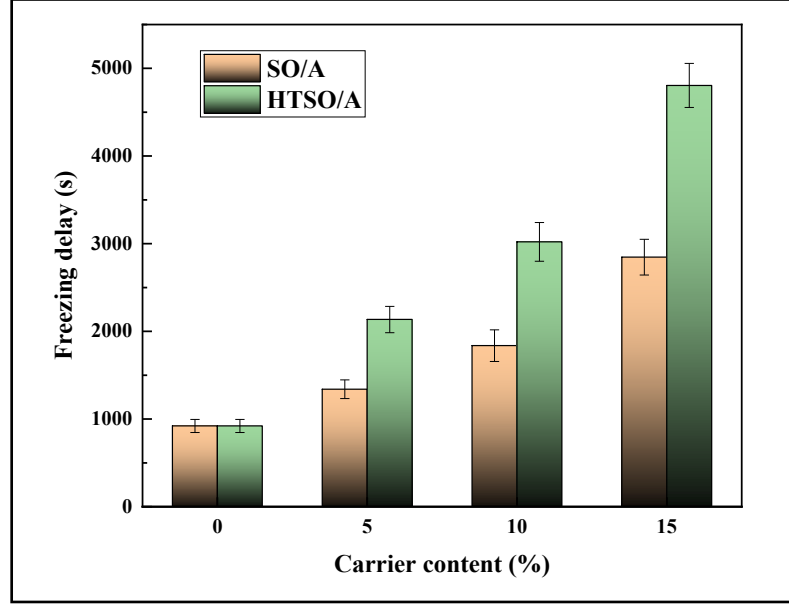
Differential scanning calorimetry was used to evaluate ice nucleation temperature on the coating in contact with the water droplet. As illustrated in Figure 3-6 the ice nucleation temperature on the reference sample was  $-16.25\text{ }^{\circ}\text{C}$  and it continuously decreased by increasing the percentage of lubricant-loaded carrier powders of HTSO/A and SO/A. Incorporating lubricant-loaded powders within the polymeric matrix reduced ice nucleation temperature, and this effect was greater for the HTSO/A samples ( $-23.53\text{ }^{\circ}\text{C}$  at 15 wt.%) than for SO/A samples ( $-21.26\text{ }^{\circ}\text{C}$  at 15%).



**Figure 3-6.** Evaluation by differential scanning calorimetry (DSC) of ice nucleation temperatures corresponding to samples containing carriers loaded with (a) silicone oil-infused aerogels (SO/A) and (b) hydroxyl-terminated silicone oil-infused aerogels (HTSO/A).

To better understand the effect of type and content of lubricant on the anti-icing characteristics of the coating, we also measured freezing times. Figure 3-7 presents the icing delay measurement of different surfaces. Water droplets on the reference froze on average after 921 s. This freezing time extended to 1340, 1837, and 2846 s for samples containing 5, 10, and 15 wt.% of SO/A, respectively. These times reached 2135, 3021, and 4805 s for samples containing 5, 10, and 15 wt. % of HTSO/A, respectively. This pattern agreed with the DSC results, as samples containing HTSO/A demonstrated a better anti-icing performance than SO/A-filled samples, and they could prolong icing time more effectively. This desirable effect on ice nucleation and freezing time relates to how heat insulation affects the lubricant layer. The silicone oils have a lower thermal conductivity than silicone elastomeric matrices. Increasing the lubricant content within the matrix reduces the total thermal conductivity of the coating. This

affects the heat transfer through the water droplet–coating interface, which has an essential role in ice nucleation, leading to a delay in freezing time.



**Figure 3-7.** Water droplet freezing time on the surface of the samples containing silicone oil–infused aerogels (SO/A) and hydroxyl-terminated silicone oil–infused aerogels.

The better anti-icing performance of HTSO/A-infused samples can be attributed to the hydroxyl groups of the lubricant, which enhance hydrogen bonding between the lubricant layer on the surface and the water molecules. The bonding could contribute to the ice nucleation delay. To improve our understanding of this phenomenon, we applied Eq. 3-1, in which the ice nucleation rate  $J$  can be obtained.

$$J \propto \frac{k_B T}{h} \exp\left(-\frac{\Delta G_f^*}{k_B T} - \frac{\Delta g_{act}}{k_B T}\right) \quad (\text{Eq. 3-1})$$

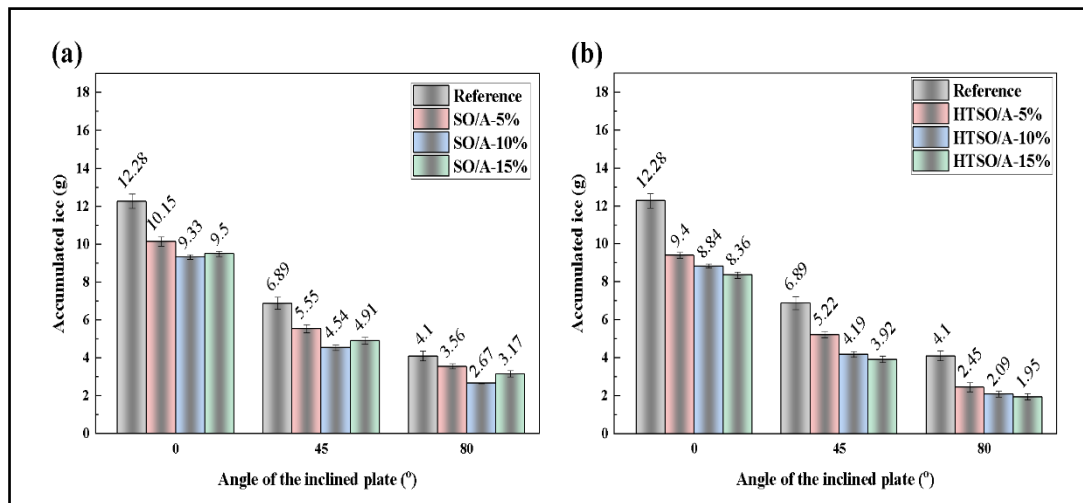
where  $\Delta g_{act}$  and  $\Delta G_f^*$  are the activation energy barriers and the Gibbs free energy, respectively. Furthermore,  $K_B$  and  $h$  are constants, and  $T$  is the absolute temperature. In the process of nucleation, water molecules must diffuse into an ice–water interfacial layer to join an ice embryo. In the above equation,  $\Delta g_{act}$  is described as an energy barrier corresponding to the diffusion of water molecules. The formation of hydrogen bonds between the water molecules and the hydroxyl groups of the lubricant slows the transfer of water molecules because of an increased viscosity [275]. Thus, it leads to increased  $\Delta g_{act}$  and, subsequently, increase of the ice nucleation rate  $J$ , which prolongs the ice nucleation time.

#### 3.6.4.1.1 Ice accumulation

Ice accumulation occurs as supercooled water droplets contact the surface at subzero temperatures. The SAT method evaluates the amount of ice accumulated on the surface at various inclinations (in our case 0°, 45°, and 80°). Generally, increased lubricant-loaded carrier content decreased ice accumulation on the surface (Figure 3-8).

For samples containing HTSO/A, this trend was apparent at all angles and samples, and ice accumulation decreased from 12.28, 6.89, and 4.1 g (for the reference) to 8.36, 3.92, and 1.95 g (at 15% carrier content) at 0°, 45°, and 80°, respectively. However, increasing SO/A content from 0% to 10% in the coating decreased the amount of ice accumulated on the samples at all angles. Ice accumulation increased at all angles when SO/A content was 15%. On an inclined surface, the tangential component of gravity force—equal to  $W \sin \alpha$  ( $W$ , droplet weight;  $\alpha$ , angle corresponding inclination)—acts as the key factor for removing ice from the surface.

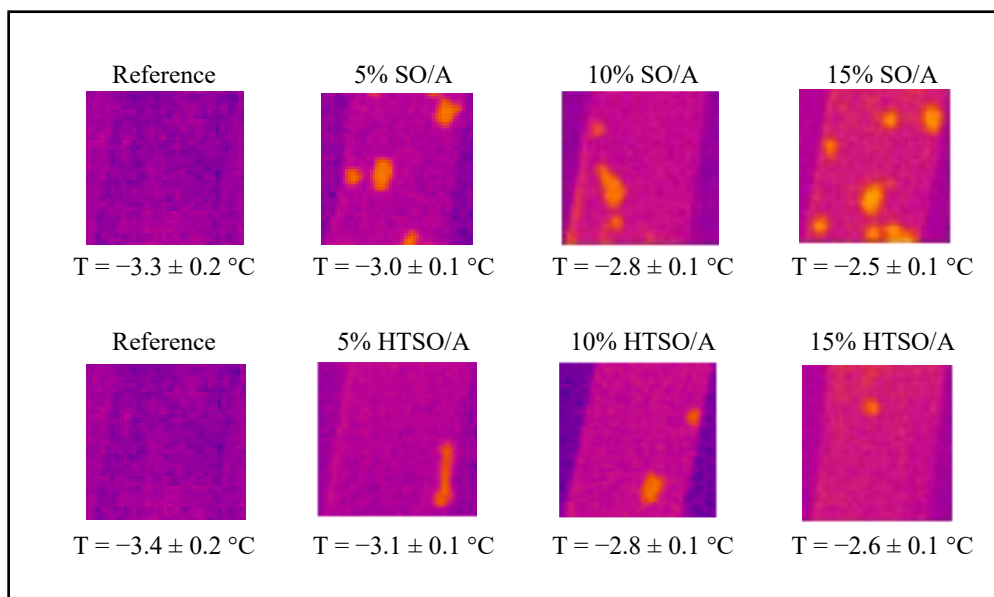
Therefore, a greater inclination ( $\alpha$ ) enhances ice removal. At an inclination of  $0^\circ$ , there is no tangential component of the gravitational force ( $\sin 0^\circ = 0$ ), and this angle is usually used to determine the intensity of the precipitation. However, ice accumulation at  $0^\circ$  experienced a similar trend as ice accumulation at  $45^\circ$  and  $80^\circ$  for both types of lubricant-loaded carrier. Moreover, we expected to have less ice accumulation at  $80^\circ$  than at  $45^\circ$  because the tangential component corresponding to  $80^\circ$  is greater than that at  $45^\circ$  ( $\sin 80^\circ > \sin 45^\circ$ ). On the other hand, ice adhesion strength is the main force resisting ice detachment from the surface. Therefore, evaluating the ice adhesion can help explain the observed ice accumulation on the surfaces (see Section 3.3.3).



**Figure 3-8.** Ice accumulation on samples containing (a) silicone oil-infused aerogels (SO/A) and (b) hydroxyl-terminated silicone oil-infused aerogels (HTSO/A) on surfaces inclined at  $0^\circ$ ,  $45^\circ$ , and  $80^\circ$ , as measured by a static accumulation test.

Furthermore, infrared thermographs of the samples tilted at  $80^\circ$  after 5 minutes of precipitation showed that the surfaces of the samples were not fully covered by the supercooled water droplets. This indicates that the higher temperature observed in samples containing the lubricant-loaded carrier is caused by the oil's impact on the

overall heat insulation of the coatings (Figure 3-9). This effect agrees to a large degree with the observations for ice nucleation and freezing time.



**Figure 3-9.** Infrared thermographs of the samples on surfaces inclined at  $80^{\circ}$  after 5 min of precipitation.

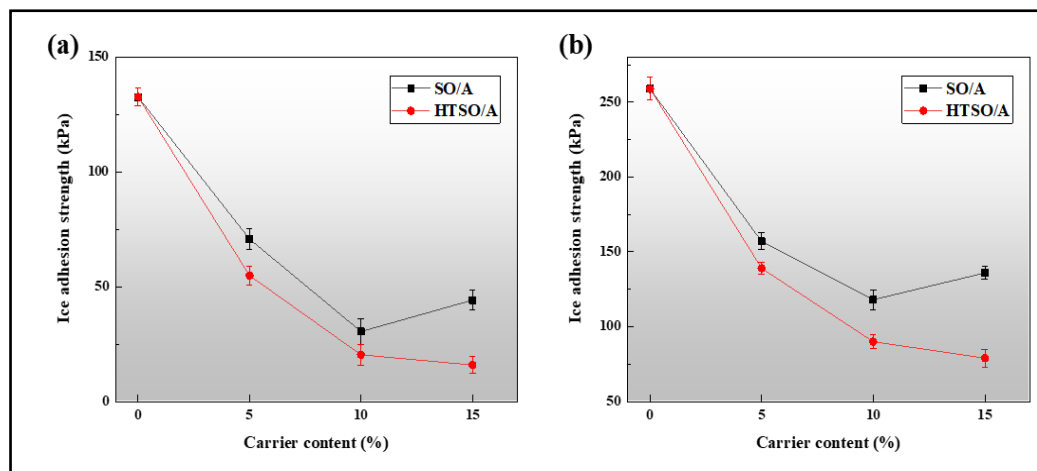
#### 3.6.4.2 Ice adhesion

To expand upon the interaction between the ice and the surface highlighted by the ice accumulation tests in the preceding section, we applied two different methods to examine ice adhesion strength. Ice adhesion is influenced by multiple factors, including surface elasticity, surface topography, liquid extent, and surface chemistry [168]. We used two methods, the push-off and centrifugal adhesion tests, to test nonimpact bulk ice and glaze ice, respectively. The glaze ice conditions represent harsher icing conditions than those analyzed by the push-off adhesion test. The blend of alkoxy siloxane resin and PDMS, used as the matrix, had a lower ice adhesion strength (133 kPa) than the PDMS coating (about 270 kPa), measured by a push-off

test (Figure 3-10a). This difference relates to the difference in the modulus of the alkoxy siloxane resin and that of PDMS, which promotes stress localization during ice detachment [194]. Since polymeric blends are generally immiscible, and it is rare to obtain a homogenous blend in molecular scale [273][276], so, the blends would consist of two soft (PDMS) and hard (alkoxy siloxane). Therefore, under the applied stress, each part can produce different strain value than other. By considering the high modulus of ice, it can promote the localized stress on the surface, resulting in produce micro cracks in ice-surface interface and consequently, ice detachment.

Adding HTSO/A to the coating decreased ice adhesion strength from 133 to 15.9 kPa, whereas SO/A-containing samples experienced a decreasing ice adhesion until 10% to 30 kPa, then increased to about 44 kPa for the 15% SO/A-containing samples. In general, the reduced ice adhesion of both silicone oil groups can be attributed to the effective role of the oil that spreads over these surfaces, allowing the ice to slide over the surface. By increasing the amount of lubricant-loaded carrier, the availability of oil over the surface was greater. Consequently, the smaller direct contact area between the ice and the substrate reduced ice adhesion. Furthermore, the ice adhesion strength for samples containing HTSO/A decreased faster than for SO/A-containing samples; therefore, lower ice adhesion strengths were achieved using HTSO/A at all concentrations. In samples containing HTSO/A, in addition to the mechanism of the slippery surface, there is another factor that affects ice adhesion. The hydrophilic groups of the hydroxyl-terminated silicone oil interact with water molecules to form hydrogen-bonded molecules. These molecules can remain unfrozen even at subzero temperatures and reduce ice adhesion strength [168]. In another words, combining three different anti-icing mechanisms, namely producing localized stress

(matrix), slipperiness (lubricant), and formation of unfrozen molecules (hydroxyl groups) play the main role in lowering ice adhesion in coatings containing HTSO/A. TGA demonstrated that HTSO/A had a lower oil content than SO/A; nonetheless, because of the synergistic effect of the above-mentioned mechanisms, this lower lubricant content still accompanied a lower ice adhesion strength for HTSO/A-containing samples than SO/A-containing samples. Moreover, the greater ice adhesion strength of SO/A-containing samples at concentrations greater than 10% may relate to the increased surface roughness (see Figure 3-4), which enhances the mechanical interlocking between the ice and the surface asperities.



**Figure 3-10.** Ice adhesion strength of samples containing silicone oil–infused aerogels (SO/A) and hydroxyl-terminated silicone oil–infused aerogels (HTSO/A), obtained using (a) push-off and (b) centrifuge tests.

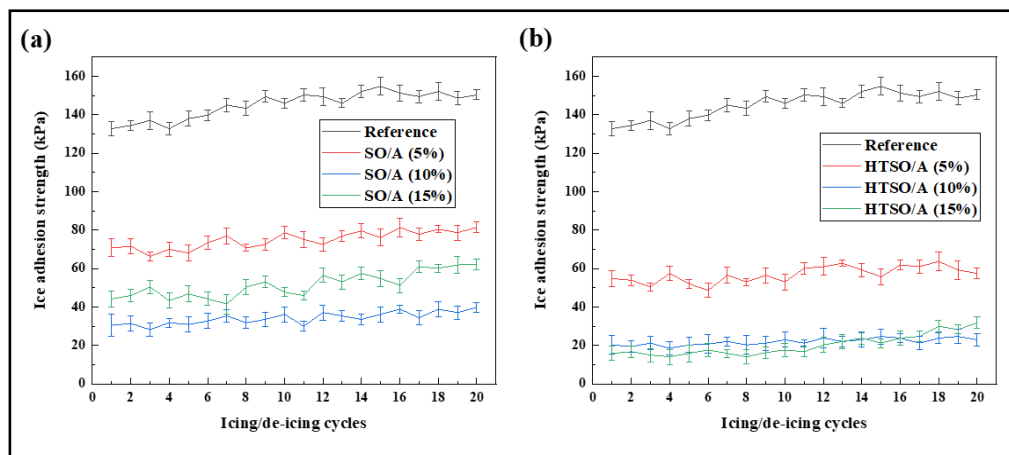
The results of the centrifugal tests of the samples showed similar trends to those of the push-off tests (Figure 3-10b). For samples containing HTSO/A, ice adhesion decreased from 259 to 79 kPa as the carrier quantity increased. For samples containing SO/A, the ice adhesion strength dropped to its lowest value, 118 kPa at 10%; it then



increased to 136 kPa at 15%. The ice adhesion strengths obtained by the centrifuge tests were generally higher than those measured by the push-off tests because of the harsher ice conditions in the former.

### 3.6.5 Coating durability

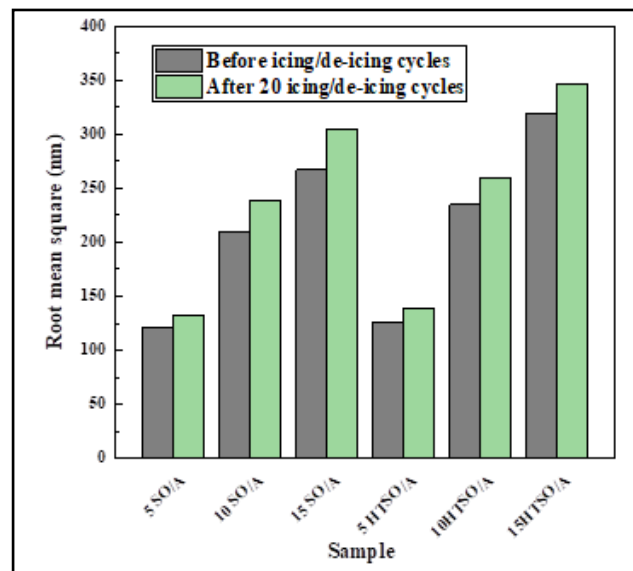
The durability of the coatings was evaluated by monitoring ice adhesion measured via a push-off test during 20 icing/deicing cycles (Figure 3-11). For samples containing SO/A at lower concentrations, namely 5% and 10%, we observed relative stability in ice adhesion during repeated icing/deicing cycles; ice adhesion remained below 81 kPa and 40 kPa, respectively. For samples containing 15% SO/A, ice adhesion strength varied between icing/de-icing cycles and showed an increasing trend associated with a loss of silicone oil and increased roughness relative to the samples having less aerogel.



**Figure 3-11.** Ice adhesion strength in samples containing (a) silicone oil-infused aerogels (SO/A) and (b) hydroxyl-terminated silicone oil-infused aerogels (HTSO/A) over 20 icing/de-icing cycles, as measured by push-off tests.

For all samples containing 5% and 10% HTSO/A, the ice adhesion was, to a great extent, stable over the 20 icing/de-icing cycles. For samples containing 15% HTSO/A, we observed no considerable change in ice adhesion until the 12<sup>th</sup> cycle; beyond this point, ice adhesion gradually increased, probably because of oil consumption and increased surface roughness.

To confirm these results, we also compared the surface roughness of the original samples with that of samples having undergone 20 repeated icing/de-icing tests (Figure 1-12). In general, the surface roughness of all samples increased after 20 icing/de-icing cycles, probably because of oil consumption. However, the roughness of the SO/A-containing samples increased to a greater degree than those containing HTSO/A. This difference stemmed from the additional icephobic mechanism of the HTSO/A-containing samples, which lowered the ice adhesion strength of the surfaces, in turn limiting oil depletion and improving the coating durability.



**Figure 3-12.** Root mean square ( $R_q$ ) of surface roughness after 20 icing/deicing cycles.

The porous aerogel enhanced the locking of oil within the coating. Removal of the oil layer from the uppermost surface transfers lubricant from the microporous structure of the carriers to the upper surface because of the capillary effect. Therefore, as the available oil layer on the surface was eliminated during contact with ice, an oil concentration gradient developed between the surface and the bulk material. This difference acts as the driving force for transferring oil toward the surface. Using a lubricant-loaded carrier slows this migration and ensures the availability of a slippery behavior for a more extended period. Moreover, the icephobic performance of the HTSO/A-containing samples is more desirable than for other surfaces, a performance that can be attributed to the hydroxyl groups of the HTSO/A lubricant. The hydrogen bonding between the water molecules and hydroxyl groups on the oil help stabilize ice adhesion strength, even with a greater oil content.

### **3.7 Conclusions**

We fabricated slippery coatings by infusing lubricant-loaded carriers into a polymeric matrix. The lubricant-loaded carriers were prepared by infusing two different lubricants, namely silicone oil and a hydroxyl-terminated silicone oil, into a hydrophobic-modified aerogel. Thermographic analysis demonstrated that about 47% and 63% of the lubricant-loaded carrier mass consisted of silicone oil and hydroxyl-terminated silicone oil, respectively. A decrease in the pore volume and surface area of the powders after lubricant loading confirmed that the oil was accommodated within the micropores of the aerogel. Various concentrations of each type of lubricant-loaded carrier were then added into an alkoxysiloxane resin-PDMS blend. Incorporating the lubricant-loaded carriers and altering their content positively affected the anti-icing

characteristics of the coatings. Increasing the HTSO/A content produced a lower ice nucleation temperature and a longer freezing time relative to those containing SO/A. Furthermore, ice accumulation on the surfaces was generally lower as the amounts of lubricant-loaded carrier increased. Ice accumulation for the SO/A-containing samples increased for all surface inclinations once the lubricant concentration was above 10%, likely because of increased surface roughness.

Evaluating ice adhesion can explain the observed trends in ice accumulation. Samples containing HTSO/A benefited from a reduced ice adhesion because of the presence of the slippery-surface mechanism and the formation of hydrogen bonds between the hydroxyl groups of the oil and water molecules. Thus, HTSO/A-containing samples had lower amounts of accumulated ice on their surfaces than samples containing SO/A. The three-step preparation of lubricant carriers improved the stability of lubricant within the matrix and heightened its anti-icing performance over 20 icing/deicing cycles. By slowing the release rate of the lubricant, issues related to oil depletion can be controlled to improve the life service and durability of the coatings. Combining three different mechanisms, namely stress localization (matrix), slippery and the formation of unfrozen molecules can help us to achieve acceptable icephobic characteristics with lower oil content, compared to the previous studies. Therefore, such coatings can be applicable to existing applications such as wind turbine and insulators.

In this chapter, we focused on investigating the icephobic performance of the coatings. As such, the HTSO/A-containing coating which has illustrated desirable icephobic properties through a comprehensive set of methods, moves forward to the

evaluation of its electrical performance. By conducting electrical tests, we aim to ensure that the selected coatings could maintain its efficiency for high voltage insulator applications while significantly reducing ice-related issues.

### **Acknowledgments**

The authors acknowledge all support from the Natural Sciences and Engineering Research Council of Canada (NSERC), Hydro-Québec, and PRIMA Québec. The authors would like to thank UQAC and CENGIVRE for providing the icing infrastructure. The authors would also like to thank Dr Mohammadreza Shamshiri at LARGIS, UQAC, for his help in conducting the DSC test.

## **Chapter 4: Icephobicity and Electrical Assessment of Slippery Coating Impregnated with a Stabilized Hydroxyl-terminated Lubricant for High Voltage Insulation Application**

Samaneh Heydarian<sup>1\*</sup>, Gelareh Momen<sup>1</sup>and, Reza Jafari<sup>1</sup>

<sup>1</sup>Department of Applied Sciences, University of Québec at Chicoutimi (UQAC), 555, boul. de

l'Université, Chicoutimi, Québec, G7H 2B1, Canada

\*Corresponding author: samaneh.heydarian-dolatabadi1@uqac.ca

### **4.1 Abstract**

In cold climate conditions, insulators are subjected to ice accretion that could affect their electrical performance and consequently lead to power outages. Besides icing, other outdoor factors, such as UV, rain, and pollution, could influence their electrical insulation efficiency. Slippery liquid-infused coatings have attracted great attention due to their icephobic applications, and they could be considered as a potential candidate to overcome the aforementioned problem. However, the problems caused by lubricant depletion could restrict their service time and thus limit their applications. Here, hydroxyl-terminated silicone oil carriers were impregnated into a silicone-based blend. The fabricated coatings exhibited long-lasting icephobic characteristics, resulting in reduced amount of ice accumulated on the surfaces. This reduction in ice adhesion is related not only to the slippery behavior of the coatings but also the formation of unfrozen hydrogen-bonded molecules. The coatings exhibited desired stability against weathering conditions, such as UV exposure and humidity. The

electrical characteristics of the prepared coatings were evaluated using dielectric spectroscopy, flashover, condensation, and inclined plane tests. Accordingly, the coatings containing lubricant-loaded carriers showed increased flashover voltage in dry, wet, and polluted states and reduced leakage currents in the condensation test. Moreover, during the inclined test, the tacking and erosion area was more restricted than that for the reference sample.

**Keywords:** Icephobic surfaces, Slippery coatings, oil absorbents, high voltage insulator, leakage current, flashover

## 4.2 Introduction

Ice formation and accumulation could cause catastrophic blackouts in a wide range of settings, particularly power transmission and distribution [277,278]. The adhesion of ice on insulators, as an essential part of transmission lines, is also considered as a devastating economical and safety issue during ice storms in cold climate regions [279]. Such components are used to provide mechanical support for electrical components and separate high-voltage line conductors. Besides ice accretion, the presence of pollution layer, including soluble mineral substances, on insulators could affect their electrical performance [280]. In fact, the migration of these contaminations towards the uppermost layer of ice could change the accumulated ice into highly conductive matter, resulting in further leakage current. Consequently, this causes formation of conductive water layer on the surface, leading to flashover. Other issues, including thermal degradation, corona discharge, and dry band arcing, are among the factors that result in electrical failure [281].

Various preventative strategies have been used to remove ice and pollution from the insulator surface. These strategies included change in insulator substance, shape, dimension and applying grease as a de-icing material [282,283]. However, most of them were ineffective, and therefore, much work has been focused on modifying the surface characteristics of insulators that are mostly gloss- and porcelain-based [284].

Hydrophobic coatings based on room-temperature-vulcanizing (RTV) silicone rubber were among the pioneer generations that were applied on glass and porcelain insulators [285–289]. They were chosen due to their water repellency characteristics and suitable long-term performance under conditions of road salt and industrial pollution [234,290–292]. However, they were not effective at harsh icing circumstances due to loss of hydrophobicity, resulting in increased discharge current. Semiconductive silicone coatings containing conducting particles, such as zinc oxide and graphene oxide (GO), were also proposed to be applied on insulators that offered enhanced anti-icing performance [105,293–295]. However, they had some drawbacks, such as high-power loss, aging, and degradation [296–298]. Superhydrophobic coatings have also shown some promising results for being applied on insulators [10,14,54,110,299,300]. These coatings present high-water repellency that could result in decreased ice accretion over insulators. Despite their optimized icephobic effectiveness, using superhydrophobic coatings demonstrated some disadvantages that limit their applications, particularly exposure to harsh environmental conditions, such as high humidity that much likely leads to losing their anti-icing characteristics [301–303]. Under such condition, water molecules condense in the porous surface structure that promotes mechanical interlocking between ice and the surface and consequently increase ice adhesion.



By imitating the morphology of *Nepenthes* pitcher plants, slippery liquid-infused porous surfaces (SLIPS) have been developed, and they do not have issues related to water condensation in high-humidity conditions [33,261,304], due to replacing air by oil within the surface pores. Infusing a lubricant into the porous substrate produces a smooth surface with fewer pinning points that exhibits low contact hysteresis and tilted angle [70,83,185]. Polymer-based SLIPS are generally fabricated by infusing lubricant in either a preformed structure or a precursor matrix [39–41]. Having greater control on composition in the latter method could prevent swelling deformation of the matrix.

SLIPS have shown high potential to be used in a wide range of applications, including anticorrosion, biomedical, and icephobic needs [35,69,71,170,241]. Aizenberg's group designed SLIPS by infusing a perfluorinated lubricant into a micro/nanostructured surfaces [33]. Besides low contact-angle hysteresis and low sliding angles, the fabricated coatings showed excellent ice-repellency characteristics. Golovin et al. investigated the effect of lubricant being infused on the stiffness of polymeric matrices and proposed the concept of interfacial slippage [94,305]. Accordingly, the combination of elasticity and the presence of lubricating layer could result in ice adhesion strength of lower than 20 kPa. In another attempt, SLIPS was fabricated by infusing liquid paraffin into polymethylsiloxane (PDMS), exhibiting a very low ice adhesion strength of 1.7 kPa at  $-30\text{ }^{\circ}\text{C}$  [158].

Due to the extraordinary icephobic characteristics of SLIPS, they could be considered as a suitable candidate to prevent ice accretion on insulators and thus electrical failure. Wang et al. prepared silicone-oil-infused PDMS coating with different lubricant contents and evaluated the ice accumulation of coated insulator in

high voltage chamber. The low surface energy of the lubricant and PDMS and the high mobility of the silicone oil within the matrix network could effectively contribute in reducing the ice adhesion strength on the insulator coated with the fabricated coatings [157]. Olad et al. developed SLIPS coatings by infusing perfluorinated lubricants into two different chemically modified porcelain substrates. The fabricated surfaces exhibited acceptable ice repellency properties, and they endured inclined plane test (IPT) at 4.5 kV for 6 h [306].

Given that oil is one of the essential components of SLIPS to have desirable icephobic properties, lubricant loss could result in limited service life and consequently restrict their applications [40]. Therefore, stabilizing the oil in the matrix structure to lengthen service life has become one of the main challenges in the fabrication of slippery coatings. Accordingly, some methods, such as using nanoparticles and nanoporous materials and micro-texturing, have been proposed [266,268,307]. These strategies for lubricant retention in slippery coatings were not used in most relevant studies regarding the fabrication of such coatings for electrical applications.

In this work, a slippery lubricant infused coating that contained silica-based carriers was developed to enhance the coating's durability. First, hydroxy-terminated silicone oil was infused into the silica aerogel pores by applying negative pressure to obtain lubricant-loaded carrier (LLC) powders. Then, the fabricated powders were impregnated in silicone-based blend. The icephobic characteristics of the prepared coatings were evaluated using different test methods, including DSC, micro-push-off adhesion test, push-off test, and static accumulation test (SAT). The weathering resistance of the coatings were assessed using QUV. A comprehensive group of electrical tests, namely, dielectric spectroscopy, flashover and condensation test, and

IPT, was also conducted. The findings showed that the fabricated coatings containing lubricant-loaded carriers could be a suitable potential candidate for application on insulators.

### **4.3 Materials and methods**

#### **4.3.1 Fabrication of coatings containing lubricant-loaded carriers**

The preparation of the coatings consisted of two general procedures, namely, loading the lubricant inside the carriers and impregnating lubricant-loaded carriers within the matrix. In the former procedure, hydroxyl-terminated silicone oil (Genesee Polymers) was loaded into the hydrophobic silica aerogel (particle size of 2–40  $\mu\text{m}$ , Enova Aerogel IC3100). To increase the loading capacity and stabilize lubricant within the aerogel's micropores, the following three-step procedure was conducted through applying negative pressure. First, 0.1 g of aerogel was mixed with 10 g of a prepared solution of the oil in hexane (60 wt.%). After 10 min of sonicating, the prepared dispersion was then, vacuumed at 60 kPa at 40 °C for 1 h. This process was repeated three times to further infuse the oil within the carrier pores. Finally, the powder-like lubricant-loaded carriers were obtained after the mixture was washed with hexane and dried for 24 h at 60 °C. The loading capacity of the carriers was evaluated using thermogravimetric analysis (TGA, Netzsch STA 449C).

The coatings were fabricated by embedding the prepared lubricant-loaded carriers within a blend of polydimethylsiloxane (PDMS) and alkoxy-siloxane resin. For this purpose, PDMS (Sylgard 184 silicone elastomer) serving as a base and a curing agent was mixed with the alkoxy-siloxane resin (DOWSIL 2405) at a ratio of 70:30, respectively. This ratio was selected based on the measurement of mechanical

properties described in APPENDIX III (Figure A-III. 1 and Figure A-III. 2). Furthermore, the SEM micrograph of the matrix with mentioned combination showed no evidence of immiscibility (see APPENDIX III- Figure A-III. 3). According to the data sheet, the alkoxy-siloxane resin could act as a co-binder that enhances the mechanical performance of silicone-based coatings. Different percentages (5 wt.%, 10 wt.%, and 15 wt.%) of the lubricant-loaded carriers, dispersed in suitable amount of xylene, were added into the prepared polymeric blend. The curing agent of PDMS was added to the mixture (ratio of 1:10), and tetraethoxysilane (TEOS, Dow Corning) as a coupling agent of alkoxy-siloxane resin. Aluminum plates polished by 800 and 1200 SiC papers were used as the substrate by using a film applicator (ZEHNTER testing instrument). After 10 min of stirring, each mixture was applied on the treated substrate by using a film applicator (ZEHNTER testing instrument). The coated samples were then placed in the oven overnight at 90 °C to complete their curing process. The samples were labeled on the basis of the content of lubricant-loaded carriers as LLC-5, LLC-10, and LLC-15; for instance, sample LLC-10 contained 10 wt.% of LLC. Furthermore, the polymeric sample without LLC was selected as a reference. The average thickness of the cured coatings was around  $100 \pm 5 \mu\text{m}$ , measured by a coating thickness gauge. The micrographs of LLCs and cross-section of the coating containing LLCs were provided in APPENDIX III (Figure A-III. 4), depicting their size and spatial distribution.

#### **4.3.2 Surface characterization**

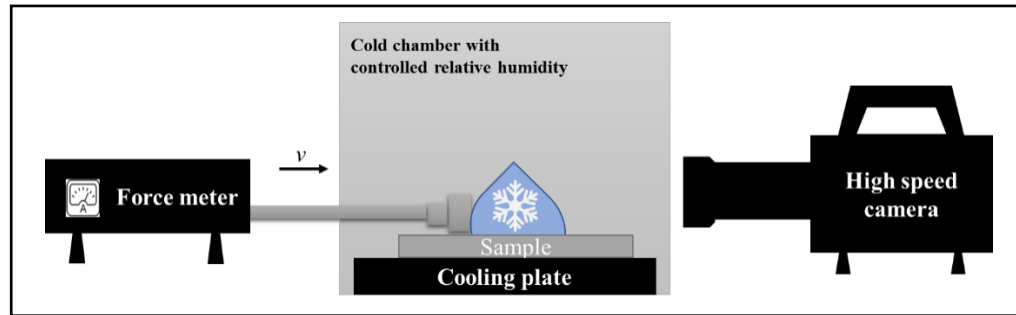
The water contact angle was measured using a Kruss DSA100 goniometer at 25 °C, based on the Young-Laplace approximation. A 4  $\mu\text{L}$  deionized water droplet

was placed onto the sample surface to determine the contact angle. The contact angle hysteresis was obtained by measuring the difference between the advancing and receding contact angles when the water droplet was moved by the needle across the sample surface. The measurement was repeated at three different points of each sample to ensure its accuracy. An optical profiler (Profil3D, Filmetrics, USA) was used to evaluate the topography of the samples and quantify the corresponding surface parameters.

### **4.3.3 Icephobic Properties**

The delayed ice nucleation temperature of the prepared samples was obtained by DSC. In this procedure, a 5 mg-deionized water droplet was placed into an aluminum DSC pan that had already been coated by each coating. After being sealed, the pan was placed on a DSC sample holder, and the measurement was conducted by cooling down the sample from 40 to  $-40$  °C with a ramp of 5 °C/min.

The ice adhesion strength of the fabricated coatings in micro and macro scales was evaluated using micro-push-off and push-off tests. In the micro-push-off test, a 10  $\mu$ L deionized water was deposited on a cooling plate located in a small cold chamber at  $-10.0$  °C  $\pm$  0.1 °C and under relative humidity of around 50%  $\pm$  3% (Figure 4-1). The freezing process was filmed via a high-speed camera. When the water droplet froze completely, the probe attached to the force meter approached the droplet at 0.5 mm/s, and the maximum force required to remove the frozen droplet from the sample surface was recorded. The ice adhesion strength of each sample was obtained by dividing the maximum force by the contact area of the frozen water droplet–sample interface.



*Figure 4-1. Schematic of micro-push-off apparatus.*

Similar to the micro-push-off test, non-impact ice was used in the push-off test, but in this procedure, the ice adhesion was evaluated in a larger scale. A cylindrical plastic mold with the diameter of 1 cm was placed onto the samples while they were kept in a cold chamber at  $-10.0\text{ }^{\circ}\text{C} \pm 0.2\text{ }^{\circ}\text{C}$ . Then, they were filled with adequate deionized water and left in the chamber for 24 h to obtain a frozen water column. In the following day, the samples were placed on the holder of the push-off apparatus, and the maximum force for ice detachment was recorded when the probe of force meter approached the cylindrical column. The ice adhesion strengths of the samples were obtained by dividing their corresponding maximum force by the cross-sectional area of the plastic mold.

The ice accumulation on the samples was also evaluated using SAT. First, the coatings were applied to  $3\text{ cm} \times 15\text{ cm}$  aluminum substrates by using a ZEHNTNER film applicator. After the curing process, they were placed onto a special-designed stand with inclined angles of  $0^{\circ}$ ,  $45^{\circ}$ , and  $80^{\circ}$  and placed in a cold chamber at  $-5.0\text{ }^{\circ}\text{C} \pm 0.2\text{ }^{\circ}\text{C}$  and, under relative humidity of around  $84 \pm 2\%$ . Then, the samples were exposed to freezing drizzle conditions by spraying supercooled water microdroplets with an average diameter of  $327\text{ }\mu\text{m}$  and a temperature of  $4.0\text{ }^{\circ}\text{C}$ . They were iced for

about 45 minutes at  $-5.0\text{ }^{\circ}\text{C}$ . The difference between the sample mass before and after icing condition was equaled to the amount of ice accumulated on each sample.

#### 4.3.4 Durability

The durability of the samples was evaluated using QUV, which included exposing to simulated outdoor circumstances. The test was conducted following the test standard of ASTM G154. The samples were exposed to about 1000 h of UV light by using UVA-340 fluorescent lamps ( $0.89\text{ W}\cdot\text{m}^{-2}$ ) as a test cycle of 8 h at a temperature of  $60\text{ }^{\circ}\text{C}$ . The UV exposure was then followed by 4 h of condensation at  $50\text{ }^{\circ}\text{C}$ .

The durability of the samples against the subsequent de-icing events was evaluated by combining the push-off test and 20 icing/de-icing cycles. For this purpose, the ice adhesion strength of the samples after each cycle was measured.

The evaluating procedure of the replenishment capability of the samples was adopted from the work of J. Zhang et al. [47]. For this purpose, the weight of the sample was measured via a Sartorius balance (precision 0.1 mg) and recorded as  $m_0$ . Then, the oil layer was removed from the surface using an oil-absorbing paper, and the weight of sample was again recorded. This process was repeated for  $n$  cycles, and the rate of weight loss was obtained using the Eq. 4-1.

$$\text{Rate of weight loss} = \frac{m_0 - m_n}{m_0} \times 100 \quad (\text{Eq. 4-1})$$

Where  $m_n$  is the weight of sample after  $n$  cycles.

#### 4.3.5 Electrical properties

The dielectric response of the samples at 25 °C was evaluated via a Novocontrol broadband dielectric spectrometer (Microtonic Alpha-A high-performance frequency analyzer). The frequency was changed from  $10^{-2}$  Hz to  $10^6$  Hz. The coatings were applied using a film applicator on circular-shaped paper substrates with a diameter of 46 mm and a thickness of 2 mm. The measurement was carried out by placing the prepared samples between two solid electrodes to form a capacitor and then applying an AC voltage of 3 V.

The flashover voltage was measured via a rod-plate configuration connected to the AC voltage source. The coatings were applied to porcelain substrates and then placed between two electrodes with a fixed distance of 36 mm (Figure 4-2a). The test procedure was conducted under two steps: rapid increase and gradual increase in voltage. The first step was continued until 50% of the predicted flashover value. Meanwhile, in the second step, the voltage was gradually increased at a rate of 0.5 kV/s until a disturbing discharge occurred, and then the corresponding voltage was recorded. The procedure was repeated 10 times on each sample. Furthermore, a 2-minute interval between each trial was allocated to dissipate the residual charges on the samples.

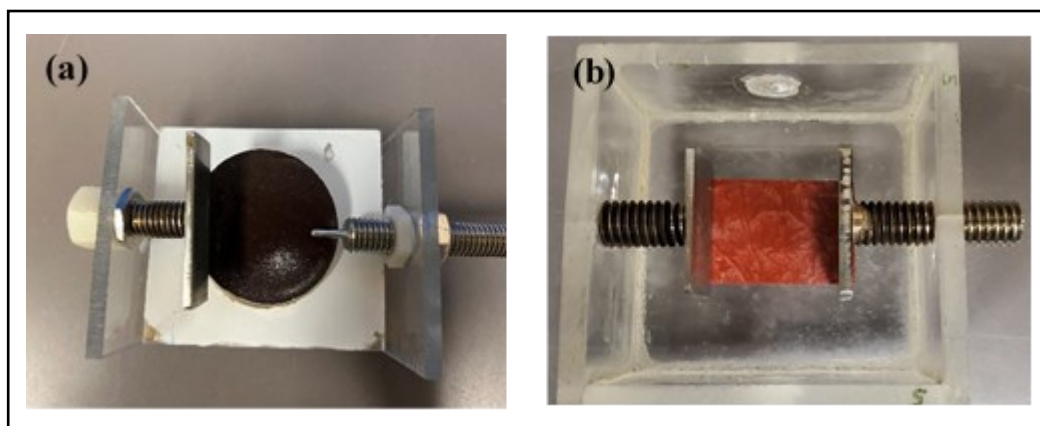
Three different conditions, namely, nonpolluted/dry, polluted/dry, and polluted/wet, were chosen for each sample. A dispersion of Kaolin in deionized water was used to pollute the samples, which were then wetted by spraying deionized water on their surface before applying the voltage.

Flashover test was carried out under sub-zero and zero temperature conditions. The rod-plate configuration was transferred into an EH40-2-3 climatic chamber with



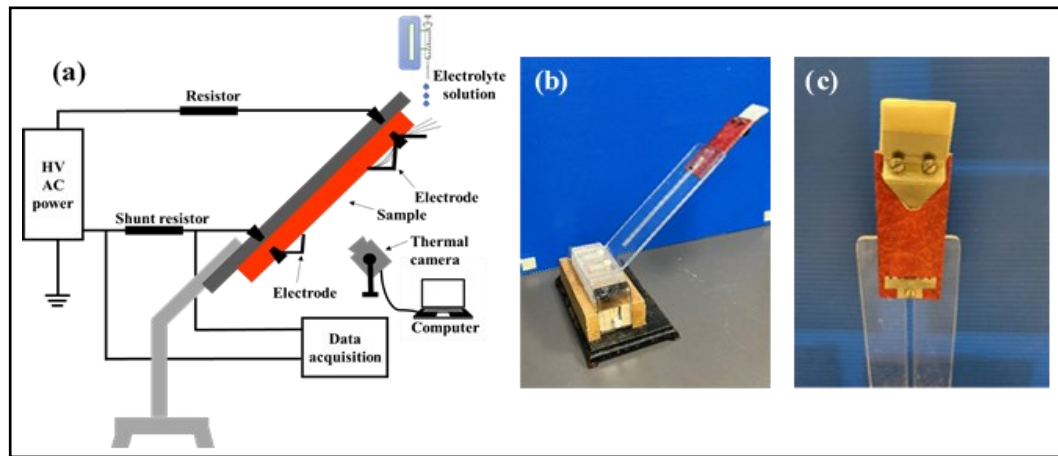
adjustable temperature. Once the temperature reached  $-10\text{ }^{\circ}\text{C}$ , deionized water was sprayed over the samples. When water was frozen, the flashover measurement was conducted on the basis of the abovementioned procedure. The flashover voltages were also measured at  $-5\text{ }^{\circ}\text{C}$  and  $0\text{ }^{\circ}\text{C}$ . The measurement was repeated five times for each sample, with a 2-minute interval between each event.

Condensation test was conducted in accordance with the test method proposed by the previous research work [308]. Under high-humidity condition, the moisture could be settled on the surface of cold insulator, resulting in the formation of a thin water layer. Therefore, the samples were placed in a chamber with variable temperature between  $10\text{ }^{\circ}\text{C}$  and  $35\text{ }^{\circ}\text{C}$  and a relative humidity of 95% (Figure 4-2b). For achievement of a uniform condensed water, the temperature of the chamber was increased to  $35\text{ }^{\circ}\text{C}$  for 30 min, resulting in condensation settlement on the surface. Then, the temperature was lowered to  $10\text{ }^{\circ}\text{C}$  for another 30 min. During the test, a low electric field of  $4\text{ kV/cm}$  was applied, and the leakage current was monitored. A leakage current greater than  $5\text{ mA}$  was considered as failure.



**Figure 4-2.** (a) Top view of the flashover and (b) condensation setups.

The inclined plane test (IPT) was used to assess the erosion and tracking resistance of the samples on the basis of the test standard of IEC 60587 [309]. This test is usually carried out either at constant voltage or by voltage steps. In the present work, the second process was used on the applied coatings on GPO3 substrates with standard dimensions of 50 mm width, 120 mm length, and 5.5 mm thickness and 5 mm diameter holes for fixing (Figure 4-3).



**Figure 4-3.** (a) Schematic illustrating the test setup for inclined plane test (IPT); (b) and (c) parts used for mounting the samples for IPT.

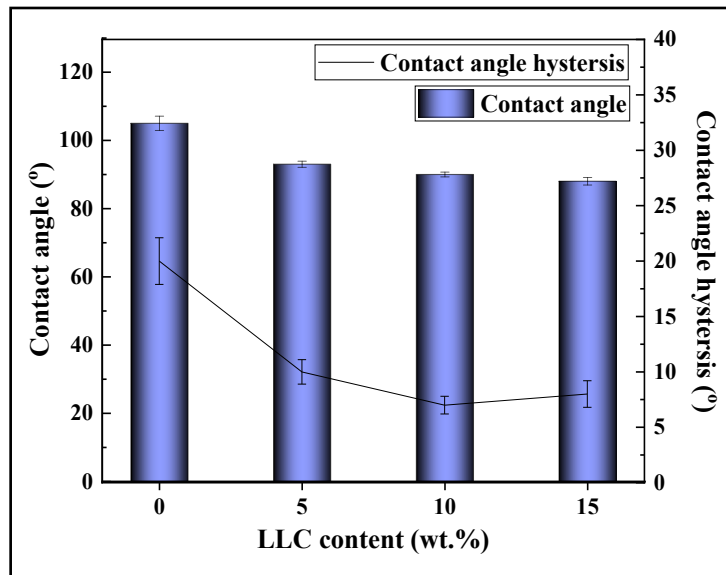
GPO-3 is a glass reinforced thermoset polyester with excellent tracking performance, and it was used in this work because its shape could allow samples to be easily produced. The prepared samples were placed on the holder that could accommodate them at an inclination angle of 45°. The contaminant consisted of an electrolyte solution of 0.1 wt.%  $\text{NH}_4\text{Cl}$  and 0.02 wt.% Triton X100 in deionized water. Once the contaminant solution was flowing evenly at a rate of 0.6 mL/min through the filter, an initial 60 Hz of high voltage was applied, followed by 2.5, 3, and 3.5 kV (each for 45 min). The carbonaceous path (track) produced on the samples due to the arcing

was used to analyse the tracking and erosion lines of the samples. Moreover, a thermal camera was used to evaluate the leakage current and the variation of temperature. The endpoint was determined when the leakage current passing through the sample exceeded 60 mA.

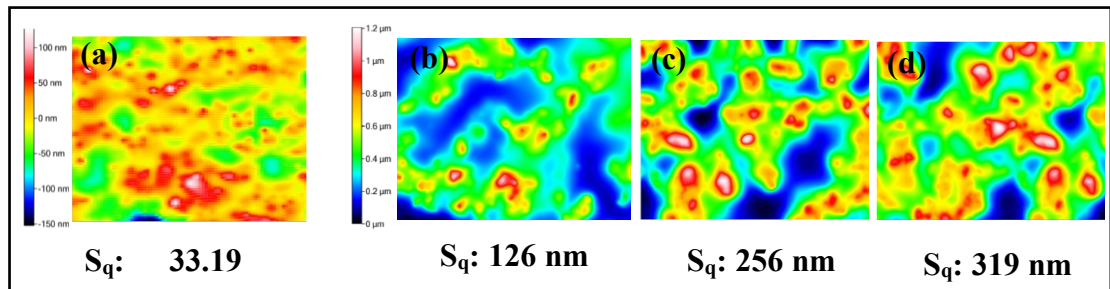
## **4.4 Results and discussion**

### **4.4.1 Surface characterization**

The water contact angle was measured to assess the effect of impregnating lubricant-loaded carriers on the coating wettability (Figure 4-4). Increasing the carrier content from 5 wt.% to 15 wt.% resulted in the contact angle decreasing from 105° for the reference to 93° (LLC-5), 90° (LLC-10), and 88° (LLC-15), respectively. In general, incorporating the carriers could result in reduced contact angle due to the lower surface energy of oil than that of the matrix. However, the variation of lubricant-loaded carrier content did not significantly affect the contact angle and the wettability of the samples containing the carriers. Water contact angle hysteresis also decreased by heightened carrier concentrations. In fact, reduced contact angle hysteresis equaled to decreased pinning points between the water droplet and the surface and consequently, easy removal of the water droplet. The topographical maps of the samples and their corresponding surface roughness values were obtained by profilometry (Figure 4-5). Accordingly, impregnating the lubricant-loaded carriers increased the surface roughness from 126 nm to 319 nm, very likely due to the presence of aerogel in the coating structure.



*Figure 4-4. Variation of contact angle and contact angle hysteresis as a function of LLC content.*



*Figure 4-5. 3D topographical maps of the (a) reference and LLC-5, (b) LLC-10, and (c) LLC-15.*

#### 4.4.2 Icephobicity

The icephobic characteristics of prepared coatings are usually evaluated using two different groups of methods. The test methods, such as measuring ice nucleation temperature, belong to the first group that characterize the samples before freezing. The

latter ones, including ice adhesion measurement and SAT, are related to the performance of the samples in removing ice from the surface.

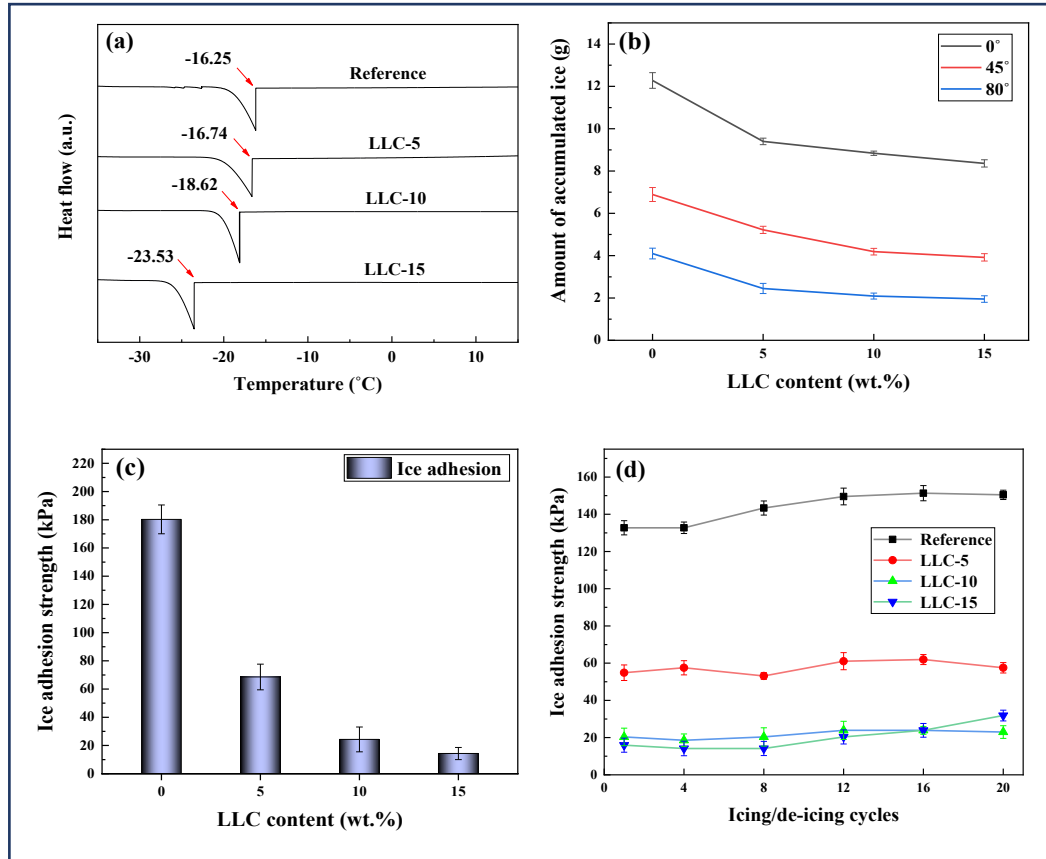
The ice nucleation temperature corresponding to each sample was evaluated using DSC. As seen in Figure 4-6a, the ice nucleation temperature continuously decreased from  $-16.25\text{ }^{\circ}\text{C}$  for the reference to  $-23.53\text{ }^{\circ}\text{C}$  for the sample containing 15% of the lubricant-loaded carriers. The reduced ice nucleation time could be related to the decreased thermal conductivity of the coating due to the presence of the lubricant. In general, the thermal conductivity of silicone oils is lower than that of the PDMS matrix. Therefore, adding the lubricant to the matrix could result in the increased heat insulation effect of the coating system and consequently, delayed ice nucleation temperature. A notable detail that even a decrease of  $1\text{ }^{\circ}\text{C}$  in ice nucleation temperature could lead to multifold increase in ice nucleation rate [275].

The de-icing performance of the prepared coating was evaluated using SAT method, which exhibited the amount of ice accumulated on the samples inclined at  $0^{\circ}$ ,  $45^{\circ}$ , and  $80^{\circ}$  (Figure 4-6b). The ice accumulation on the samples decreased by impregnating lubricant-loaded carriers. Moreover, the increased carrier content resulted in a gradual reduction in accumulated ice on the surface from 12.28, 6.89, and 4.1 g for the reference to 8.36, 3.92, and 1.95 g for LLC-15 samples at their corresponding angles, respectively.

The tangential component ( $F_{\parallel}$ ) of the gravity force ( $W$ ) equaled to  $W \cdot \sin\alpha$ , ( $\alpha$ : the inclined angle) is a key factor in removing ice from the prepared samples. Increasing the inclined angle led to greater tangential force and consequently, less ice accumulation.

Meanwhile, ice adhesion strength, as the main resisting force against ice detachment, could significantly affect the amount of ice accumulated on the surface. Micro-push off adhesion test was used to evaluate the ice adhesion strength on the samples (Figure 4-6c). By using water droplet, micro-push-off test aims to measure ice adhesion in a smaller scale than push-off test. Furthermore, in micro-push-off test, parameters such as humidity could be controlled more.

As illustrated in Figure 4-6c, adding the lubricant-loaded carriers to the coating decreased the ice adhesion strength from about 180 kPa for the reference to around 14kPa for LLC-15 samples. The presence of oil over the surface could be the reason for the reduced ice adhesion of the samples. TGA confirmed that the loaded-lubricant mass value for the prepared powders was about 47%. This infused oil could migrate from the pores towards the surface to facilitate ice sliding. This migration occurred from the inner pores of aerogels into the large free volume of the polymeric bulk due to the produced concentration gradient pressure. The lubricant is then transferred into the surface because of the mobility of the lubricant small molecules through the bulk [157]. Another possible mechanism for the reduced ice adhesion is that the hydroxyl-terminated silicone oil had hydrophilic groups that could produce hydrogen bonding with water molecules. These hydrogen-bonded molecules could preserve water in non-frozen state at or below 0 °C, resulting in an additional factor to decrease ice adhesion [157,270].



**Figure 4-6.** (a) DSC evaluation of ice nucleation temperatures corresponding to samples with LLC content. (b) Ice accumulation on samples inclined at 0°, 45°, and 80°, as measured by SAT. (c) Ice adhesion strength of samples, as obtained using micro-push-off test. (d) Ice adhesion strength in samples containing LLC over 20 icing/de-icing cycles, as obtained by push-off test.

### 4.4.3 Durability

#### 4.4.3.1 Subsequent de-icing events

A total of 20 icing/de-icing cycles were conducted in the present study (Figure 4-6d), and the ice adhesion strength was evaluated after each four trials by using push-off adhesion test. For the LLC-5 and LLC-10 samples, no significant change was observed over all subsequent cycles, Meanwhile, for LLC-15, the ice adhesion strength

increased slightly after 12 icing/de-icing cycles, very likely due to the depletion of oil on the surface, consequently increasing the surface roughness.

The presence of the micropores can promote the oil trapping within the aerogel. When the uppermost oil layer is removed from the surface, the capillary effect causes the lubricant to be transferred from the bulk towards the surface. In other words, ice detachment from the surface can eliminate the accessible oil layer, producing a concentration gradient of lubricant between the surface and the bulk that serves as a driving force for the lubricant transferring [157]. The presence of LLC results in the lubricant to be released in lower rate, and guarantees the slipperiness for longer service life. Moreover, no significant change was observed over the icing/de-icing cycles that confirmed the capability of the surface in lubricant recovery.

#### *4.4.3.2 Accelerated weathering test*

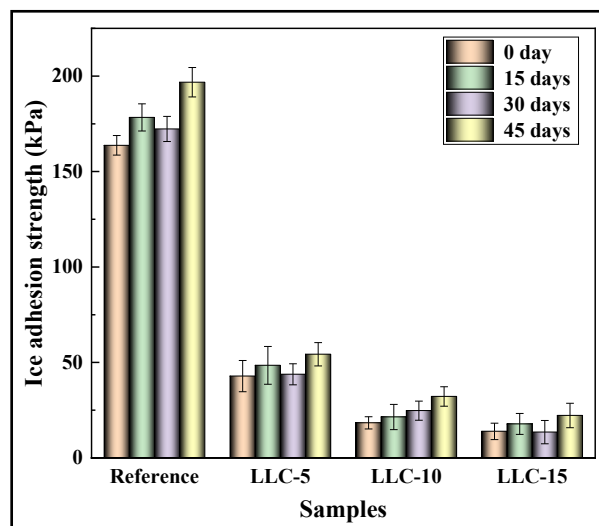
Exposure to weathering conditions, such as UV and humidity, could lead to deterioration of coatings. Therefore, the effect of these weathering conditions on the surface and icephobic characteristics of the fabricated coatings was investigated.

Figure 4-7 illustrates the evaluation of ice adhesion strength of the fabricated samples exposed to accelerated weathering conditions for 45 days, which equalled to about 5 years of real outdoor conditions [67]. In general, the coatings containing LLC maintained their icephobic performance even after a 1000-h exposure period to UV irradiation and humidity condensation. Furthermore, increasing the LLC content in the coating could result in more durable coating under these harsh conditions. This finding could be related to further availability of the oil in higher LLC content when it migrated from bulk towards the surface. The presence of the oil layer on the surface could reduce



the effect of UV light on the physical and chemical properties of the coating [310]. Thus, despite the increasing trend of ice adhesion strength for 45 days, LLC-15 maintained its ice adhesion strength to below 25 kPa. For the reference sample that had no LLC, the ice adhesion increased significantly after the exposure period.

Considering their presentation of desired icephobic characteristics and stability against weathering, LLC-10 and LLC-15 were chosen to evaluate their electrical performance in the next section.

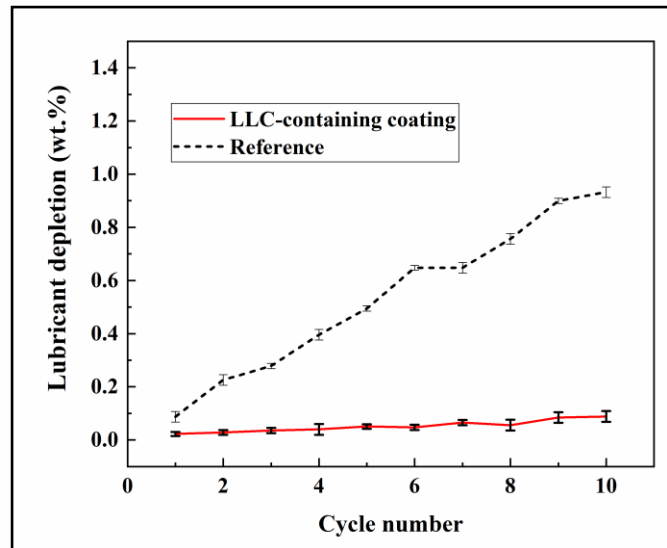


**Figure 4-7.** Evaluation of ice adhesion strength corresponding to samples during 45-day accelerated weathering test.

#### 4.4.3.3 Lubricant replenishment

The lubricant depletion is considered as one of the main challenges of the slippery coatings that affects their service life. The lubricant lost of the fabricated samples was assessed over ten cycles (Figure 4-8). We compared the lubricant weight loss of LLC-15 and the reference (the coating containing the same amount of oil but without aerogel). It was observed that both samples show a gradual loss of lubricant over repeated cycles. Although the sample containing LLC offered much better

lubricant retention properties then the reference. It can be related to using the three-step procedure that can significantly control the delivery of the lubricant on the surface, and therefore, it contributed effectively to reducing the lubricant depletion rate.



**Figure 4-8.** The rate of weight loss the coating containing LLC and the reference (the coating containing the same amount of oil but without aerogel) in relation to the number of test cycles of oil recovery/depletion.

#### 4.4.4 Electrical characterization

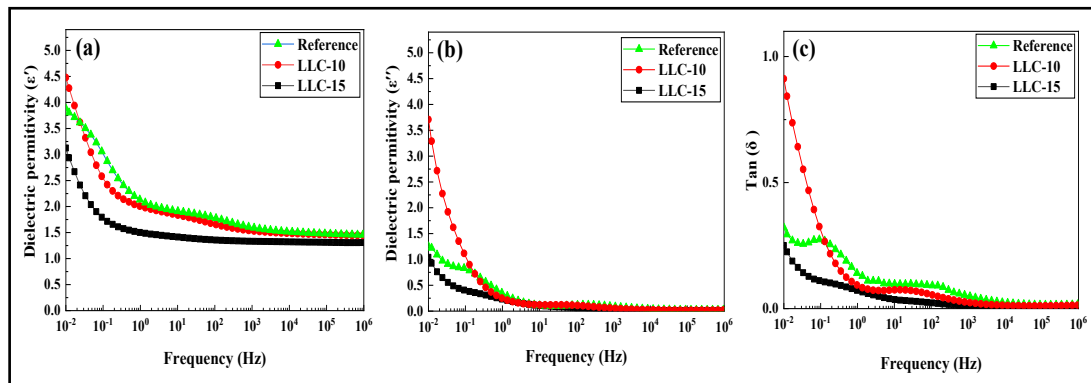
##### 4.4.4.1 Dielectric spectral analysis

Dielectric spectroscopy is a common method to measure the permittivity and loss factor of insulating materials. In a complete insulating system, having a zero resistive leakage current ( $I_R = 0$ ) is desirable. As this value could not be achievable, the insulation level is usually expressed by dissipation factor,  $\tan \delta$ , which be defined as Eq. 4-2 [311,312]:

$$\tan \delta = \frac{|I_R|}{|I_C|} \approx \frac{\varepsilon''(\omega)}{\varepsilon'(\omega)} \quad (\text{Eq. 4-2})$$

In this equation;  $\epsilon'$  is the real part of the permittivity related to material dissipation;  $\epsilon''$  is the imaginary part of permittivity, which is equal to polarization losses; and  $I_R$  and  $I_C$  are the resistive and capacitive currents, respectively. Accordingly, a dissipation factor as small as possible must be achieved.

Figure 4-9 depicts the variation of  $\epsilon'$ ,  $\epsilon''$ , and the dissipation factor ( $\tan \delta$ ). From the graphs, at low frequency,  $\epsilon'$  and  $\epsilon''$  showed increased values, which then dropped dramatically when the frequency was increased and then levelled out with the change to high frequencies. In fact, the dipoles could become readily oriented with the electrical field at lower frequencies, resulting in enhanced mobility of the segments and consequently, increased values of  $\epsilon'$  and  $\epsilon''$ . The high values of  $\epsilon'$  and  $\epsilon''$  could be attributed to conductivity and polarization losses, respectively. Meanwhile, at higher frequencies, the dipoles are not able to reorient rapidly with the electrical field due to lack of enough time.



**Figure 4-9.** Variation of (a) real ( $\epsilon'$ ) and (b) imaginary ( $\epsilon''$ ) parts of permittivity and (c) dissipation factor ( $\tan \delta$ ) in relation to frequency.

As illustrated in Figure 4-9a and Figure 4-9b, the  $\epsilon'$  and  $\epsilon''$  values of the prepared coating were lower than those of the reference. Silicone oils are generally

considered as nonpolar liquids with a low dielectric constant and loss factor and high electrical resistivity [313–315]. These liquids also offer low temperature and frequency dependency of electrical constant and dissipation factor [316]. Infusing silicone oil within the elastomeric matrix reduced the number of dipoles within coatings, resulting in reduced total dielectric constant and increased resistivity compared with reference samples.

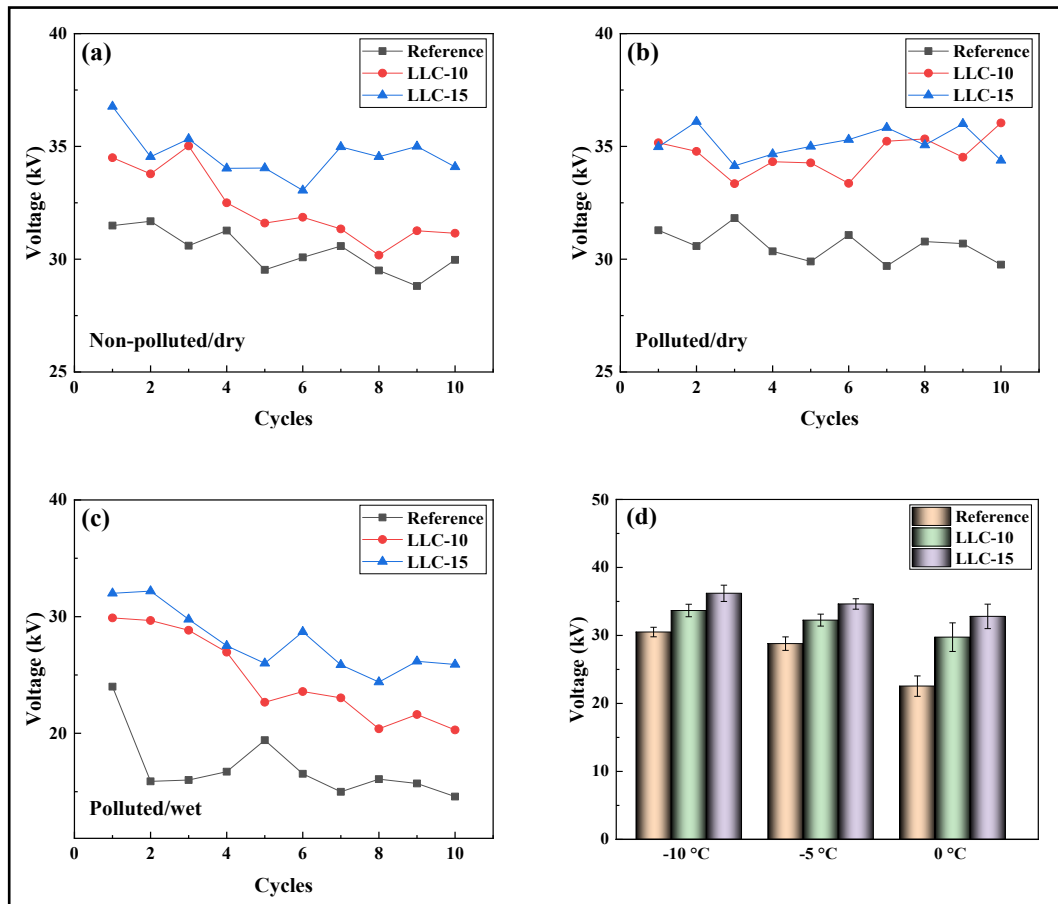
Figure 4-9c illustrates the variation of  $\tan \delta$  in terms of frequency at 25 °C. This factor obviously decreased rapidly by increasing the frequency and stabilized in high frequencies. The insulating properties of the lubricant infused within the matrix could prevent the electron mobility throughout the prepared coating at high frequencies. Moreover, LLC-15 showed the best performance in terms of  $\tan \delta$  at a power frequency of 60 Hz.

#### **4.4.5 Flashover**

High-voltage test is one of the essential techniques to evaluate the electrical performance of insulators by monitoring the flashover voltage of coated and uncoated surfaces. In this method, the maximum tolerance of surfaces is evaluated under applying high-voltage stress on a 36 mm sample. Figure 4-10a, Figure 4-10b and Figure 4-10c illustrate the variation of flashover levels for the fabricated slippery coatings and uncoated surfaces in different conditions, including clean/dry, polluted/dry, and polluted/wet states.

Under the clean/dry condition, the slippery coatings of LLC-10 and LLC-15 showed a disruptive discharge at around 35 kV, and LLC-15 could remain at this level after 10 repeated tests (Figure 4-10a). For the polluted condition in dry state (Figure

4-10b), the presence of pollution had no high negative effect on the performance of the coating under high voltage stress, and the coated surface could tolerance the same level of flashover (35 kV) as dry state, with acceptable stability after repetitive test. However, for the polluted/wet state (Figure 4-10c), a different behavior was observed between the slippery coatings containing LLC and the reference coating while water was sprayed.



**Figure 4-10.** Evaluation of flashover voltage during 10 subsequent cycles under (a) non-polluted/dry, (b) polluted/dry, and (c) polluted/wetted conditions. (d) Evaluation of first flashover voltage at  $-10\text{ }^{\circ}\text{C}$ ,  $-5\text{ }^{\circ}\text{C}$ , and  $0\text{ }^{\circ}\text{C}$ .

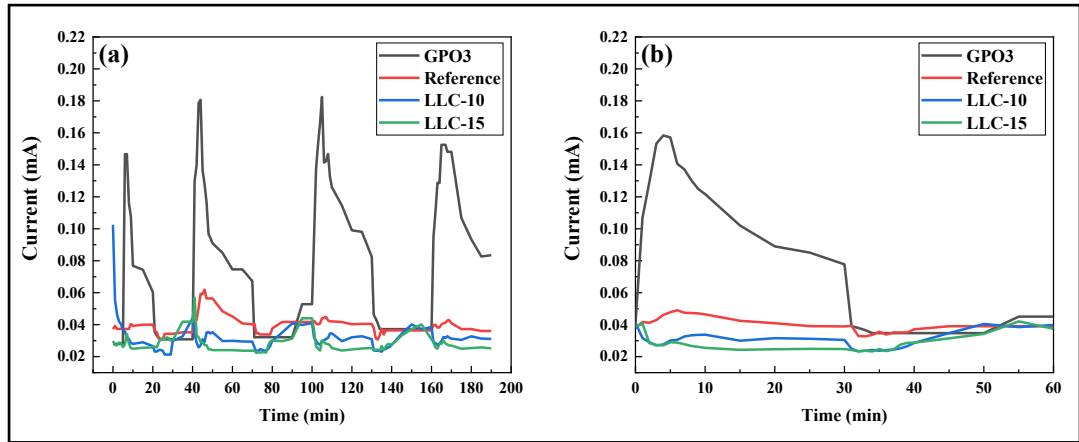
The slippery coatings did not allow the water to remain over the surface because of their slippage properties, whereas the reference coating did not have such characteristic, and the water film spread over the surface and completely wetted it. Therefore, the flashover level for reference (under 25 kV) was considerably lower than that for the fabricated coatings. After repeated cycles, the reference coating underwent electrical discharge, and the level of flashover dropped to about 15kV. The results indicated that the insulation effect of slippery coatings containing LLC not only degraded the electrical performance of the surface but also made it more stable against electrical discharge and flashover.

Figure 4-10d illustrates the evaluation of the flashover voltage at  $-10\text{ }^{\circ}\text{C}$ ,  $-5\text{ }^{\circ}\text{C}$ , and  $0\text{ }^{\circ}\text{C}$ . At  $-10\text{ }^{\circ}\text{C}$ , the samples generally showed the highest flashover voltages, and upon increasing the temperature, a reducing trend was observed for all samples.

Increasing the LLC content resulted in increased flashover voltage at all temperatures. Furthermore, for  $0\text{ }^{\circ}\text{C}$ , at which ice turned into water, the difference between the flashover voltages corresponding to the reference sample and LLC-10 was higher than those at  $-10\text{ }^{\circ}\text{C}$  and  $-5\text{ }^{\circ}\text{C}$ . This finding could be related to the presence of a lower amount of water on the coatings containing LLC, which resulted from the slippage property of the coatings.

#### **4.4.6 Condensation test**

Condensation test was conducted to evaluate the electrical performance of the prepared coatings under controlled humidity conditions [308]. Figure 4-11a, and Figure 4-11b exhibit the variation in leakage current for three cycles and the three-cycle average leakage current during subsequent heating/cooling events.



**Figure 4-11.** Evaluation of leakage current versus time on samples for a) three repetitive cycles and b) their averages, as obtained by condensation test.

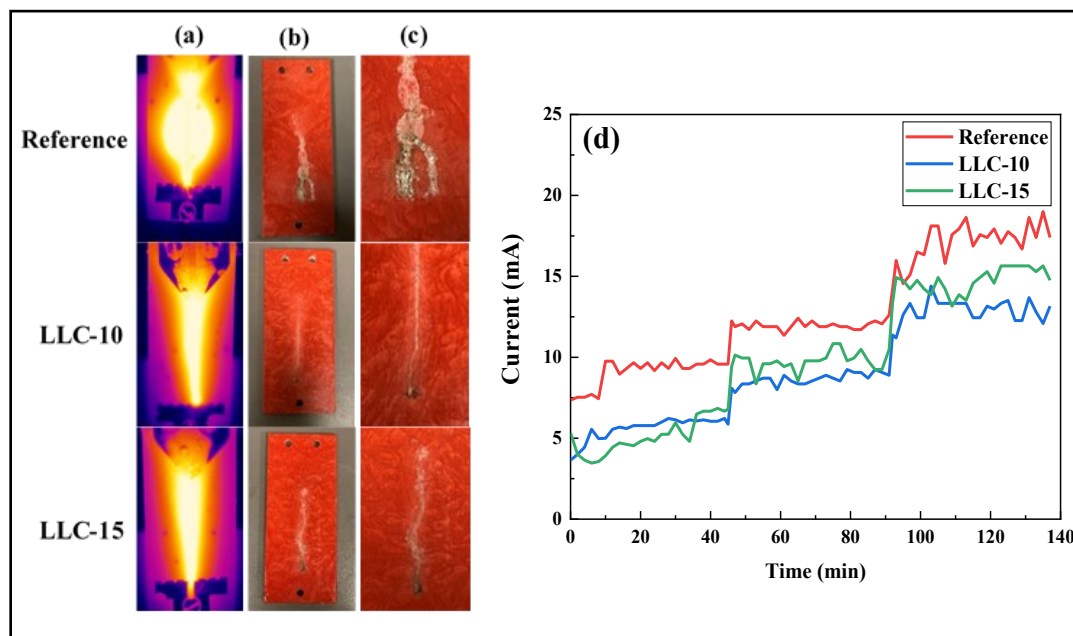
The first smaller cycle (0–40 min) is a preliminary test to carry out the subsequent tests under the same initial conditions. Increasing the LLC content led to decreased leakage current. The leakage current of LLC-15 samples dropped to around 0.02 mA, whereas for GPO3, the leakage current was 0.16 mA in wet state (0–30 min). Thus, the presence of lubricant in the coating enhanced the electrical insulation of the coatings and subsequently, the leakage current decreased considerably.

#### 4.4.7 Inclined plane test (IPT)

IPT is used to evaluate the resistance of slippery coatings against tracking and erosion when they are exposed to electrical voltage [309]. First, the contamination solution was continuously flowed over the surface, and then the voltage was applied, resulting in leakage current. Consequently, this leakage current caused the erosion and tracking of the material over the surface due to the enhanced possibility of electrical discharge. Figure 4-12a illustrates the thermal camera images of the samples at the final step of IPT. In these images, the bright yellow arcs corresponded to the erosion of the

surfaces. Accordingly, for samples containing LLC, such arcs spread in a narrower area than that for the reference. Figure 4-12b and Figure 4-12c shows the samples' surfaces after the test, in which the eroded area and tracking path were clearly visible. Accordingly, the tracks and cracks on the reference surface were wider and deeper than those on the samples containing LLC. This finding could be related to the slippage of water droplet on the sample containing lubricant, which enhanced the water droplet velocity over them, resulting in reduced polluted spots that contributed to the initiation and progress of erosion. Figure 4-12d illustrates the leakage current evolution of the slippery coatings of LLC-10, LLC-15, and reference surface. The leakage current trend of each step showed various behavior for the corresponding sample. In the first step (2.5 kV), the reference sample exhibited the highest level of leakage current at around 8 mA. Meanwhile, the leakage current of the fabricated coatings was about 4 mA. By increasing the voltage in the next step (3 kV), the leakage current increased for all the samples. However, the LLC-15 sample showed a little bit higher level of leakage than the LLC-10 sample. This behavior confirmed that the coating containing a lower content of lubricant-loaded porous particles exhibited, to some extent, more resistance towards degradation under applied voltage over time. Moreover, it could keep such a low leakage current even until the final step with a high level of voltage (3.5 kV). However, both slippery coatings generally did not allow the leakage current to increase significantly under high-voltage level. Moreover, considering that IPT is a very harsh test, the slippery coatings showed promising performance against tracking and erosion for electrical application.





**Figure 4-12.** (a) Thermal camera images of samples at the final minutes of IPT. (b) and (c) Images of the samples after the test. (d) Evaluation of leakage current over time during IPT.

#### 4.5 Conclusions

Scalable slippery coatings were designed by impregnating lubricant-loaded carriers into a silicone-based blend. The lubricant-loaded carriers were obtained through a three-step procedure by applying negative pressure to enhance the infusing oil within the aerogel's pores. The icephobic and electrical properties of the coatings with various carrier contents were evaluated to obtain an optimized formulation. Using hydroxyterminated silicone oil as a lubricant could promote the production of nonfrozen hydrogen-bonded molecules, which probably contributed to the enhancement of icephobic properties. The coatings containing lubricant-loaded carriers showed acceptable resistance against weathering conditions, including harsh condensation cycles and UV exposure. The electrical properties of the coatings were also assessed using a comprehensive set of test methods under various conditions.

The coatings exhibited decreased dielectric permittivity and loss factor under applied frequency range of  $10^{-4}$ – $10^3$  Hz, very likely due to the nonpolar characteristics of the infused lubricant. Furthermore, due to the insulating effect of the fabricated coatings, they had desirable resistance against electrical discharge and flashover voltage, particularly under wet and polluted conditions. The condensation test also confirmed that the coatings enhanced the insulation performance of the insulators under controlled high-humidity circumstances. The adapted inclined plane test was carried out to evaluate the erosion and tracking resistance of the samples under applied voltage steps. The results confirmed that the coatings with lubricant-loaded-carriers were more resistant against the degradation caused by applied voltage over time, and they preserved a low leakage current even under a high voltage of 3.5 kV.

In summary, the coating containing LLC exhibited desirable anti-icing and electrical performance that opens an avenue towards designing efficient strategies to tackle icing-related challenges on high-voltage insulators.

### **Acknowledgement**

The authors acknowledge all support from the Natural Sciences and Engineering Research Council of Canada (NSERC), Hydro-Québec, and PRIMA Quebec. The authors would like to thank CENGIVRE for providing the icing infrastructure and Ms Caroline Blackburn at the Anti-icing Materials International Laboratory (AMIL), UQAC, for helping carry out the SAT test. They also would like to give very special thanks to Frederick Munger for performing the high voltage test.

## Chapter 5: Conclusions

In this section, the main findings of this project are summarized as the partial and general conclusions. The main results achieved in each paper are first presented, followed by the general conclusion.

### **Fabrication of liquid-infused textured surfaces (LITS): the effect of surface textures on anti-icing properties and durability**

- LIS and liquid-infused textured surfaces (LITS) were produced by combining textured micromorphology and the concept of slipperiness. Then, the morphology and icephobic characteristics of the fabricated surfaces were evaluated in terms of viscosity and infusion percentages of the lubricant. Furthermore, the effect of microtexturing on long-lasting durability was assessed.

- The replication method was employed to produce microtextures on LITS. In this method, the surface of aluminium coupons was chemically etched to obtain microtextured templates. In the next step, the microtextures of the templates were transferred to lubricant-infused silicone elastomer. The silicone oil of two viscosities (50cSt, 500cSt) were infused into the polydimethylsiloxane matrix at five various oil contents.

- The water contact angles of samples containing silicone oil with 50 cSt were higher than those of the samples containing silicone oil with 500 cSt viscosity. This property can be attributed to the contribution of microstructures to the de-wetting characteristics. Moreover, the presence of microtextures and lubricant thickness can affect the droplet velocity on the fabricated surfaces. Depletion/recovery cycle test also confirmed that

the LITS samples had a lower rate of lubricant depletion than the LIS samples, regardless of lubricant viscosity.

- DSC test demonstrated that the oil viscosity had no considerable effect on ice nucleation temperature. The samples containing oil with lower viscosity had a slightly lower ice nucleation temperature than those with the viscosity of 500 cSt possibly because of the heat insulation effect.

- The ice adhesion measurements showed that the LITS samples had an ice adhesion strength of less than 20 kPa that can be related to the synergetic effect of microtextures and infused oil. Moreover, microtextures have a key role in reducing the rate of oil depletion. Therefore, LITS samples presented more durable and stable icephobic characteristics than the LIS samples.

#### **Icephobic behavior of a slippery coating containing nanoporous particles as lubricant-loaded carriers**

- An icephobic coating was designed by embedding lubricant-loaded carriers within a polymeric blend. A three-step procedure was employed to enhance the loading capacity of the carriers and therefore lengthen the durability of the prepared coatings. Furthermore, two different lubricants, namely, silicone oil and hydroxyl-terminated silicone oil, were used to study the effect of oil type on the icephobicity and durability of the coatings.

- TGA results showed that the loaded-lubricant mass percentages for the carriers infused by silicone oil and hydroxyl-terminated silicone oil were approximately 47%

and 63%, respectively. Moreover, BET test confirmed that the lubricants were accommodated within the micropores of the carrier.

- The coating's performance against icing was evaluated using a comprehensive set of methods. In general, the incorporation of lubricant-loaded carriers within the matrix can reduce the ice nucleation temperature. Notably, for samples containing hydroxyl-terminated silicone oil, the reduction in ice nucleation temperature was greater than that for samples containing the silicone oil. The evaluation of the freezing delay time supports this pattern, because samples containing hydroxyl-terminated silicone oil could prolong the icing time more effectively compared with the other group. These improved anti-icing properties can stem from the formation of hydrogen bonding between the hydroxyl groups of the oil and water molecules.

- Generally, heightened lubricant-loaded carrier percentage in the polymeric matrix decreased the amount of ice that accumulated on the surface. This trend can be attributed to the reduced ice adhesion caused by the presence of the slippery-surface mechanism. For samples containing hydroxyl-terminated silicone oil, in addition to the mentioned mechanism, the formation of hydrogen bonds between hydrophilic groups and water molecules produced unfrozen structures, thus further reducing the ice adhesion strength compared with the samples containing silicone oil.

- Monitoring ice adhesion evaluated via the push-off test during 20 subsequent de-icing events confirmed that generally, samples at lower carrier contents showed relative durability in their icephobic performance. This phenomenon can be attributed to the enhanced stability of the lubricant within the coating caused by the three-step

preparation of lubricant carriers that slowed the release rate of the lubricant during the icing/de-icing cycles.

**Icephobicity and electrical assessment of durable slippery coating impregnated with lubricant absorbent materials for application on high-voltage insulators**

- Considering the high demand for durable icephobic coatings for application on high-voltage insulators, a slippery coating was fabricated by incorporating the lubricant-loaded carriers into a polymeric matrix. A three-step procedure based on the application of negative pressure was followed to promote the infusion of the lubricant within the carrier's pores, thus enhancing the service life of the coatings.

- DSC analysis results confirmed that embedding the lubricant-loaded carriers into the silicone-based blend decreased the ice nucleation temperature from approximately  $-16\text{ }^{\circ}\text{C}$  (for the reference) to approximately  $-23.5\text{ }^{\circ}\text{C}$  (for the sample containing 15% lubricant-loaded carrier). Moreover, the slippery-surface mechanism and the production of unfrozen molecules at the ice-coating interface can contribute to the enhanced de-icing performance of the prepared coatings.

- After exposure to UV irradiation and humidity condensation, the effect of the weathering conditions on the icephobic performance was assessed. The coating containing the lubricant-loaded carriers showed relative stability in the icephobic characteristics after harsh condensation cycles and UV exposure. Moreover, considering the application of the prepared coating for insulators, their electrical properties were evaluated using a comprehensive set of electrical tests, including dielectric spectroscopy, flashover, condensation, and inclined plane tests.

- The dielectric spectroscopy confirmed that the coatings containing lubricant-loaded carriers exhibited lower dielectric permittivity and loss factor than the reference, which lacks the carriers under an applied frequency of  $10^{-4}$ – $10^3$  Hz.
- The flash over voltage of the slippery coatings and the uncoated substrates were investigated under various conditions, namely, clean/dry, polluted/dry, and polluted/wet states. Under all conditions, the samples containing lubricant-loaded carriers showed higher flashover levels than those for the bare porcelain substrates. Under wet and polluted condition, the flashover level corresponding to the reference lowered more considerably than that of the samples containing lubricant-loaded carriers.
- Condensation test was performed to assess the electrical performance of the slippery coating under controlled humidity condition. For coatings containing lubricant-loaded carriers, the leakage current remarkably decreased possibly because of the presence of the lubricant, thus enhancing the insulation performance of the coating.
- An adapted version of the inclined plane test for thin films was employed to assess the resistance of the prepared coatings to erosion and tracking as electrical voltage was applied. IPT results confirmed that the coating containing lubricant-loaded carriers showed higher resistance to the degradation caused by the applied voltage compared with the pristine sample. This slippery coating preserved a low leakage current event until the last step, including the high-voltage condition (3.5 kV).

### **General Conclusions**

Ice accretion on the surface of high voltage insulators can result in severe damages, such as deformation, flashover, and power outages. Therefore, two approaches were presented to create slippery LIS with enhanced durable icephobic

characteristics. Inspired by the *Nepenthes* pitcher plant, such coatings can offer an efficient anti-icing solution to protect the infrastructure subjected to harsh cold-weather environment. The replication process was first used to fabricate the slippery surfaces by infusing lubricants into the silicone-based matrix. Then, the icephobic characteristics of the prepared samples were evaluated to determine the effect of the lubricant content and viscosity on their durability. The water droplet velocity increased on the surface containing the lubricant with lower viscosity than that with higher viscosity. The synergistic effect of the combination of microstructures and the slipperiness in the prepared surfaces can reduce ice adhesion strength by four orders of magnitude compared with the reference sample. Moreover, the presence of the microstructures can effectively contribute to the reduction of the rate of lubricant loss by keeping it within the superficial asperities. Therefore, the prepared slippery surfaces can offer more long-lasting icephobic characteristics.

In terms of the low durability of the oil-infused coatings caused by oil depletion, a slippery coating was designed by incorporating lubricant-loaded carriers into a polymeric blend. A three-step method was used by applying the negative pressure, and it increased the loading capacity of the aerogel carriers and controlled the rate of oil migration toward the surface. Therefore, the coating containing lubricant-loaded carriers offered enhanced anti-icing and de-icing properties for a longer service life. The combination of three different mechanisms, namely stress localization (matrix), slippery, and the production of hydrogen bonds between water molecules and the hydroxyl groups of the lubricant played an essential role in obtaining desirable icephobic characteristics.



Third, the coatings containing aerogel carriers infused by hydroxyl-terminated silicone oil, and their electrical performance was assessed using a comprehensive set of tests. Dielectrical spectroscopy showed that incorporating the lubricant-loaded carriers into the coating reduced dielectric permittivity and loss factors. Moreover, the insulation effect of such coatings enhanced their resistance against electrical stresses specially under wet and polluted conditions. Condensation test showed that the coating containing lubricant-loaded carriers could reduce leakage current under high humidity. Moreover, the prepared coating exhibited a desirable level of resistance against degradation under applied voltage.

## Chapter 6: Recommendations

In this Ph.D. thesis, the fabrication of slippery liquid infused surfaces through different strategies is reported. These strategies include the production of micro textures over elastomeric surface and the use of lubricant loaded carriers to guarantee long-lasting surfaces. The fabricated surfaces exhibited remarkable results in terms of icephobicity, lubricant stability, durability, and electrical performances. Some recommendations are worth considering for more investigation in this field.

- In the present work, the effect of microtexturing on lubricant depletion, anti-icing durability, and water droplet velocity was assessed extensively. The use of other types of textures such as nano, micro-nano, hierarchical, and ordered structures could be beneficial. Various structural parameters such as pore size, and pillar dimension could affect the rate of lubricant depletion and durability.
- The use of lubricant absorbent materials could open a new horizon toward increasing the stability of lubricant inside the polymeric matrix and over the surface. Here, silica aerogel with specific pore size and surface area was used. The synthesis of porous particles to control the pore size and surface properties can be employed, and this method can optimize the adsorption-desorption of the lubricant.
- The lubricant was physically infused into the polymeric matrix. It can also be chemically stabilized within the matrix to enhance durability. Moreover, the new category of substance, called SOCAL, can covalently attach to the surface and create a liquid-like layer.

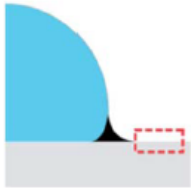



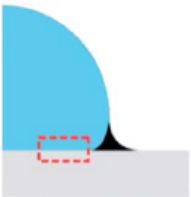


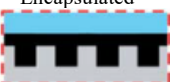
- The use of the proposed strategies remarkably affected the coating durability and lubricant retention, and slippery coatings are still vulnerable under harsh cold-weather conditions. Recently, the idea of lubricant-free slippery materials has gained more attention in eliminating the problems related to lubricant depletion. For this type of surface, solid lubricants such as organogels and polymer brushes can be used, and these materials do not suffer from oil evaporation and shear loss.
- Among the modifications carried out in this research work was the improvement of the mechanical properties by using the appropriate material selection. The selection of other types of either polymeric blends or inorganic lubricant absorbents that are compatible with desired lubricant could lead to obtain slippery coatings with remarkable mechanical robustness.
- The electrical performance of the fabricated coatings was assessed in laboratory scale, including small samples and setups. Scaling-up the experiments in other whole porcelain insulators could provide a better understanding of the performance of the fabricated coatings.

## APPENDIX I

### SUPPORTING INFORMATION FOR LITRATURE REVIEW

**Table A-I.1.** Illustration of wetting configurations, the associated calculations of total interface energies per unit area, and their respective equivalent stability requirements [130].

**Table A-I.2.** Summary of the slippery surface fabrication methods.

Interface	Configuration	Total interface energy per unit area	Equivalent criteria
 <b>Oil-Solid-Air</b>	A1 Dry 	$E_{A1} = r\gamma_{sa}$	$E_{A1} < E_{A2}, E_{A3}$ $S_{os(a)} < -\gamma_{oa} \left( \frac{r-1}{r-\phi} \right)$ $\theta_{os(a)} > \theta_c$
	A2 Impregnated, emerged 	$E_{A2} = (r-\phi)\gamma_{os} + \phi\gamma_{sa} + (1-\phi)\gamma_{oa}$	$E_{A2} < E_{A1}, E_{A3}$ $-\gamma_{oa} \left( \frac{r-1}{r-\phi} \right) < S_{os(a)} < 0$ $0 < \theta_{os(a)} < \theta_c$
	A3 Encapsulated 	$E_{A3} = \gamma_{oa} + r\gamma_{os}$	$E_{A3} < E_{A2}, E_{A1}$ $S_{os(a)} \geq 0$ $\theta_{os(a)} = 0$
 <b>Oil-Solid-Water</b>	W1 Impaled 	$E_{w1} = r\gamma_{sw}$	$E_{w1} < E_{w2}, E_{w3}$ $S_{os(w)} < -\gamma_{ow} \left( \frac{r-1}{r-\phi} \right)$ $\theta_{os(w)} > \theta_c$
	W2 Impregnated, emerged 	$E_{w2} = (r-\phi)\gamma_{os} + \phi\gamma_{sw} + (1-\phi)\gamma_{ow}$	$E_{w2} < E_{w1}, E_{w3}$ $-\gamma_{ow} \left( \frac{r-1}{r-\phi} \right) < S_{os(w)} < 0$ $0 < \theta_{os(w)} < \theta_c$
	W3 Encapsulated 	$E_{w3} = \gamma_{ow} + r\gamma_{os}$	$E_{w3} < E_{w1}, E_{w2}$ $S_{os(w)} \geq 0$ $\theta_{os(w)} = 0$

<b>Surface fabrication method</b>	<b>Category</b>	<b>Material composition</b>	<b>Infused lubricant</b>	<b>Characteristics</b>
<b>Photolithography</b> [48]	Ordered	Silicon wafer/OTS (octadecyl trichlorosilane)	Silicone oil/tetramethyl tetraphenyl trisiloxane	Dependency of the ice adhesion strength of the slippery surface on the texture density.
<b>Laser irradiation/ replication</b> [145]	Ordered	Al/PDMS polymer	Silicone oil	Fabrication of oil-infused slippery surfaces with superhydrophobicity characteristics. - Optimizing the results in terms of viscosity and oil content.
<b>Spraying method</b> [134]	Disordered	SiO <sub>2</sub> nanoparticles/poly (methyl methacrylate) (PMMA)	Perfluorotripentyl amin	Comparison the water repellency of slippery coating with superhydrophobic surfaces. - Development of the one-step substrate-independent,
<b>Spin coater</b> [32]	Disordered	Polytetrafluoroethylene (PTFE)	Perfluoropolyether (PFPE)	transparent SLIPSs. -Evaluation of liquid-repellency, self-cleaning,

<b>Electrodeposition</b> [33]	Disordered	Polypyrrole (PPy) /Al	Perfluoroalkylether (Krytox 100)	icing-delay, and ice adhesion. - Controlling the morphology of the surface by deposition variables and monomer concentration. - Reduction of ice adhesion considerably compared to bare Al.
<b>Double-layered structure/ hydrothermal method</b> [147]	Disordered	$Mg_5(CO_3)_4(OH)_2/Mg_6Al_2(OH)_{18-4}$ phases	Perfluoropolyether (PFPE)	Superior corrosion resistance and anti-icing performance with enhanced durability compared with the SHS coatings.
<b>Liquid Flame Spray</b> [317]	Disordered	Titanium-oxide nanoparticles/ low density polyethylene (LDPE)	Silicone oil	Superior corrosion resistance and anti-icing performance with enhanced durability compared with the SHS coatings.

## APPENDIX II

### SUPPORTING INFORMATION FOR ARTICLE 1

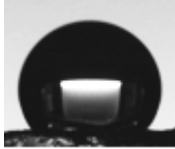
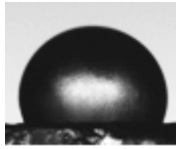
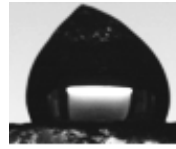

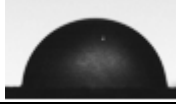
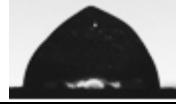


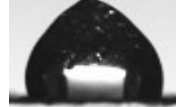



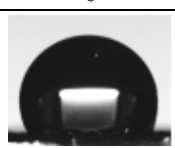

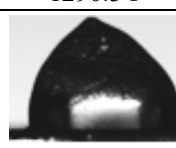
#### **Fabrication of liquid-infused textured surfaces (LITS): the effect of surface textures on anti-icing properties and durability**

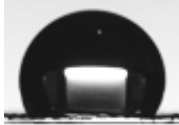
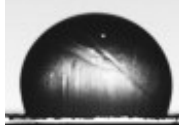
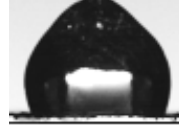

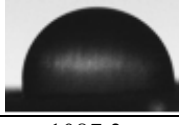
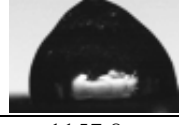
Samaneh Heydarian<sup>1\*</sup>, Khosrow Maghsoudi<sup>1</sup>, Reza Jafari<sup>1</sup>, Hellene Gauthier<sup>2</sup>,  
Gelareh Momen<sup>1</sup>

<sup>1</sup>Department of Applied Sciences, University of Quebec at Chicoutimi (UQAC), 555, boul. de l'Université, Chicoutimi, Quebec, G7H 2B1, Canada.

<sup>2</sup>Institut de recherche d'Hydro-Québec (IREQ) 1800 boul. Lionel-Boulet, Varennes (Québec), J3X 1S1, Canada

\*Corresponding author: E-mail address: samaneh.heydarian-dolatabadi1@uqac.ca. Tel:001(418) 545-5011

Sample	T=0 s	Unset nucleation	Complete freezing
No oil			
	0	120.2 s	188.1 s
10-50			
	0	275.1 s	330.4 s
30-50			
	0	783.5 s	870.1 s
50-50			
	0	1210.2 s	1290.3 s
10-500			
	0	210.2 s	290.7 s

<b>30-500</b>			
	0	701.4 s	775.1 s
<b>50-500</b>			
	0	1087.3 s	1157.8 s

**Figure A-II.1.** Ice nucleation time on the surface of LITS samples.



## APPENDIX III

### SUPPORTING INFORMATION FOR ARTICLE 3

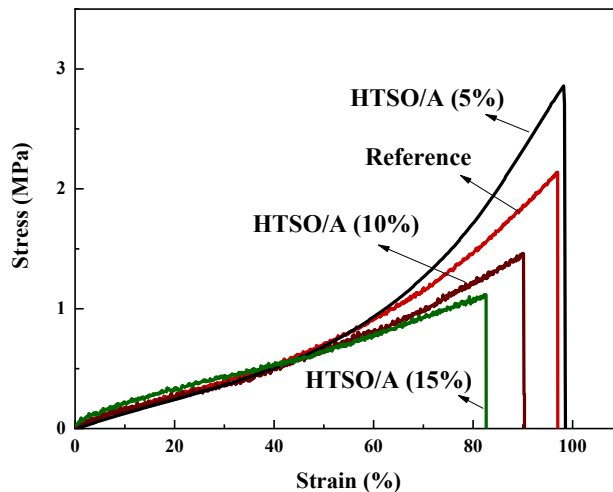
# Icephobicity and Electrical Assessment of Slippery Coating Impregnated with a Stabilized Hydroxyl-terminated Lubricant for High Voltage Insulation Application

Samaneh Heydarian<sup>1\*</sup>, Gelareh Momen<sup>1</sup>, and Reza Jafari<sup>1</sup>

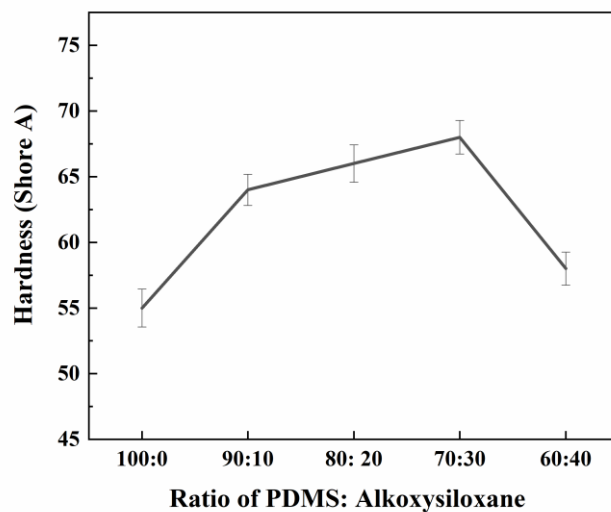
<sup>1</sup>Department of Applied Sciences, University of Québec at Chicoutimi (UQAC), 555, boul. de

l'Université, Chicoutimi, Québec, G7H 2B1, Canada

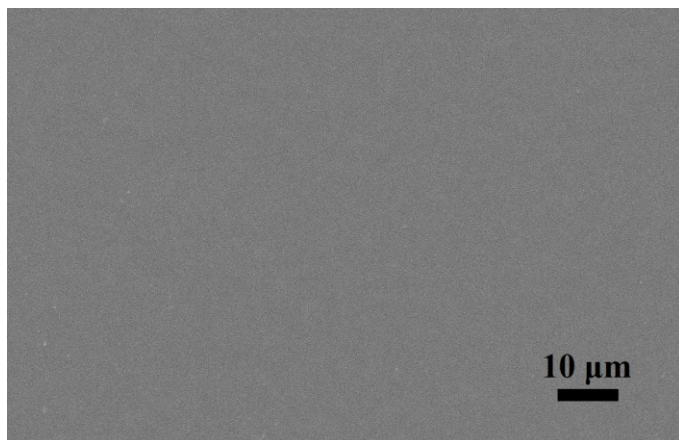
\*Corresponding author: samaneh.heydarian-dolatabadi1@uqac.ca



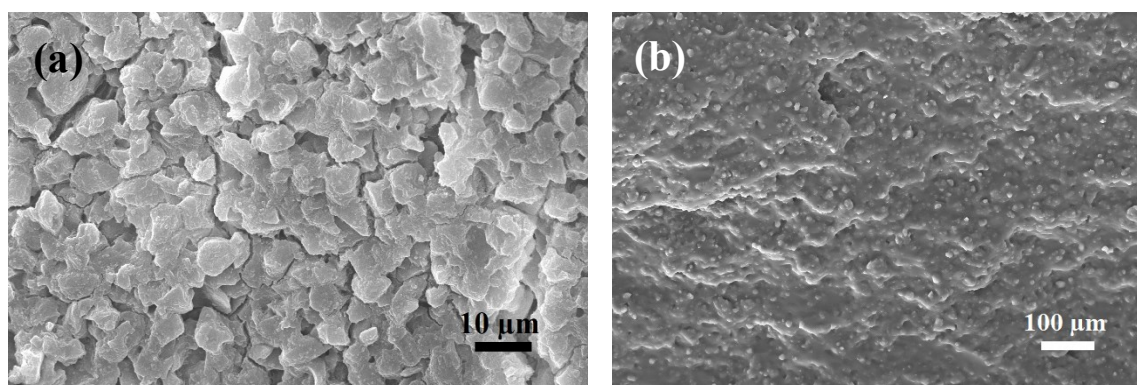
**Figure A-III.1.** Strain-stress curves of the samples containing different HTSPO/A content. The tensile test was conducted using a TA.XTPlus 100 apparatus equipped with a 5 kg load cell. The free films with dimensions of 10 mm × 1 mm × 2 mm. were prepared for the measurements.



**Figure A-III. 2.** Hardness values of the matrixes with different combinations. The hardness of the samples was evaluated via a 2000 max-hand Shore A durometer (Rex Gauge, USA). The measurement was carried out at five points on each sample having a thickness of about  $4.0 \pm 0.1$  mm.



**Figure A-III. 3.** SEM image of the matrix obtaining by mixing PDMS with the alkoxy-siloxane resin (DOWSIL 2405) at a ratio of 70:30, illustrating no evidence of immiscibility in the matrix surface.



**Figure A-III. 4.** Micrographs of the (a) lubricant-loaded carriers (LLCs), and (b) cross-section of the coating containing LLC. These images show that the LLC had the particle size ranged between approximately 5 and 30  $\mu\text{m}$ , and they dispersed, to a larger extent, homogeneously throughout the matrix.

## References

- [1] M. Farzaneh, Ice accretions on high-voltage conductors and insulators and related phenomena, *Philos. Trans. R. Soc. A Math. Phys. Eng. Sci.* 358 (2000) 2971–3005. <https://doi.org/10.1098/rsta.2000.0692>.
- [2] M. Farzaneh, Atmospheric icing of power networks, 2008. <https://doi.org/10.1007/978-1-4020-8531-4>.
- [3] C. Armenakis, N. Nirupama, Urban impacts of ice storms: Toronto December 2013, *Nat. Hazards.* 74 (2014) 1291–1298. <https://doi.org/10.1007/s11069-014-1211-7>.
- [4] M. Farzaneh, Ice accretions on high-voltage conductors and insulators and related phenomena, *Philos. Trans. R. Soc. A Math. Phys. Eng. Sci.* (2000). <https://doi.org/10.1098/rsta.2000.0692>.
- [5] R. Liao, Z. Zuo, C. Guo, A. Zhuang, Y. Yuan, X. Zhao, Y. Zhang, Ice accretion on superhydrophobic insulators under freezing condition, *Cold Reg. Sci. Technol.* (2015). <https://doi.org/10.1016/j.coldregions.2015.01.006>.
- [6] M. Farzaneh, W.A. Chisholm, *Insulators for Icing and Polluted Environments*, 2009. <https://doi.org/10.1002/9780470496251>.
- [7] S.M. Brainsi, *Coatings for Outdoor High Voltage*, (2013).
- [8] V.F. Petrenko, C.R. Sullivan, V. Kozlyuk, F. V. Petrenko, V. Veerasamy, Pulse electro-thermal de-icer (PETD), *Cold Reg. Sci. Technol.* (2011). <https://doi.org/10.1016/j.coldregions.2010.06.002>.
- [9] R.W. Gent, N.P. Dart, J.T. Cansdale, Aircraft icing, *Philos. Trans. R. Soc. A Math. Phys. Eng. Sci.* (2000). <https://doi.org/10.1098/rsta.2000.0689>.
- [10] Arshad, G. Momen, M. Farzaneh, A. Nekahi, Properties and applications of superhydrophobic coatings in high voltage outdoor insulation: A review, *IEEE Trans. Dielectr. Electr. Insul.* 24 (2017) 3630–3646. <https://doi.org/10.1109/TDEI.2017.006725>.
- [11] H. Koivuluoto, C. Stenroos, R. Ruohomaa, G. Bolelli, L. Lusvarghi, P. Vuoristo, Research on icing behavior and ice adhesion testing of icephobic surfaces, *Iwais* 2015. (2015) 1–14. [http://windren.se/IWAIS\\_p/IWAIS2015/IWAIS2015\\_pa/49\\_05\\_04\\_Paper\\_Koivuluoto\\_et\\_al\\_Research\\_on\\_icing\\_behavior\\_and\\_ice\\_adhesion\\_testing\\_of\\_ice\\_phobic\\_surfaces\\_49\\_WAIS\\_2015.pdf](http://windren.se/IWAIS_p/IWAIS2015/IWAIS2015_pa/49_05_04_Paper_Koivuluoto_et_al_Research_on_icing_behavior_and_ice_adhesion_testing_of_ice_phobic_surfaces_49_WAIS_2015.pdf).
- [12] M. Farzaneh, Coatings for the protection of power network equipment in winter conditions, in: *Int. Conf. Mater. Sci. Eng. Technol. (MSET 2014)*, 2014.
- [13] E.A. Cherney, R.S. Gorur, RTV silicone rubber coatings for outdoor insulators, *IEEE Trans. Dielectr. Electr. Insul.* (1999). <https://doi.org/10.1109/94.798117>.
- [14] J. Li, Y. Zhao, J. Hu, L. Shu, X. Shi, Anti-icing performance of a superhydrophobic PDMS/modified nano-silica hybrid coating for insulators, *J. Adhes. Sci. Technol.* (2012). <https://doi.org/10.1163/016942411X574826>.
- [15] G. Momen, M. Farzaneh, Survey of micro/nano filler use to improve silicone rubber for outdoor insulators, *Rev. Adv. Mater. Sci.* (2011).
- [16] X. Li, B. Yang, Y. Zhang, G. Gu, M. Li, L. Mao, A study on superhydrophobic coating in anti-icing of glass/porcelain insulator, *J. Sol-Gel Sci. Technol.* (2014). <https://doi.org/10.1007/s10971-013-3243-y>.

- [17] S.A. Seyedmehdi, H. Zhang, J. Zhu, Superhydrophobic RTV silicone rubber insulator coatings, *Appl. Surf. Sci.* 258 (2012) 2972–2976. <https://doi.org/10.1016/j.apsusc.2011.11.020>.
- [18] Y. Lin, H. Chen, G. Wang, A. Liu, Recent progress in preparation and anti-icing applications of superhydrophobic coatings, *Coatings*. (2018). <https://doi.org/10.3390/coatings8060208>.
- [19] T. Kim, J. Yi, Application of hydrophobic coating to reduce leakage current through surface energy control of high voltage insulator, *Appl. Surf. Sci.* 578 (2022). <https://doi.org/10.1016/j.apsusc.2021.151820>.
- [20] K. Manoharan, S. Bhattacharya, Superhydrophobic surfaces review: Functional application, fabrication techniques and limitations, *J. Micromanufacturing*. 2 (2019) 59–78. <https://doi.org/10.1177/2516598419836345>.
- [21] H.C. Hillborg, Loss and recovery of hydrophobicity of polydimethylsiloxane after exposure to electrical discharges of polydimethylsiloxane after exposure to electrical discharges, 2001.
- [22] M. Nosonovsky, V. Hejazi, Why superhydrophobic surfaces are not always icephobic, *ACS Nano*. 9 (10) (2012) 8488–8491. <https://doi.org/10.1021/nm302138r>.
- [23] A.J. Meuler, G.H. McKinley, R.E. Cohen, Exploiting topographical texture to impart icephobicity, *ACS Nano*. 4 (2010) 7048–7052. <https://doi.org/10.1021/nm103214q>.
- [24] Y. Bai, H. Zhang, Y. Shao, H. Zhang, J. Zhu, Recent progresses of superhydrophobic coatings in different application fields: An overview, *Coatings*. 11 (2021) 1–30. <https://doi.org/10.3390/coatings11020116>.
- [25] A. Hooda, M.S. Goyat, J.K. Pandey, A. Kumar, R. Gupta, A review on fundamentals, constraints and fabrication techniques of superhydrophobic coatings, *Prog. Org. Coatings*. 142 (2020). <https://doi.org/10.1016/j.porgcoat.2020.105557>.
- [26] P. Nguyen-Tri, H.N. Tran, C.O. Plamondon, L. Tuduri, D.V.N. Vo, S. Nanda, A. Mishra, H.P. Chao, A.K. Bajpai, Recent progress in the preparation, properties and applications of superhydrophobic nano-based coatings and surfaces: A review, *Prog. Org. Coatings*. (2019). <https://doi.org/10.1016/j.porgcoat.2019.03.042>.
- [27] M.A. Samaha, M. Gad-el-Hak, Slippery surfaces: A decade of progress, *Phys. Fluids*. 33 (2021). <https://doi.org/10.1063/5.0056967>.
- [28] F. Song, C. Wu, H. Chen, Q. Liu, J. Liu, R. Chen, R. Li, J. Wang, Water-repellent and corrosion-resistance properties of superhydrophobic and lubricant-infused super slippery surfaces, *RSC Adv*. 7 (2017) 44239–44246. <https://doi.org/10.1039/c7ra04816e>.
- [29] V.T.H. Hanh, M.X. Truong, T.Q. Tan, T.B. Nguyen, Nature-inspired slippery polymer thin film for ice-repellent applications, *Bioinspired, Biomim. Nanobiomaterials*. 10 (2021) 107–113. <https://doi.org/10.1680/jbibr.21.00027>.
- [30] H. Niemelä-Anttonen, H. Koivuluoto, M. Tuominen, H. Teisala, P. Juuti, J. Haapanen, J. Harra, C. Stenroos, J. Lahti, J. Kuusipalo, J.M. Mäkelä, P. Vuoristo, Icephobicity of Slippery Liquid Infused Porous Surfaces under Multiple Freeze–Thaw and Ice Accretion–Detachment Cycles, *Adv. Mater. Interfaces*. 5 (2018) 1800828. <https://doi.org/10.1002/admi.201800828>.

- [31] C. Wei, G. Zhang, Q. Zhang, X. Zhan, F. Chen, Silicone Oil-Infused Slippery Surfaces Based on Sol-Gel Process-Induced Nanocomposite Coatings: A Facile Approach to Highly Stable Bioinspired Surface for Biofouling Resistance, *ACS Appl. Mater. Interfaces.* 8 (2016) 34810–34819. <https://doi.org/10.1021/acsami.6b09879>.
- [32] M. Liu, Y. Hou, J. Li, L. Tie, Z. Guo, Transparent slippery liquid-infused nanoparticulate coatings, *Chem. Eng. J.* 337 (2018) 462–470. <https://doi.org/10.1016/j.cej.2017.12.118>.
- [33] P. Kim, T.S. Wong, J. Alvarenga, M.J. Kreder, W.E. Adorno-Martinez, J. Aizenberg, Liquid-infused nanostructured surfaces with extreme anti-ice and anti-frost performance, *ACS Nano.* 6 (2012) 6569–6577. <https://doi.org/10.1021/nn302310q>.
- [34] C. Wei, B. Jin, Q. Zhang, X. Zhan, F. Chen, Anti-icing performance of super-wetting surfaces from icing-resistance to ice-phobic aspects: Robust hydrophobic or slippery surfaces, *J. Alloys Compd.* (2018). <https://doi.org/10.1016/j.jallcom.2018.06.041>.
- [35] S. Heydarian, R. Jafari, G. Momen, Recent progress in the anti-icing performance of slippery liquid-infused surfaces, *Prog. Org. Coatings.* 151 (2021) 106096. <https://doi.org/10.1016/j.porgcoat.2020.106096>.
- [36] G. Liu, Y. Yuan, R. Liao, L. Wang, X. Gao, Fabrication of a porous slippery icephobic surface and effect of lubricant viscosity on anti-icing properties and durability, *Coatings.* 10 (2020). <https://doi.org/10.3390/COATINGS10090896>.
- [37] M. Villegas, Y. Zhang, N. Abu Jarad, L. Soleymani, T.F. Didar, Liquid-Infused Surfaces: A Review of Theory, Design, and Applications, *ACS Nano.* (2019). <https://doi.org/10.1021/acsnano.9b04129>.
- [38] M. Shamshiri, R. Jafari, G. Momen, Icephobic properties of aqueous self-lubricating coatings containing PEG-PDMS copolymers, *Prog. Org. Coatings.* 161 (2021) 106466. <https://doi.org/10.1016/j.porgcoat.2021.106466>.
- [39] L.B. Boinovich, E. V. Chulkova, K.A. Emelyanenko, A.G. Domantovsky, A.M. Emelyanenko, The mechanisms of anti-icing properties degradation for slippery liquid-infused porous surfaces under shear stresses, *J. Colloid Interface Sci.* 609 (2022) 260–268. <https://doi.org/10.1016/j.jcis.2021.11.169>.
- [40] S. Peppou-Chapman, J.K. Hong, A. Waterhouse, C. Neto, Life and death of liquid-infused surfaces: a review on the choice, analysis and fate of the infused liquid layer, *Chem. Soc. Rev.* 49 (2020) 3688–3715. <https://doi.org/10.1039/D0CS00036A>.
- [41] T. Li, Y. Zhuo, V. Håkonsen, S. Rønneberg, J. He, Z. Zhang, Epidermal gland inspired self-repairing slippery lubricant-infused porous coatings with durable low ice adhesion, *Coatings.* 9 (2019) 602. <https://doi.org/10.3390/coatings9100602>.
- [42] C. Urata, G.J. Dunderdale, M.W. England, A. Hozumi, Self-lubricating organogels (SLUGs) with exceptional syneresis-induced anti-sticking properties against viscous emulsions and ices, *J. Mater. Chem. A.* 3 (2015) 12626–12630. <https://doi.org/10.1039/c5ta02690c>.
- [43] C. Urata, G.J. Dunderdale, M.W. England, A. Hozumi, Self-lubricating organogels (SLUGs) with exceptional syneresis-induced anti-sticking properties against viscous emulsions and ices, *J. Mater. Chem. A.* 3 (2015) 12626–12630.

- <https://doi.org/10.1039/c5ta02690c>.
- [44] I. Sotiri, A. Tajik, Y. Lai, C.T. Zhang, Y. Kovalenko, C.R. Nemr, H. Ledoux, J. Alvarenga, E. Johnson, H.S. Patanwala, J.V.I. Timonen, Y. Hu, J. Aizenberg, C. Howell, Tunability of liquid-infused silicone materials for biointerfaces, *Biointerphases*. (2018). <https://doi.org/10.1116/1.5039514>.
- [45] W. Cui, T.A. Pakkanen, Icephobic performance of one-step silicone-oil-infused slippery coatings: Effects of surface energy, oil and nanoparticle contents, *J. Colloid Interface Sci.* 558 (2019) 251–258. <https://doi.org/10.1016/j.jcis.2019.09.119>.
- [46] R. Mukherjee, M. Habibi, Z.T. Rashed, O. Berbert, X. Shi, J.B. Boreyko, Oil-Impregnated Hydrocarbon-Based Polymer Films, *Sci. Rep.* 8 (2018). <https://doi.org/10.1038/s41598-018-29823-7>.
- [47] S. Heydarian, K. Maghsoudi, R. Jafari, H. Gauthier, G. Momen, Fabrication of liquid-infused textured surfaces (LITS): The effect of surface textures on anti-icing properties and durability, *Mater. Today Commun.* 32 (2022) 103935. <https://doi.org/10.1016/J.MTCOMM.2022.103935>.
- [48] S.B. Subramanyam, K. Rykaczewski, K.K. Varanasi, Ice adhesion on lubricant-impregnated textured surfaces, *Langmuir.* 29 (2013) 13414–13418. <https://doi.org/10.1021/la402456c>.
- [49] C. Howell, A. Grinthal, S. Sunny, M. Aizenberg, J. Aizenberg, Designing Liquid-Infused Surfaces for Medical Applications: A Review, *Adv. Mater.* (2018). <https://doi.org/10.1002/adma.201802724>.
- [50] J.S.A. Cortez, B.I. Kharisov, T.E.S. Quezada, T.C.H. García, Micro- and nanoporous materials capable of absorbing solvents and oils reversibly: the state of the art, *Pet. Sci.* (2017). <https://doi.org/10.1007/s12182-016-0143-0>.
- [51] A. Gong, Y. Zheng, Z. Yang, X. Guo, Y. Gao, X. Li, Spray fabrication of superhydrophobic coating on aluminum alloy for corrosion mitigation, *Mater. Today Commun.* 26 (2021). <https://doi.org/10.1016/j.mtcomm.2020.101828>.
- [52] E. Vazirinasab, R. Jafari, G. Momen, Evaluation of atmospheric-pressure plasma parameters to achieve superhydrophobic and self-cleaning HTV silicone rubber surfaces via a single-step, eco-friendly approach, *Surf. Coatings Technol.* 375 (2019) 100–111. <https://doi.org/10.1016/j.surfcoat.2019.07.005>.
- [53] A. Pozzato, S.D. Zilio, G. Fois, D. Vendramin, G. Mistura, M. Belotti, Y. Chen, M. Natali, Superhydrophobic surfaces fabricated by nanoimprint lithography, *Microelectron. Eng.* 83 (2006) 884–888. <https://doi.org/10.1016/j.mee.2006.01.012>.
- [54] Y.Y. Quan, Z. Chen, Y. Lai, Z.S. Huang, H. Li, Recent advances in fabricating durable superhydrophobic surfaces: A review in the aspects of structures and materials, *Mater. Chem. Front.* 5 (2021) 1655–1682. <https://doi.org/10.1039/d0qm00485e>.
- [55] Y. Zhuo, S. Xiao, A. Amirfazli, J. He, Z. Zhang, Polysiloxane as icephobic materials – The past, present and the future, *Chem. Eng. J.* 405 (2021) 127088. <https://doi.org/10.1016/j.cej.2020.127088>.
- [56] S. Heydarian, K. Maghsoudi, R. Jafari, H. Gauthier, G. Momen, Fabrication of liquid-infused textured surfaces (LITS): The effect of surface textures on anti-icing properties and durability, *Mater. Today Commun.* 32 (2022) 103935. <https://doi.org/10.1016/j.mtcomm.2022.103935>.

- [57] S. Heydarian, R. Jafari, G. Momen, Icephobic Behavior of a Slippery Coating Containing Nanoporous Particles as Lubricant-Loaded Carriers, *Surfaces and Interfaces*. 103306 (2023). <https://doi.org/10.1016/j.surfin.2023.103306>.
- [58] S. Heydarian, G. Momen, R. Jafari, Icephobicity and electrical assessment of slippery coating impregnated with a stabilized hydroxyl-terminated lubricant for high voltage insulation application, *J. Mater. Sci.* 58 (2023) 9264–9281. <https://doi.org/10.1007/s10853-023-08600-6>.
- [59] S. Zhang, J. Huang, Y. Cheng, H. Yang, Z. Chen, Y. Lai, Bioinspired Surfaces with Superwettability for Anti-Icing and Ice-Phobic Application: Concept, Mechanism, and Design, *Small*. (2017). <https://doi.org/10.1002/sml.201701867>.
- [60] J. Li, Y. Luo, J. Zhu, H. Li, X. Gao, Subcooled-Water Nonstickiness of Condensate Microdrop Self-Propelling Nanosurfaces, *ACS Appl. Mater. Interfaces*. (2015). <https://doi.org/10.1021/acsami.5b09719>.
- [61] C.W. Lo, V. Sahoo, M.C. Lu, Control of Ice Formation, *ACS Nano*. (2017). <https://doi.org/10.1021/acsnano.6b07348>.
- [62] P. Van Dyke, D. Havard, A. Laneville, Effect of ice and snow on the dynamics of transmission line conductors, in: *Atmos. Icing Power Networks*, 2008. [https://doi.org/10.1007/978-1-4020-8531-4\\_5](https://doi.org/10.1007/978-1-4020-8531-4_5).
- [63] H. Sojoudi, M. Wang, N.D. Boscher, G.H. McKinley, K.K. Gleason, Durable and scalable icephobic surfaces: Similarities and distinctions from superhydrophobic surfaces, *Soft Matter*. 12 (2016) 1938–1963. <https://doi.org/10.1039/c5sm02295a>.
- [64] T. Vasileiou, T.M. Schutzius, D. Poulikakos, Imparting Icephobicity with Substrate Flexibility, *Langmuir*. 33 (2017) 6708–6718. <https://doi.org/10.1021/acs.langmuir.7b01412>.
- [65] O. Parent, A. Ilinca, Anti-icing and de-icing techniques for wind turbines: Critical review, *Cold Reg. Sci. Technol.* 65 (2011) 88–96. <https://doi.org/10.1016/j.coldregions.2010.01.005>.
- [66] E. Vazirinasab, K. Maghsoudi, R. Jafari, G. Momen, A comparative study of the icephobic and self-cleaning properties of Teflon materials having different surface morphologies, *J. Mater. Process. Technol.* 276 (2020) 116415. <https://doi.org/10.1016/j.jmatprotec.2019.116415>.
- [67] K. Maghsoudi, E. Vazirinasab, G. Momen, R. Jafari, Icephobicity and durability assessment of superhydrophobic surfaces: The role of surface roughness and the ice adhesion measurement technique, *J. Mater. Process. Technol.* 276 (2021) 116415. <https://doi.org/10.1016/j.jmatprotec.2020.116883>.
- [68] R. Jafari, G. Momen, M. Farzaneh, Durability enhancement of icephobic fluoropolymer film, *J. Coatings Technol. Res.* 13 (2016) 405–412. <https://doi.org/10.1007/s11998-015-9759-z>.
- [69] X. Zeng, Z. Guo, W. Liu, Recent advances in slippery liquid-infused surfaces with unique properties inspired by nature, *Bio-Design Manuf.* 4 (2021) 506–525. <https://doi.org/10.1007/s42242-021-00133-8>.
- [70] W. Yao, L. Wu, L. Sun, B. Jiang, F. Pan, Recent developments in slippery liquid-infused porous surface, *Prog. Org. Coatings*. 166 (2022). <https://doi.org/10.1016/j.porgcoat.2022.106806>.
- [71] S.S. Latthe, R.S. Sutar, A.K. Bhosale, S. Nagappan, Recent developments in air-



- trapped superhydrophobic and liquid-infused slippery surfaces for anti-icing application, *Prog. Org. Coatings.* 137 (2019) 105373. <https://doi.org/10.1016/j.porgcoat.2019.105373>.
- [72] Q. Liu, Y. Yang, M. Huang, Y. Zhou, Y. Liu, X. Liang, Durability of a lubricant-infused Electrospray Silicon Rubber surface as an anti-icing coating, *Appl. Surf. Sci.* 346 (2015) 68–76. <https://doi.org/10.1016/j.apsusc.2015.02.051>.
- [73] N. Vogel, R.A. Belisle, B. Hatton, T.S. Wong, J. Aizenberg, Transparency and damage tolerance of patternable omniphobic lubricated surfaces based on inverse colloidal monolayers, *Nat. Commun.* 4 (2013) 2176. <https://doi.org/10.1038/ncomms3176>.
- [74] X. Huang, J.D. Chrisman, N.S. Zacharia, Omniphobic slippery coatings based on lubricant-infused porous polyelectrolyte multilayers, *ACS Macro Lett.* 2 (2013) 826–829. <https://doi.org/10.1021/mz400387w>.
- [75] Y. Tuo, H. Zhang, W. Chen, X. Liu, Corrosion protection application of slippery liquid-infused porous surface based on aluminum foil, *Appl. Surf. Sci.* (2017). <https://doi.org/10.1016/j.apsusc.2017.06.170>.
- [76] P. Wang, D. Zhang, R. Qiu, Liquid/solid contact mode of super-hydrophobic film in aqueous solution and its effect on corrosion resistance, *Corros. Sci.* (2012). <https://doi.org/10.1016/j.corsci.2011.08.050>.
- [77] Z. Wang, L. Heng, L. Jiang, Effect of lubricant viscosity on the self-healing properties and electrically driven sliding of droplets on anisotropic slippery surfaces, *J. Mater. Chem. A.* (2018). <https://doi.org/10.1039/c7ta10439a>.
- [78] J. Yong, F. Chen, Q. Yang, Y. Fang, J. Huo, J. Zhang, X. Hou, Nepenthes Inspired Design of Self-Repairing Omniphobic Slippery Liquid Infused Porous Surface (SLIPS) by Femtosecond Laser Direct Writing, *Adv. Mater. Interfaces.* (2017). <https://doi.org/10.1002/admi.201700552>.
- [79] B. Jin, M. Liu, Q. Zhang, X. Zhan, F. Chen, Silicone Oil Swelling Slippery Surfaces Based on Mussel-Inspired Magnetic Nanoparticles with Multiple Self-Healing Mechanisms, *Langmuir.* (2017). <https://doi.org/10.1021/acs.langmuir.7b02691>.
- [80] D. Daniel, M.N. Mankin, R.A. Belisle, T.S. Wong, J. Aizenberg, Lubricant-infused micro/nano-structured surfaces with tunable dynamic omniphobicity at high temperatures, *Appl. Phys. Lett.* 102 (2013) 231603. <https://doi.org/10.1063/1.4810907>.
- [81] I. Sotiri, J.C. Overton, A. Waterhouse, C. Howell, Immobilized liquid layers: A new approach to anti-adhesion surfaces for medical applications, *Exp. Biol. Med.* (2016). <https://doi.org/10.1177/1535370216640942>.
- [82] C. Huang, Z. Guo, Fabrications and Applications of Slippery Liquid-infused Porous Surfaces Inspired from Nature: A Review, *J. Bionic Eng.* (2019). <https://doi.org/10.1007/s42235-019-0096-2>.
- [83] M.A. Samaha, M. Gad-el-Hak, Polymeric slippery coatings: Nature and applications, *Polymers (Basel).* (2014). <https://doi.org/10.3390/polym6051266>.
- [84] L.B. Boinovich, A.M. Emelyanenko, Anti-icing potential of superhydrophobic coatings, *Mendeleev Commun.* (2013). <https://doi.org/10.1016/j.mencom.2013.01.002>.
- [85] B.P. Jelle, The challenge of removing snow downfall on photovoltaic solar cell roofs in order to maximize solar energy efficiency - Research opportunities for

- the future, *Energy Build.* (2013). <https://doi.org/10.1016/j.enbuild.2013.08.010>.
- [86] S.N. Gorb, E. V. Gorb, Anti-icing strategies of plant surfaces: the ice formation on leaves visualized by Cryo-SEM experiments, *Sci. Nat.* 109 (2022) 24. <https://doi.org/10.1007/s00114-022-01789-7>.
- [87] L. Foroughi Mobarakeh, R. Jafari, M. Farzaneh, Robust icephobic, and anticorrosive plasma polymer coating, *Cold Reg. Sci. Technol.* (2018). <https://doi.org/10.1016/j.coldregions.2018.03.009>.
- [88] S. Jin, J. Liu, J. Lv, S. Wu, J. Wang(s), Interfacial Materials for Anti-Icing: Beyond Superhydrophobic Surfaces, *Chem. - An Asian J.* (2018). <https://doi.org/10.1002/asia.201800241>.
- [89] R. Menini, M. Farzaneh, Advanced icephobic coatings, *J. Adhes. Sci. Technol.* 25 (2011) 971–992. <https://doi.org/10.1163/016942410X533372>.
- [90] Peyman Irajizad, S. Nazifi, H. Ghasemi, Icephobic surfaces: Definition and figures of merit, *Adv. Colloid Interface Sci.* 269 (2019) 203–218. <https://doi.org/10.1016/j.cis.2019.04.005>.
- [91] M. Yamazaki, A. Jemcov, H. Sakaue, A review on the current status of icing physics and mitigation in aviation, *Aerospace.* 8 (2021) 188. <https://doi.org/10.3390/aerospace8070188>.
- [92] A. Azimi Yancheshme, G. Momen, R. Jafari Aminabadi, Mechanisms of ice formation and propagation on superhydrophobic surfaces: A review, *Adv. Colloid Interface Sci.* 279 (2020) 102155. <https://doi.org/10.1016/j.cis.2020.102155>.
- [93] Y. Zhuo, V. Håkonsen, Z. He, S. Xiao, J. He, Z. Zhang, Enhancing the Mechanical Durability of Icephobic Surfaces by Introducing Autonomous Self-Healing Function, *ACS Appl. Mater. Interfaces.* 10 (14) (2018) 11972–11978. <https://doi.org/10.1021/acsami.8b01866>.
- [94] K. Golovin, S.P.R. Kobaku, D.H. Lee, E.T. DiLoreto, J.M. Mabry, A. Tuteja, Designing durable icephobic surfaces, *Sci. Adv.* 2 (2016) e1501496. <https://doi.org/10.1126/sciadv.1501496>.
- [95] K. Rykaczewski, S. Anand, S.B. Subramanyam, K.K. Varanasi, Mechanism of frost formation on lubricant-impregnated surfaces, *Langmuir.* 29 (2013) 5230–5238. <https://doi.org/10.1021/la400801s>.
- [96] W. Li, Y. Zhan, S. Yu, Applications of superhydrophobic coatings in anti-icing: Theory, mechanisms, impact factors, challenges and perspectives, *Prog. Org. Coatings.* 152 (2021) 106117. <https://doi.org/10.1016/j.porgcoat.2020.106117>.
- [97] V. Hejazi, K. Sobolev, M. Nosonovsky, From superhydrophobicity to icephobicity: Forces and interaction analysis, *Sci. Rep.* (2013). <https://doi.org/10.1038/srep02194>.
- [98] H. Koivuluoto, C. Stenroos, M. Kylmälahti, M. Apostol, J. Kiilakoski, P. Vuoristo, Anti-icing Behavior of Thermally Sprayed Polymer Coatings, *J. Therm. Spray Technol.* (2017). <https://doi.org/10.1007/s11666-016-0501-x>.
- [99] V. Hejazi, K. Sobolev, M. Nosonovsky, From superhydrophobicity to icephobicity: Forces and interaction analysis, *Sci. Rep.* 3 (2013) 2194. <https://doi.org/10.1038/srep02194>.
- [100] Y. Wang, Y. Sun, Y. Xue, X. Sui, F. Wang, W. Liang, Q. Dong, Multifunctional electro-thermal superhydrophobic shape memory film with in situ reversible wettability and anti-icing/deicing properties, *Colloids Surfaces A Physicochem.*

- Eng. Asp. 654 (2022) 129960. <https://doi.org/10.1016/j.colsurfa.2022.129960>.
- [101] X. Zhou, G. Yang, C. Li, J. Wu, Functional microdroplet self-dislodging icephobic surfaces: A review from mechanism to synergic morphology, *Appl. Therm. Eng.* 215 (2022) 118928. <https://doi.org/10.1016/j.applthermaleng.2022.118928>.
- [102] Q. He, W. He, F. Zhang, Y. Zhao, L. Li, X. Yang, F. Zhang, Research Progress of Self-Cleaning, Anti-Icing, and Aging Test Technology of Composite Insulators, *Coatings*. 12 (2022) 1224. <https://doi.org/10.3390/coatings12081224>.
- [103] A.B.D. Cassie, S. Baxter, Wettability of porous surfaces, *Trans. Faraday Soc.* (1944). <https://doi.org/10.1039/TF9444000546>.
- [104] W. Liao, Z. Jia, Z. Guan, L. Wang, J. Yang, J. Fan, Z. Su, J. Zhou, Reducing ice accumulation on insulators by applying semiconducting RTV silicone coating, *IEEE Trans. Dielectr. Electr. Insul.* (2007). <https://doi.org/10.1109/TDEI.2007.4401227>.
- [105] G. Momen, M. Farzaneh, Study of ice accumulation on nanocomposite semiconducting coatings, in: *Annu. Rep. - Conf. Electr. Insul. Dielectr. Phenomena, CEIDP, 2010*. <https://doi.org/10.1109/CEIDP.2010.5724058>.
- [106] A. Aparna, A.S. Sethulekshmi, A. Saritha, K. Joseph, Recent advances in superhydrophobic epoxy based nanocomposite coatings and their applications, *Prog. Org. Coatings*. 166 (2022). <https://doi.org/10.1016/j.porgcoat.2022.106819>.
- [107] H. He, Z. Guo, Superhydrophobic materials used for anti-icing Theory, application, and development, *IScience*. 24 (2021). <https://doi.org/10.1016/j.isci.2021.103357>.
- [108] J.T. Simpson, S.R. Hunter, T. Aytug, Superhydrophobic materials and coatings: A review, *Reports Prog. Phys.* (2015). <https://doi.org/10.1088/0034-4885/78/8/086501>.
- [109] Y. Wang, J. Xue, Q. Wang, Q. Chen, J. Ding, Verification of icephobic/anti-icing properties of a superhydrophobic surface, *ACS Appl. Mater. Interfaces*. 5 (2013) 3370–3381. <https://doi.org/10.1021/am400429q>.
- [110] A. Allahdini, G. Momen, F. Munger, S. Brettschneider, I. Fofana, R. Jafari, Performance of a nanotextured superhydrophobic coating developed for high-voltage outdoor porcelain insulators, *Colloids Surfaces A Physicochem. Eng. Asp.* 649 (2022) 129461. <https://doi.org/10.1016/J.COLSURFA.2022.129461>.
- [111] H. Jin, P. Jin, R. Niu, Y. Li, B. He, N. Gao, H. Zhang, Flashover characteristics of discrete water droplets on the surface of super-hydrophobic silicone rubber, *IEEE Trans. Dielectr. Electr. Insul.* (2014). <https://doi.org/10.1109/TDEI.2014.004281>.
- [112] I. Ramalla, R.K. Gupta, K. Bansal, Effect on superhydrophobic surfaces on electrical porcelain insulator, improved technique at polluted areas for longer life and reliability, *Int. J. Eng. Technol.* (2015). <https://doi.org/10.14419/ijet.v4i4.5405>.
- [113] F. Z.Kamand, B. Mehmood, R. Ghunem, M.K. Hassan, A. El-Hag, L. Al-Sulaiti, A. Abdala;, Self-Healing Silicones for Outdoor High Voltage Insulation: Mechanism, Applications and Measurements, *Energies*. 15 (2022) 1677. <https://doi.org/10.3390/en15051677>.

- [114] A.C. Ribeiro, B.G. Soares, J.G.M. Furtado, A.A. Silva, N.S.S.E. Couto, Superhydrophobic nanocomposite coatings based on different polysiloxane matrices designed for electrical insulators, *Prog. Org. Coatings*. 168 (2022) 106867. <https://doi.org/10.1016/J.PORGCOAT.2022.106867>.
- [115] Y. Zhao, J. Li, J. Hu, S. Grzybowski, Icing performances of super-hydrophobic PDMS/nano-silica hybrid coating on insulators, *2010 Int. Conf. High Volt. Eng. Appl. ICHVE* 2010. (2010) 489–492. <https://doi.org/10.1109/ICHVE.2010.5640721>.
- [116] M. Ma, R.M. Hill, Superhydrophobic surfaces, *Curr. Opin. Colloid Interface Sci.* (2006). <https://doi.org/10.1016/j.cocis.2006.06.002>.
- [117] S. Wang, K. Liu, X. Yao, L. Jiang, Bioinspired surfaces with superwettability: New insight on theory, design, and applications, *Chem. Rev.* 115 (2015) 8230–8293. <https://doi.org/10.1021/cr400083y>.
- [118] T. Li, T. Ren, J. He, The Inspiration of Nature: Natural Counterparts with Self-cleaning Functions, *RSC Smart Mater.* 2017–Janua (2017) 1–24. <https://doi.org/10.1039/9781782623991-00001>.
- [119] C. Liu, F. Su, J. Liang, P. Huang, Facile fabrication of superhydrophobic cerium coating with micro-nano flower-like structure and excellent corrosion resistance, *Surf. Coatings Technol.* (2014). <https://doi.org/10.1016/j.surfcoat.2014.08.032>.
- [120] P. Roach, N.J. Shirtcliffe, M.I. Newton, Progress in superhydrophobic surface development, *Soft Matter*. (2008). <https://doi.org/10.1039/b712575p>.
- [121] J. He, *Self-cleaning Coatings Structure, Fabrication and Application*, The Royal Society of Chemistry, Cambridge, 2017.
- [122] R.H.A. Ras, A. Marmur, *Non-wettable Surfaces: Theory, Preparation and Applications*, The Royal Society of Chemistry, Cambridge, 2016. <https://doi.org/10.1039/9781782623953>.
- [123] T. Maitra, C. Antonini, M.K. Tiwari, A. Mularczyk, Z. Imeri, P. Schoch, D. Poulikakos, Supercooled water drops impacting superhydrophobic textures, *Langmuir*. (2014). <https://doi.org/10.1021/la502675a>.
- [124] K. Ji, V. Tomchak, K. Xu, F. Jee, Super-antiwetting with High Adhesion Property of Pitcher Plant, *Nanomedicine Nanotechnol.* 8 (2017) 8–10. <https://doi.org/10.4172/2157-7439.1000424>.
- [125] S.C. Rahul Sharma, Sankha Shuvra Das, Udit Uday Ghosh, Sunando DasGupta, Pitcher Plant Inspired Biomimetic Liquid Infused Slippery Surface Using Taro Leaf, *Arxiv Soft Condens. Matter*. (2018).
- [126] S. Sunny, N. Vogel, C. Howell, T.L. Vu, J. Aizenberg, Lubricant-Infused Nanoparticulate Coatings Assembled by Layer-by-Layer Deposition, *Adv. Funct. Mater.* (2014). <https://doi.org/10.1002/adfm.201401289>.
- [127] C. Howell, T.L. Vu, C.P. Johnson, X. Hou, O. Ahanotu, J. Alvarenga, D.C. Leslie, O. Uzun, A. Waterhouse, P. Kim, M. Super, M. Aizenberg, D.E. Ingber, J. Aizenberg, Stability of surface-immobilized lubricant interfaces under flow, *Chem. Mater.* 27 (2015) 1792–1800. <https://doi.org/10.1021/cm504652g>.
- [128] T.S. Wong, S.H. Kang, S.K.Y. Tang, E.J. Smythe, B.D. Hatton, A. Grinthal, J. Aizenberg, Bioinspired self-repairing slippery surfaces with pressure-stable omniphobicity, *Nature*. 477 (2011) 443–447. <https://doi.org/10.1038/nature10447>.

- [129] S. Yuan, S. Luan, S. Yan, H. Shi, J. Yin, Facile Fabrication of Lubricant-Infused Wrinkling Surface for Preventing Thrombus Formation and Infection, *ACS Appl. Mater. Interfaces*. (2015). <https://doi.org/10.1021/acsami.5b05865>.
- [130] J.D. Smith, R. Dhiman, S. Anand, E. Reza-Garduno, R.E. Cohen, G.H. McKinley, K.K. Varanasi, Droplet mobility on lubricant-impregnated surfaces, *Soft Matter*. 9 (2013) 1772–1780. <https://doi.org/10.1039/c2sm27032c>.
- [131] F. Schellenberger, J. Xie, N. Encinas, A. Hardy, M. Klapper, P. Papadopoulos, H.J. Butt, D. Vollmer, Direct observation of drops on slippery lubricant-infused surfaces, *Soft Matter*. 11 (2015) 7617–7626. <https://doi.org/10.1039/c5sm01809a>.
- [132] A. Keiser, L. Keiser, C. Clanet, D. Quéré, Drop friction on liquid-infused materials, *Soft Matter*. 13 (2017) 6981–6987. <https://doi.org/10.1039/c7sm01226h>.
- [133] A. Hosseini, M. Villegas, J. Yang, M. Badv, J.I. Weitz, L. Soleymani, T.F. Didar, Conductive Electrochemically Active Lubricant-Infused Nanostructured Surfaces Attenuate Coagulation and Enable Friction-Less Droplet Manipulation, *Adv. Mater. Interfaces*. (2018). <https://doi.org/10.1002/admi.201800617>.
- [134] N. Wang, D. Xiong, Y. Lu, S. Pan, K. Wang, Y. Deng, Y. Shi, Design and Fabrication of the Lyophobic Slippery Surface and Its Application in Anti-Icing, *J. Phys. Chem. C*. (2016). <https://doi.org/10.1021/acs.jpcc.6b04778>.
- [135] J. Sun, W. Cheng, J.L. Song, Y. Lu, Y.K. Sun, L. Huang, X. Liu, Z.J. Jin, C.J. Carmalt, I.P. Parkin, Fabrication of superhydrophobic micro post array on aluminum substrates using mask electrochemical machining, *Chinese J. Mech. Eng. (English Ed.)*. (2018). <https://doi.org/10.1186/s10033-018-0270-1>.
- [136] R. Jafari, C. Cloutier, A. Allahdini, G. Momen, Recent progress and challenges with 3D printing of patterned hydrophobic and superhydrophobic surfaces, *Int. J. Adv. Manuf. Technol.* 103 (2019) 1225–1238. <https://doi.org/10.1007/s00170-019-03630-4>.
- [137] C. Lee, C.H. Choi, C.J. Kim, Structured surfaces for a giant liquid slip, *Phys. Rev. Lett.* 101 (2008) 064501. <https://doi.org/10.1103/PhysRevLett.101.064501>.
- [138] K. Maghsoudi, R. Jafari, G. Momen, M. Farzaneh, Micro-nanostructured polymer surfaces using injection molding: A review, *Mater. Today Commun.* 13 (2017) 126–143. <https://doi.org/10.1016/j.mtcomm.2017.09.013>.
- [139] M. Shamshiri, A. Manaia, T. Vuchkov, A. Carvalho, G. Gaspar, A. Fernandes, S.H. Dolatabadi, F. Costa, A. Cavaleiro, Influence of laser structural patterning on the tribological performance of C-alloyed W-S coatings, *Surf. Coatings Technol.* 394 (2020) 125822. <https://doi.org/10.1016/j.surfcoat.2020.125822>.
- [140] R. Jafari, G. Momen, E. Eslami, Fabrication of icephobic aluminium surfaces by atmospheric plasma jet polymerisation, *Surf. Eng.* 35 (2019) 450–455. <https://doi.org/10.1080/02670844.2018.1509813>.
- [141] B. Qian, Z. Shen, Fabrication of superhydrophobic surfaces by dislocation-selective chemical etching on aluminum, copper, and zinc substrates, *Langmuir*. 21 (2005) 9007–9009. <https://doi.org/10.1021/la051308c>.
- [142] S. Nagappan, J.J. Park, S.S. Park, C.-S. Ha, Preparation of superhydrophobic and transparent micro-nano hybrid coatings from polymethylhydroxysiloxane and silica ormosil aerogels, *Nano Converg.* (2014).

- <https://doi.org/10.1186/s40580-014-0030-6>.
- [143] Y. Song, C. Wang, X. Dong, K. Yin, F. Zhang, Z. Xie, D. Chu, J. Duan, Controllable superhydrophobic aluminum surfaces with tunable adhesion fabricated by femtosecond laser, *Opt. Laser Technol.* (2018). <https://doi.org/10.1016/j.optlastec.2017.12.024>.
- [144] K. Maghsoudi, G. Momen, R. Jafari, M. Farzaneh, Direct replication of micro-nanostructures in the fabrication of superhydrophobic silicone rubber surfaces by compression molding, *Appl. Surf. Sci.* 458 (2018) 619–628. <https://doi.org/10.1016/j.apsusc.2018.07.099>.
- [145] Y.H. Yeong, C. Wang, K.J. Wynne, M.C. Gupta, Oil-infused superhydrophobic silicone material for low ice adhesion with long-term infusion stability, *ACS Appl. Mater. Interfaces.* 8 (2016) 32050–32059. <https://doi.org/10.1021/acsami.6b11184>.
- [146] A.J. Meuler, J.D. Smith, K.K. Varanasi, J.M. Mabry, G.H. McKinley, R.E. Cohen, Relationships between water wettability and ice adhesion, *ACS Appl. Mater. Interfaces.* 2 (11) (2010) 3100–3110. <https://doi.org/10.1021/am1006035>.
- [147] J. Zhang, C. Gu, J. Tu, Robust Slippery Coating with Superior Corrosion Resistance and Anti-Icing Performance for AZ31B Mg Alloy Protection, *ACS Appl. Mater. Interfaces.* (2017). <https://doi.org/10.1021/acsami.7b00972>.
- [148] S. Anand, A.T. Paxson, R. Dhiman, J.D. Smith, K.K. Varanasi, Enhanced condensation on lubricant-impregnated nanotextured surfaces, *ACS Nano.* 6 (2012) 10122–10129. <https://doi.org/10.1021/nn303867y>.
- [149] J. Lv, Y. Song, L. Jiang, J. Wang, Bio-inspired strategies for anti-icing, *ACS Nano.* (2014). <https://doi.org/10.1021/nn406522n>.
- [150] X. Yao, S.S. Dunn, P. Kim, M. Duffy, J. Alvarenga, J. Aizenberg, Fluorogel elastomers with tunable transparency, elasticity, shape-memory, and antifouling properties, *Angew. Chemie - Int. Ed.* 53 (2014) 4418–4422. <https://doi.org/10.1002/anie.201310385>.
- [151] C. Howell, T.L. Vu, J.J. Lin, S. Kolle, N. Juthani, E. Watson, J.C. Weaver, J. Alvarenga, J. Aizenberg, Self-replenishing vascularized fouling-release surfaces, *ACS Appl. Mater. Interfaces.* (2014). <https://doi.org/10.1021/am503150y>.
- [152] X. Yao, S. Wu, L. Chen, J. Ju, Z. Gu, M. Liu, J. Wang, L. Jiang, Self-Replenishable Anti-Waxing Organogel Materials, *Angew. Chemie - Int. Ed.* (2015). <https://doi.org/10.1002/anie.201503031>.
- [153] J. Cui, D. Daniel, A. Grinthal, K. Lin, J. Aizenberg, Dynamic polymer systems with self-regulated secretion for the control of surface properties and material healing, *Nat. Mater.* (2015). <https://doi.org/10.1038/nmat4325>.
- [154] T.V.J. Charpentier, A. Neville, S. Baudin, M.J. Smith, M. Euvrard, A. Bell, C. Wang, R. Barker, Liquid infused porous surfaces for mineral fouling mitigation, *J. Colloid Interface Sci.* (2015). <https://doi.org/10.1016/j.jcis.2014.12.043>.
- [155] A.B. Tesler, P. Kim, S. Kolle, C. Howell, O. Ahanotu, J. Aizenberg, Extremely durable biofouling-resistant metallic surfaces based on electrodeposited nanoporous tungstite films on steel, *Nat. Commun.* (2015). <https://doi.org/10.1038/ncomms9649>.
- [156] I. Okada, S. Shiratori, High-transparency, self-standable Gel-SLIPS fabricated

- by a facile nanoscale phase separation, *ACS Appl. Mater. Interfaces*. (2014). <https://doi.org/10.1021/am404077h>.
- [157] L. Zhu, J. Xue, Y. Wang, Q. Chen, J. Ding, Q. Wang, Ice-phobic coatings based on silicon-oil-infused polydimethylsiloxane, *ACS Appl. Mater. Interfaces*. 5 (2013) 4053–4062. <https://doi.org/10.1021/am400704z>.
- [158] Y. Wang, X. Yao, J. Chen, Z. He, J. Liu, Q. Li, J. Wang, L. Jiang, Organogel as durable anti-icing coatings, *Sci. China Mater.* 58 (2015) 559–565. <https://doi.org/10.1007/s40843-015-0069-7>.
- [159] G. Zhang, Q. Zhang, T. Cheng, X. Zhan, F. Chen, Polyols-Infused Slippery Surfaces Based on Magnetic Fe<sub>3</sub>O<sub>4</sub>-Functionalized Polymer Hybrids for Enhanced Multifunctional Anti-Icing and Deicing Properties, *Langmuir*. 34 (2018) 4052–4058. <https://doi.org/10.1021/acs.langmuir.8b00286>.
- [160] J. Chen, R. Dou, D. Cui, Q. Zhang, Y. Zhang, F. Xu, X. Zhou, J. Wang, Y. Song, L. Jiang, Robust prototypical anti-icing coatings with a self-lubricating liquid water layer between ice and substrate, *ACS Appl. Mater. Interfaces*. 5 (2013) 4026–4030. <https://doi.org/10.1021/am401004t>.
- [161] J. Chen, Z. Luo, Q. Fan, J. Lv, J. Wang, Anti-Ice coating inspired by ice skating, *Small*. 10 (2014) 4693–4699. <https://doi.org/10.1002/sml.201401557>.
- [162] J. Chen, K. Li, S. Wu, J. Liu, K. Liu, Q. Fan, Durable Anti-Icing Coatings Based on Self-Sustainable Lubricating Layer, *ACS Omega*. 2 (2017) 2047–2054. <https://doi.org/10.1021/acsomega.7b00359>.
- [163] R. Dou, J. Chen, Y. Zhang, X. Wang, D. Cui, Y. Song, L. Jiang, J. Wang, Anti-icing coating with an aqueous lubricating layer, *ACS Appl. Mater. Interfaces*. 6 (2014) 6998–7003. <https://doi.org/10.1021/am501252u>.
- [164] Z. He, W.J. Xie, Z. Liu, G. Liu, Z. Wang, Y.Q. Gao, J. Wang, Tuning ice nucleation with counterions on polyelectrolyte brush surfaces, *Sci. Adv.* (2016). <https://doi.org/10.1126/sciadv.1600345>.
- [165] Z. Liu, Z. He, J. Lv, Y. Jin, S. Wu, G. Liu, F. Zhou, J. Wang, Ion-specific ice propagation behavior on polyelectrolyte brush surfaces, *RSC Adv.* (2017). <https://doi.org/10.1039/c6ra24847k>.
- [166] B. Weber, Y. Nagata, S. Ketzetzi, F. Tang, W.J. Smit, H.J. Bakker, E.H.G. Backus, M. Bonn, D. Bonn, Molecular Insight into the Slipperiness of Ice, *J. Phys. Chem. Lett.* (2018). <https://doi.org/10.1021/acs.jpcclett.8b01188>.
- [167] G. Amit, Why is ice slippery?, *New Sci.* (2015). [https://doi.org/10.1016/S0262-4079\(15\)31136-2](https://doi.org/10.1016/S0262-4079(15)31136-2).
- [168] D. Chen, M.D. Gelenter, M. Hong, R.E. Cohen, G.H. McKinley, Icephobic surfaces induced by interfacial nonfrozen water, *ACS Appl. Mater. Interfaces*. 9 (2017) 4202–4214. <https://doi.org/10.1021/acsami.6b13773>.
- [169] S. Chernyy, M. Järn, K. Shimizu, A. Swerin, S.U. Pedersen, K. Daasbjerg, L. Makkonen, P. Claesson, J. Iruthayaraj, Superhydrophilic polyelectrolyte brush layers with imparted anti-icing properties: Effect of counter ions, *ACS Appl. Mater. Interfaces*. 6 (2014) 6487–6496. <https://doi.org/10.1021/am500046d>.
- [170] X. Wang, J. Huang, Z. Guo, Overview of the development of slippery surfaces: Lubricants from presence to absence, *Adv. Colloid Interface Sci.* 301 (2022). <https://doi.org/10.1016/j.cis.2022.102602>.
- [171] F. Barca, T. Caporossi, S. Rizzo, Silicone oil: Different physical proprieties and clinical applications, *Biomed Res. Int.* 2014 (2014).

- <https://doi.org/10.1155/2014/502143>.
- [172] L. Xiao, J. Li, S. Mieszkin, A. Di Fino, A.S. Clare, M.E. Callow, J.A. Callow, M. Grunze, A. Rosenhahn, P.A. Levkin, Slippery liquid-infused porous surfaces showing marine antibiofouling properties, *ACS Appl. Mater. Interfaces*. 5 (2013) 10074–10080. <https://doi.org/10.1021/am402635p>.
- [173] M. Zhang, M. Dong, S. Chen, Z. Guo, Slippery liquid-infused porous surface fabricated on aluminum maintains stable corrosion resistance at elevated temperatures, *Eng. Sci.* 3 (2018) 67–76. <https://doi.org/10.30919/es8d732>.
- [174] W. Ma, Y. Higaki, H. Otsuka, A. Takahara, Perfluoropolyether-infused nano-texture: A versatile approach to omniphobic coatings with low hysteresis and high transparency, *Chem. Commun.* 49 (2013) 597–599. <https://doi.org/10.1039/c2cc37576a>.
- [175] J.G. Drobny, S. Ebnesajjad, Fluoroelastomers, in: *Introd. to Fluoropolymers Mater. Technol. Appl. A Vol. Plast. Des. Libr. Second Ed.*, 2020: pp. 271–319. <https://doi.org/10.1016/B978-0-12-819123-1.00016-1>.
- [176] H.L. Hays, D. Mathew, J. Chapman, Fluorides and Fluorocarbons Toxicity, 2020. <http://www.ncbi.nlm.nih.gov/pubmed/28613550>.
- [177] J.W. Clayton, The toxicity of fluorocarbons with special reference to chemical constitution, *J. Occup. Med.* 4 (1962) 262–273.
- [178] K. Manabe, K.H. Kyung, S. Shiratori, Biocompatible slippery fluid-infused films composed of chitosan and alginate via layer-by-layer self-assembly and their antithrombogenicity, *ACS Appl. Mater. Interfaces*. 7 (2015) 4763–4771. <https://doi.org/10.1021/am508393n>.
- [179] X.Q. Wang, C.D. Gu, L.Y. Wang, J.L. Zhang, J.P. Tu, Ionic liquids-infused slippery surfaces for condensation and hot water repellency, *Chem. Eng. J.* 343 (2018) 561–571. <https://doi.org/10.1016/j.cej.2018.03.045>.
- [180] Y. Galvan, K.R. Phillips, M. Haumann, P. Wasserscheid, R. Zarraga, N. Vogel, Ionic-Liquid-Infused Nanostructures as Repellent Surfaces, *Langmuir*. 34 (2018) 6894–6902. <https://doi.org/10.1021/acs.langmuir.7b03993>.
- [181] S. Ozbay, C. Yuceel, H.Y. Erbil, Improved Icephobic Properties on Surfaces with a Hydrophilic Lubricating Liquid, *ACS Appl. Mater. Interfaces*. (2015). <https://doi.org/10.1021/acsami.5b07265>.
- [182] D.F. Miranda, C. Urata, B. Masheder, G.J. Dunderdale, M. Yagihashi, A. Hozumi, Physically and chemically stable ionic liquid-infused textured surfaces showing excellent dynamic omniphobicity, *APL Mater.* 2 (2014). <https://doi.org/10.1063/1.4876636>.
- [183] Y. Chen, Z. Guo, An ionic liquid-infused slippery surface for temperature stability, shear resistance and corrosion resistance, *J. Mater. Chem. A*. 8 (2020) 24075–24085. <https://doi.org/10.1039/d0ta08717c>.
- [184] Q. Rao, A. Li, J. Zhang, J. Jiang, Q. Zhang, X. Zhan, F. Chen, Multi-functional fluorinated ionic liquid infused slippery surfaces with dual-responsive wettability switching and self-repairing, *J. Mater. Chem. A*. 7 (2019) 2172–2183. <https://doi.org/10.1039/c8ta08956f>.
- [185] J. Li, E. Ueda, D. Paulssen, P.A. Levkin, Slippery Lubricant-Infused Surfaces: Properties and Emerging Applications, *Adv. Funct. Mater.* (2019). <https://doi.org/10.1002/adfm.201802317>.
- [186] G. Wang, Z. Guo, Liquid infused surfaces with anti-icing properties, *Nanoscale*.



- 11 (2019) 22615–22635. <https://doi.org/10.1039/c9nr06934h>.
- [187] H. Tsuchiya, M. Tenjimbayashi, T. Moriya, R. Yoshikawa, K. Sasaki, R. Togasawa, T. Yamazaki, K. Manabe, S. Shiratori, Liquid-Infused Smooth Surface for Improved Condensation Heat Transfer, *Langmuir*. (2017). <https://doi.org/10.1021/acs.langmuir.7b01991>.
- [188] Y. Zhang, M.R. Klittich, M. Gao, A. Dhinojwala, Delaying Frost Formation by Controlling Surface Chemistry of Carbon Nanotube-Coated Steel Surfaces, *ACS Appl. Mater. Interfaces*. (2017). <https://doi.org/10.1021/acsami.6b11531>.
- [189] S. Sett, X. Yan, G. Barac, L.W. Bolton, N. Miljkovic, Lubricant-Infused Surfaces for Low-Surface-Tension Fluids: Promise versus Reality, *ACS Appl. Mater. Interfaces*. (2017). <https://doi.org/10.1021/acsami.7b10756>.
- [190] Q. Li, Z. Guo, Fundamentals of icing and common strategies for designing biomimetic anti-icing surfaces, *J. Mater. Chem. A*. 6 (2018) 13549–13581. <https://doi.org/10.1039/c8ta03259a>.
- [191] Y. Yang, Z.G. Zhang, E.A. Grulke, W.B. Anderson, G. Wu, Heat transfer properties of nanoparticle-in-fluid dispersions (nanofluids) in laminar flow, *Int. J. Heat Mass Transf.* (2005). <https://doi.org/10.1016/j.ijheatmasstransfer.2004.09.038>.
- [192] X. Dai, B.B. Stogin, S. Yang, T.S. Wong, Slippery Wenzel State, *ACS Nano*. (2015). <https://doi.org/10.1021/acs.nano.5b04151>.
- [193] B.R. Solomon, K.S. Khalil, K.K. Varanasi, Drag reduction using lubricant-impregnated surfaces in viscous laminar flow, *Langmuir*. (2014). <https://doi.org/10.1021/la5021143>.
- [194] P. Irajizad, M. Hasnain, N. Farokhnia, S.M. Sajadi, H. Ghasemi, Magnetic slippery extreme icephobic surfaces, *Nat. Commun.* (2016). <https://doi.org/10.1038/ncomms13395>.
- [195] P. Irajizad, S. Nazifi, H. Ghasemi, Icephobic surfaces: Definition and figures of merit, *Adv. Colloid Interface Sci.* 269 (2019) 203–218. <https://doi.org/10.1016/j.cis.2019.04.005>.
- [196] H. Geng, X. Liu, G. Shi, G. Bai, J. Ma, J. Chen, Z. Wu, Y. Song, H. Fang, J. Wang, Graphene Oxide Restricts Growth and Recrystallization of Ice Crystals, *Angew. Chemie - Int. Ed.* (2017). <https://doi.org/10.1002/anie.201609230>.
- [197] Y. Shen, X. Wu, J. Tao, C. Zhu, Y. Lai, Z. Chen, Icephobic materials: Fundamentals, performance evaluation, and applications, *Prog. Mater. Sci.* (2019). <https://doi.org/10.1016/j.pmatsci.2019.03.004>.
- [198] M.J. Coady, M. Wood, G.Q. Wallace, K.E. Nielsen, A.M. Kietzig, F. Lagugné-Labarthe, P.J. Ragona, Icephobic Behavior of UV-Cured Polymer Networks Incorporated into Slippery Lubricant-Infused Porous Surfaces: Improving SLIPS Durability, *ACS Appl. Mater. Interfaces*. 10 (2018) 2890–2896. <https://doi.org/10.1021/acsami.7b14433>.
- [199] X. Sun, V.G. Damle, S. Liu, K. Rykaczewski, Bioinspired Stimuli-Responsive and Antifreeze-Secreting Anti-Icing Coatings, *Adv. Mater. Interfaces*. 2 (5) (2015) 1400479. <https://doi.org/10.1002/admi.201400479>.
- [200] K. Golovin, A. Tuteja, A predictive framework for the design and fabrication of icephobic polymers, *Sci. Adv.* 3 (2017) e1701617. <https://doi.org/10.1126/sciadv.1701617>.
- [201] X. Zhao, L. Bi, B. Khatir, J.E. Wulff, K. Golovin, Crosslinking Inert Liquidlike

- Polydimethylsiloxane Brushes Using Bis-Diazirine Chemical Insertion for Enhanced Mechanical Durability, *SSRN Electron. J.* (2022). <https://doi.org/10.2139/ssrn.4009563>.
- [202] Z.A. Dijvejin, M.C. Jain, R. Kozak, M.H. Zarifi, K. Golovin, Smart low interfacial toughness coatings for on-demand de-icing without melting, *Nat. Commun.* 13 (2022) 5119. <https://doi.org/10.1038/s41467-022-32852-6>.
- [203] L.O. Andersson, C.G. Golander, S. Persson, Ice adhesion to rubber materials, *J. Adhes. Sci. Technol.* 8 (1994) 117–132. <https://doi.org/10.1163/156856194X00104>.
- [204] K. Zhang, X. Li, Y. Zhao, K. Zhu, Y. Li, C. Tao, X. Yuan, UV-curable POSS-fluorinated methacrylate diblock copolymers for icephobic coatings, *Prog. Org. Coatings.* 93 (2016) 87–96. <https://doi.org/10.1016/j.porgcoat.2016.01.005>.
- [205] R.J. Good, Theory of “Cohesive” vs “Adhesive” Separation in an Adhering System, *J. Adhes.* (1972). <https://doi.org/10.1080/00218467208072218>.
- [206] S.H. Anastasiadis, H. Retsos, S. Pispas, N. Hadjichristidis, S. Neophytides, Smart polymer surfaces, *Macromolecules.* (2003). <https://doi.org/10.1021/ma0211129>.
- [207] S. Wooh, D. Vollmer, Silicone Brushes: Omniphobic Surfaces with Low Sliding Angles, *Angew. Chemie - Int. Ed.* (2016). <https://doi.org/10.1002/anie.201511895>.
- [208] L. Wang, T.J. McCarthy, Covalently Attached Liquids: Instant Omniphobic Surfaces with Unprecedented Repellency, *Angew. Chemie - Int. Ed.* (2016). <https://doi.org/10.1002/anie.201509385>.
- [209] H. Zhao, C.A. Deshpande, L. Li, X. Yan, M.J. Hoque, G. Kuntumalla, M.C. Rajagopal, H.C. Chang, Y. Meng, S. Sundar, P. Ferreira, C. Shao, S. Salapaka, S. Sinha, N. Miljkovic, Extreme Antiscaling Performance of Slippery Omniphobic Covalently Attached Liquids, *ACS Appl. Mater. Interfaces.* (2020). <https://doi.org/10.1021/acsami.9b22145>.
- [210] J.W. Krumpfer, T.J. McCarthy, Rediscovering silicones: “unreactive” silicones react with inorganic surfaces, *Langmuir.* (2011). <https://doi.org/10.1021/la202583w>.
- [211] Y. Tsuge, T. Moriya, Y. Moriyama, Y. Tokura, S. Shiratori, Slippery Liquid-Immobilized Coating Films Using in Situ Oxidation-Reduction Reactions of Metal Ions in Polyelectrolyte Films, *ACS Appl. Mater. Interfaces.* (2017). <https://doi.org/10.1021/acsami.7b01869>.
- [212] D. Ceylan, S. Dogu, B. Karacik, S.D. Yakan, O.S. Okay, O. Okay, Evaluation of butyl rubber as sorbent material for the removal of oil and polycyclic aromatic hydrocarbons from seawater, *Environ. Sci. Technol.* 43 (2009) 3846–3852. <https://doi.org/10.1021/es900166v>.
- [213] H. Li, L. Liu, F. Yang, Hydrophobic modification of polyurethane foam for oil spill cleanup, *Mar. Pollut. Bull.* 64 (2012) 1648–1653. <https://doi.org/10.1016/j.marpolbul.2012.05.039>.
- [214] B.I.K. Javier S. Acevedo Cortez, T.E.S. Quezada, T.C.H. García, Micro- and nanoporous materials capable of absorbing solvents and oils reversibly: the state of the art, *Pet. Sci.* 14 (2017) 84–104. <https://doi.org/10.1007/s12182-016-0143-0>.
- [215] S. Zhao, L. Yin, Q. Zhou, C. Liu, K. Zhou, In situ self-assembly of zeolitic

- imidazolate frameworks on the surface of flexible polyurethane foam: Towards for highly efficient oil spill cleanup and fire safety, *Appl. Surf. Sci.* 506 (2020). <https://doi.org/10.1016/j.apsusc.2019.144700>.
- [216] J. Lin, Y. Shang, B. Ding, J. Yang, J. Yu, S.S. Al-Deyab, Nanoporous polystyrene fibers for oil spill cleanup, *Mar. Pollut. Bull.* 64 (2012) 347–352. <https://doi.org/10.1016/j.marpolbul.2011.11.002>.
- [217] Q.F. Wei, R.R. Mather, A.F. Fotheringham, Oil removal from used sorbents using a biosurfactant, *Bioresour. Technol.* 96 (2005) 331–334. <https://doi.org/10.1016/j.biortech.2004.04.005>.
- [218] J.L. Gurav, I.K. Jung, H.H. Park, E.S. Kang, D.Y. Nadargi, Silica aerogel: Synthesis and applications, *J. Nanomater.* 2010 (2010). <https://doi.org/10.1155/2010/409310>.
- [219] P.C. Thapliyal, K. Singh, Aerogels as Promising Thermal Insulating Materials: An Overview, *J. Mater.* 2014 (2014) 1–10. <https://doi.org/10.1155/2014/127049>.
- [220] J. Lin, G. Li, W. Liu, R. Qiu, H. Wei, K. Zong, X. Cai, A review of recent progress on the silica aerogel monoliths: synthesis, reinforcement, and applications, *J. Mater. Sci.* 56 (2021) 10812–10833. <https://doi.org/10.1007/s10853-021-05997-w>.
- [221] A. Du, B. Zhou, Z. Zhang, J. Shen, A special material or a new state of matter: A review and reconsideration of the aerogel, *Materials (Basel)*. (2013). <https://doi.org/10.3390/ma6030941>.
- [222] C. Wu, K. Li, X. Li, Z. Fei, Z. Zhang, Z. Yang, Research progress on preparation of silica aerogels at ambient pressure drying, *Huagong Jinzhan/Chemical Ind. Eng. Prog.* 41 (2022) 837–847. <https://doi.org/10.16085/j.issn.1000-6613.2021-0552>.
- [223] W.J. Malfait, S. Zhao, R. Verel, S. Iswar, D. Rentsch, R. Fener, Y. Zhang, B. Milow, M.M. Koebel, Surface Chemistry of Hydrophobic Silica Aerogels, *Chem. Mater.* 27 (2015) 6737–6745. <https://doi.org/10.1021/acs.chemmater.5b02801>.
- [224] J.H. Kim, M.J. Kim, B. Lee, J.M. Chun, V. Patil, Y.S. Kim, Durable ice-lubricating surfaces based on polydimethylsiloxane embedded silicone oil infused silica aerogel, *Appl. Surf. Sci.* 512 (2020). <https://doi.org/10.1016/j.apsusc.2020.145728>.
- [225] J.D. Menczel, R.B. Prime, *Thermal Analysis of Polymers: Fundamentals and Applications*, 2008. <https://doi.org/10.1002/9780470423837>.
- [226] S. Kinzy, R. Falcone, Thermogravimetric Analysis Of Polymers, in: *Handb. Plast. Anal.*, 2003. <https://doi.org/10.1201/9780203911983.ch4>.
- [227] H.M. Ng, N.M. Saidi, F.S. Omar, K. Ramesh, S. Ramesh, S. Bashir, Thermogravimetric Analysis of Polymers, in: *Encycl. Polym. Sci. Technol.*, 2018: pp. 1–29. <https://doi.org/10.1002/0471440264.pst667>.
- [228] O. Nabinejad, D. Sujan, M.E. Rahman, I.J. Davies, Determination of filler content for natural filler polymer composite by thermogravimetric analysis, *J. Therm. Anal. Calorim.* 122 (2015) 227–233. <https://doi.org/10.1007/s10973-015-4681-2>.
- [229] K.S. Walton, R.Q. Snurr, Applicability of the BET method for determining surface areas of microporous metal-organic frameworks, *J. Am. Chem. Soc.* 129

- (2007) 8552–8556. <https://doi.org/10.1021/ja071174k>.
- [230] F. Ambroz, T.J. Macdonald, V. Martis, I.P. Parkin, Evaluation of the BET theory for the characterization of meso and microporous MOFs, *Small Methods*. 2 (2018). <https://doi.org/10.1002/smt.201800173>.
- [231] D. Borisova, H. Möhwald, D.G. Shchukin, Mesoporous silica nanoparticles for active corrosion protection, *ACS Nano*. 5 (2011) 1939–1946. <https://doi.org/10.1021/nn102871v>.
- [232] E. Shchukina, D. Shchukin, D. Grigoriev, Effect of inhibitor-loaded halloysites and mesoporous silica nanocontainers on corrosion protection of powder coatings, *Prog. Org. Coatings*. 102 (2017) 60–65. <https://doi.org/10.1016/j.porgcoat.2016.04.031>.
- [233] J.M. Falcón, L.M. Otubo, I. V. Aoki, Highly ordered mesoporous silica loaded with dodecylamine for smart anticorrosion coatings, *Surf. Coatings Technol.* 303 (2016) 319–329. <https://doi.org/10.1016/j.surfcoat.2015.11.029>.
- [234] M. Shamshiri, R. Jafari, G. Momen, Potential use of smart coatings for icephobic applications: A review, *Surf. Coatings Technol.* 424 (2021) 127656. <https://doi.org/10.1016/j.surfcoat.2021.127656>.
- [235] L. Foroughi Mobarakeh, R. Jafari, M. Farzaneh, Robust icephobic, and anticorrosive plasma polymer coating, *Cold Reg. Sci. Technol.* 151 (2018) 89–93. <https://doi.org/10.1016/j.coldregions.2018.03.009>.
- [236] E. Vazirinasab, R. Jafari, G. Momen, Application of superhydrophobic coatings as a corrosion barrier: A review, *Surf. Coatings Technol.* 341 (2018) 40–56. <https://doi.org/10.1016/j.surfcoat.2017.11.053>.
- [237] H.M. Ali, M.A. Qasim, S. Malik, G. Murtaza, Techniques for the Fabrication of Super-Hydrophobic Surfaces and Their Heat Transfer Applications, in: *Heat Transf. - Model. Methods Appl.*, 2018. <https://doi.org/10.5772/intechopen.72820>.
- [238] A.B.D. Cassie, S. Baxter, Large contact angles of plant and animal surfaces, *Nature*. 155 (1945) 21–22. <https://doi.org/10.1038/155021a0>.
- [239] A. Chi Wang, C. Wu, D. Pisignano, Z. Lin Wang, L. Persano, A.M. Wagner, D.S. Spencer, N.A. Peppas, *J. Appl Polym Sci*, R. Muthuraj, M. Misra, A. Kumar Mohanty, J. Appl, P. Sarkar, A.K. Bhowmick, S. Stratton, O.S. Manoukian, R. Patel, A. Wentworth, S. Rudraiah, S.G. Kumbar, *J. Appl Polym*, C. Wang, M.C. Gupta, Y. Han Yeong, K.J. Wynne, J. Li, J. Zhu, J. Wang, S. Yuan, J. Lin, J. Shen, B. Van der Bruggen, J. Li, A.I. Isayev, Q. Wang, M.D. Soucek, Factors affecting the adhesion of ice to polymer substrates, *J. Appl. Polym. Sci.* 135 (2018) 45734. <https://doi.org/10.1002/APP.45734>.
- [240] F.M. Fowkes, ATTRACTIVE FORCES AT INTERFACES, *Ind. Eng. Chem.* 56 (2002) 40–52. <https://doi.org/10.1021/IE50660A008>.
- [241] J. Zhang, B. Liu, Y. Tian, F. Wang, Q. Chen, F. Zhang, H. Qian, L. Ma, Facile one-step method to fabricate a slippery lubricant-infused surface (lis) with self-replenishment properties for anti-icing applications, *Coatings*. (2020). <https://doi.org/10.3390/coatings10020119>.
- [242] W.W. Scott, B. Bhushan, Use of phase imaging in atomic force microscopy for measurement of viscoelastic contrast in polymer nanocomposites and molecularly thick lubricant films, *Ultramicroscopy*. 97 (2003) 151–169. [https://doi.org/10.1016/S0304-3991\(03\)00040-8](https://doi.org/10.1016/S0304-3991(03)00040-8).

- [243] D. Raghavan, X. Gu, T. Nguyen, M. VanLandingham, A. Karim, Mapping polymer heterogeneity using atomic force microscopy phase imaging and nanoscale indentation, *Macromolecules*. 33 (2000) 2573–2583. <https://doi.org/10.1021/ma991206r>.
- [244] C.D. Onal, B. Sümer, M. Sitti, Cross-talk compensation in atomic force microscopy, *Rev. Sci. Instrum.* 79 (2008) 103706. <https://doi.org/10.1063/1.3002483>.
- [245] G. Mistura, M. Pierno, Advances in Physics: X Drop mobility on chemically heterogeneous and lubricant-impregnated surfaces, *Adv. Phys. X*. 6149 (2017) 0. <https://doi.org/10.1080/23746149.2017.1336940>.
- [246] X. Zhu, J. Lu, X. Li, B. Wang, Y. Song, X. Miao, Z. Wang, G. Ren, Simple Way to a Slippery Lubricant Impregnated Coating with Ultrastability and Self-Replenishment Property, 58 (2019) 8148–8153. <https://doi.org/10.1021/acs.iecr.9b01176>.
- [247] L. Zhu, J. Xue, Y. Wang, Q. Chen, J. Ding, Q. Wang, Ice-phobic Coatings Based on Silicon-Oil-Infused Polydimethylsiloxane, 5 (2013) 4053–4062.
- [248] A. Chremos, C. Jeong, J.F. Douglas, Influence of polymer architectures on diffusion in unentangled polymer melts, *Soft Matter*. 13 (2017) 5778–5784. <https://doi.org/10.1039/C7SM01018D>.
- [249] X. Xu, J. Chen, J. Zhou, B.X. Li F Xu, J. Chen, J. Zhou, X.F. Xu, B.W. Li, Thermal Conductivity of Polymers and Their Nanocomposites, *Adv. Mater.* 30 (2018) 1705544. <https://doi.org/10.1002/ADMA.201705544>.
- [250] L.J. Fetters, D.J. Lohse, D. Richter, T.A. Witten, A. Zirkel, Connection between Polymer Molecular Weight, Density, Chain Dimensions, and Melt Viscoelastic Properties, *Macromolecules*. 27 (1994) 4639–4647. <https://doi.org/10.1021/ma00095a001>.
- [251] M. Tonelli, S. Peppou-Chapman, F. Ridi, C. Neto, Effect of Pore Size, Lubricant Viscosity, and Distribution on the Slippery Properties of Infused Cement Surfaces, *J. Phys. Chem. C*. 123 (2019) 2987–2995. <https://doi.org/10.1021/acs.jpcc.8b11221>.
- [252] Y.H. Yeong, A. Milionis, E. Loth, J. Sokhey, Self-lubricating icephobic elastomer coating (SLIC) for ultralow ice adhesion with enhanced durability, *Cold Reg. Sci. Technol.* 148 (2018) 29–37. <https://doi.org/10.1016/j.coldregions.2018.01.005>.
- [253] H. Lan, T.A. Venkatesh, On the relationships between hardness and the elastic and plastic properties of isotropic power-law hardening materials, *Philos. Mag.* 94 (2014) 35–55. <https://doi.org/10.1080/14786435.2013.839889>.
- [254] M. P. LANGLEBE, YOUNG’S MODULUS FOR SEA ICE, *Can. J. Phys.* 40 (1962).
- [255] Y. Zhuo, S. Xiao, A. Amirfazli, J. He, Z. Zhang, Polysiloxane as icephobic materials – The past, present and the future, 405 (2021) 127088.
- [256] C. Wang, T. Fuller, W. Zhang, K.J. Wynne, Thickness dependence of ice removal stress for a polydimethylsiloxane nanocomposite: Sylgard 184, *Langmuir*. 30 (2014) 12819–12826. <https://doi.org/10.1021/la5030444>.
- [257] C. Larson, J.R. Smith, G.J. Armstrong, Current research on surface finishing and coatings for aerospace bodies and structures - A review, *Trans. Inst. Met. Finish.* (2013). <https://doi.org/10.1179/0020296713Z.000000000102>.

- [258] M. Shamshiri, R. Jafari, G. Momen, Potential use of smart coatings for icephobic applications: A review, *Surf. Coatings Technol.* 424 (2021) 127656. <https://doi.org/10.1016/j.surfcoat.2021.127656>.
- [259] H. Sojoudi, M. Wang, N.D. Boscher, G.H. McKinley, K.K. Gleason, Durable and scalable icephobic surfaces: Similarities and distinctions from superhydrophobic surfaces, *Soft Matter*. 12 (2016) 1938–1963. <https://doi.org/10.1039/c5sm02295a>.
- [260] C. Wangab, Z. Guo, A comparison between superhydrophobic surfaces (SHS) and slippery liquid-infused porous surfaces (SLIPS) in application, *Nanoscale*. 12 (2020) 22398–22424. <https://doi.org/10.1039/D0NR06009G>.
- [261] C.G.J. Prakash, R. Prasanth, Recent trends in fabrication of nepenthes inspired SLIPs: Design strategies for self-healing efficient anti-icing surfaces, *Surfaces and Interfaces*. 21 (2020). <https://doi.org/10.1016/j.surfin.2020.100678>.
- [262] Z. Gao, T. Xu, X. Miao, J. Lu, X. Zhu, Y. Song, G. Ren, Y. Jia, X. Li, A thermal-driven self-replenishing slippery coating, *Surfaces and Interfaces*. 24 (2021). <https://doi.org/10.1016/j.surfin.2021.101022>.
- [263] G. Zhang, Q. Zhang, T. Cheng, X. Zhan, F. Chen, Polyols-Infused Slippery Surfaces Based on Magnetic Fe<sub>3</sub>O<sub>4</sub>-Functionalized Polymer Hybrids for Enhanced Multifunctional Anti-Icing and Deicing Properties, *Langmuir*. 34 (2018) 4052–4058. <https://doi.org/10.1021/acs.langmuir.8b00286>.
- [264] A. Hozumi, L. Jiang, H. Lee, M. Shimomura, Toward Environmentally Adaptive Anti-icing Coating, in: *Stimuli-Responsive Dewetting/Wetting Smart Surfaces and Interfaces*, Springer International Publishing AG, 2018: pp. 259–286.
- [265] K. Golovin, S.P.R. Kobaku, D.H. Lee, E.T. DiLoreto, J.M. Mabry, A. Tuteja, Designing durable icephobic surfaces, *Sci. Adv.* 2 (2016) e1501496. <https://doi.org/10.1126/sciadv.1501496>.
- [266] A.S. Aghdam, F.C. Cebeci, Tailoring the Icephobic Performance of Slippery Liquid-Infused Porous Surfaces through the LbL Method, *Langmuir*. 36 (2020) 14145–14154. <https://doi.org/10.1021/acs.langmuir.0c02873>.
- [267] M. Zhang, J. Yu, R. Chen, Q. Liu, J. Liu, D. Song, Peili Liu, L. Gao, J. Wang, Highly transparent and robust slippery lubricant-infused porous surfaces with anti-icing and anti-fouling performances, *J. Alloys Compd.* 803 (2019) 51–60. <https://doi.org/10.1016/j.jallcom.2019.06.241>.
- [268] L. Zhou, H. Liu, A. Liu, L. Zhou, C. Du, Y. Li, Easily fabricated icephobic surface with external and self-replenishing properties, *Appl. Surf. Sci.* 579 (2022) 152069. <https://doi.org/10.1016/j.apsusc.2021.152069>.
- [269] S. Alwin, X.S. Shajan, Aerogels: promising nanostructured materials for energy conversion and storage applications, *Mater. Renew. Sustain. Energy*. 9 (2020). <https://doi.org/10.1007/s40243-020-00168-4>.
- [270] A.A. Mahani, S. Motahari, A. Mohebbi, Sol-gel derived flexible silica aerogel as selective adsorbent for water decontamination from crude oil, *Mar. Pollut. Bull.* 129 (2018) 438–447. <https://doi.org/10.1016/j.marpolbul.2017.10.012>.
- [271] Zhiwei He, H. Xie, M.I. Jamil, T. Li, Q. Zhang, Electro-/Photo-Thermal Promoted Anti-Icing Materials: A New Strategy Combined with Passive Anti-Icing and Active De-Icing, *Adv. Mater. Interfaces*. 9 (2022) 2200275. <https://doi.org/10.1002/admi.202200275>.
- [272] J. Ma, T. Ma, W. Duan, W. Wang, J. Cheng, J. Zhang, Superhydrophobic, multi-

- responsive and flexible bottlebrush-network-based form-stable phase change materials for thermal energy storage and sprayable coatings, *J. Mater. Chem. A*. 8 (2020) 22315–22326. <https://doi.org/10.1039/d0ta07619h>.
- [273] T. Ougizawa, T. Inoue, Morphology of Polymer Blends, in: L.A. Utracki, C.A. Wilkie (Eds.), *Polym. Blends Handb.*, 2nd ed., Springer Science+Business Media Dordrecht, 2014: pp. 875–918.
- [274] K. Ahmed, An investigation on chloroprene-compatible acrylonitrile butadiene rubber/high density polyethylene blends, *J. Adv. Res.* 6 (2014) 811–817. <https://doi.org/10.1016/j.jare.2014.06.003>.
- [275] A. Amirfazli, C. Antonini, Fundamentals of Anti- Icing Surfaces, in: *Non-Wettable Surfaces Theory, Prep. Appl. Non-Wettable Surfaces*, Royal Society of Chemistry, 2016: p. 319–346.
- [276] R. Fayt, R. Jerome, P. Teyssié, Molecular Design of Multicomponent Polymer Systems. VII. Emulsifying Effect of Poly(ethylene- styrene) Copolymer in High-Density Polyethylene/Polystyrene Blends, *Polym. Lett.* 19 (1981) 79–84.
- [277] J. Xu, F. Yin, L. Li, Q. Wen, H. Wang, S. Liu, Z. Jia, M. Farzaneh, Wet snow flashover characteristics of 500-kV AC insulator strings with different arrangements, *Appl. Sci.* 9 (2019). <https://doi.org/10.3390/app9050930>.
- [278] C. Zong, Y. Hu, X. Jiang, R. Xian, Z. Liu, J. Sun, AC flashover characteristics and arc development process of glaze ice-covered insulators in natural environment, *Int. J. Electr. Power Energy Syst.* 135 (2022). <https://doi.org/10.1016/j.ijepes.2021.107559>.
- [279] M. Farzaneh, Insulator flashover under icing conditions, *IEEE Trans. Dielectr. Electr. Insul.* 21 (2014) 1997–2011. <https://doi.org/10.1109/TDEI.2014.004598>.
- [280] S. Sanyal, F. Aslam, T. Kim, S. Jeon, Y.J. Lee, J. Yi, I.H. Choi, J.A. Son, J. Bin Koo, Deterioration of Porcelain Insulators Utilized in Overhead Transmission Lines: A Review, *Trans. Electr. Electron. Mater.* 21 (2020) 16–21. <https://doi.org/10.1007/s42341-019-00143-5>.
- [281] Q. Hu, S. Wang, H. Yang, L. Shu, X. Jiang, H. Li, J. Qi, Y. Liu, Effects of icing degree on ice growth characteristics and flashover performance of 220 kV composite insulators, *Cold Reg. Sci. Technol.* 128 (2016) 47–56. <https://doi.org/10.1016/j.coldregions.2016.04.010>.
- [282] X. Jiang, Z. Xiang, Z. Zhang, J. Hu, Q. Hu, L. Shu, Comparison on ac icing flashover performance of porcelain, glass, and composite insulators, *Cold Reg. Sci. Technol.* 100 (2014) 1–7. <https://doi.org/10.1016/j.coldregions.2013.12.010>.
- [283] Y. Huang, X. Jiang, M.S. Virk, Study of inverted T-shape insulator strings in icing conditions, *Cold Reg. Sci. Technol.* 173 (2020). <https://doi.org/10.1016/j.coldregions.2020.103021>.
- [284] M. Farzaneh et al., Coatings for Protecting Overhead Power Network Equipment in Winter Conditions, *CIGRE, Electra.* 283 (2015) 41–45.
- [285] A.N. Chaudhry, N.C. Billingham, Characterisation and oxidative degradation of a room-temperature vulcanised poly(dimethylsiloxane) rubber, *Polym. Degrad. Stab.* 73 (2001) 505–510. [https://doi.org/10.1016/S0141-3910\(01\)00139-2](https://doi.org/10.1016/S0141-3910(01)00139-2).
- [286] Suwarno, A. Basuki, F. Lendy, Sumedi, Improving outdoor insulator performances installed at coastal area using silicone rubber coating, in: *Proc. 2012 IEEE Int. Conf. Cond. Monit. Diagnosis, C. 2012*, 2012: pp. 1143–1146.

- <https://doi.org/10.1109/CMD.2012.6416361>.
- [287] I. Ahmadi-Joneidi, M. Rezaei, H. Kahuri, J. Sahragard, A. Sayani, Evaluation of actual field ageing on room temperature vulcanized silicone rubber coating of ceramic insulators on 230/63 substation, *Life Sci. J.* 10 (2013) 833–838.
- [288] M. Isa, M. Othman, A.Z. Abdullah, M.A.M. Piah, N.A. Rahman, M.N. Mazlee, Characteristics of RTV Coating on Ceramic Insulator, in: 2019 IEEE Int. Conf. Autom. Control Intell. Syst. I2CACIS 2019 - Proc., 2019: pp. 114–117. <https://doi.org/10.1109/I2CACIS.2019.8825080>.
- [289] G. Momen, M. Farzaneh, R. Jafari, Wettability behaviour of RTV silicone rubber coated on nanostructured aluminium surface, *Appl. Surf. Sci.* 257 (2011) 6489–6493. <https://doi.org/10.1016/j.apsusc.2011.02.049>.
- [290] I. Ramirez, R. Hernandez, G. Montoya, Salt fog testing of RTV coated ceramic insulators and comparison with HTV silicone rubber insulators, in: *Annu. Rep. - Conf. Electr. Insul. Dielectr. Phenomena, CEIDP*, 2012: pp. 794–797. <https://doi.org/10.1109/CEIDP.2012.6378900>.
- [291] K. Siderakis, D. Agoris, Performance of RTV silicone rubber coatings installed in coastal systems, *Electr. Power Syst. Res.* 78 (2008) 248–254. <https://doi.org/10.1016/j.epsr.2007.02.013>.
- [292] T. Sorqvist, Long-term field experience with RTV coated porcelain insulators, in: *Conf. Rec. IEEE Int. Symp. Electr. Insul.*, 2000: pp. 201–206. <https://doi.org/10.1109/elinsl.2000.845489>.
- [293] A.Y. Yassin, A.R. Mohamed, A.M. Abdelghany, E.M. Abdelrazek, Enhancement of dielectric properties and AC electrical conductivity of nanocomposite using poly (vinyl chloride-co-vinyl acetate-co-2-hydroxypropyl acrylate) filled with graphene oxide, *J. Mater. Sci. Mater. Electron.* 29 (2018) 15931–15945. <https://doi.org/10.1007/s10854-018-9679-7>.
- [294] X. Qiao, Z. Zhang, X. Jiang, R. Sundararajan, X. Ma, X. Li, AC failure voltage of iced and contaminated composite insulators in different natural environments, *Int. J. Electr. Power Energy Syst.* 120 (2020). <https://doi.org/10.1016/j.ijepes.2020.105993>.
- [295] X. Wei, Z. Jia, Z. Sun, W. Liao, Y. Qin, Z. Guan, Z. Xu, X. Peng, Study of anti-icing performance of insulator strings bottom-coated with semiconductive silicone rubber coating, *IEEE Trans. Dielectr. Electr. Insul.* 19 (2012) 2063–2072. <https://doi.org/10.1109/TDEI.2012.6396966>.
- [296] M. Taghvaei, M. Sedighizadeh, N. NayebPashae, A. Sheikhi Fini, Thermal stability of nano RTV vs. RTV coatings in porcelain insulators, *Therm. Sci. Eng. Prog.* 20 (2020). <https://doi.org/10.1016/j.tsep.2020.100696>.
- [297] E. Cherney, M. Marzinotto, R. Gorur, I. Ramirez, S. Li, A. El-Hag, A. Tzimas, End-of-life and replacement strategies for RTV silicone rubber coatings, *IEEE Trans. Dielectr. Electr. Insul.* 21 (2014) 253–261. <https://doi.org/10.1109/TDEI.2013.004185>.
- [298] M. Taghvaei, M. Sedighizadeh, N. NayebPashae, A.S. Fini, Reliability assessment of RTV and nano-RTV-coated insulators concerning contamination severity, *Electr. Power Syst. Res.* 191 (2021). <https://doi.org/10.1016/j.epsr.2020.106892>.
- [299] S. Xu, Q. Wang, N. Wang, Chemical Fabrication Strategies for Achieving Bioinspired Superhydrophobic Surfaces with Micro and Nanostructures: A



- Review, *Adv. Eng. Mater.* 23 (2021). <https://doi.org/10.1002/adem.202001083>.
- [300] Q. Zeng, H. Zhou, J. Huang, Z. Guo, Review on the recent development of durable superhydrophobic materials for practical applications, *Nanoscale*. 13 (2021) 11734–11764. <https://doi.org/10.1039/d1nr01936h>.
- [301] H.Y. Erbil, Practical Applications of Superhydrophobic Materials and Coatings: Problems and Perspectives, *Langmuir*. 36 (2020) 2493–2509. <https://doi.org/10.1021/acs.langmuir.9b03908>.
- [302] A. Allahdini, R. Jafari, G. Momen, Transparent non-fluorinated superhydrophobic coating with enhanced anti-icing performance, *Prog. Org. Coatings*. 165 (2022). <https://doi.org/10.1016/j.porgcoat.2022.106758>.
- [303] H. de Santos, M. Sanz-Bobi, Research on the pollution performance and degradation of superhydrophobic nano-coatings for toughened glass insulators, *Electr. Power Syst. Res.* 191 (2021). <https://doi.org/10.1016/j.epsr.2020.106863>.
- [304] C. Wang, Z. Guo, A comparison between superhydrophobic surfaces (SHS) and slippery liquid-infused porous surfaces (SLIPS) in application, *Nanoscale*. 12 (2020) 22398–22424. <https://doi.org/10.1039/d0nr06009g>.
- [305] K. Golovin, A. Tuteja, A predictive framework for the design and fabrication of icephobic polymers, *Sci. Adv.* 3 (2017) e1701617. <https://doi.org/10.1126/sciadv.1701617>.
- [306] A. Olad, F. Maryami, A. Mirmohseni, A.A. Shayegani-Akmal, Potential of slippery liquid infused porous surface coatings as flashover inhibitors on porcelain insulators in icing, contaminated, and harsh environments, *Prog. Org. Coatings*. 151 (2021). <https://doi.org/10.1016/j.porgcoat.2020.106082>.
- [307] S. Heydarian, K. Maghsoudi, R. Jafari, H. Gauthier, G. Momen, Fabrication of Liquid-Infused Textured Surfaces (Lits): The Effect of Surface Textures on Anti-Icing Properties and Durability, *Mater. Today Commun.* 32 (2022) 103935. <https://doi.org/10.1016/j.mtcomm.2022.103935>.
- [308] J. Wu, A. Schnettler, Degradation assessment of nanostructured superhydrophobic insulating surfaces using multi-stress methods, *IEEE Trans. Dielectr. Electr. Insul.* 15 (2008) 73–80. <https://doi.org/10.1109/T-DEI.2008.4446738>.
- [309] A. Krivda, L.E. Schmidt, X. Kornmann, H. Ghorbani, A. Ghorbandaeipour, M. Eriksson, H. Hillborg, Inclined-Plane Tracking and Erosion Test According to the IEC 60587 Standard, *IEEE Electr. Insul. Mag.* 25 (2009) 14–22. <https://doi.org/10.1109/MEI.2009.5313706>.
- [310] I. Ullah, M. Amin, H. Hussain, M.T. Nazir, Impact of Accelerated Ultraviolet Weathering on Polymeric Composite Insulators Under High Voltage DC Stress, *J. Power Energy Syst.* 8 (2022) 922–932. <https://doi.org/10.17775/CSEEJPES.2020.01900>.
- [311] I. Latif, T. B. Alwan, A. H. Al-Dujaili, Low Frequency Dielectric Study of PAPA-PVA-GR Nanocomposites, *Nanosci. Nanotechnol.* 2 (2013) 190–200. <https://doi.org/10.5923/j.nn.20120206.07>.
- [312] S.M. Gubanski, P. Boss, G. Cseépes, V. Der Houbanessian, J. Filippini, P. Guuinic, U. Gaäfvert, V. Karius, J. Lapworth, G. Urbani, P. Werelius, W. Zaengl, Dielectric response methods for diagnostics of power transformers, *IEEE Electr. Insul. Mag.* 19 (2003) 12–18.

- <https://doi.org/10.1109/MEI.2003.1203017>.
- [313] R.M. Hakim, R.G. Olivier, H. St-Onge, The Dielectric Properties of Silicone Fluids, *IEEE Trans. Electr. Insul.* EI-12 (1977) 360–370. <https://doi.org/10.1109/TEI.1977.298043>.
- [314] T. Teranishi, A. Ohashi, M. Ueda, Dielectric Characteristics of Silicone Oils in Low Temperature Regions, *IEEJ Trans. Fundam. Mater.* 95 (1975) 118–124. <https://doi.org/10.1541/ieejfms1972.95.118>.
- [315] A. Betie, F. Meghnefi, I. Fofana, Z. Yeo, H. Ezzaidi, Neural network approach to separate aging and moisture from the dielectric response of oil impregnated paper insulation, *IEEE Trans. Dielectr. Electr. Insul.* 22 (2015) 2176–2184. <https://doi.org/10.1109/TDEI.2015.004731>.
- [316] T. Teranishi, A. Ohashi, M. Ueda, Dielectric characteristics of silicone oils at low temperature, *Electr. Eng. Japan.* 95 (1975) 118–124. <https://doi.org/10.1002/ej.4390950201>.
- [317] P. Juuti, J. Haapanen, C. Stenroos, H. Niemelä-Anttonen, J. Harra, H. Koivuluoto, H. Teisala, J. Lahti, M. Tuominen, J. Kuusipalo, P. Vuoristo, J.M. Mäkelä, Achieving a slippery, liquid-infused porous surface with anti-icing properties by direct deposition of flame synthesized aerosol nanoparticles on a thermally fragile substrate, *Appl. Phys. Lett.* 110 (2017). <https://doi.org/10.1063/1.4981905>.

## Publications

### *Journal Articles*

- 1. Icephobicity and Electrical Assessment of Slippery Coating Impregnated with a Stabilized Hydroxyl-Terminated Lubricant for High Voltage Insulation Application**, S. Heydarian, G. Momen and R. Jafari. *Journal of Material Science*. 58, 9264–9281 (2023).
- 2. Icephobic Behavior of a Slippery Coating Containing Nanoporous Particles as Lubricant-Loaded Carriers**, S. Heydarian, R. Jafari and G. Momen. *Surfaces and Interfaces Journal*,103306 (2023).
- 3. Fabrication of liquid-infused textured surfaces (LITS): the effect of surface textures on anti-icing properties and durability**, S. Heydarian, K. Maghsoudi, R. Jafari, H. Gauthier, G. Momen. *Materials Today Communications*,32,103935, (2022).
- 4. Recent progress in anti-icing performance of slippery liquid-infused surfaces**, S. Heydarian, R. Jafari and G. Momen, *Progress in Organic Coatings*, *Progress in Organic Coatings*,151, 106096, (2021).

### *Conference papers*

- 1. Development of Slippery Surfaces Embedded with Silicone Oil-loaded Materials for Anti-icing Application**, CCEC 2022, Vancouver, Canada, October, 2022.
- 2. Fabrication of lubricant-impregnated Icephobic surfaces with Improved Stability**, Proceedings – Int. Workshop on Atmospheric Icing of Structures IWAIS 2022 -Montreal, Canada, June 2022.
- 3. Fabrication of Icephobic Slippery surfaces bioinspired by Nepenthe Pitcher Plant**, Conference of the Polymer Processing Society (PPS36), Montreal, Canada, September 2021 (Selected as the best presentation by the Next-Gen Committee).
- 4. Recent Progress in Fabrication of Icephobic Slippery Surfaces**, QCAM Student symposium (Webinar), 2020. (Best Presentation Award).
- 5. Slippery coatings to outdoor structures against ice accumulation**, QCAM Student symposium, Montreal, Canada, October 2019.